Theses & Dissertations   Graduate Studies

Spring 5-7-2016

Exploitation of the Ligand-Binding Properties of the Mannose 6-Phosphate/Insulin-Like Growth Factor II (IGF-II) Receptor to Inhibit IGF-II-Dependent Growth of Cancer Cells

Megan Zavorka Thomas
University of Nebraska Medical Center

EXPLOITATION OF THE LIGAND-BINDING PROPERTIES OF THE MANNOSE 6-PHOSPHATE/INSULIN-LIKE GROWTH FACTOR II (IGF-II) RECEPTOR TO INHIBIT IGF-II-DEPENDENT GROWTH OF CANCER CELLS

By

Megan E. Zavorka Thomas

A Dissertation

Presented to the Faculty of

The Graduate College in the University of Nebraska

In Partial Fullfilment of the Requirements

For the Degree of Doctor of Philosophy

Department of Biochemistry and Molecular Biology

Under the Supervision of Professor Richard G. MacDonald

University of Nebraska Medical Center
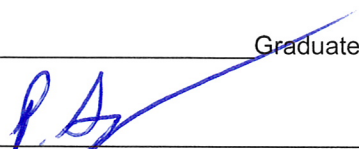
Omaha, Nebraska

April, 2015

THE UNIVERSITY OF NEBRASKA
REPORT ON DOCTORAL DEGREE

Date **April 22, 2016**

TO THE REGISTRAR:

Megan E. Zavorka Thomas has been reported as follows concerning the requirements for the Doctor of Philosophy degree.

All requirements established by the **Biochemistry & Molecular Biology** Graduate Program have been satisfied, as attested by:

_____
Graduate Program Director (signature)

and each member of the student's Supervisory Committee (signatures):

_____ Chair

_____ Co-Chair (if applicable)
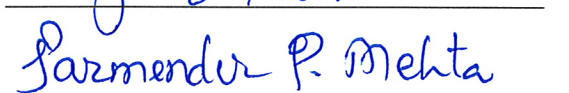
Dissertation Title:

Exploitation of the Ligand-Binding Properties of the Mannose 6-Phosphate/Insulin-like Growth Factor II (IGF-II) Receptor to Inhibit IGF-II-Dependent Growth of Cancer Cells

Under the supervision of **Dr. Richard MacDonald**

The candidate is therefore to be reported to the Faculty of the Graduate College as having fulfilled all requirements for the above mentioned degree.

_____
Dean for Graduate Studies

EXPLOITATION OF THE LIGAND-BINDING PROPERTIES OF THE MANNOSE 6-PHOSPHATE/INSULIN-LIKE GROWTH FACTOR II (IGF-II) RECEPTOR TO INHIBIT IGF-II-DEPENDENT GROWTH OF CANCER CELLS

Megan E. Zavorka Thomas, Ph.D.

University of Nebraska, 2016

Advisor: Richard G. MacDonald, Ph.D.

The mannose 6-phosphate/insulin-like growth factor II receptor (M6P/IGF2R) is a multifunctional, type I transmembrane receptor that is a member of the P-type lectin family. A large, extracytoplasmic (EC) region of the M6P/IGF2R binds various ligands, allowing the receptor to regulate multiple biological functions, including the role as a tumor suppressor. Two major classes of ligands, M6P-glycosylated (i.e. any proteins that bear M6P due to post-translational modification in the trans-Golgi network (TGN)) and non-glycosylated (i.e., the mitogen insulin-like growth factor II (IGF-II)), bind within distinct regions of the EC of the receptor and are trafficked to the lysosome. The M6P/IGF2R as well as the cation-dependent mannose 6-phosphate receptor (CD-MPR) are mostly involved in lysosomal biogenesis, trafficking newly synthesized lysosomal enzymes from the TGN to the early endosomes, where the vesicles mature into lysosomes. The receptors undergo recycling during the late endosomal phase where they are retrograde transported back to the TGN for another round of trafficking. However, a fraction of the receptors is found on the cell surface, where the M6P/IGF2R, but not the CD-MPR, is able to bind extracellular ligands. Through this action, IGF-II can bind to the M6P/IGF2R and will be degraded in the lysosome, reducing the bioavailability of the growth factor for the mitogenic insulin-like growth factor I receptor (IGF1R); thus, the M6P/IGF2R is considered a clearance receptor and tumor suppressor. Due to its growth suppressive function, the M6P/IGF2R is believed to play a role in cancer biology.

High-affinity, bivalent M6P-based ligands, such as lysosomal enzymes, bind and stabilize the dimeric M6P/IGF2R at the cell surface, leading to its internalization at a faster rate than when there is no M6P-based ligand bound. Therefore, the major goal of our work is to produce a panel of M6P-based ligands capable of bi- or multivalent binding to the M6P/IGF2R that could suppress IGF-II-dependent growth of cancer cells. Additionally, the M6P receptors (MPR) are well conserved through evolution, with the earliest form of "true" MPR known to date in the invertebrates such as mollusk. However, the social amoeba, *D. discoideum*, produces lysosomal enzymes that bind to the M6P/IGF2R, a discovery that predated identification of a receptor capable of transporting these acid hydrolases within this organism. We provide evidence of a putative MPR protein that retains all the necessary components of a M6P receptor homology domain that also binds M6P. The studies presented herein further our understanding of the origin of the M6P/IGFR as well as exploiting this receptor as a novel therapeutic target against IGF-II-dependent cancers.

Table of Contents

Abbreviations

α, alpha, anti- (reference to an antibody's antigenic target)

Å, Angstrom

A_{280}, absorbance at 280 nm

ADP, adenosine 5'-diphosphate

AKT, protein kinase B

Ala, A, alanine

ALS, acid-labile subunit

Amp, ampicillin

AMPK, 5' adenosine monophosphate-activated protein kinase

ANOVA, analysis of variance

AP, adaptor protein complexes

APC, adenomatous polyposis coli

AR, androgen receptor

Arg, R, arginine

Asp, D, aspartic acid

Ax3, Ax4, D. discoideum Axenic strains

A-T, adenine-thymine

Ax3 strain (Hit 1 nucleotide accession: XM_630458.1; Hit 1 protein accession

β-ME, 2-mercaptoethanol

Bax, Bcl-2 antagonist killer

Bcl-2, B-cell lymphoma 2

BH3, Bcl-2 homology domain

BL21, *E. coli* BL21(DE3) competent cell

BLAST, basic local alignment search tool

bp, base pair

BrdU, 5-bromo-2'-deoxyuridine

°C, degrees Celsius

C41, *E. coli* C41(DE3)pLysS competent cell

CAFs, cancer associated fibroblasts

Cam, chloramphenicol

cAMP, cyclic adenosine 5'-monophosphate

CD, circular dichroism

CD222, cluster of differentiation antigen of 222 kDa

CD-MPR, cation-dependent mannose 6-phosphate receptor

cDNA, complementary deoxyribonucleic acid

CI-MPR, cation-independent mannose 6-phosphate receptor

cm, centimeter(s)

CM, conditioned medium

CPM, counts per minute

CREG, cellular repressor of E1A-stimulated genes

CSCs, cancer stem cells

C-terminal, carboxyl-terminal

CLL, chronic lymphocytic leukemia

CTCF, CCCTC-binding factor

CuAAC, copper(I)-catalyzed azide-alkyne cycloaddition

Cys, C, cysteine

DAPI, 4',6-diamidino-2-phenylindole

D. discoideum, Dictyostelium discoideum, slime mold or social amoeba

DDMPR, *D. discoideum* mannose 6-phosphate receptor

DDMPR R1-3, regions 1-3 of the DDMPR

DDMPR R3, Region 3 of DDMPR

DEAE, diethylaminoethyl

DMEM, Dulbecco's modified Eagle medium

DMR, differentially methylated region

DMSO, dimethyl sulfoxide

DNA, deoxyribonucleic acid

DPBS, Dulbecco's phosphate-buffered saline

DTT, dithiothreitol

DNase, deoxyribonuclease

DU145, prostate cancer cell line

EC, extracellular

EDTA, ethylenediamnetetraacetic acid

EGFR, epidermal growth factor receptor

ERK1/2, extracellular signal regulated kinases 1 and 2

F1P, fructose 1-phosphate

FBS, fetal bovine serum

Fc, fragment crystallizable region

FnII, fibronectin-like type II domain

FPLC, fast protein liquid chromatography

g, gram(s)

G6P, glucose 6-phosphate

GAA, acid α-glucosidase

GGA, Golgi-localized gamma-ear-containing ADP-ribosylation factor-binding

GH, growth hormone

GlcNAc, N-acetyl glucosamine

Gln, Q, glutamine

Glu, E, glutamic acid

Gly, G, glycine

h, hour(s)

H, His, histidine

H19 locus ER, endoplasmic reticulum

HBS, HEPES-buffered saline

HBST, HEPES-buffered saline plus 0.05% Triton X-100

HCC, hepatocellular carcinoma

HEK 293, human embryonic kidney cells

HEK 293T, human embryonic kidney cells expressing SV40 large T antigen

HEPES, (4-(2-hydroxyethyl)-1-piperazineethanesulfonic acid)

His, H, histidine

HuH-7, hepatocellular carcinoma cell line

hGUS, human β-glucuronidase

HSA, human serum albumin

IC50, concentration that yields 50% inhibition

IGF1R, insulin-like growth factor 1 receptor

IGF2BP, insulin-like growth factor II mRNA binding protein

IGFBP, insulin-like growth factor binding protein

IGF-I, insulin-like growth factor I

IGF-II, insulin-like growth factor II

IgG$_1$, immunoglobulin G subtype 1

Ile, I, isoleucine

IMM2, immunoprecipitation buffer 2: 50 mM HEPES, pH 7.4, 0.15 M NaCl, 0.05%
      Triton X-100, pH 7.4

INS, insulin

IPTG, isopropyl β-D-1-thiogalactopyranoside

IR, insulin receptor

IR-A/B, insulin receptor isoform A or B

IRS, insulin receptor substrate

JEG-3, choriocarcinoma

JRC1, *E. coli* C41(DE3)pRARE2pLysS competent cell

JRC3, *E. coli* C43(DE3)pRARE2pLysS competent cell

Kb, kilobases

K_D, dissociation constant (equilibrium)

kDa, kilodalton

λ280, wavelength at 280 nm

L, liter(s)

LAMP1, Lysosomal-associated membrane protein 1

LB, Luria broth

LC3, microtubule-associated protein 1A/1B-light chain 3

LERP, lysosomal enzyme receptor protein

Leu, L, leucine

LOI, loss of imprinting

Lys, K, lysine

M, molar

μL, microliter(s)

μM, micromolar

mCi, millicurie(s)

mL, milliliter(s)

mM, millimolar

mAbs, monoclonal antibodies

MALDI-TOF, matrix-assisted laser-desorption ionization-time of flight

M6P, mannose 6-phosphate

M6P/IGF2R, mannose 6-phosphate/insulin-like growth factor II receptor

M6P-GlcNAc, M6P-N-acetyl-glucosamine

M6P-OCH$_3$, methyl phosphodiester

M6S, mannose 6-sulfate

MAPK, mitogen-activated protein kinase

Mcl-1, Myeloid cell leukemia-1

MES, 2-(N-morpholino)ethanesulfonic acid

MiaPaCa-2, pancreatic adenocarcinoma cell line

µM, micromolar

µg, microgram

mg, milligram

mM, millimolar

min, minute

miRNA, micro-ribonucleic acid

MMP, matrix metalloproteinase

MOPS, (3-(N-morpholino)propanesulfonic acid)

MPR, mannose 6-phosphate receptor

mRNA, messenger ribonucleic acid

MRH, mannose 6-phosphate receptor homology domain

Mrl1p, yeast mannose 6-phosphate receptor-like protein 1

mTOR, mammalian target of rapamycin

MTT, 3-(4,5-dimethylthiazol-2-yl)-2,5-diphenyltetrazolium bromide

MWCO, molecular weight cut-off

N-linked, asparagine-linked

N-terminal, amino-terminal

ng, nanogram

Ni^{2+}-NTA, Nickel-Nitrilotriacetic acid

nm, nanometer

nM, nanomolar

nmol/L, nanomoles per liter

NMR, nuclear magnetic resonance

nt, nucleotide(s)

O.D.$_{600}$, optical density at 600 nm

OVA, ovalbumin

p53, tumor protein p53

p70S6K, p70 ribosomal protein S6 kinase

PANC-1 pancreatic adenocarcinoma cell line

PAPEA, *p*-aminophenyl-ethanolamine

PARP, poly-adenosine diphosphate ribose polymerase

PBG, polybutylene glycol

PBS, phosphate-buffered saline

PC, phosphomannan core

PC-3, prostate cancer cell line

pCOLD-GST, pCOLD vector encoding glutathione S-transferase tag

pCMV5RIX, pCMV5 vector with *Eco*RI restriction site removed

PCR, polymerase chain reaction

PEG, polyethylene glycol

pelB, periplasmic leader sequence

Phe, F, phenylalanine

pI, isoelectric point

PI, propidium iodide

PI3P, phosphatidylinositol-3-phosphate

PKC, protein kinase C

pM, picomolar

PMP, pentamannosyl 6-phosphate

PMP-BSA, pentamannosyl 6-phosphate -bovine serum albumin

PMP-INS, pentamannosyl 6-phosphate -insulin

PMP-KYK, pentamannosyl 6-phosphate -Lysyl-tyrosyl-lysine

PMP-OVA, pentamannosyl 6-phosphate -ovalbumin

PMP-SYK, Seryl-tyrosyl-lysine

Pro, P, proline

PS, phosphatidylserine

PUMA, p53 upregulated modulator of apoptosis

RA, retinoic acid

RBA, relative binding affinity

RIA, radioimmunoassay

rpm, revolutions per minute

RT, room temperature

RT-PCR, real-time polymerase chain reaction

Ru(II)-mediated AAC (RuAAC)

sec, s, second

Ser, S, serine

S2-013, Suit-2 subline 13 pancreatic cancer cell line

SDS, sodium dodecyl sulfate

SDS-PAGE, sodium dodecyl sulfate/polyacrylamide gel electrophoresis

SHC, src homology domain-containing

Shh, Sonic hedgehog

SK-N-AS, Sloan Kettering neuroblastoma cell line

sM6P/IGF2R, soluble mannose 6-phosphate/insulin-like growth factor II receptor

SMC, smooth muscle cells

SSB, single-strand DNA break

SPR, surface plasmon resonance

$t_{1/2}$, half-life

TBS, Tris-buffered saline

Thr, T, threonine

TCA, Trichloroacetic acid

TGF-β, transforming growth-factor β

TGN, *trans*-Golgi network

TKI, tyrosine kinase inhibitors

TM, transmembrane

TNF-α, tumor necrosis factor-alpha

Tris, tris(hydroxymethyl)aminomethane

uPAR, urokinase-type plasminogen activator receptor

Val, V, valine

VPS10, vacuolar protein sorting 10 gene

X, any amino acid (single letter code)

Xkr8, scramblase Xk-related protein 8

Y, Tyr, tyrosine

Z-VAD-FMK, pan-kinase inhibitor

List of Tables and Figures

Acknowledgments

Dedication

I would like to thank everyone at the University of Nebraska Medical Center, in particular the Department of Biochemistry and Molecular Biology, for providing me the opportunity to pursue my education in a supportive environment. I would like to thank the members of my supervisory committee, Dr. Ming-Fong Lin, Dr. Parmender Mehta, and Dr. Joyce Solheim, for all of their guidance and invaluable advice throughout my graduate education.

I wish to express my graditude for my advisor, Dr. Richard MacDonald, for his wonderful mentorship, support, and encourgement throughout my entire graduate career. He has spent great time and effort into fostering my scientific mind and developing my skills. I could not have done as well throughout graduate school without his great understanding of my work-life balance. He has been supportive of my rigourous marathon training schedule and has been instrumental in preparing me for my future in science.

I thank all of the fellow BMB students and the friends that I have made along the way, which have provided an enthusiastic and positive environment. Thank you to all of my family that has supported me over the years, from being away from home throughout undergraduate and graduate school. Their support and encouragement has helped me survive the sometimes stressful nature of the process. I would like to thank my husband, York, for his constant understanding, love, and support. He is my best friend and has always been supportive of my work and has helped bring balance to my life when I needed it most. Finally, I thank God for His love and support of me for who I am and not giving up on me when I feel that I have lost my strength to continue.

Chapter I

Introduction

A.   Overview

The mannose 6-phosphate/insulin-like growth factor II receptor (M6P/IGF2R) is a multifunctional, type I transmembrane receptor that is a member of the P-type lectin family. A large, extracytoplasmic (EC) region of the M6P/IGF2R binds various ligands, allowing the receptor to regulate multiple biological functions, including the role as a tumor suppressor. Two major classes of ligands, M6P-glycosylated (i.e. any proteins that bear M6P due to post-translational modification in the trans-Golgi network (TGN)) and non-glycosylated (i.e., the mitogen insulin-like growth factor II (IGF-II)), bind within distinct regions of the EC of the receptor and are trafficked to the lysosome. The M6P/IGF2R as well as the cation-dependent mannose 6-phosphate receptor (CD-MPR) are mostly involved in lysosomal biogenesis, binding newly synthesized lysosomal enzyme from the TGN to the early endosomes, where the vesicles mature into lysosomes. The receptors undergo recycling during the late endosomal phase where they are retrograde transported back to the TGN for another round of trafficking. However, a fraction of the receptors is found on the cell surface, where the M6P/IGF2R, but not the CD-MPR, is able to bind extracellular ligands. Through this action, IGF-II can bind to the M6P/IGF2R and be degraded in the lysosome, reducing the bioavailability of the growth factor for the mitogenic insulin-like growth factor I receptor (IGF1R); thus, the M6P/IGF2R is considered a clearance receptor and tumor suppressor. Due to its growth suppressive function, the M6P/IGF2R is believed to play a role in cancer biology. With the recent knowledge on the M6P/IGF2R's structure and function on cellular biology, there is still much to be learned that may have significant impacts on health and disease. Our goal is to exploit the M6P/IGF2R as a novel therapeutic target in limiting IGF-II from the cell milieu in IGF-II-dependent cancers.

B.   M6P Receptors

The lysosomes are acidic intracellular organelles containing hydrolytic enzymes that function in degradation of proteins and other macromolecules. The lysosomes contain over 60 acid hydrolases that degrade endogenous and exogenous materials. Newly synthesized lysosomal enzymes are delivered from the *trans*-Golgi network to the lysosome by the mannose 6-phosphate receptors (MPRs). The MPRs have M6P-binding sites that recognize the M6P recognition marker on the glycoprotein's *N*-linked oligosaccharides. Lysosomes void of the proper complement of acid hydrolases can result in over 50 different lysosomal storage diseases (*1-5*).

There are two MPRs that transport glycosylated proteins: the cation-dependent MPR (46 kDa) and the cation-independent MPR (CI-MPR; 300 kDa) (*6*) which the latter is also called CD222 or M6P/IGF2R. The CD-MPR and CI-MPR belong to the P-type lectin family of type-1 integral membrane glycoproteins and are found mostly within the TGN and endosome trafficking network, but a small portion is trafficked to the plasma membrane. The MPRs have some redundant functions, yet they differ in their binding affinities and specificities for their ligands. Also, the M6P/IGF2R is distinct in that it has evolved into a multifunctional protein that binds many types of ligands.

B.1.   Discovery of M6P/IGF2R

Studies in the 1970s by Neufeld and colleagues on lysosomal storage diseases observed that there was a deficit of acid hydrolases in cultured fibroblast cells from I-cell patients yet these enzymes were present in the culture medium. When "corrective factors" (lysosomal enzymes from normal fibroblasts) were added to the culture medium of the I-cell fibroblasts, the cells took up the enzymes; the normal fibroblasts were

unable to endocytose the enzymes secreted by the I-cell fibroblasts (*7*). This similar phenomenon was seen in Mucoliidosis-II (*8*). It was noticed that "high uptake" form of the acid hydrolases were internalized at a faster rate than the "low uptake" forms. The "high uptake" forms were endocytosed while the "low uptake" forms were not, yet the "low uptake" forms were still enzymatically active. It was thought that a recognition marker must be allowing uptake of the enzyme through a receptor-mediated pathway (*9*) but the recognition marker was not necessary for enzyme activity. It was later determined that the phosphate on the M6P moiety on these "high uptake" forms of lysosomal enzymes is critical for recognition and internalization of the enzymes as incubation with alkaline phosphatase transformed the higher endocytosed ligand to a lower uptake, and that M6P competitively inhibited endocytosis (*10*). Kinetic studies validated these results using iduronidase as the enzyme added to cells deficient in this enzyme, which was inhibited by addition of M6P and the stereoisomer fructose 1-phosphate (F1P) (*11*). Together, it was proposed that a M6P recognition receptor on the cell surface was responsible for uptake of the enzymes possessing M6P residues. This receptor was soon named the CI-MPR, which was purified and characterized in the early 1980's, and was found to have a molecular weight of 215 kDa (*12-17*).

Around the same time that the M6P receptor was discovered, a human somatomedin (otherwise known as IGF-II) was used to partially purify a receptor greater than 240 kDa in molecular weight that was distinct from the insulin receptor (IR) (*18*). Work from three laboratories was able to determine that the sequence for the two receptors were identical, and that the receptor could bind both M6P ligands and IGF-II; thus, the receptor for somatomedin was the CI-MPR (*19-21*).

The CD-MPR was discovered in CI-MPR-deficient cells, yet lysosomal enzymes were still properly sorted (*14, 22*). Further analysis revealed that the CD-MPR differed

from the larger MPR in that it required divalent cations to bind to its ligands, and that the CD-MPR is coded from a different location within the genome than its larger counterpart (*14, 23, 24*).

B.2.   M6P/IGF2R Evolution

The MPRs have been well conserved in evolution. The CD-MPR has a similar sequence and protein structure as one of the 15 EC domains of the M6P/IGF2R, suggesting that the M6P/IGF2R may have evolved from duplications of the CD-MPR (*25*). The M6P/IGF2R has been sequenced or characterized in many species with the greatest characterization in human and mouse. To date, the complete cDNA sequences of the M6P/IGF2R have been obtained from multiple mammals, including bovine (*20*), human (*21, 26*), mouse (*27*), rat (*19*), pig, and many others (*28*). There are also incomplete sequences for sheep, kangaroo (*29*), and goat (*30*).

The M6P/IGF2R orthologs from non-mammalian vertebrates, such as chicken, bind to M6P but bind only very weakly to IGF-II (*31*). Further analysis showed that the M6P/IGF2R in the chicken shared only 61% identity with the mammalian receptor, indicating that the receptor acquired the property of IGF-II binding some time after the divergence of mammals from birds (*32*). Interestingly, the M6P/IGF2R isolated from the oriental garden lizard (*Calotes versicolor*) can bind human IGF-II (*25*), which may be attributed to convergent evolution. The MPR is conserved in fish; however, there is less sequence identity with the mammalian receptor (48-50% identity) and has amino acid substitutions in key ligand binding sites (*33*). The M6P/IGF2R was characterized from zebrafish and found to be 51% identical to the human receptor, making this the most primitive vertebrate species with the MPR (*34*).

Invertebrates also have conserved a version of the M6P/IGF2R. This has been seen in the starfish (*35*) and mollusk (*36, 37*), and there is a MPR-like binding protein in *Drosophila melanogaster* (*38*). The mollusk does have an interesting domain that interacts with the alpha-fucosidase enzyme that has not been seen with the other species, suggesting a different potential role of the receptor (*25, 30*). Since *Drosophila* has only 23-29% homology to the human M6P/IGF2R, it is considered to be only a MPR-like protein called lysosomal enzyme receptor protein (LERP) (*25, 38*).

Although it was thought that yeast did not have an MPR and that they sorted their lysosomal enzymes via the *VPS10* gene product through a specific amino acid sequence unrelated to M6P binding, Whyte and Munro discovered that yeast do in fact have a yeast homolog of MPR, which they termed Mrl1p (*39*). Unlike the mammalian MPRs, Mrl1p does not seem to be as important in lysosome biogenesis in yeast as the mammalian counterparts, since knockout of the *MRL1* gene did not substantially affect lysosome maturation (*39*). Still, the Mrl1p protein may be an evolutionary precursor to the MRPs in the subsequent domain.

Dictyostelium discoideum, a social amoeba, possesses M6P-methylesters on its lysosomal enzymes that can recognize and bind the mammalian M6P/IGF2R (*40-42*). However, *D. discoideum* has unique characteristics about its lysosomal enzymes that differ from the higher-order species. *D. discoideum's* acid hydrolases have phosphodiesters and these methylphosphomannosyl groups resist acid hydrolysis (*41, 43*). In addition, *D. discoideum* has many sulfate residues in lysosomal enzymes, mainly existing as mannose 6-sulfate (M6S). In fact, only about 2% of the oligosaccharide residues within the lysosomal enzymes exist as phosphomonoesters (*41, 44*). Thus, even though *D. discoideum* acid hydrolases can bind to the mammalian M6P/IGF2R, it may have its own version of MPR that favors the phosphodiester- or M6S-binding, but to

date, no MPR-like receptor has been found. Work from the MacDonald and Berkowitz laboratories has found a putative mannose 6-phosphate receptor in *D. discoideum*. This *D. discoideum* mannose 6-phosphate receptor (DDMPR) has five mannose 6-phosphate receptor homology (MRH) domains and is predicted to have a similar sequence and fold as the mammalian domain 3. If this receptor is in fact an MPR, the DDMPR would be a very interesting protein to characterize, because it would be the first such MPR-like protein discovered in a species in the slime mold branch after divergence from the lineage leading to animals, fungi, ciliates and plants within Eukaryota.

B.3.   Genomic structure of M6P/IGF2R

The genes encoding the M6P/IGF2R in both mouse and human map to different loci than both the genes encoding IGF-II (chromosome 11 in human) (*45*) and CD-MPR (chromosome 12 with 7 exons and total length of 12 kb in human) (*46, 47*). The *M6p/Igf2r* gene locus is mapped to chromosome 17 in mouse, and is maternally imprinted. The murine *M6p/Igf2r* gene is about 93 kilobases (kb) long and has 48 exons and is predicted to code for 2482 amino acids (*48*). Exons 1-46 code for the 15 EC domains that are similar to the bovine and human M6P/IGF2R EC domains. Each domain is encoded by 3-5 exons, and the fibronectin-like domain within repeat 11 is encoded by exon 39. Part of exon 46 codes for the transmembrane domain while exons 46-48 code for the cytoplasmic tail (*48*). In human, the *M6P/IGF2R* gene maps to chromosome 6q26 and has 48 exons comparable to the mouse, with a total size of 136 kb (*49*). There is no correspondence of the exon boundaries of the M6P/IGF2R with the EC domain structure, with each EC domain encoded by three to five exons, similar to the CD-MPR. The 226-bp promoter region has a 54-bp enhancer with two E-box motifs, and

putative binding sites for the transcription factors Sp1 and nerve growth factor-1A (*46*). The human and mouse genes encoding the M6P/IGF2R are differentially imprinted. In the mouse, the *M6p/Igf2r* gene is maternally imprinted and expressed in all tissues, but the IGF2R gene in human is biallelically expressed (*49-51*), as is the *Igf2* and *M6p/Igf2r* in chicken (*52*). Contrary, the *IGF2* in human is maternally imprinted, and with loss of imprinting there is increased risk of cancer (*53*). Furthermore, when *M6P/IGF2R* is monoallelically imprinted, it increases the risk of cancers, such as Wilms' tumors (*49*).

Expression of *M6P/IGF2R* is developmentally regulated and tissue-specific (*54-58*), with the highest expression of *M6P/IGF2R* and *IGF2* around prenatal 16-20 days of development, dropping postnatally in rat and mouse tissues (*59*). In human, the M6P/IGF2R level is non-significantly higher in prenatal tissues compared to postnatal tissues, with high expression in all tissues studied (*57*). The MP6/IGF2R plays a crucial role in development, as knockout of this gene leads to fetal overgrowth and neonatal lethality (*60*). According to Matzner *et al.,* there was differential expression of the two MPRs in specific tissues during early and late-stage embryogenesis, suggesting that these two receptors have non-redundant roles in lysosome biogenesis that are cell- and stage-dependent, despite their overlapping functions (*54*).

B.4.   M6P/IGF2R protein structure

The M6P/IGF2R is a 300-kDa type-1 integral membrane glycoprotein consisting of a 44-residue amino-terminal signal sequence, 2269-residue EC region, 23-residue transmembrane region, and a163- residue carboxyl-terminal cytoplasmic tail (Figure 1.1) (*20*). There are 15 contiguous MRH repeat domains, each consisting of ~147 amino acid residues, that share 14-38% sequence identity and cysteine distribution (*20, 46*). Each

EC repeat of the M6P/IGF2R, as well as the single EC domain of the CD-MPR, has nine β-strands forming a flattened β-barrel structure, stabilized by 3-4 disulfide bonds and held together by a flexible linker. Sequence alignment and homology mapping predict that all of the domains have the overall similar structure with the exception of domain 13 having a fibronectin-like extra loop that protrudes out and supports the binding of IGF-II to domain 11 (*61, 62*).

To date, only domains 1-3 of the bovine M6P/IGF2R and 11-14 of the human M6P/IGF2R have been structurally solved using x-ray crystallography techniques (*61, 63, 64*), which have revealed great detail about the receptor's structure and function. The tertiary structures of the other EC domains have been predicted through sequence alignment and molecular modeling using the solved domains as a reference (Figure 1.2).

The crystal structure of domains 1-3 indicates that repeat 3 sits above repeats 1 and 2, suggesting that the M6P/IGF2R forms distinct structural units in groups of three repeats of the EC, producing five tri-repeats, oriented back-to-front (*63*). The IGF-II binding site in this proposed model would be on the opposite side of the receptor from the M6P-binding sites. However, the crystal structure of domains 11-14 showed the structure was a more open or linear configuration, resembling beads on a string where each repeat was a bead (*64*). Collectively, the two crystal structures suggest a structure that is more tightly packed with the tri-repeats retaining a compact architecture at the amino-terminal end while repeats 10-15 form a more linear, open conformation (Figure 1.1).
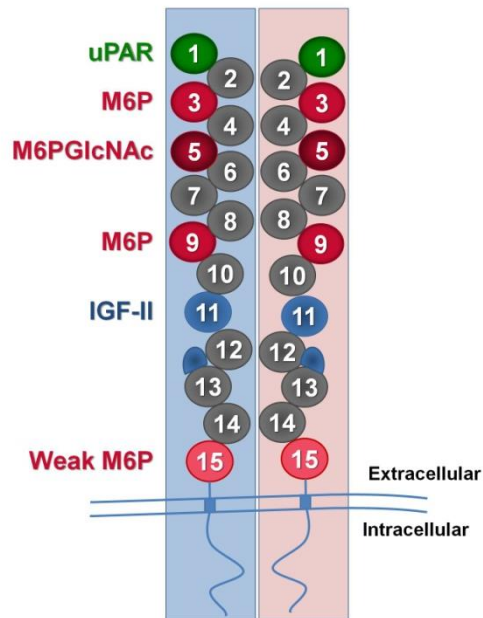
Figure 1.1: Schematic diagram of the M6P/IGF2R, indicating its dimeric nature and major structural domains having known functions. Abbreviations: uPAR, urokinase-type plasminogen activator receptor; M6P, mannose 6-phosphate monoester binding preference; M6P-GlcNAc, mannose 6-phosphate diester binding preference; IGF-II, insulin-like growth factor-II binding preference.
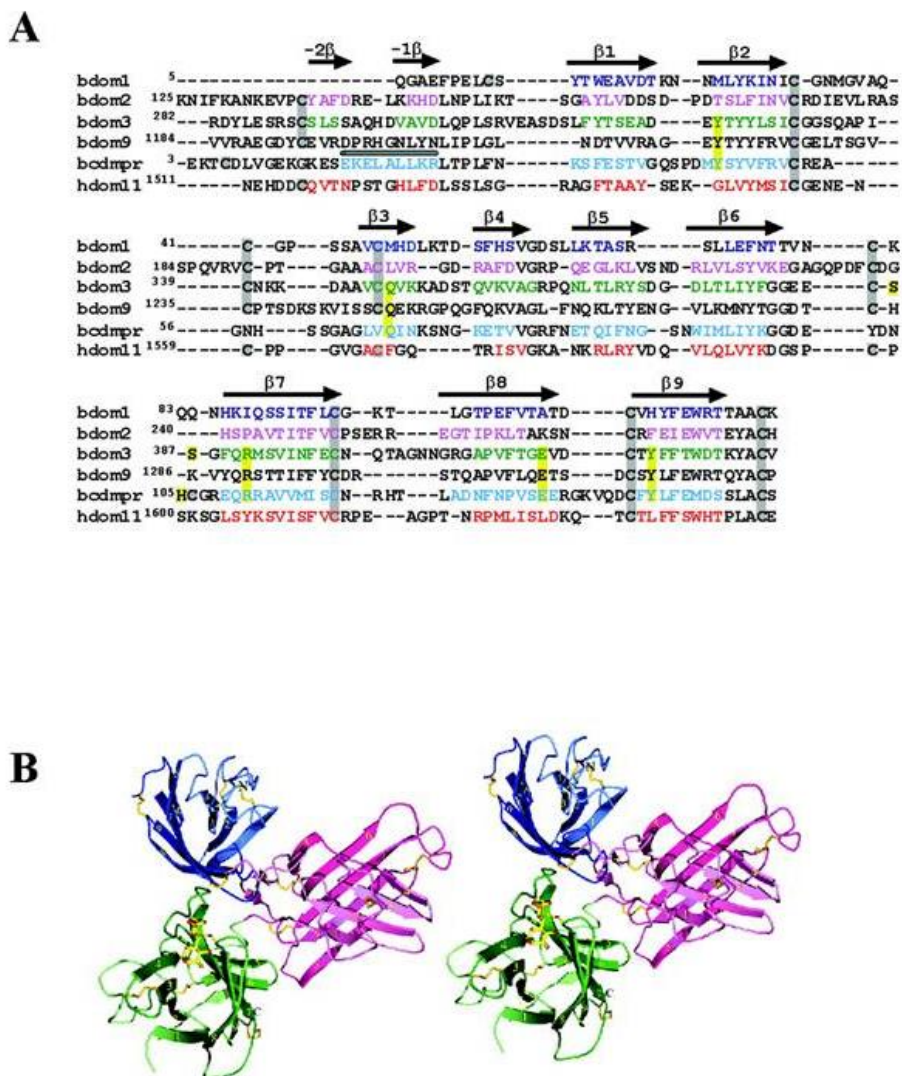
Figure 1.2: Sequences and tertiary structures of the MRH domains of the M6P/IGF2R. A) Sequence alignment of domains 1, 2, 3, 9, and 11 of the bovine M6P/IGF2R with the extracellular domain of the bovine CD-MPR. Arrows represent the extent of the β-sheets. There are 6-8 conserved cysteine residues in these domains, indicated in gray highlighting. B) A ribbon diagram of the tertiary structure of the bovine M6P/IGF2R domains 1 (blue), 2 (pink), and 3 (green). The disulfide bonds that interconnect the overall β -barrel sandwich structure are indicated in yellow. This figure was originially published in *The Journal of Biological Chemistry* and has been reprinted with permission of the publisher. Olson, L. J., Dahms, N. M., and Kim, J.-J. P. (2004) The N-terminal carbohydrate recognition site of the cation-independent mannose 6-phosphate receptor, *J. Biol. Chem. 279*, 34000-34009. The American Society for Biochemistry and Molecular Biology, Inc.

Several motifs important for protein-protein interactions, phosphorylation, and trafficking are located within the cytoplasmic tail of the M6P/IGF2R (Figure 1.3). The adaptor protein (AP) complexes interact with the single tyrosine-based motif, YSKV, which promotes clathrin-mediated endocytosis of the receptor at the plasma membrane (*1*). The acidic-cluster dileucine motif (SFHDDS**D**ED**LL** for human M6P/IGF2R) in the cytoplasmic tail interacts with the Golgi-localized γ-ear-containing ADP-ribosylation factor-binding (GGA) proteins and AP-1, allowing for trafficking of the receptor from the TGN to the endosome (*65*). Also, there have been reports of tyrosine phosphorylation at one of the four consensus motifs that are potential substrates for protein kinase C (PKC), cyclic adenosine 5'-monophosphate (cAMP)-dependent protein kinase and casein kinases (CK) 1 and 2 (*66-69*), which may play a role in internalization and trafficking.

B.5. Biosynthesis and processing of the M6P/IGF2R (co- and post-translational modifications)

There are nineteen potential *N*-linked glycosylation sites within the EC domain of the M6P/IGF2R (*20, 46*). However, the molecular mass differences of unglycosylated and glycosylated receptor forms in H-35 hepatoma cells suggest that there are 4-6 high-mannose oligosaccharide side chains (*70*). Studies show that most of these high-mannose oligosaccharide modifications converted to complex-type oligosaccharide forms when the receptor is mature (*46, 68, 71*). Even though the M6P/IGF2R has *N*-linked glycosylation, glycosylation is not necessary for M6P or IGF-II to bind to the receptor (*46, 68, 72*); however, it has not yet been determined if glycosylation affects the folding of the receptor.
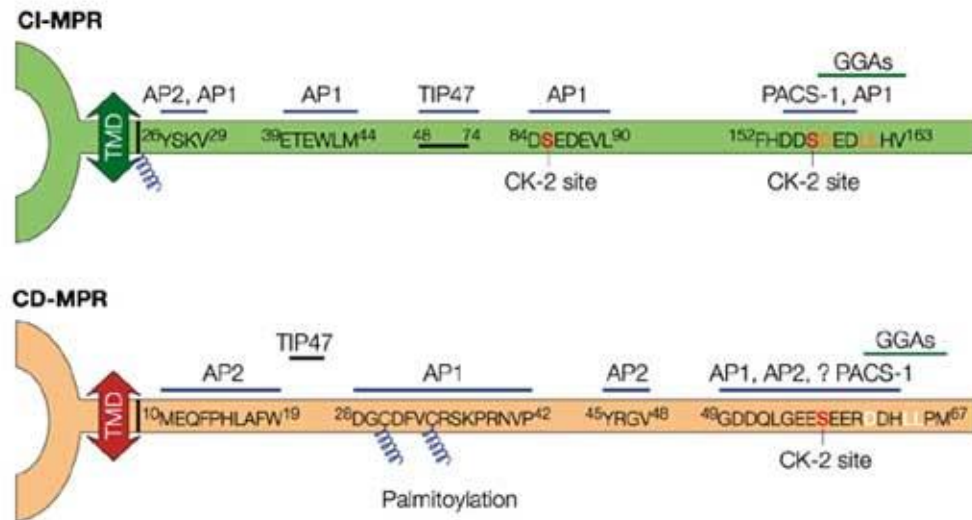
Figure 1.3: The cytoplasmic tail of the MPRs contains the trafficking signals. The CI-MPR (M6P/IGF2R) and CD-MPR have multiple motifs within the cytoplasmic tail that mediate interactions with binding partners, which influences trafficking and recycling of the receptors. This figure was originially published in *Nature Reviews Molecular Cell Biology* and has been reprinted with permission of the publisher. Ghosh, P., Dahms, N. M., and Kornfeld, S. (2003) Mannose 6-phosphate receptors: new twists in the tale, *Nat. Rev. Mol. Cell Biol. 4*, 202-213. Nature Publishing Group. License number: 3840350587925.

Using the CD-MPR as a reference of the disulfide-bond pattern, the 15 EC domains of the M6P/IGF2R have similarities in the locations of the cysteine residues (*46*). Studies using reducing agents indirectly confirmed that the MP6/IGF2R has intramolecular disulfide bonds (*46, 68, 72-75*). It is thought that the disulfide bond formation is an essential early step in the proper folding of the M6P/IGF2R. Additional post-translational modifications include phosphorylation of threonine, serine and tyrosine residues in the cytoplasmic domain of the M6P/IGF2R (*67, 68, 76, 77*), but only the phosphorylation at serine residues has been thoroughly studied at this time. Ser19, Ser85, and Ser156 are potential phosphorylation sites within the cytoplasmic domain of the receptor. When Ser86 and Ser156, which lie within the casein kinase-like motifs, are phosphorylated, there is an association with TGN and clathrin-coated vesicle localization in Chinese hamster ovary cells, indicating that its phosphorylation status may regulate M6P/IGF2R trafficking (*46, 78*). The amount of M6P/IGF2R present on the cell surface may be regulated by serine phosphorylation by PKC or the inhibition of sensitive phosphatases via okadaic acid (*46, 69, 79, 80*). Plasma membrane M6P/IGF2R can be phosphorylated on serine by type V transforming growth factor (TGF)-β, which has serine/threonine kinase activity (*80*), and can have a two-fold increase in internalization of a lysosomal enzyme; this suggests that the internalization rate of M6P/IGF2R can be modulated via the phosphorylation of its cytoplasmic tail (*46, 81*). If these serine residues are mutated, abolishing phosphorylation, the steady-state sorting of the acid hydrolases is unaffected in bovine (*46, 82*) or mouse (*46, 83*) cells. The acidic-cluster dileucine motif in the carboxyl-terminal tail provides the critical sorting signals that are recognized by GGA proteins in the TGN (*46, 65, 83-85*), suggesting that phosphorylation may be more important for modulating kinetics. One last modulation of the M6P/IGF2R is palmitoylation in the cytoplasmic domain, but the attachment sites and functional significance are unknown, unlike the CD-MPR (*46, 86*). Palmitoylation at Cys30 and

Cys34 of the cytosolic tail of CD-MPR is important for anchoring the receptor in the lipid bilayer and normal trafficking of the receptor (*87*).

C.   Ligand binding properties of the M6P/IGF2R

The M6P/IGF2R binds a diverse array of ligands, conferring multiple functions on this receptor. Not long after the receptor was discovered, it was predicted that each of the 15 EC repeats may bind its own specific ligand (*22*). Today, we now know that nearly half of the EC repeats play functional roles by binding certain ligands; interestingly, all of these functions reside in the odd-numbered repeats. The polypeptide growth factor IGF-II or glycoproteins with M6P modifications on their *N*-linked oligosaccharides are the best-characterized ligands for the M6P/IGF2R.

C.1.   Carbohydrate recognition by the MPRs: Binding of M6P-based ligands

The M6P/IGF2R and CD-MPR have an overlapping yet distinct distribution of ligands. There are over 60 acid hydrolases that need to be transported to the lysosome following their synthesis in the endoplasmic reticulum and post-translational processing and folding in the *trans* Golgi where they acquire M6P moities. Each of these ligands varies in size, positioning and number of N-linked oligosaccharides, phosphomannosyl modifications, and glycosidic linkage between mannose residues on high-mannose structures. This makes a complex network of lysosomal enzymes to be trafficked. The MPRs are expressed in most cell types and have been studied extensively to determine the role that each receptor plays in lysosomal enzyme targeting. The MPRs have different affinities for the different lysosomal enzymes, with some ligands showing

preferential binding to one MPR over the other. Mouse fibroblast cell lines with knockout of one of the MPRs or both were used for multiple studies on the lysosomal enzyme trafficking. When both MPRs were absent, there was severe mis-sorting of lysosomal enzymes, but when either receptor on its own was absent, there was only partial mis-sorting of enzymes, where the lysosomes remained normal or near-normal. The secretions from these single-knockout studies showed that the same species of enzymes were mis-sorted but in different ratios depending on which receptor was missing (*88*). Additionally, an excess of one receptor could not fully compensate for the absence of the other receptor, suggesting that the receptors preferentially recognize different features on the acid hydrolases (*89*). However, the excess amounts of M6P/IGF2R can compensate for loss of the CD-MPR using a secretion-recapture mechanism, where the receptor is able to take up secreted lysosomal enzymes from the medium rather than binding them in the Golgi and sorting internally to the lysosome directly (*68, 90*). The differences in binding affinities of the lysosomal enzymes to the MPRs confirmed that the receptors have overlapping binding repertoires, yet each preferentially binds to a unique subset of the lysosomal enzymes (*91*). Furthermore, a M6P proteomic analysis of serum from MPR-deficient mice indicated that some of the acid hydrolases (i.e., heparanase and α-mannosidase B1) have distinct preferences, respectively, for either the CD-MPR or the M6P/IGF2R (*92*). The M6P/IGF2R appears to be more efficient at lysosomal targeting than the CD-MPR, as there is an increase in M6P-capped glycoproteins in the medium when the M6P/IGF2R is absent relative to the absence of the CD-MPR (*91*). It is still not known how and for what reason two MPRs have evolved that display overlapping yet distinct specificities for lysosomal targeting, but further studies are necessary to determine the functional significance of the two MPRs.

C.1.a. Structural characteristics of M6P-glycans for M6P/IGF2R binding

M6P monoesters bind to the M6P/IGF2R with micromolar affinity (K_D = 5-8 x 10^{-6} M) (*93*) and utilize hydrogen bond interactions for productive binding. The phosphate on the sixth carbon hydrogen-bonds with a Ser residue and water molecules while the 2-hydroxyl group of the mannosyl ring forms a hydrogen bond with Gln and Arg residues, and this hydroxyl must be in the axial position as opposed to the equatorial position to do so (i.e., compared with the geometry of glucose 6-phosphate (G6P) at carbon 2) (*63*). If the mannose does not have a phosphate or the sugar has the hydroxyl in the wrong configuration, there is a 10,000-fold reduction in M6P-binding affinity for the M6P/IGF2R (*94*). The phosphate positioning and glycosidic linkage within the oligosaccharide is also important for optimal binding. Chemically synthesized oligomannosides or pseudoglycoproteins have been used as inhibitors to determine whether the phosphate group on the ultimate mannose is required for productive binding as well as varying the glycosidic linkages between mannose groups, α(1,2), α(1,3), and α(1,6). Radioligand displacement analysis determined that the α(1,2)-linked mannose structures had stronger inhibition of ^{125}I-β-galactosidase binding to the M6P/IGF2R. The penultimate glycosidic linkages did not have an inhibitory effect (*95, 96*). When the final glycosidic linkage was α(1,3)- or α(1,6)-linked, the affinity was reduced by 6-fold compared to the α(1,2)-linkage. Increasing the mannose-chain length improved the inhibition for binding to the M6P/IGF2R, suggesting that the two mannose groups leading up to the ultimate M6P may make contacts with the M6P-binding pocket of the receptor (*95*). Crystallography of the CD-MPR, which has a structurally homologous M6P-binding domain, in complex with pentamannosyl 6-monophosphate (PMP) or a phosphorylated α(1,2)-linked tri-mannoside confirmed that there are hydrogen bonds formed between the two mannose groups leading up to the final M6P and the M6P-binding pocket of the

receptor (*97, 98*). Two moles of M6P or one mole of a high-mannose oligosaccharide bearing two M6P moieties bind to one mole of M6P/IGF2R, as demonstrated by equilibrium dialysis experiments (*46, 93, 95*); however, the high-mannose oligosaccharide improved binding affinity by 100-1000-fold (1-10 nM) over M6P, indicating that these ligands have a multivalent interaction with the M6P/IGF2R (*91, 93*).

C.1.b. Structural requirements of the M6P/IGF2R for M6P recognition

Several laboratories have contributed to our understanding of the specific requirements for the recognition of M6P-containing moieties by the M6P/IGF2R. These biochemical and biophysical studies have determined the pH dependency for M6P-based binding, the specific amino acid residues required to make functional contacts with the ligand, and the binding sites' specific preferences for glycosidic modifications. Optimal binding of M6P-bearing ligands by the M6P/IGF2R occurs at a pH of approximately 6.4 while the receptor is unable to bind at a pH below 5.5, supporting the observations of the dissociation of lysosomal enzymes and other cargo from the M6P/IGF2R in the acidic environment of the endosome (*46*). The M6P/IGF2R, but not the CD-MPR, maintains M6P-binding ability at neutral pH, permitting the receptor to internalize extracellular M6P-based ligands (*93, 94*). Furthermore, the M6P/IGF2R recognizes M6P-GlcNAc phosphodiesters and hydrolase enzymes from *D. discoideum* that do not contain M6P modifications but rather mannose 6-sulfate (M6S) and methyl phosphodiester (M6P-OCH$_3$) (*99, 100*).   The capacity to bind different glycosyl modifications on M6P-based ligands at various pH conditions is attributed to four individual M6P-binding locations within the EC domain of the receptor (*93, 101, 102*).

Site-directed mutagenesis studies have determined that Gln348, Arg391, Glu416, Tyr421, and Ser387 within domain 3 of the bovine M6P/IGF2R are important for high-affinity binding of glycosylated proteins. The same motif of amino acid residues is conserved within domain 9 (Gln1292, Arg1334, Glu1354, Tyr1360) of the bovine M6P/IGF2R (*103*) as well as the bovine CD-MPR (Gln66, Arg111, Glu133, Tyr143) (*104*). These amino acid residues are able to directly interact with M6P groups, with Glu and Tyr forming hydrogen bonds with the 4- and 3-hydroxyl groups and Gln and Arg hydrogen bonding with the 2-hydroxyl of the mannose ring (*63*). This same motif in domain 5 is assigned as Gln644, Arg687, Glu709, and Tyr714 and for domain 15 as Gln2160, Arg2170, Glu2227, Tyr2233 (*101, 105*), indicating that these residues are essential for carbohydrate recognition by the bovine M6P/IGF2R in all four M6P-binding sites (Figure 1.4). Moreover, crystallographic studies have determined additional residues within the M6P-binding pockets that hydrogen bond with the two mannose groups leading up to the ultimate mannose group; mutation of Arg435/1334 to Ala or Lys abrogates nearly all M6P-based binding by the M6P/IGF2R (*106*).

M6P binds to distinct carbohydrate recognition sites in domains 3 and 9 with high affinity, and domains 5 and 15 with low affinity (*46, 93, 95, 101, 106, 107*). Recombinant M6P/IGF2R mini-receptors allowed for characterization and ligand-type preferences of the four M6P-binding sites. There are two high-affinity M6P sites (K_D=1 nM) located in domains 3 and 9 and two lower-affinity M6P-binding sites within domains 5 (K_D= 20 mM for M6P and 1 mM for M6P-diester) and 15 (K_D=13 μM), where domain 5 prefers phosphodiester-modified ligands (*101, 104, 108*). To date, only domains 1-3 (M6P-binding) and 11-14 (IGF-II binding) have been solved through x-ray
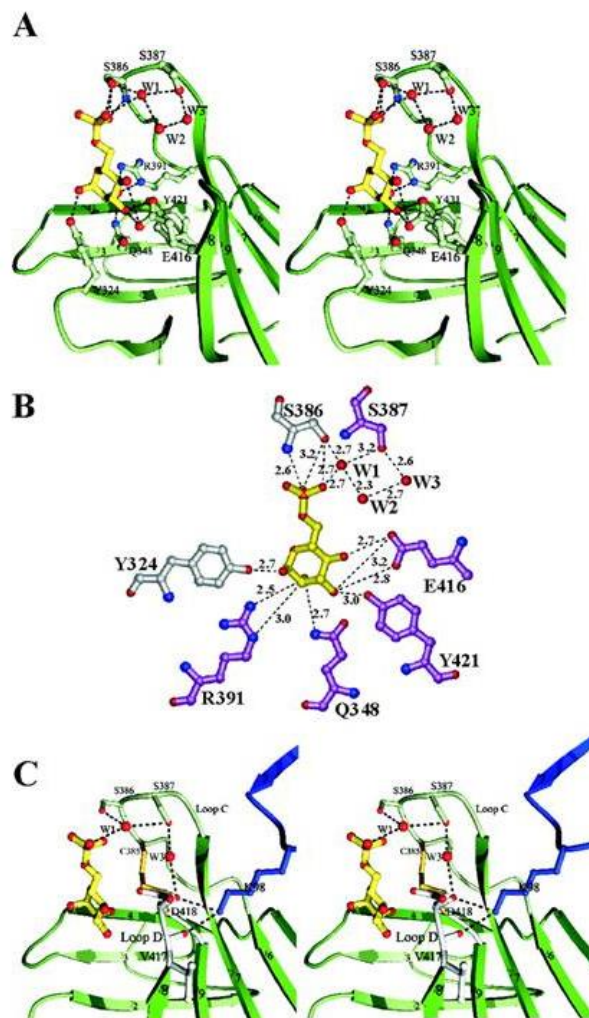
Figure 1.4: The M6P recognition by the M6P/IGF2R. A) Ribbon diagram of domain 3 (green) with bound M6P (yellow). B) M6P forms multiple hydrogen bonds within the binding pocket. The phosphate group of M6P makes contact with Ser386 and is stabilized by the involvement of three water molecules (W1-3) depicted as red spheres. Glu416 and Tyr421 form hydrogen bonds with the 4- and 3-hydroxyl groups. Gln348 and Arg 391 hydrogen bonds with the 2-hydroxyl of the mannose ring. C) Ribbon diagram indicating the contribution that Ser386 has in ligand binding. This figure was originially published in *The Journal of Biological Chemistry* and has been reprinted with permission of the publisher. Olson, L. J., Dahms, N. M., and Kim, J.-J. P. (2004) The N-terminal carbohydrate recognition site of the cation-independent mannose 6-phosphate receptor, *J. Biol. Chem. 279*, 34000-34009. The American Society for Biochemistry and Molecular Biology, Inc.

crystallography. The crystal structure of domains 1-3 indicates that domains 1-2 act to stabilize the M6P-binding site of domain 3 and are necessary to produce a high-affinity binding pocket (*63*).

Further analysis of the binding properties of the M6P-binding domains was done using affinity chromatography and acid-dependent dissociation analysis (*108*). Domain 9 has a more acidic pH optimum for binding (pH of 6.4-6.5) compared to the N-terminal binding domain (pH of ~6.9). Furthermore, domain 9 is able to retain more binding of M6P-based ligands as the pH drops below 5.5 compared with domain 3 (*108*). The ability of the M6P/IGF2R to bind M6P-based ligands throughout a broader pH range may account for how the receptor binds ligands at slightly alkaline conditions (pH 7.4 at the cell surface) and in slightly acidic luminal compartments (pH 6.5 at the TGN and endosomes), allowing for an expansive repertoire of ligand binding. Moreover, domain 3, with the aid of domains 1 and 2, forms a broader M6P-binding pocket that may allow this site to be more promiscuous in the type of ligand that it binds, such as M6P, M6S, M6P-phosphodiester, etc.) (*108*). Acid α-glucosidase (GAA) with a M6P or M6P-OCH$_3$ modification on its *N*-linked oligosaccharides was used in surface plasmon resonance (SPR) studies to determine whether domain 5 preferred mono- or diester M6P binding. Domain 5 displayed 14- to 18-fold higher affinity for M6P-phosphodiester than M6P, which explains the delivery of phosphodiester-containing lysosomal enzymes (such as those that escaped the uncovering enzyme's action in the TGN, where the *N*-acetylglucosamine linked to the M6P is enzymatically removed to reveal the M6P moiety) to the lysosome by this domain of the M6P/IGF2R (*105*). Unlike domains 3 and 9 of the M6P/IGF2R, domain 5 lacks two critical cysteines that form a disulfide bond, which may allow for M6P-phosphodiester recognition (*105*). Recently, domain 15 has been determined to have very low affinity M6P-binding ability, as it has only three of the

four critical amino acid residues that are required for high-affinity M6P binding and lacks two cysteine residues (*101*). This site binds its ligands with a K_D of 13 µM; thus, the physiological significance of this binding functionality is not clear at this time. In summary, each M6P-binding site has similar yet unique structural features and binding specificities that allow the M6P/IGF2R to recognize a diverse repertoire of M6P-modified proteins

C.2.   Structural requirements for IGF-II binding by the M6P/IGF2R

IGF-II is a small, acidic polypeptide that has many biological effects, with the most important roles in growth and development, cell division and differentiation (*109*). IGF-II is 67 amino acid residues in length in its mature form, which has a high sequence and structure homology to IGF-I and insulin (*110-113*), yet the latter polypeptides are unable to bind the M6P/IGF2R.

IGF-II binds to a hydrophobic cleft in domain 11 of the M6P/IGF2R while the fibronectin-like repeat in domain 13 enhances the binding affinity (*114, 115*). IGF-II binding is mostly attributed to I1572, as mutagenesis studies have shown that binding is abrogated by a substitution with threonine (*116-118*).   Furthermore, the core hydrophobic cluster within domain 11 of the bovine M6P/IGF2R contains amino acid residues Tyr1542, Glu1544, Phen1567, Thr1570 that form an overall positively charged surface for the negatively charged IGF-II surface to bind (Phe19 of IGF-II) (*64*). Additionally, binding affinity for IGF-II can be increased 6-fold with an E1544L substitution, which may increase the binding affinity with electrostatic interaction between E1544 and D20 on IGF-II (*119*).

A crystal structure of IGF-II in complex with an M6P/IGF2R fragment (domains 11-13) provided details on the mechanism of IGF-II binding to the receptor (*64*). The IGF-II binding site in domain 11 involves the same four implicated loops that are found within the M6P-binding sites of domains 3 and 9. A hydrophobic cluster consisting of Thr1542, Phe1567 and Leu1629 lying at the mouth of the β-barrel forms a patch that surrounds the IGF-II anchor residue Phe19 (Figure 1.5). Phe19 and Leu53 of the IGF-II polypeptide mediate binding to the hydrophobic cluster (*64*). The FnII domain within domain 13 does not directly interact with the IGF-II binding, but minor solvent accessible surface area changes in Trp1939 and Phe1941 are in proximity to IGF-II side chains and affect the AB-loop flexibility (*64*).

The binding pocket produced by domain 11 by itself is enough for productive binding of IGF-II to the M6P/IGF2R (*46, 120*); however, binding of IGF-II to the receptor is improved 5-10-fold when domain 13 with the fibronectin-like domain is also present (*114, 115, 120*). This fibronectin-like domain is a 43-residue insert in domain 13 that has approximately 50% sequence identity to the fibronectin type II (FnII) domain. FnII domains are found in many proteins, with their most prominent role in collagen binding; additionally, Devi *et al.* suggested that FnII within domain 13 was important for the high-affinity binding of the M6P/IGF2R for IGF-II (*114*), which was shown by Linnell *et al.* not to interact directly with the polypeptide but rather to act as a stabilizer for the binding pocket. In support of this, the predicted IGF-II binding pocket within domain 11 is adjacent to domain 13 containing the FnII fragment, thus allowing repeat 13 to slow the rate of IGF-II dissociation from the M6P/IGF2R, which enhances binding affinity (*61, 114, 116*).

An interesting observation was made from purified M6P/IGF2R from opossum and kangaroo indicating that the receptors of the metatherian mammals (marsupials)

exhibited lower binding affinities for IGF-II than the receptors of eutherian mammals; other animal species such as monotremes, chicken and frog do not display significant affinity for IGF-II (*29, 31, 46, 121-124*). These differences may have arisen from divergent evolution, as the IGF-II non-binding species have substantially different amino acid sequences in their domain 11 regions when compared with most eutherian mammals (*46, 123, 125*). On the contrary, the receptors of non-mammalian vertebrate fish (trout) appear to bind IGF-II (*46, 126*), while the zebrafish has a conserved isoleucine important for IGF-II-binding, but lacks conserved flanking regions involved in binding (*127*).

Furthermore, the dimeric M6P/IGF2R does not seem to affect IGF-II binding to the receptor. M6P-based ligands can bind to the M6P/IGF2R dimeric structure producing bivalent, high affinity binding that requires cooperation between subunits of the monomers, which may or may not affect IGF-II binding. To address this, co-immunoprecipitation studies of differentially expressed epitope-tagged soluble mini-receptors determined that IGF-II can bind to each monomer independently and there was no inhibitory effect on IGF-II binding induced by the formation of M6P/IGF2R dimers (*128*). While M6P/IGF2R dimerization does not affect IGF-II binding, prior studies propose that some phosphomannosylated ligands can block IGF-II binding (*129, 130*), although others determine that the receptor can accommodate both types of ligands simultaneously (*131*). Therefore, the binding of IGF-II and M6P-based ligands by the M6P/IGF2R is in part mutually exclusive.
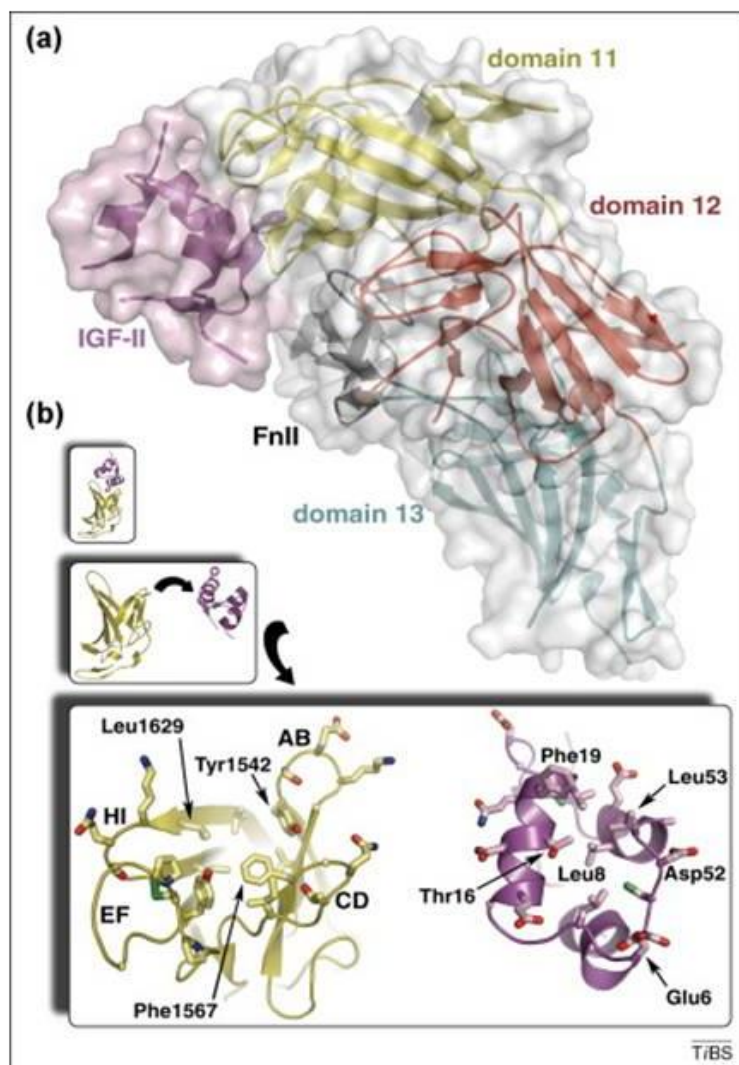
Figure 1.5: The interface of the M6P/IGF2R interaction with IGF-II. A) The IGF-II binding pocket is formed by domains 11-13 of the bovine M6P/IGF2R. The primary binding site for IGF-II (magenta) is located within domain 11 (yellow) but contacts are made from the type II fibronectin-like domain (FnII) of domain 13 (black). B) Side chains within domain 11 undergo a shift, changing the surface area upon IGF-II binding. This figure was originially published in *Trends in Biomedical Sciences* and has been reprinted with permission of the publisher. Brown, J., Jones, E.Y., Forbes, B.E. (2009) Keeping IGF-II under control: Lessons from the IGF-II-IGF2R crystal structure, *Trends in Biochemical Sciences. 34(12)*, 589-648. Elesvier. Licesnse number: 3840351012018.

C.3.   Additional non-M6P-modified M6P/IGF2R ligands

The M6P/IGF2R has been shown to bind other ligands apart from IGF-II and M6P-based glycoproteins, although their binding properties are far less studied than for IGF-II and the M6P ligands. There are a number of other ligands that interact by M6P-independent or unknown mechanisms, including: urokinase-type plasminogen activator receptor (uPAR) (*132*), plasminogen (*133*), retinoic acid (RA) (*134*), serglycin (*135*), and heparanase (*136*). The interaction between RA and the M6P/IGF2R is not completely understood at this time. Studies using full-length and soluble M6P/IGF2R have indicated that the receptor's cytoplasmic domain is necessary for RA binding. Additionally, binding of RA to the M6P/IGF2R enhances the internalization rate of the receptor and of passenger ligands (IGF-II and secreted lysosomal enzymes) that results in decreased cell proliferation and increased apoptosis (*134*). Plasminogen and uPAR binding sites have both been mapped to domain 1 of the M6P/IGF2R (*137*); however, there is some controversy as to the precise interaction. Kreiling *et al.* used co-immunoprecipitation assays to show that soluble M6P/IGF2R can bind uPAR in an M6P-dependent manner, but the full-length membrane-associated receptor displays weak binding to uPAR that is M6P-independent (*138*). The M6P/IGF2R may function to regulate activation of plasminogen (*137*). Heparanase appears to bind the M6P/IGF2R in the EC domain that acts as a tether for this enzyme to be stretched further out into the EC matrix for degradation of heparan sulfate (*136*), but the receptor may also function as an internalization route for heparanase into the cell (*139*). Serglycin has varying glycosaminoglycan chains depending on the cell type, which can consist of heparin, heparan sulfate, or chondroitin sulfate chains. Serglycin plays a role in lysosome biogenesis of hematopoietic cells (*135*).

C.4. Biochemical and structural evidence for M6P/IGF2R dimerization

It has been observed that M6P/IGF2R exists as homodimers at the cell surface independent of bound ligand (*140, 141*), but in detergent-solubilized preparations, the receptor mostly exists as a monomer (*131, 142*). Interestingly, this is unlike the CD-MPR that is detected as a dimeric or tetrameric complex under most conditions (*46, 143*). Even though the M6P/IGF2R is monomeric in detergent-solubilized preparations, there is strong evidence that M6P/IGF2R forms dimers with bound multivalent ligands, such as the naturally occurring lysosomal enzyme human β-glucuronidase (hGUS) (*131, 141, 144*). Using soluble, epitope-tagged M6P/IGF2R constructs, it has been demonstrated that the EC region of the receptor is sufficient to produce oligomerization (*141, 144*). Further analysis using forced expression of chimeric receptors (EC and TM regions of the M6P/IGF2R fused to the cytoplasmic tail of the EGFR) revealed the formation of dimers in the absence of M6P-based multivalent ligands (*141*). Furthermore, sedimentation coefficient studies demonstrated possible dimer formation using a truncation of the M6P/IGF2R encompassing domains 11-13, but did not see any dimeric formation when using a separate mini-receptor of domains 11-12 (*64*). Even though the authors of that study saw only weak interactions between these domains, it is thought that additional contacts made throughout the EC domain may enhance the dimeric structure of the M6P/IGF2R. Based upon the current literature, the M6P/IGF2R exists as a monomer but forms weak dimers in membranes that can be further stabilized with the binding of multivalent M6P-based ligands. Moreover, the internalization rate study done by York *et al.* revealed an enhanced internalization of IGF-II bound to the M6P/IGF2R when hGUS was present, further supporting the hypothesis that multivalent M6P-based ligands stabilize receptor dimers and alter the kinetics of internalization (*131*).

Even though weak, dimeric structures of the M6P/IGF2R form in the plasma membrane, the precise domain responsible for dimerization has yet to be determined. Nevertheless, multiple interactions may occur along the EC domain with domain 12 being most critical in influencing dimerization (*64, 140, 141*). Crystal structures for the dimer of domains 11-14 of the M6P/IGF2R indicate that this region forms the bulk of the receptor dimer (*64*), while domain 5 in the bovine M6P/IGF2R has also been shown to contribute to dimerization (*102*), suggesting that additional contacts within domain 5 of each monomer may further support dimerization (Figure 1.6).

Although there is increasing evidence suggesting that M6P/IGF2R forms a dimeric complex in membranes, the exact mechanism and interplay between the domains of each monomer has yet to be defined. Additionally, it is believed that multivalent M6P-based ligands can stabilize the dimeric receptor, but they are not necessary for initiation of the dimer complex. This was seen when an epitope-tagged double mutant of the soluble form of the M6P/IGF2R encompassing domains 1-15 was pulled down with a different epitope-tagged wild-type mini-receptor of domains 1-15 in the absence of multivalent ligand (*128*). Nevertheless, it remains unclear how multivalent M6P-based ligands, when bound to the dimeric M6P/IGF2R, can accelerate the internalization of the receptor and passenger ligands as seen with hGUS (*131*). Whether the increased rate of receptor internalization is mediated by the clathrin-dependent endocytosis pathway is still up for debate. One hypothesis is that when the multivalent M6P-based ligands bind to the dimeric or oligimeric M6P/IGF2R structure, it leads to clustering of the internalization signals that are present in the C-terminal tail (*131, 145*). Another explanation is that a conformational change within the EC domain caused by ligand binding can result in an optimal presentation of the internalization signals within the cytoplasmic tail that allows a greater interaction with the clathrin-
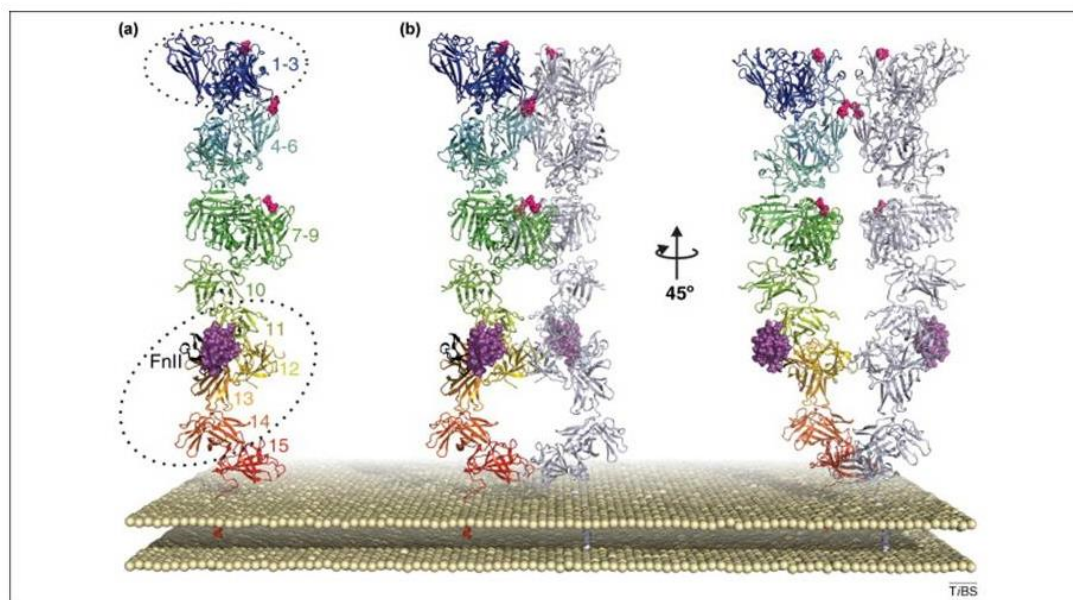
Figure 1.6: Model of the ectodomain of the M6P/IGF2R tertiary structure. A) The monomeric M6P/IGF2R ectodomain is depicted as a series of ribbons for each domain, folding into tri-repeats. The crystal structure of domains 1-3 and 11-14 have been solved, and the remaining domains have been modeled through sequence alignment. B) The M6P/IGF2R forms a dimer in membranes where multiple contacts are made throughout the length of the ectodomain. Domain 12 is predominantly involved in the dimeric structure. This figure was originially published in *Trends in Biomedical Sciences* and has been reprinted with permission of the publisher. Brown, J., Jones, E.Y., Forbes, B.E. (2009) Keeping IGF-II under control: Lessons from the IGF-II-IGF2R crystal structure, *Trends in Biochemical Sciences. 34(12)*, 589-648. Elesvier. Licesnse number: 3840351012018.

mediated endocytosis machinery (*131*). It is also unknown at this time if the M6P/IGF2R can form higher-order oligomeric states through multivalent ligand interactions and the potential effect they would have on the receptor's intracellular trafficking.

D.   M6P/IGF2R function

D.1.   M6P/IGF2R localization and trafficking

The MPRs are predominantly found in the TGN and lysosomal network, with about 10% of receptor found at the plasma membrane at most times, but the actual amount varies among cell types (*46, 146-150*). The MRPs undergo constitutive trafficking that is not dependent on ligand binding (*151, 152*). However, upon binding of different ligands (insulin, IGF-I, IGF-II, or M6P-based) to receptors, these ligands may cause a type-dependent shift in the distribution of that receptor from the intracellular compartments to the cell surface to decrease EC ligand (*151, 153*). The MPRs mainly function in lysosome biogenesis, but also function to recapture any M6P-capped acid hydrolases that escape sorting and were secreted by the cell, as well as certain extracellular ligands such as IGF-II that are internalized from the plasma membrane and trafficked to the lysosome for degradation.

D.2.   Lysosome biogenesis

Lysosomes are acidic membrane-bound organelles that function in degradation of cellular macromolecules. Lysosomes contain over 60 soluble acid hydrolases and over 120 accessory proteins. These proteins are the enzymatic machinery for degradation and need to be continuously replenished in the lysosomes (*154*). Newly

synthesized acid hydrolases undergo specific modifications and follow a specific trafficking pathway in order for them to reach their destination in the lysosome. These enzymes are synthesized in the endoplasmic reticulum and undergo co-translational glycosylation on specific asparagine residues (*N*-linkages) (*46*). As they continue through the ER-Golgi biosynthesis pathway, their *N*-linked oligosaccharides are processed in two steps to produce the terminal mannose 6-phosphate structure. In the first step, *N*-acetylglucosamine-1-phosphotransferase transfers α-*N*-acetylglucosamine 1-phosphate from UDP-*N*-acetylglucosamine to the 6th carbon of terminal mannose residues on biantennary high-mannose structures, forming an intermediate of M6P-OGlcNAc-acid hydrolase (*46, 155, 156*). Then in the TGN, the uncovering enzyme (*N*-acetyl-glucosamine 1-phosphodiester-α-*N*-acetylglucosaminidase removes a GlcNAc to expose a M6P moiety (*157, 158*). M6P signals on the acid hydrolases are recognized by the P-type lectins (M6P/IGF2R and CD-MPR) in the TGN and then sorted to the early endosome (*46, 158, 159*). Additionally, if these lysosomal enzymes are mis-sorted and trafficked to the plasma membrane where they are exocytosed, they can be recaptured by the M6P/IGF2R (CD-MPR is unable to bind ligands at slightly alkaline pH) on the cell surface and brought back to the early endosome. At either case, the cytosolic tails of the MPRs interact with trafficking proteins and mediate the transport of MPR-containing vesicles (*46, 159-161*). Upon arrival at the early endosome, the ligands remain bound to the MPRs until the acidic pH of <6 is reached in the late endosome, where the MPRs release their cargo. The MPRs then undergo recycling via retrograde transport back to the TGN to be used for another round of trafficking newly synthesized M6P-capped enzymes, while the acid hydrolases continue from the late endosome to the lysosome (Figure 1.7) (*46, 162*).
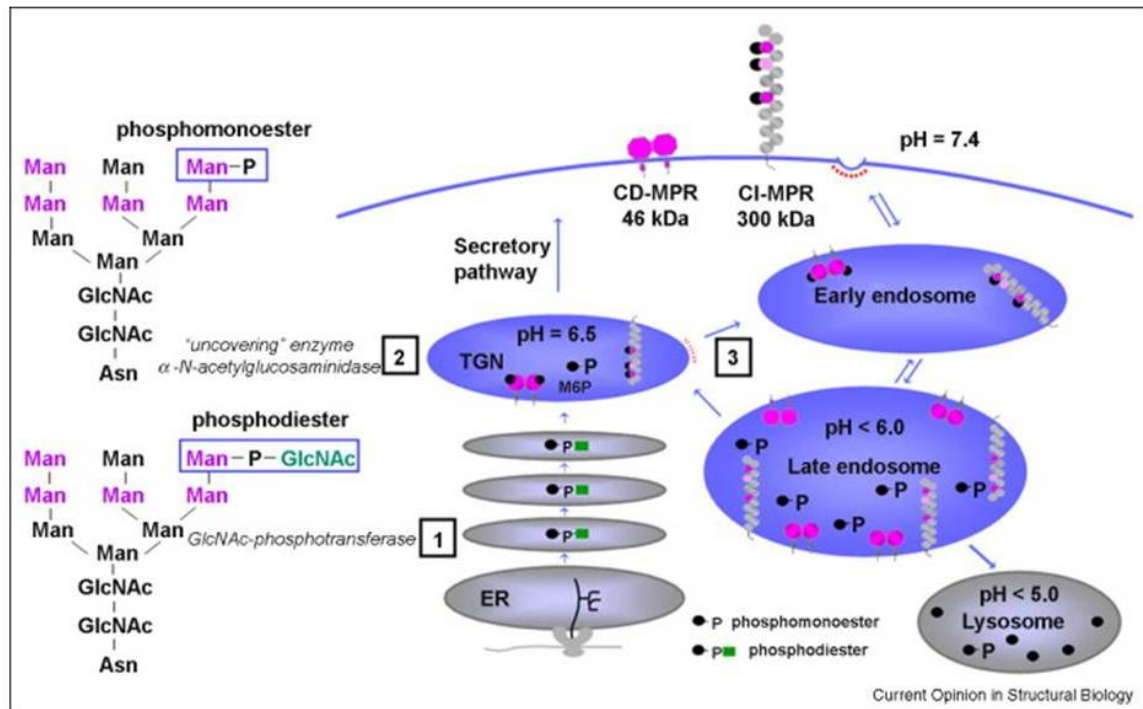
Figure 1.7: Localization and trafficking of the MPRs. M6P/IGF2R and CD-MPR are found mostly within the intracellular compartments, trafficking newly synthesized acid hydrolases from the TGN to the early endosome. The M6P/IGF2R also binds extracellular ligands and internalizes them to the early endosome. Upon maturation of the endosome, ligands dissociate from the MPRs and arrive at the lysosome while the receptors are recycled through signals in the cytoplasmic tails. The MPRs recognize the M6P signal on oligosaccharide chains, which bind to the extracellular domains of the receptors. This figure was originially published in *Current Opinion in Structural Biology* and has been reprinted with permission of the publisher. Kim, J.J.P., Olson, L.J., Dahms, N.M. (2009) Carbohydrate recoginition by the mannose 6-phosphate receptors, *Current Opinion in Structural Biology. 19(5):* 534-542. Elesvier. Liscense number: 3840360859638.

It is interesting to note that when the M6P/IGF2R has mutations in its EC domain that affect M6P-based binding, more lysosomal enzymes are mis-sorted and secreted at the plasma membrane, contributing to cellular invasiveness (*59*), and can result in more immature lysosomes that do not contain enough acid hydrolases. Furthermore, there are over 40 diseases related to genetic defects in synthesis, sorting, or targeting of lysosomal enzymes, (*163*), resulting in the storage diseases known as mucolipidoses or mucopolysaccharidoses. This is why proper lysosomal biogenesis is biomedically important. Moreover, diseases such as cancer progression, Alzheimer's disease, rheumatoid arthritis and atherosclerosis have been associated with defects in the lysosomal system (*164-166*).

D.3. The IGF axis

The IGF axis is quite complex, comprising multiple cellular transmembrane receptors, binding proteins and growth factor peptides that regulate diverse biological processes including cell proliferation and survival, death, differentiation, development and malignancy (*113, 167-169*). The classical IGF axis is composed of two polypeptide growth factors (IGF-I and –II), three IGF receptors (IGF1R, insulin receptor isoform A (IR-A), and M6P/IGF2R), and six IGF binding proteins (IGFBP) (*170, 171*). The IGF axis can also be expanded to include regulatory factors such as proteases that cleave the IGFBPs and regulate the bioavailability of the IGFs (*172*) (Figure 1.8). Insulin can also be considered a distant relative of this axis as binding of insulin to IR-A or IGF1R/IR-A hybrid receptors can result in mitogenic outcomes as opposed to metabolic outcomes through IR-B (*173*). Each member of the IGF axis plays a unique role in maintaining cellular homeostasis. The M6P/IGF2R, which transports M6P-glycosylated proteins and

non-glycosylated proteins to the lysosome, regulates pericellular levels of IGF-II by mediating its degradation in the lysosome (*153*). Changes in the M6P/IGF2R regulatory activity have been associated with the onset of diseases, such as cancer, diabetes, and neurodegeneration (*174-177*).

D.3.a. The IGFs

IGF-I and –II are small polypeptide growth factors that act by endocrine, paracrine, or autocrine mechanisms to exert mitogenic and anti-apoptotic effects on many types of normal and tumor cells (*167, 168, 170, 178*). IGF-I and –II (approximately 7.5-7.6 kDa) are 49% and 47%, respectively, identical in sequence and structure to proinsulin, and the two human IGFs share 76% identity (*179, 180*). IGFs are expressed in numerous organs and tissues and exhibit regulation of expression throughout developmental stages. Transcription of *IGF1* is predominantly regulated by growth hormone (GH) and synthesized and secreted by the liver (*168, 181, 182*). *IGF1* expression is relatively low prenatally and increases postnatally until maximal expression is reached around puberty development and early adulthood. The levels of circulating IGF-I remain fairly constant throughout most of adult life but steadily decline with age (*183*). IGF-I regulates growth of the muscles, tendons, and bones and is the primary IGF during adult life (*181, 184*). IGF-II has a different expression pattern from IGF-I; it is mostly involved in growth of tissues in the fetal development stages and then declines postnatally in many mammals (*185*). *IGF2* expression exhibits regulation by complex maternal imprinting, in which the gene shares an enhancer region with the *H19* locus (*186*). Differential methylation allows maternal expression of H19 but only paternal expression of *IGF2* (*187*). Furthermore, the methylation pattern of *IGF2* changes,
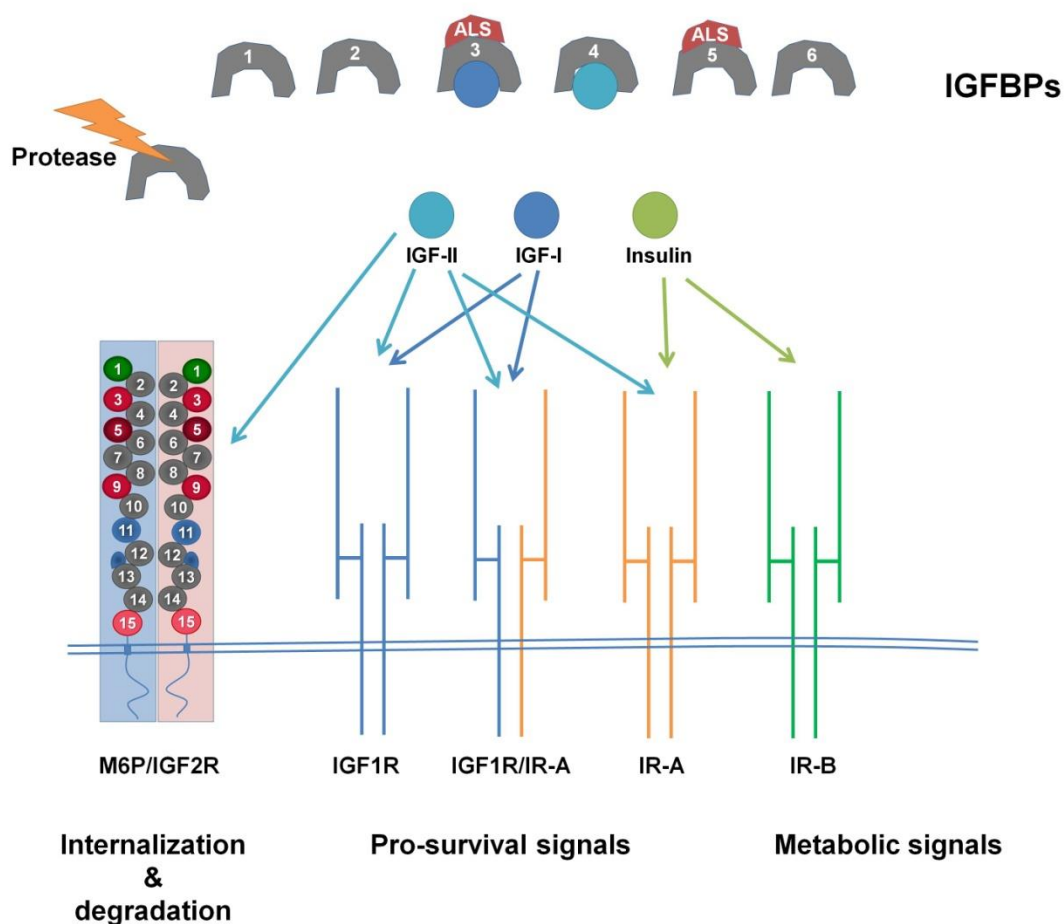
Figure 1.8: The IGF axis is complex with multiple different levels of regulation. The IGF receptors are composed of M6P/IGF2R (clearance receptor that clears excess IGF-II signal that does not have a tyrosine kinase domain), and the receptor tyrosine kinases: IGF1R, IGF1R/IR-A, IR-A, and IR-B. IR-B is mostly involved in metabolic signaling through insulin. The ligands in this pathway are IGF-II, IGF-I, and insulin that are homologous in structure and sequence and bind with varying affinities for their receptors. IGFBPs regulate the stability and bioavailability of the IGFs by binding and sequestering them from the receptors. However, proteases may cleave the IGFBPs, which release the IGFs. IGFBP-3 and IGFBP-5 have an acid labile subunit (ALS) which further extends the half-life of the IGFBP and IGF complex.

allowing for transcription from a different promoter in adult tissues (*53, 188, 189*). However, dysregulation of the epigenetics of the *IGF2* gene can lead to disease progression (*53*) as discussed later in this chapter.

D.3.b. The IGFBPs

There are six IGFBPs (labeled IGFBP-1 through -6) that regulate the bioavailability of IGF-I and IGF-II. IGF-I and –II in the circulation are unstable and subjected to degradation; thus, the IGFBPs modulate their bioavailability as well as extend their half-lives. IGF-I (20 nmol/L) and IGF-II (90 nmol/L) circulate at substantially higher concentrations than insulin (0.5 nmol/L) in adult human blood, but most of the IGFs are bound to IGFBPs (*169*). The IGFBPs have differing affinities for IGF-I vs IGF-II yet negligible affinity for insulin (*168, 169, 181*). The IGFBPs are homologous in structure and sequence but they each have unique post-translational modifications, susceptibility to proteolysis, and preferences for the IGFs (*190*). IGFBPs limit IGF interactions with the cell-surface receptors IGF1R and IGF1R/IR-A to regulate the effects of these ligands. Along with the IGFBPs facilitating the transport of the IGFs in the circulation and increasing their half-lives, these binding proteins allow cell type- and tissue-specific localization of the IGFs (*168*). There has been speculation as to whether increased expression of IGFBP-2 and -5 increases cancer risk due to concentrating the IGF ligands near the tumor microenvironment or if IGFBPs have activity on their own that is not dependent on IGF ligands (*169*); however, this aspect of IGFBPs is not the focus of this work and will focus solely on a brief summary of their roles in regulating IGF-II.

IGFBPs are expressed in many tissues at various times during development, in the adult, and in disease, allowing the change in bioavailability of the IGFs. For example, there is a shift in the IGFBP expression profile of developing mice that occurs postnatally and continues to change until the mice are considered adolescent (data submitted). The most predominant IGFBP that appears to serve the greatest role in IGF-II regulation is IGFBP-3 in complex with an acid-labile subunit (ALS) that greatly extends the half-life (16 hours or longer) of the growth factor compared to other binary IGFBP complexes (20-30 minutes) or free ligand (just a few minutes) (*190*). Additionally, there are specific proteases that cleave the IGFBPs, lowering the affinity of these binding proteins for the IGFs and subsequently releasing the IGFs into the extracellular environment where they are free to bind the receptors of this axis (*190*).

There is also a group of lower-affinity IGF binding proteins that are confusingly referred to as being part of the IGFBP superfamily but are classified as IGFBP-related proteins, and the consensus in the field is to exclude them from the IGFBP family (*190-192*).

D.3.c. The IGF Receptors

Multiple cell-surface receptors are included in the IGF axis, each with a different biological response to IGF binding. IGF1R, IR-A, and hybrids of these two receptors are responsible for the biological activity of the IGFs, while the M6P/IGF2R functions as a clearance receptor for IGF-II. The IGF1R is fairly specific for IGF-I, having a dissociation constant for IGF-I of 0.2 to 1 nM. The receptor's affinity for IGF-I is 100- to 1000-fold higher than for insulin and 2- to 15-fold higher than for IGF-II (*111, 173*). The IGF1R is composed of four polypeptide chains held together by disulfide bonds: two α-subunits on

the extracellular surface that bind ligands and two transmembrane β-subunits that have intrinsic tyrosine kinase activity (*193*). Following synthesis, processing and protein folding, the IGF1R is transported to the plasma membrane as a heterotetramer, where ligand binding in the EC domain causes a conformational change that results in β-subunit transphosphorylation. The phosphorylated and activated IGF1R recruits and phosphorylates adaptor proteins in the insulin receptor substrate (IRS) family or src homology domain-containing (SHC) proteins, which serve as docking sites for effector molecules. This leads to the activation of several downstream pathways, such as the classical phosphatidylinositol 3-kinase (PI3K)/protein kinase B (Akt) or extracellular signal-regulated kinase 1 and 2/mitogen-activated protein kinase (ERK/MAPK) pathways (*194*). One such outcome is a decrease in apoptosis activation. There must be a balance between cell division and programmed cell death in order to maintain proper development and maintenance of tissues in order to keep pathological conditions at bay, such as disruptions in embryogenesis, neurodegenerative diseases, and cancer development and progression. Apoptosis, also known as programmed cell death, is necessary to protect the health of an organism. In cancer, decreased apoptosis can lead to faster tumor growth resulting in a greater tumor burden and metastasis. In the classical caspase-dependent apoptosis, there are two pathways that activate cell death: intrinsic and extrinsic. In short, the extrinsic pathway is activated when ligands bind to the death receptors on the cell surface that leads to the activation of the executioner caspases (namely caspase 3). The intrinsic pathway results from growth factor starvation, DNA damage due to radiation, toxins, and free radicals, or ER stress that is sensed by the Bcl-2 family proteins. These sensors ultimately result in the release of cytochrome c from the mitochondria and activation of the executioner caspase-3 (*195*). Endonuclease activation that leads to degradation of chromosomal DNA, protease activation that degrades the nuclear and cytoskeletal proteins leading to cytoskeletal

reorganization, and extensive morphological changes with nuclear fragmentation and the formation of apoptotic bodies are all characteristics of apoptosis (*196*). Interestingly, the gene expression profile following IGF1R activation can be different depending on which ligand binds to and activates the receptor (*197*).

In addition to the IGF1R, the insulin receptor (IR) has two isoforms that may play a role in the IGF axis: a more mitogenic isoform (isoform A) and the classical metabolic isoform (isoform B). The IR has a high degree of homology with the IGF1R, with 50-60% overall identity and 84% identity in the intracellular kinase domain (*198*). Alternative splicing of the IR gene product leads to the two aforementioned isoforms, where IR-A lacks 12 amino acid residues correlating to exclusion of exon 11. IR-B does not bind any ligands except insulin with high affinity, while the IR-A is a bit more promiscuous and can bind insulin and IGF-II with high affinity, leading to different outcomes by ultimately activating the expression of different genes (*173, 199*). IR-A is thought to be a more mitogenic receptor and has been expressed in many tumor cells (*173, 200, 201*), while IR-B has mainly metabolic functions (*202*). Interestingly, IGF-I does not bind with appreciable affinity to IR-A. Due to the high degree of homology between the IGF1R and IR, these two hemireceptors can form a heterotetrameric hybrid (IGF1R/IR) using one α- and one β-subunit from each hemi-receptor. IGF-I can bind either IGF1R/IR-B or IGF1R/IR-A, but IGF-II can only bind the latter hybrid, while insulin does not bind to either hybrid (*203*), making these receptors complex with a greater repertoire of combinatory outcomes. It is interesting to note that IGF-II responsiveness changes with the receptor tyrosine kinase expression. IR-A expression is increased during embryogenesis (*200, 204*), and the IR-A:IR-B ratio is increased during de-differentiation. Taken together, these receptors have overlapping functions, yet they

differ in physiological outcomes, tissue distribution, and relative cellular localization (*205*).

D.4.   Role of the M6P/IGF2R within the IGF axis (cell surface actions)

Numerous studies have sought to elucidate the function of the M6P/IGF2R at the cell surface. As previously mentioned, the majority of the receptor is found within the cell, trafficking newly synthesized lysosomal enzymes to the lysosome and recycling back to the TGN. However, the M6P/IGF2R can bind both glycosylated (M6P-bearing) and non-glycosylated proteins at the cell surface, where they are endocytosed. Unlike the IGF1R and IGF1R/IR-A hybrids, the M6P/IGF2R lacks intrinsic tyrosine kinase activity, and acts as a clearance receptor for an increasing repertoire of ligands. The M6P/IGF2R functions as an endocytic recapture mechanism of M6P-bearing lysosomal enzymes that escaped proper sorting at the TGN (*46, 90, 206, 207*). In addition to the acid hydrolases, the M6P/IGF2R also binds IGF-II at the cell surface, causing it to be internalized and degraded in the lysosome which is one way of regulating IGF-II in the extracellular space. Furthermore, the M6P/IGF2R can bind additional ligands that include proliferin (*208*), prorenin (*209*), thyroglobulin (*210*), and the latent form of TGF-β (*46, 133, 211-216*). Binding prorenin by the M6P/IGF2R leads to prorenin cleavage to renin, but unlike the canonical activation of the angiotensin-renin pathway, prorenin is internalized and degraded; thus, the M6P/IGF2R serves as a clearance receptor for this protein (*217*). Also upon binding to the M6P/IGF2R, TGF-β can become cleaved by hydrolysis from the latency-associated form to mature, active TGF-β (*46, 133, 211-216*). Plasminogen and urokinase-type plasminogen activator receptor (uPAR) bind to the M6P/IGF2R, most likely in domain 1; where these proteins complex with M6P/IGF2R.

Plasminogen is converted to plasmin, which in turn can proteolytically activate latent TGF-β bound to the M6P/IGF2R (*46, 132, 133*). Proliferin binds the M6P/IGF2R in a M6P-dependent manner and is important for proliferin-induced endothelial cell migration and neovascularization in the developing embryo (*208, 218*). There is a growing list of ligands that are recognized by and bind the M6P/IGF2R that play many different biological roles (*46*).

It has been observed in adipocytes and hepatoma cells that insulin stimulation shifts the receptor distribution from intracellular trafficking to the cell membrane (*219*). Fibroblasts treated with IGFs or insulin exhibited this same event of receptor relocalization (*220, 221*). It is thought that the M6P/IGF2R trafficks to the plasma membrane in order to compensate for increases in IGF-II from the cell milieu to dampen fluctuations in growth factor availability and maintain a steady-state cellular rate of growth. It is important to note that IGF-II binds to the M6P/IGF2R with high affinity (K_D=0.017-0.7 nM) (*168*), which is about a 500-fold higher affinity than for IGF-I (K_D=0.4 µM), and insulin does not bind to this receptor (*93*).

D.4.a. Binding of multivalent M6P-based ligands: Effects on IGF-II endocytosis

The M6P/IGF2R in rat adipocytes is constitutively internalized from the plasma membrane ($t_{1/2}$ of 3.5 min) and recycled regardless if ligand was bound or not (*151, 153*). Moreover, receptor internalization mediates IGF-II degradation, which was enhanced following insulin stimulation in adipocytes that redistributed the M6P/IGF2R to the plasma membrane and allowed more available receptor to take up IGF-II for degradation (*153*). Studies in the early 1990's showed that several cell-surface receptors can undergo rapid internalization and recycling, which is mediated by a unique tyrosine-

based sorting motif within the cytoplasmic tail (*222-226*). This same motif was discovered in the M6P/IGF2R and determined to be necessary for proper internalization (*227*). Utilizing a panel of cell lines stably expressing wild-type or point mutants of the receptor to track the internalization of radiolabeled hGUS, it was determined that a functional tyrosine-based motif was critical for hGUS internalization by the M6P/IGF2R ($t_{1/2}$= 45 sec). A functional internalization signal required an aromatic residue (tyrosine) followed by any two amino acids and then a large, hydrophobic residue (YXXφ). The internalization of the M6P/IGF2R was uninhibited when the YSKV sequence (residues 26 to 29 of the cytoplasmic tail) was either translocated or substituted with another tyrosine-based internalization motif from other cell-surface receptors that undergo rapid internalization (*227*).

Studies on the stoichiometry of multidendate M6P-ligands, monodentate M6P-based ligands, and non-glycosylated proteins determined that these ligands bind with different ratios to the M6P/IGF2R (*93*). The multidentate ligands (β-galactosidase and high-mannose oligosaccharide bearing two or more M6P groups) and non-glycosylated IGF-II bound to the M6P/IGF2R with a 1:1 molar ratio (ligand:receptor), while the monodentate ligands (M6P and pentamannose phosphate) bound to the receptor with a 2:1 ratio. This was suggestive that the M6P/IGF2R has two M6P-binding sites, in which monovalent binding occurs to each site with monodentate ligands. Moreover, there was 100- to 1000-fold higher affinity of the receptor for multidentate M6P-based ligands than the monodentate M6P-based ligands, indicative of multivalent binding by the multidentate ligands that comprises one M6P molecule binding to one M6P-binding site on two separate M6P/IGF2R monomers simultaneously (*93, 94*).

York *et al.* observed that the natural-occurring, M6P-based lysosomal enzyme (hGUS) stimulated an increased rate of M6P/IGF2R internalization, suggesting that bi- or

multivalent interaction of a M6P-based ligand (hGUS) was cross-bridging the M6P/IGF2R into a dimeric structure that increases the receptor's internalization rate (*131*). Furthermore, the bi- or multivalent binding of hGUS was able to accelerate the internalization of IGF-II ($t_{1/2}$ of 45 sec vs 3 min, respectively). Additionally, the monovalent ligand (M6P) was unable to accelerate the internalization of IGF-II, indicating that bivalent interactions may allow the M6P/IGF2R to suppress the proliferative actions of IGF-II. This was the first study to indicate that bivalent M6P-based ligands can bind to the M6P/IGF2R and increase internalization of the receptor and receptor-bound ligands, such as IGF-II, by 3-4-fold (*131*). Since monovalent ligands (M6P and IGF-II) were unable to produce the same response, it is believed that intermolecular, and not intramolecular, cross-bridging of the M6P/IGF2R is important for receptor dimerization and increased uptake. This hypothesis was supported by the finding that hGUS stimulated the enhanced internalization rate of the M6P/IGF2R in a cell line that was engineered to stably express a mutant form of the receptor that had only one functional M6P-binding site per monomer (*131*).

These conclusions were made biologically relevant when subsequent studies tested these principles with a natural ligand. Di Bacco *et al.* demonstrated that overexpression of the M6P-glycoprotein cellular repressor of E1A-stimulated genes (CREG) could induce G1 cell cycle arrest and inhibit the anchorage-independent growth of a teratocarcinoma cell line, NTERA-2, in a M6P/IGF2R-dependent manner (*228*). Furthermore, knockdown of CREG in NIH3T3 fibroblasts promoted cell proliferation by increasing IGF-II accumulation in the conditioned medium. These experiments indirectly supported the idea that CREG was affecting pericellular IGF-II bioavailability, but they did not prove that the M6P/IGF2R was involved. Subsequently, it was shown that the increased proliferation could be reversed when recombinant human CREG or an αIGF-

II-neutralizing antibody were added back to the cultured medium (*229*). Migration of human vascular smooth muscle cells (SMC) is inhibited by down-regulation of activity of matrix metalloproteinase-9 (MMP-9) as well as enhanced IGF-II endocytosis mediated by CREG binding to the M6P/IGF2R (*229*). When CREG was knocked down in these cells, the increased IGF-II secretion activated the PI3K pathway, most likely via activation of IGF1R. The direct interaction of CREG with M6P/IGF2R was confirmed by immunoprecipitation and immunofluorescence studies (*229*). CREG binds directly to the receptor between domains 7-10 of the M6P/IGF2R in a glycosylation-dependent manner, as multiglycosylated CREG has preferential binding over monoglycosylated CREG, and both are displaceable by M6P, suggesting that CREG is binding to domain 9 of the receptor. Deglycosylated CREG showed minimal binding to domains 11-13, indicating that there is some glycosylation-independent binding of CREG for the receptor (*228-230*), which calls into question how IGF-II is simultaneously able to bind to repeat 11 of the receptor. Nonetheless, when a M6P/IGF2R-neutralizing antibody or recombinant soluble M6P/IGF2R was added to smooth muscle cells in culture, the CREG-induced increase in extracellular IGF-II accumulation was inhibited, suggesting that M6P/IGF2R was responsible for enhanced IGF-II internalization in the presence of CREG overexpression (*231*). Taken together, these studies further supported the role of multivalent ligands in cross-bridging the M6P/IGF2R dimeric structure. Apparently, this leads to internalization of IGF-II and decreased cell proliferation in some cells. If this is a universal property of the receptor in many types of cells, particularly tumor cells, it may be further exploited to treat IGF-II-dependent cancers.

E.   IGF-II in cancer

IGF-II has contributing roles in development and tumor progression signaling through the IGF1R or IGF1R/IR-A in an autocrine or paracrine fashion (*232*). Upon binding to the EC binding domain, activation of these receptors causes cross-phosphorylation of the receptor within the tyrosine kinase domain of the carboxyl-terminal region. This then leads to the activation of signaling cascades, including PI3K/Akt and MAPK/ERK pathways that ultimately promote cell survival and proliferation (*233*). Under normal conditions, IGF-II is intricately regulated to control IGF-II signaling during embryogenesis, development, and in adult tissues (*234, 235*). IGF-II is regulated on multiple levels including transcriptional regulation through methylation, mRNA stability, and IGFBPs. However, dysregulation of IGF-II-mediated signaling has been implicated in many cancers, such as liver, breast, prostate, lung, and colorectal cancer as well as neuroblastoma and Wilms' tumor (*236*).

Transcription of *IGF2* is regulated by maternal imprinting of the differentially methylated region (DMR), restricting expression to the paternal allele (*53*). *IGF2* has four promoters (P1-P4) that allow for tissue-specific transcription. During embryonal development, promoters P2-P4 are responsible for transcriptional start of *IGF2*, which is monoallelic expression. However, the adult liver expression of *IGF2* is from P1 and is biallelically expressed, which allows for a relatively high IGF-II expression in the adult circulation in humans, compared with rodents (*53, 188, 237*). Additionally, loss of imprinting (LOI) of the *IGF2* gene normally occurs by a decrease in binding of the enhancer-blocking element CCCTC-binding factor (CTCF) to the control region, but does not necessarily indicate disease (*234, 238*). One study determined that healthy Chinese babies had 20% of LOI in cord blood cells (*239*), while a smaller percentage was observed in neonates in the USA (*234, 240*).

Conversely, biallelic expression has been extensively observed in many types of cancers. One such cancer type, epithelial ovarian cancer, has hypomethylation of the *IGF2* DMR compared to normal lymphocyte *IGF2* gene (*234, 241*). Furthermore, hypermethylation of the CTCF binding sites further increases IGF-II expression. Clinical samples of ovarian cancer revealed changes in the methylation of the fetal promoters, where patients with methylated P2 and unmethylated P3 had higher IGF-II expression and significantly worse prognosis compared to the patients with unmethylated P2 and methylated P3 (*234, 242*). Patients with the inherited disorder Beckwith-Wiedemann syndrome exhibit site-specific mutations that relax the *IGF2* imprinting, which leads to biallelic expression of *IGF2*. The outcome is somatic overgrowth that is associated with increased risk of childhood cancers (*243, 244*). Wilms' tumor, a childhood cancer of the kidney, was the first tumor to show aberrant *IGF2* imprinting (*245*). Since then, several adult cancers, including liver cancer, have been found to have LOI at the *IGF2* locus (*246, 247*). Moreover, it has also been observed that epigenetic changes of the *IGF2* gene have been linked to IGF-II overexpression and drug resistance in cancer cells (*234, 248*).

In addition to LOI of the *IGF2 (249)* gene, whole gene amplifications also occur in some cancers. There was a focal amplification of *IGF2* in 7% of tumors studied from The Cancer Genome Atlas (TGCA) study of colorectal cancer, leading to increased IGF-II expression in these tumors. Furthermore, the miRNA transcript *miR-483* was also increased, which localizes to an *IGF2* intron (*234*). Overexpression of *miR-483* in a Ewing sarcoma cell line did not increase the stability of the *IGF2* mRNA, but rather increased the number of transcripts (*234, 250*). Additional miRNAs may regulate the over- or under-expression of *IGF2* mRNA (*234*) indicating that expression of IGF-II is intricately regulated in normal tissues, and that dysregulation on different levels may

lead to cancer progression. *IGF2* mRNA binding protein (IGF2BP) is a family of RNA binding proteins (IGF2BP1-3) that bind and stabilize the expression of *IGF2* transcripts (among others) during fetal development. However, IGF2BP1 and -3 are repressed in adult tissues but can be reactivated in cancer (*234, 251*), and cause dysregulation of *IGF2* (*252, 253*). The regulation of *IGF2* mRNA adds another layer of complexity to this system that can have detrimental consequences during tumor progression.

In addition to LOI, gene amplifications, and the role of miRNAs, other factors can lead to the overexpression of IGF-II, including transcription factors. Sonic hedgehog (Shh) transcriptionally activates *Igf2* in mice by activating Gli, which is a transcription factor that induces a number of target genes (*254*). Mouse mesenchymal cells treated with Shh or transfected with Gli1 have increased *Igf2* mRNA expression (*255*). Inactivating mutations in the tumor suppressor gene *patched* result in constitutive activation of Gli with the end result of IGF-II elevation in some rhabdomyosarcomas and medulloblastomas (*256*). An embryonic stem cell-specific transcription factor, ZFP57, binds to the imprinting control region of *IGF2*, and overexpression of this transcription factor leads to anchorage-independent growth of a fibrosarcoma cell line, 3T3. Additionally, this transcription factor is increased in tumor samples from pancreas, esophagus and breast relative to their normal tissues, leading to overexpression of IGF-II (*234, 257*). E2F3, another transcription factor, regulates *IGF2* expression during development, specifically binding to P3 and regulating transcription. E2F3 is downregulated postnatally, which is vital for decreased *IGF2* expression. However, this transcription factor is overexpressed in some cancers, correlating to an increase in IGF-II in samples of human bladder and prostate cancers but not in Wilms' tumor, which indicates the complexity of IGF-II expression in malignancies (*234, 258*). Other transcription factors interplay to regulate the expression of *IGF2*, which can be

dysregulated in tumor progression (*234*), indicating multiple mechanisms of IGF-II overexpression.

It has been suggested that IGF-II influences tumor growth through an increased autocrine or paracrine mechanism (*259-261*), as circulating IGF-II is increased ~40% in patients with hepatocellular carcinoma (HCC) (*249, 262*). Many laboratories have studied IGF-II in the circulation, including in malignancies of the prostate, breast, colon, and liver (*263-266*). The IGFBPs regulate bioavailability of IGF-II, and limit the interaction of the growth factor with its receptors; thus, one would think that increased IGFBP expression would decrease cancer incidence. Incidentally, it was suggested that IGFBPs may contribute to cancer progression in preliminary studies of prostate cancer (*267, 268*). Additionally, bioavailable IGF-II contributes to IGF1R activation, as small-molecule inhibitors in murine xenograft transplants of HCC significantly reduced IGF-II-dependent activation of the IGF1R receptor tyrosine kinase (*264*). Furthermore, blocking the kinase activity of the IGF1R abolished the formation of aberrant crypt foci in an *Igf2* LOI murine model, which restored the colonic crypt cells to wild-type proliferation rates, but did not affect the wild-type mice. The authors suggested that the colonic crypt cells in the LOI mice were addicted to IGF-II and that this growth factor was essential for cellular proliferation, proposing that the dynamics of signal transduction may cause epigenetic changes in cancer progression (*265, 269*).

In toto, these studies indicate that the regulation of IGF-II is complex and multi-leveled, with multiple potential steps where dysregulation can lead to tumorigenesis. It is important to disrupt the signaling caused by IGF-II in order to decrease tumor progression in cancers that express IGF-II. To date, the majority of therapies targeting IGF-II have focused on targeting the receptor tyrosine kinases, which can have increased off-target effects and toxicity (*270*). We have developed a novel therapeutic

agent to restrict the bioavailability of IGF-II using M6P/IGF2R-mediated internalization and degradation of IGF-II, thereby limiting this mitogenic growth hormone to the IGF1R.

F.   M6P/IGF2R's role as a tumor suppressor: regulating growth and motility

The M6P/IGF2R regulates lysosomal enzyme targeting, modulates circulating levels of glycosylated leukemia inhibitory factor, granzyme B (which regulates cytotoxic T cell-induced apoptosis), facilitates activation of the growth inhibitor TGF-β, and targets IGF-II for degradation. All of these functions are important for proper cell maintenance, but aberrant regulation and disruption in any of these processes has been associated with cancer progression, supporting the notion that M6P/IGF2R acts as a tumor suppressor (*46, 271*). When overexpressed, the M6P/IGF2R suppresses growth both *in vitro* and *in vivo*, and loss of function is implicated in tumorigenesis (*46, 272-276*). Loss of heterozygosity at the *IGF2R* locus has been reported in a number of human tumors, including those of the liver (*277-280*), breast (*281-283*), lung (*284*), and ovary (*283*). Additionally, mutations in the remaining *IGF2R* allele have also been reported in cancers (*278, 280, 281, 284, 285*). Furthermore, transgenic mice engineered to express soluble M6P/IGF2R (deletion of the transmembrane domain) displayed reduced organ size. Crossing these mice with mice overexpressing *Igf2* resulted in offspring with reduced organomegaly that is observed in *Igf2* overexpressing mice, indicating that the soluble M6P/IGF2R was able to stunt the mitogenic effects of IGF-II (*273*). Furthermore, M6P/IGF2R mutation or downregulation in mice caused tissue over-growth and perinatal lethality. Knockout of *Igf2* revealed viable offspring. The double mutant knockout (*Igf2r* and *Igf2*) also produced viable mice yet these mice were smaller than wild-type mice (*201*). A decrease in cell growth was also seen in JEG-3 choriocarcinoma cells treated

with *M6P/IGF2R* cDNA *in vitro* and decreased tumor growth in nude mice, that was characterized by increased latent TGF-β secretion and activation (*274*). Furthermore, there was abnormal lysosomal enzyme trafficking in *M6p/Igf2r*-null mouse mammary tumor cell line (66c14), as expected without one of two MPRs, which was rescued upon stable transfection of the receptor back into these cells. With the addition of the M6P/IGF2R into these cells, there was no effect on cell proliferation or invasiveness *in vitro*; however, sub-cutaneous injections of these receptor-expressing mammary tumor cells into BALB/c mice had inhibited tumor formation, with a 3-fold decrease in proliferation and no observable apoptosis (*286*).

To date, only one single point mutation (P2379T) has been found in the cytoplasmic tail of the M6P/IGF2R, yet there have been several identified in the EC domain: in the M6P-binding domain 9 (C1262S, G1296R), domain 10 (Q1445H, G1449V, G1464E), and IGF-II-binding domain 11 (G1564R, I1572T, A1618T, G1619R) (*46*). Additionally, point mutations D1317G in domain 9 and Y2024Stop in domain 14 both result in early stop codons and truncations of the M6P/IGF2R (*287*). The majority of these mutations and truncations have been characterized with significant alterations in M6P and/or IGF-II binding and have been associated with cancer. This supports the hypothesis that the M6P/IGF2R functions as a tumor suppressor, and loss of function to the receptor has tumor-promoting properties.

G. Current therapeutic strategies targeting the IGF axis

G.1. Therapies against the IGF axis in clinical trials

Targeting the IGF axis in cancer has proven to be difficult as this system is quite complex. There are three typical therapy classifications when targeting the IGF axis:

monoclonal antibodies (mAbs) against the IGF1R and IGF1R/IR-A; mAbs against IGF ligands; and IGF1R tyrosine kinase inhibitors (TKI). All of these therapies differ in their effectiveness, mechanisms of action, and targets. Examples of each type have entered different stages of clinical trials.

There have been at least eight humanized anti-IGF1R mAbs that have entered clinical trials, but several have been discontinued, mostly due to side effects and lack of efficacy. Typically, these mAbs are highly specific for IGF1R and do not cross-react with IR, and they usually block the ligand-binding site on the receptor and cause internalization and degradation of the receptor. Anti-IGF1R mAbs are typically well tolerated as a monotherapy, but hyperglycemia is a common side effect. Early clinical trials indicate that these therapies have target effects that include down-regulation of the IGF1R, increases in human growth hormone (GH) and IGF-I, and can increase circulating insulin levels (*270, 288*). The mAbs in Ewing sarcoma treated in Phase 1 trials induced complete or partial responses, which led to a series of phase 2 and 3 trials. The most common examples of mAbs against the IGF1R are figitumumab, cixutumumab, and ganitumab, which are all used as monotherapies or in combination therapies with or without chemotherapy. Even though initial studies showed promise, these mAb therapies still had low success rates, with the largest study having a complete or partial response rate of only 10% and a median overall survival of 7.6 months (*270*). These therapies have also been used in phase 1 and 2 trials in other cancers, such as those of the liver, thymus, prostate, liver, thymus, adrenal cortex and lung. Again, all of these studies had varying responses to the treatment but with marginal improvements (*270, 289*). This class of drug target often leads to insulin resistance, hyperinsulinemia, and hyperglycemia. The mechanism of the adverse side effects is believed to occur as a result of increased GH secretion and some IGFBPs due

to a direct blockage of IGF1R in the pituitary, disrupting the feedback regulation (*288*). The various studies in these cancer cell models using IGF1R-targeted mAb therapy suggest that inhibition of the receptor is beneficial for a small subset of patients.

TKI against IGF1R have a range of specificities for the receptor, as many can inhibit other receptor tyrosine kinases; linsitinib and BVP 51004 are the most specific for the IGF1R (*270*). Typically, the mechanism of action of these inhibitors is by competition for the ATP-binding site within the kinase domain of these receptors (*288*). There is a high degree of homology between the IGF1R and IR isoforms, so targeting the IGF1R frequently interferes with IR signaling. The cross-reactivity is usually not detrimental in tumors that have over-activation of IGF1R, IR-A, or IGF1R/IR-A. However, interference with IR-B, the receptor responsible for regulating metabolic processes, can cause significant side effects, such as hyperglycemia and can contribute to the metabolic syndrome (*270*). Unfortunately, many of these studies resulted in little to no improvement of the treatment *versus* the control.

There are fewer studies on the IGF-neutralizing mAbs. These mAbs function by binding the IGFs and preventing their subsequent binding and activation of the receptor, and are able to inhibit without affecting the glucose metabolism (*288*). MEDI-573 is the first antibody that neutralized both IGF-I and –II in clinical trials (*290*) and does have promise, but further clinical trials are needed.

G.2. Current therapeutics targeting IGF-II and M6P/IGF2R in cancer

Many groups have proposed different approaches to target the M6P/IGF2R as a treatment option in cancer. Work done by Poelstra's group utilized the M6P/IGF2R as a conduit for uptake of ligand-carrier toxins. In this model, human serum albumin was

modified with M6P groups and conjugated to cytotoxic drugs such as doxorubicin. The ligand-carrier toxin was then internalized by binding the M6P-binding sites of the M6P/IGF2R in hepatic stellate cells, and the toxin was subsequently released to the cell interior via the lysosome. The internalization of this ligand-carrier toxin was specific for the M6P/IGF2R, as doxorubicin by itself is not internalized nearly as effectively as the ligand-carrier toxin. This drug was internalized in tumors and various organs such as the liver, lungs, spleen, kidney, stomach, and small intestine, but did not internalize in the fat, testis, bladder, thymus, brain, skin, muscle, bone, colon, prostate, heart, or large intestine (*291, 292*).

In addition to using the M6P/IGF2R as a conduit for drugs to enter specific cells, the receptor can be used to limit cellular migration and invasion by improved targeting of lysosomal enzymes. It has been noted that the expression of M6P/IGF2R in receptor-deficient murine squamous cell carcinoma cells had decreased invasion, restoration of dense lysosomes, and reduced anchorage-independent proliferation and tumor growth (*293*). Additionally, a functional IGF-II-binding site is not required for the inhibition of growth and invasion, suggesting that these effects were independent of IGF-II; however, a functional domain 3 was required for these effects (*294*). Additionally, M6P/IGF2R-deficient fetal rat liver cells hyper-secrete lysosomal enzymes such as cathepsins, which degrade the EC matrix, but expression of the receptor restores the functional intracellular transport of lysosomal enzymes to the lysosomes, thereby reducing invasion (*295*).

Another therapeutic approach is to suppress cell growth by sequestering and degrading IGF-II, such as by means of ligand traps. Modified sM6P/IGF2R and IGFBPs have been designed to function as such ligand traps. Soluble M6P/IGF2R administered to an IGF-II-overexpressing colon cancer mouse model rescued the colon cancer

phenotype (*296*). Furthermore, domain 11 of the M6P/IGF2R is the high-affinity IGF-II-binding domain, and a single substitution of Glu1554 to a lysine increases the affinity for IGF-II by 6-fold, and the fusion with the carboxyl-terminal human IgG1 Fc domain increases the affinity for IGF-II and the half-life of the ligand trap to a greater extent (*297*). Proliferation was inhibited in HaCaT human keratinocytes and *Igf2*$^{-/-}$ mouse embryonic fibroblast cells by treatment with this ligand trap. Additionally, a modified, protease-resistance IGFBP-2 has been shown to bind IGF-I and –II with high affinity and inhibit cancer cell proliferation in breast cancer cells (*298*). The difference of using a modified IGFBP over a modified sM6P/IGF2R is that the IGFBP can bind and sequester both IGF-I and -II, whereas the receptor can sequester only IGF-II.

M6P-based ligands can target the M6P/IGF2R by stabilizing the dimeric receptor and increasing the rate of ligand-receptor internalization, thereby internalizing IGF-II as a passenger ligand that becomes degraded in the lysosome. Work done in our laboratory has synthesized a panel of high-affinity, bivalent M6P-based ligands that are discussed in chapter III of this dissertation. We have evidence that our ligands bind to the M6P/IGF2R and promote accelerated internalization of IGF-II from the conditioned medium of cancer cells. Additionally, these ligands reduce cell viability in both a M6P- and IGF-II-dependent manner. We, in collaboration with the Berkowitz laboratory, have developed a panel of M6P-based ligands that would be resistant to inactivating hydrolysis catalyzed by proteases, glycosidases and phosphatases. However, we have not yet achieved bivalent binding with these bidentate molecules. Nevertheless, targeting the M6P/IGF2R to clear the IGF-II signal from the pericellular milieu remains a promising approach to inhibiting IGF-II-dependent growth of cancer cells.

Autocrine and paracrine growth-factoring signaling loops within the tumor microenvironment play a significant role in influencing tumor progression. Interrupting

these signals from the stroma may benefit cancer therapy. Cancer stem cells (CSCs) are exposed to IGF-II in a paracrine fashion from cancer-associated fibroblasts, and this signal induces the IGF-II-mediated events that ultimately result in increased *Nanog* and *Oct3/4* transcription to promote the CSC phenotype (*299*). Disruption of this paracrine loop can lead to differentiation of the CSC, which would increase its responsiveness to chemotherapy. In summary, there are numerous potential alternative therapeutic approaches to target IGF-II-dependent growth of cancer cells that may be more efficacious than the IGF1R approaches that have failed or had low success in clinical trials.

H.   Summary

In summary, the M6P/IGF2R is mostly involved in lysosome biogenesis, trafficking acid hydrolases to the lysosome. It also internalizes EC proteins and is implicated in many diseases and cancer. The M6P/IGF2R undergoes constitutive internalization, yet multivalent ligands are able to accelerate the receptor's rate of internalization as well as any passenger ligands, namely IGF-II. It is believed that these multivalent ligands are able to stabilize the receptor dimer, which either by receptor clustering or a conformational change in the cytoplasmic tail to offer a better presentation of the internalization signal, internalizes the complex more prominently. We wanted to take advantage the known receptor properties in order to exploit the M6P/IGF2R as a novel therapeutic target in IGF-II-dependent cancers. Thus, our objectives were as follows:

1.   Develop a panel of high-affinity, bivalent ligands that function in cross-bridging the dimeric receptor and decrease IGF-II from the cell milieu, thereby inhibiting the IGF-II-dependent growth of cancer cells.

2.   Develop and test a panel of hydrolase-, phosphatase-, and protease-resistant M6P-based surrogates that can stabilize the dimeric M6P/IGF2R and function as a more clinically relevant anti-cancer agent.

3.   Characterize the ligand binding properties of the putative MPR from *D. discoideum* to understand a) the differences between this receptor and the mammalian M6P/IGF2R, and b) the possible common ancestral origin of the MPRs.

Chapter II

Experimental Methods

A. Preparation of pentamannosyl 6-phosphate (PMP)-derivatized pseudoglycan proteins and peptides

The yeast *Pichia holstii* (NRRL-Y2448) produces a secreted phosphomannan when grown under aerobic conditions in a nitrogen-limited medium that used D-glucose as the carbon source and contains an excess of orthophosphate. The phosphomannan is composed of a highly branched, high-molecular-weight (5-39 x 10^6) phosphomannan core (PC). Oligosaccharide chains composed principally of repeating PMP are linked α(1,6) to the terminal phosphate of the PC and make up approximately 90% of the phosphomannan. These side chains, which are capped by unphosphorylated residues, are susceptible to mild-acid hydrolysis of the phosphodiester linkages producing products consisting of the PC and PMP.

A.1. Preparation of phosphomannan

Hydrolysis of phosphomannan was carried out by a modification of Murray and Neville's protocol (*300*) as previously described (*301*). Briefly, prior to hydrolysis, 1 g of phosphomannan was weighed into a 250 mL Erlenmeyer flask fitted with a stopper and rehydrated overnight in an aqueous solution containing 1% KCl at 4°C. The rehydrated phosphomannan was warmed to RT (room temperature) and the hydrolysis was carried out for 6-10 h in a boiling water bath heated to 100°C at a concentration of ~50-100 g/L, pH 2.2-2.5 using 1 M HCl as the catalyst and in the present of 1% KCl. Throughout the course of the hydrolysis, the pH was closely monitored and found to rise slightly (up to pH 3) over the first hour of the reaction as the phosphomannan went back into solution and as HCl vaporized. Therefore, the pH was readjusted, as needed, to pH 2.2-2.5 by addition of 1 M HCl. Additionally, re-addition of preheated water to the bath over the course of the hydrolysis was necessary to compensate for loss to evaporation.

Following the hydrolysis, the reaction was cooled to RT and neutralized (pH 6.9-7.0) with 1 N NaOH. After neutralization of the hydrolysate, the pH was adjusted to 9.0-9.5 with 1 M NaOH, followed by separation of the PMP from the PC by ultrafiltration through a 10,000 nominal molecular weight cuff-off membrane (MWCO) (Amicon Ultra-15, Millipore, Billerica, MA). The PMP and salts permeated through the membrane while the high-molecular-weight PC was retained. The filtrate was further purified by ion-exchange chromatography on DEAE-Sepharose resin equilibrated with 0.01 M NH_4HCO_3. The PMP bound to the resin while unphosphorylated products washed through. PMP was eluted off the column with 0.25 M NH_4HCO_3 and the pooled fractions containing PMP were concentrated and desalted by reverse membrane filtration and then lyophilized to dryness. The resultant white powered was stored in a desiccator at -20°C.

B. Preparation of PMP-derivatized proteins and peptides

Conjugation of PMP to various proteins and peptides was carried out according to the procedure of Braulke *et al.* as modified previously (*144, 302*). Bovine serum albumin (BSA), insulin (INS), lysyl-tyrosyl-lysine (KYK) tripeptide, and seryl-tyrosyl-lysine (SYK) tripeptide were conjugated with PMP previously in the laboratory and not discussed in this dissertation. PMP was coupled to ovalbumin (OVA) by incubation at 15 mg/ml concentration in the presence of 0.2 M PMP and 160 mM $NaCNBH_3$ at 37°C for 4-5 days. The resultant PMP-OVA product of this reductive amidation was dialyzed against 50 mM HEPES, pH 7.4, 150 mM NaCl using Pierce Slide-A-Lyzer® Dialysis Cassettes G2 (10K MWCO). The size and overall purity of the PMP-OVA was measured using SDS-PAGE and compared to the absorbance at 280 nm (A_{280}). The resolved gels were stained with Coomassie blue R250 for protein detection. Successful derivatization of PMP to ovalbumin was determined by comparing the molecular weight

shifts of the PMP-modified protein to lanes containing underivatized protein. PMP-BSA was done previously following the same protocol. The PMP-peptide products were synthesized previously in the lab and were purified on a 30 mL QAE Sephadex A25 column and eluted by stepwise increases of the salt concentration from 0 to 1 M NaCl of a 10 mM HEPES, pH 7.4 buffer. Fractions were collected and PMP-derivatized peptides were monitored by absorbance of tyrosine at 285 nm. The size and overall purity of the PMP-peptides was measured using MALDI-TOF mass spectrometry (UNMC Mass Spectrometry and Proteomics Core Facility).

C. Preparation of ^{125}I-labeled tracers

C.1. Preparation of ^{125}I-IGF-II

Iodination of IGF-II was carried out by a modification of the Chloramine-T method as described by GroPep (Bulletin #3001: Procedure for Iodination of IGFs; http://www.gropep.com.au/index.php/article/view/109/1/21). Briefly, aliquots (6 µg in 15 µL 5 mM HCl) of recombinant human IGF-II (Bachem; Torrance, CA) were diluted in 0.3 M sodium phosphate buffer (60 µL), pH 7.4, and incubated for 30 min with 2.0-2.5 mCi (~20 µL) of carrier-free Na[125]I (PerkinElmer Life Sciences; Boston, MA). The resulting reaction mix was combined with a 0.4 mg/mL solution of Chloramine-T (20 µL) (Sigma; St. Louis, MO), mixed thoroughly, and incubated for 60 s at room temperature (RT) (to a specific activity of ~30-60 Ci/g). At the end of the incubation, the oxidation reaction was quenched by addition of a 0.6 mg/mL solution of sodium metabisulfite (20 µL). The sample was thoroughly mixed, allowed to incubate for 5 min at RT, then prepared for size exclusion chromatography by adding 200 µL column buffer (phosphate buffered saline (PBS); 10 mM sodium phosphate, pH 7.4; 150 mM NaCl) containing 1% BSA. The ^{125}I-IGF-II was separated from the free iodine on a 30 mL Sephadex G-50 column

equilibrated with column buffer. The fractions containing radiolabeled IGF-II were collected, pooled, and stored at -20°C.

C.2. Preparation of ^{125}I-PMP-BSA and ^{125}I-hGUS

Aliquots of PMP-BSA (25 µg) and hGUS (15 µg) were iodinated to specific activities of ~50-150 Ci/g by incubation in 0.3 M sodium phosphate buffer, pH 7.4, with 2 mCi Na[125]I in IODOGEN tubes (Pierce, Rockford, IL) pre-coated with the oxidizing agent, 1,3,4,6-tetrachloro-3a,6a-diphenylglycoluril, for 15 min, according to the manufacturer's specifications. The product was separated from free iodine on a Sephadex G-50 column equilibrated with PBS + 1% BSA. The iodinated PMP-BSA and hGUS were collected from the flow-through fractions and stored at -20°C.

C.3. Preparation of ^{125}I-soluble M6P/IGF2R

Soluble M6P/IGF2R (sM6P/IGF2R) was purified as described in section E below. Approximately 20 µg of lyophilized sM6P/IGF2R was dissolved in 0.3 M sodium phosphate buffer, pH 7.4, and added to a pre-wetted IODOGEN coated tube. The Na[125]I (1.5 mCi) was then added, followed by a 15 min incubation. The radiolabeled sM6P/IGF2R was purified on a Sephadex G-50 column. Radioactive fractions from the void volume were pooled and stored at -20°C until use.

D. Preparation of PMP-Sepharose 4B

To make PMP-Sepharose, PMP was first conjugated to (p)-aminophenyl-ethanolamine (PAPEA), also called 2-(4-aminophenyl)-ethylamine, to provide a primary amine for coupling to cyanogen bromide (CNBr)-activated Sepharose 4B (Sigma) as previously described (*303*). PMP (50 mg) was incubated with 0.5 mL of PAPEA for 16 h at RT. To complete the coupling reaction, 12 mg of NaBH$_3$ was dissolved in 1.5 mL of

100% ethanol and added to the reaction. This mixture was incubated at RT for 5 h, and remaining $NaBH_3$ was quenched on ice with the addition of 4 mL H_2O and glacial acetic acid to a pH of 5.6. The product was lyophilized, and PMP-PAPEA was separated from unreacted PAPEA on a 30 mL Sephadex G10 column equilibrated in 50 mM ammonium acetate, pH 6.0. The purified PMP-PAPEA was lyophilized and stored -20°C until use. A PMP-Sepharose resin coupled to a density of 10 mg protein per ml resin was prepared using CNBr-activated Sepharose 4B (Sigma) following the manufacturer's instructions.

E. Purification of sM6P/IGF2R from fetal bovine serum (FBS)

Soluble bovine M6P/IGF2R was purified from FBS by the procedure of Valenzano *et al.* (*304*) as modified by Byrd *et al.* (*141*), with additional modifications. In brief, an aliquot of serum was diluted with an equal volume of buffer to yield final concentrations of 25 mM HEPES, pH 7.4, 0.15 M NaCl, 0.1% Triton X-100, 5 mM β-glycerophosphate (column buffer conditions). This diluted serum was incubated with PMP-Sepharose 4B resin, end-over-end, overnight and then poured through a 10 mL column. The column was subsequently washed with 5 x 5 mL of column buffer, 5 x 5 mL column buffer supplemented with 10 mM G6P, and eluted with 5 x 5 mL 10 mM M6P. The fractions containing purified receptor were identified by SDS-PAGE with Coomassie blue R-250 staining and pooled. The pooled material was dialyzed to remove M6P, lyophilized and stored at -20°C. Analysis of material purified by these methods using gel filtration chromatography and native gel electrophoresis indicated that the receptor is present as both a monomer (~70%) and a dimer (~30%) (*141*).

E.1. Coupling of sM6P/IGF2R to Sepharose 4B

sM6P/IGF2R-Sepharose 4B resin was used in ligand binding assays and prepared by coupling the purified, redissolved sM6P/IGF2R to CNBr-activated

Sepharose 4B according to the manufacturer's instructions. For coupling, 1 g of CNBr-activated Sepharose 4B dry resin was rehydrated in 15 mL of 1 mM HCl for 15 min at RT, then washed with 4 x 10 mL of 1 mM HCl followed by 2 x 10 mL of coupling buffer (0.1 M $NaHCO_3$, pH 8.0, 0.5 M NaCl). The wet resin cake (~3 mL volume) was transferred to a tube containing 1.2-1.4 mg of purified receptor dissolved in 5 mL of coupling buffer. The mixture was incubated on an end-over-end mixer a 4°C for 16 h for coupling. Uncoupled sites on the resin were blocked by incubation at 4°C with 0.5 M glycine, pH 8.0, to produce a final affinity reagent of ~0.5 mg M6P/IGF2R per mL resin beads. This material was stored as a 50% slurry at 4°C in 25 mM HEPES, pH 7.4, 0.15 M NaCl, 0.02 mM NaN_3, 0.05% Triton X-100 until use. Prior to use, the resin was washed in assay buffer twice to remove the NaN_3.

F. Measurement of IC_{50} values by radioligand displacement analysis

A sM6P/IGF2R-Sepharose 4B resin-based radioligand displacement assay was used to evaluate the ability of each of the PMP-ligands to bind the receptor. Aliquots (20 µL) of receptor resin (50% slurry) were incubated with 1.5 nM ^{125}I-PMP-BSA or ^{125}I-hGUS (used as tracers) in the presence of increasing concentrations of PMP-pseudoglycan ligands (1 pM to 10 µM) in assay buffer (50 mM HEPES, pH 7.4, 0.15 M NaCl, 0.05% Triton X-100) in a volume of 0.2 mL per tube, for 16 h at 4°C on an end-over-end clinical mixer. As positive and negative controls, parallel assays were done that had increasing concentrations of M6P (0.1 µM to 10 mM) or G6P (1 to 10 mM), respectively. The resin pellets were collected by centrifugation for 1 min at 6,000 x g at 4°C, and were washed with 2 x 1 mL of assay buffer. The tips of the tubes containing the resin pellets were cut and quantified in a WIZARD 1470 Automatic Gamma Counter (PerkinElmer, Inc.). The data were converted into percent binding values based on comparison with the ligand-free controls (designated as 100% radioligand binding). The

competitive binding data were graphed as semi-log plots of percent binding vs. concentration of M6P, G6P, or the PMP-ligands. Best-fit curves were generated by nonlinear regression analysis using Prism GraphPad software (San Diego, CA), which also estimated the IC_{50} values, the concentration that displaces 50% of radioligand binding. Values for relative binding affinity (RBA) for the PMP-ligands were normalized to M6P for a given experiment and are reported as the mean of at least three replicate experiments.

G. Expression of M6P/IGF2R constructs

Transient expression of soluble receptors was done in HEK 293 cells. Transfection was carried out by a modification of the calcium phosphate method as described previously (*305*). At 24 h post-transfection, the medium was replaced with serum-free Dulbecco's modified Eagle medium (DMEM) followed by incubation for 3 days to permit the cells to condition the medium. To recover the secreted, epitope-tagged soluble receptors, the conditioned medium was recovered and cellular debris was pelleted on a tabletop centrifuge at 7000 RPM. The medium was supplemented with 1 mM PMSF and 1 mM sodium fluoride, and concentrated to ~250 μL using Amicon Ultracel 10K centrifugal filters as per the manufacturer's specifications, and then stored at -20°C until use. For full-length receptors, cells were harvested three days post-transfection and lysates were prepared by solubilization with 50 mM HEPES, pH 7.4, 1% Triton X-100, 1 mM $MgCl_2$, 1 mM PMSF, and PIC as previously described (*116*). After conditioned media and lysates were prepared, 25 μL aliquots were electrophoresed on 8 or 10% SDS-PAGE gel under reducing conditions and immunoblotted with α-FLAG M2 antibody (1:1000) (see full immunoblot protocol below).

H. Immunoprecipitation of soluble mini-receptors with M2 α-FLAG affinity resin and competitive binding analysis of PMP-ligands

Aliquots of HEK 293 cell conditioned media and lysates, containing equimolar amounts of expressed FLAG-tagged soluble receptors as determined by the bicinchoninic acid assay, were incubated with 6 μL of packed M2 affinity resin in HEPES-buffered saline (HBS; 50 mM HEPES, pH 7.4, 0.15 M NaCl) plus 1% BSA and 5 mM M6P with mixing for 16 h at 4°C. The resin was collected by centrifugation at 8,000 x g for 30 s. The resulting resin pellets were washed four times with 1 mL HBS containing 0.05% Triton X-100 (HBST). The immunoprecipitated soluble receptors were incubated with 2 nM ^{125}I-PMP-BSA in the presence of increasing concentrations of the PMP-ligands (0 mM, or 1 pM to 10 μM) in assay buffer with mixing for 4 h at 4°C. Resin pellets were processed and the binding data were quantified and calculated as described above for the receptor-resin experiments.

I. SDS-PAGE and immunoblot analysis

All SDS-PAGE gels run were 6%, 10%, or 10-16% gradient maxi- and mini-gels. Samples were prepared in 2x loading buffer (5% SDS, 10% sucrose, 100 mM Tris, 0.02% Bromophenol Blue) with or without dithiothreitol (DTT) as a reductant and boiled for 5 min before loading the gel. Gels were run at 6 mA overnight or 28 mA for 4 h and transferred to BA85 nitrocellulose membrane (Schleicher & Schuell, Keene, NH, USA). The blots were blocked in 4% nonfat dry milk in 50 mM HEPES, pH 7.4, 150 mM NaCl, 0.1% Tween-20, and probed with the appropriate primary antibody (Table 2.2) overnight and appropriate goat α-rabbit or goat α-mouse secondary antibody coupled to HRP (1:40,000). The resulting antibody complex was developed using enhanced chemiluminescence (ECL) and detected by means of autoradiography and quantified

using Li-Cor C-DiGit® Blot Scanner (Li-Cor Biosciences, Lincoln, NE, USA) and Image Studio Lite Software.

J. Cell viability studies

To investigate kinetics and dosage of PMP-pseudoglycan ligand effects on cultured cells, growth studies were performed using a modification of the previously described MTT vital dye assays (*306*). Briefly, cells were seeded into 96-well plates at 100 to 1,000 viable cells/well, in full serum-containing medium.   The cells were incubated for 24 h at 37°C before switching to reduced serum (1-3% FBS) for acclimation prior to drug treatment. At this point for the time course studies, designated day 0, a set of wells was subjected to the MTT assay while the remaining wells were incubated with reduced-serum medium supplemented with the various treatments indicated in the figures (vehicle control, M6P, PMP-ligands or IGF-II) and continued for 1-5 days. MTT at a concentration of 1 mg/mL in phenol red-free medium was added to culture wells for an incubation period of 3 h at 37°C, 5% CO_2. Wells containing purple formazan were solubilized with isopropanol and the absorbance of 100 μL solution was measured using a SpectraMax 190 (Molecular Devices, Sunnyvale, CA, USA) at 570 nm corrected for background absorbance at 690 nm and plotted as a function of time.

Antibodies	Source	Dillution	Company	Product Number
β-actin	Mouse monoclonal	1:4000	Sigma	A5441
Akt	Rabbit polyclonal	1:1000	Cell Signaling	9272
phospho-Akt (Ser473)	Mouse monoclonal	1:1000	Cell Signaling	4051
phospho-Akt (Thr308)	Rabbit monoclonal	1:1000	Cell Signaling	4056
CD222 (MEM-238)	Mouse monoclonal	1:1000	Abcam	ab8093
Cyclin D1	Rabbit polyclonal	1:500	Santa Cruz	sc-718
ERK1/2	Rabbit polyclonal	1:4000	Santa Cruz	sc-94
phospho-ERK1/2 (Thr202/Tyr204)	Rabbit polyclonal	1:400	Cell Signaling	9101
IGF-II	Rabbit polyclonal	1:500	Cell Sciences	PAC1
LC3B/MAP1 LC3B	Rabbit polyclonal	1:500	Novus	NB1002220SS
MCL-1	Rabbit polyclonal	1:1000	Santa Cruz	sc-819
mTOR	Rabbit monoclonal	1:1000	Cell Signaling	2983
phospho-mTOR (Ser2448)	Rabbit monoclonal	1:1000	Cell Signaling	5536
p53	Rabbit monoclonal	1:1000	Cell Signaling	sc-6243
p70S6K	Rabbit polyclonal	1:1000	Cell Signaling	9202
phospho-p70S6K (Thr389)	Rabbit polyclonal	1:1000	Cell Signaling	9205
PARP1	Rabbit polyclonal	1:1000	Cell Signaling	9542
PUMAα/β	Rabbit polyclonal	1:1000	Santa Cruz	sc-28226

Table 2.1: Primary antibodies used for immunoblot analysis.

K. IGF-II degradation studies

K.1. IGF-II detection via SDS-PAGE and slot blot analysis

To detect IGF-II through imunnoblotting, an IGF-II standard curve was diluted in serum-containing medium or concentrated conditioned medium was run on a 10-16% SDS-PAGE under reducing conditioned and transferred to BA85 nitrocellulose membrane. The blot was probed for α-IGF-II antibody. To concentrate the conditioned medium, medium collected from cells was concentrated to 800 µL via Amicon Ultra centrifuge filters or by lyophilization.   Concentrated conditioned medium was electrophoresed and probed as described above.

For the slot blot analysis, an IGF-II standard curve supplemented with a known amount of ^{125}I-IGF-II was added to a slot-blot apparatus that was connected to the in-house vacuum system, which drew the fluid down into the BA85 membrane. The IGF-II was contained in either HBS or 10% FBS-containing medium as a carrier. The blot was exposed to autographic film.

K.2. Trichloroacetic acid (TCA) precipitation of IGF-II

IGF-II from medium not exposed to cells was precipitated by a trichloroacetic acid protein precipitation assay. Medium (3% FBS) containing both unlabeled IGF-II (60 ng) and 500,000 cpm ^{125}I-IGF-II was incubated with 50% TCA (20% total volume) at 4°C, end-over-end, overnight. Samples were pelleted at 13,200 rpm, 4°C, 25 min. The supernatants were discarded and the pellets were washed twice with cold acetone. The washed pellets were then resolubilized in SDS-PAGE loading buffer supplemented with NaOH to account for the acidic pH. Samples were then electrophoresed, transblotted to nitrocellulose, and the blots exposed to autographic film.

K.3. Size exclusion chromatography and ^{125}I-IGF-II radioimmunoassay (RIA)

The detection of IGF-II was performed using size-exclusion chromatography followed by an IGF-II radioimmunoassay (RIA) as previously described with some modifications (*307*). SK-N-AS, Capan-1 or JEG-3 cells were seeded in 6-cm dishes in complete medium and grown at 37°C in a humidified 5% CO_2/95% air atmosphere overnight. The medium was replaced with low-serum (3%) medium and cells were grown for an additional 24 h. Cells were then treated with 100 nM PMP-OVA with or without 10 nM IGF-II in 1% serum medium. Conditioned medium was collected at 24 or 48 h, and was supplemented with 1 mM PMSF and 10 mM NaF before concentration via lyophilization. Concentrated conditioned medium was reconstituted in 1 M acetic acid and centrifuged at 9,000 x g for 5 minutes. The supernatant fraction was collected and immediately run on a 100-mL size-exclusion column containing Bio-Gel P-10 (mesh 50-100) and eluted in 0.1 M acetic acid in 2-mL fractions. Fractions containing IGF-II were collected and lyophilized. IGF-II was reconstituted in 200 µL 1 mM HCl, and aliquots of 15 or 30 µL were used in a radioimmunoassay (RIA). For the RIA, 15 µL of Protein A-Sepharose resin (50% slurry) was added to 1 mL blocking buffer (1% BSA, 25 mM HEPES, 150 mM NaCl, pH 7.4) for 5 min on ice, and centrifuged at 6,000 x g for 1 min before the buffer was aspirated. Rabbit IGF-II antibody (20 ng/µL) of was incubated with the resin in RIA buffer (50 mM sodium phosphate, 0.1% NaCl, 0.1% EDTA disodium salt, 0.1% sodium azide, 0.05% Tween 20, pH 7.5) for 16 h at 4°C on an end-over-end clinical mixer. The IGF-II-conjugated Protein A-Sepharose resin was washed twice in 1 mL RIA buffer via centrifugation at 6,000 x g, 4°C. An IGF-II standard curve was made using increasing concentrations of IGF-II (0 ng to 1000 ng) in 5 mM HCl. The IGF-II standard curve and unknown samples were diluted in 30 µL 1 mM HCl before being added to the resin containing RIA buffer. Tracer ^{125}I-IGF-II was added to each tube to

0.3 nM and the tubes were incubated for 16 h at 4°C on an end-over-end clinical mixer. The resin pellets were washed twice in 1 mL RIA buffer as described above, and the tips of the tubes containing the resin pellet were cut and quantified in a WIZARD 1470 Automatic Gamma Counter (PerkinElmer, Inc.). The data were converted to binding percentages and graphed as semi-log plots of percent binding vs. concentration of IGF-II as described above for the competitive binding assays. The concentrations of IGF-II in the unknown samples were determined from the semi-log plot and converted to the amount of IGF-II in the total sample.

K.4. ^{125}I-IGF-II Internalization assay with TCA precipitation

HuH-7, Capan-1, and SK-N-AS cells were seeded into 24-well plates. After 24 h and again at 90% confluency, cells were treated with 100 nM PMP-OVA, 100 or 200 nM IGF-II, 100 nM PMP-OVA, 100 or 200 nM IGF-II, 50 nM sM6P/IGF2R, 50 nM sM6P/IGF2R + 100 nM IGF-II, 10 mM M6P, or 10 mM M6P + 100 nM IGF-II and compared to the vehicle control (HBS + HCl) along with radiolabeled IGF-II and cold-carrier IGF-II in 3% FBS-containing medium. Each treatment had 0.3 nM ^{125}I-IGF-II to visualize the degradation of exogenous IGF-II as a result of the treatments. The low concentration was chosen as it was enough radioactive counts to determine slight differences between the groups without being high enough to overwhelm the cells and illicit its own activation response. Additionally, 1 nM of cold carrier IGF-II was provided to the cells to protect the radioligand from adsorption to matrix surfaces that bind IGF-II, such as vitronectin within the EC matrix (*308*) or IGFBPs in the medium. In the IGF-II treatment group, 100-200 nM concentration was chosen in order to inhibit degradation of ^{125}I-IGF-II by out-competing the radioligand for the available receptor binding domains; thus, there would be more radioactive counts in the conditioned medium correlating to intact ^{125}I-IGF-II as the assay progresses. Furthermore, sM6P/IGF2R and M6P were

used as controls to also inhibit the assay. The M6P would competitively displace our PMP-OVA ligand from the M6P-binding sites of the M6P/IGF2R on the cell membrane; thus, the receptor would internalize at a slower rate than when PMP-OVA binds, resulting in a slower degradation of ^{125}I-IGF-II. The sM6P/IGF2R acts as a ligand trap and scavenges any bioavailable IGF-II in the medium, such as ^{125}I-IGF-II. Since there is only one available IGF-II-binding domain within the soluble receptor, it can sequester only 1 molecule of ligand, which would manifest as IGF-II sparing, i.e., there would be more intact ^{125}I-IGF-II in the conditioned medium. Cells were treated with 900 µL of medium containing their respective treatments and allowed to internalize the ^{125}I-IGF-II for 6, 24, 48, or 72 h. At the different time points, two aliquots (250 µL and 50 µL) were withdrawn and frozen at -20°C until further use. Cells were treated in triplicate and each well was compared to itself among the different time points. For clarity, the first tube at each time point represented the first control well, which eliminates potential pipetting error between the wells upon addition of the radiolabled IGF-II-containing treatment.

Following treatments and collection of the conditioned media at all time points, TCA precipitation was performed on the conditioned media to determine the amount of radioactivity that is soluble (representing degraded IGF-II) and insoluble (intact IGF-II). The 200 µL aliquots were thawed and 150 µL of 10% BSA (2.3% final concentration) were added as bulk carrier prior to addition of 300 µL 100% TCA (46% final concentration). Samples were vigorously vortexed and incubated on ice for 1 h. TCA precipitates intact IGF-II (as demonstrated in experiments validating the assay), so the soluble and insoluble fractions were separated via centrifugation at 13,200 rpm, 4°C, 10 min. The supernatants were immediately drawn off and collected in 5 mL gamma counter tubes. The bottoms of the tubes containing the pellets that represent the precipitated, intact IGF-II with carrier protein were cut off and collected into 5 mL gamma

counter tubes. Both TCA fractions were counted on a WIZARD 1470 Automatic Gamma Counter (PerkinElmer, Inc., Waltham, MA) and compared to the total counts in the 50 µL aliquots (multiplied by 4 to account for the differences in aliquot size). Each sample from the same well was normalized before the mean and the standard error of mean (SEM) were calculated for each treatment at each time point. Radiolabled IGF-II was incubated in cell-free medium for the duration of the assay to validate the amount of precipitable IGF-II. There was approximately 70% precipitable IGF-II in all time points (0, 24, 48, 72 h), indicating that our radioligand is stable and our assay is valid since any effect seen will be due to processing by the cells.   Additionally, the sum of the recovered supernatant and pellet was approximately 80-100% of the total counts added to the assay.

L. Cell Cycle Analysis using flow cytometry

JEG-3, Capan-1, and SK-N-AS cells were seeded into 4 cm dishes. Once cells reached 70% confluency, cells were treated with the various treatments for 0-48 h. At the different time points, cells were harvested, and fixed in 70% ethanol for 15-60 min on ice. The ethanol was washed away with FACS buffer (1x PBS, 5% FBS), and then the cells were stained with Telford Reagent (1x PBS, 57.5 mM EDTA, RNAse A, 37.4 mM propidium iodide (PI), 0.1% Triton X-100) for 1 h or overnight. Cells were filtered using flow cytometry tubes, and data were collected visualizing PI staining on the Calibur I in the Flow Cytometry Core Facility (UNMC).

For JEG-3 cells that were synchronized via a serum deprivation protocol prior to cell cycle analysis, cells were seeded as above except once the cells reached 30% confluency, they were washed in DPBS and serum starved (0.1% FBS) for 48-72 h. Cells were then released into the various treatments in 1% FBS-containing medium.

For SK-N-AS cells that were synchronized using a double thymidine block, cells were seeded as above, but after 24 h the medium was changed to full medium containing 3 mM thymidine. After 16 h incubation, the cells were released into 3% serum medium for 8 hours before another thymidine block (3 mM in 3% serum medium). After 16 h, the cells were released into the treatments in 1% FBS-containing medium.

For BrdU incorporation using the APC BrdU Flow Kit (BD Pharmagen, San Jose, CA), SK-N-AS cells were seeded into 6-cm dishes. The serum was reduced (3% FBS) after 24 h, and the cells were allowed to grow for an additional 24 h. Cells were treated with various treatments in 1% FBS-containing medium for 24 h. Prior to harvesting, BrdU was added directly to the conditioned medium, and cells were allowed to incorporate the label into their DNA for 3 h. Cells were harvested and fixed, DNA cleaved, and stained following the manufacturer's instructions. Cells were then analyzed on a Calibur III flow cytometer analyzing the APC and 7AAD staining.

M. Apoptosis analysis studies

M.1. DAPI staining of apoptotic nuclei

Cells were seeded into 24-well plates, and once 70% confluency was reached, the cells were incubated with the treatments in 3% FBS-containing medium. DAPI (1 µL/well) was added directly to the conditioned medium. The plates were gently rocked for 10 seconds and incubated at 37°C, 5% CO_2 for 10 min. Representative images (3-6 images) of the DAPI fluorescence and phase contrast were taken on a Leica DMI6000B (Leica Microsystems, Buffalo Groove, IL) fluorescent microscope. The number of apoptotic nuclei, as determined by fragmented and blue staining, and total number of cells were counted, and the percentage of dead cells was determined. The mean of the treatment groups were compared to the control.

M.2. Caspase 3/7 activity assay

Capan-1, S2-013, and SK-N-AS cells were seeded into 96-well black, clear bottom plates, similar to the MTT assay in section J. After 24 h, the serum was stepped down for an additional 24 h before treatments. 24 h following the treatments, Apo-ONE® Homogeneous Caspase 3/7 Activity Assay (Promega, Madison, WI) was performed according to manufacturer's instructions. The fluorescence at 499/521 nm was determined by a Tecan Infinite® M200 Pro fluorescent spectrometer (Tecan,Systems, Inc, San Jose, CA).

M.3. Annexin V and PI staining of apoptotic and necrotic cells

JEG-3, HuH-7, and Capan-1 cells were grown in 6-cm dishes. After 24 h, the serum was reduced (3% FBS) and the cells allowed to grow for an additional 24 h. Cells were then treated in 3% FBS-containing medium for 6-24 h. At each time point, the cells were harvested, washed in cold 1x PBS, and stained following the TACS annexin V (Trevigen, Gaithersburg, MD) protocol provided by the manufacturer. Cells were then analyzed on a Calibur III flow cytometer to visualize annexin V and PI staining.

N. Migration assays

N.1. Scratch wound-healing assay

Capan-1 and HuH-7 cells were seeded into 6-well plates. Once the cells reached 80% confluency, 3 scratches were made in each well using a pipet tip (time point 0) prior to treatment. Phase contrast images (2 per scratch; 6 per well) were taken every 24 h until the 96 h time point on a Leica fluorescent microscope. The area of the wound area was measured using ImageJ (University of Wisconsin-Madison, Madison

WI) and the mean of means were determined. The rate of wound closure of the treatment groups was compared to that of the control.

N.2. Transwell migration assay

Capan-1 and HuH-7 cells were seeded into 24-well plate inserts in 100 µL volume in serum-free medium containing the PMP-OVA treatment or vehicle control. The well below the membrane insert contained 600 µL of 3% FBS-containing medium with or without 10 nM IGF-II. After 48 h to allow the cells to migrate, the inserts were retrieved, cells were fixed in isopropanol and the tops of the membranes were swabbed of cells. The cells were then treated with DAPI, washed once in 1x PBS, and mounted on slides. Representative images (3 images) of the DAPI fluorescence and phase contrast were taken on a Leica fluorescent microscope. The number of cells that migrated was counted, and the treatments were compared to the control.

O. Chemical synthesis of hydrolase-resistant M6P-surrogates

O.1. General overview of chemical synthesis

Chemical synthesis for our M6P-based surrogates were carried out by Xiang Fei and Guillaume Malik from the laboratory of our collaborator, David Berkowitz at the University of Nebraska-Lincoln. The first panel of synthetic, hydrolase- and phosphatase-resistant M6P-based ligands was synthesized by Xiang in his doctoral work, while the second panel was a collaborative effort of Xiang and Guillaume. For details on the synthesis, please refer to Xiang Fei's dissertation, chapter IV of this dissertation, and previous papers (Fei X and Berkowitz 2008). In short, the ligands were synthesized using different chemistry to control the linker orientation and tether length using polybutylene glycol and polyethylene glycol units.

P. Radioligand displacement analysis of M6P-surrogates

These assays and graphical analysis was performed as described in section F with the following changes: the concentration of M6P analogues (0 mM, or 0.0001 to 1 mM).

Q. Generation of *Dictyostelium discoideum* MPR-FLAG expression-constructs

A recombinant cDNA construct encoding a 442-amino-acid-residue portion (residues 578-1020) of the 2441-residue *Dictyostelium discoideum*-MPR (DDMPR) protein sequence (NCBI Accesion: XP_635466) was previously made in our laboratory by Dr. Chris Connelly. The gene sequence encoding the endogenous protein (NCBI Accession: XM_630374.1) is located on chromosome 5 within the *D. discoideum* genome. The 1326-nucleotide (nt) sequence encoding a part of the putative EC region of the DDMPR, corresponding to the 442-residude putative M6P-binding region of the protein, was designed to contain a 24-nt sequence encoding a C-terminal FLAG-epitope tag (DYKDDDDK) with 6-nt *Eco*RI and *Xba*I resctriction enzyme sites of the 5' and 3' ends, respectively, flanking the coding region. The optimized codon usage-adjusted insert (synthesized by GenScript Corporation (Piscataway, NJ)) was excised out of the pUC57 vector and cloned into the eukaryotic expression vector, pCMV5 (provided by Dr. David Russell, University of Texas Southwestern Medical Center, Dallas, TX). The pCMV5 vector had been previously engineered in our laboratory to destroy the *Eco*RI site in the multiple cloning sequence, to yield a pCMV5RIX vector (*116*).

The cDNA constructs prepared in bacterial expression vectors are shown in Table 2.2 and Figure 5.2. The two bacterial expression vectors used were pCOLD-GST and pET-22b(+). The pCold-GST vector was provided by Dr. Steve Caplan of BMB and encodes a 6x histidine (His)-tag and 26-kDa GST fusion at the N-terminal region of the

insert. This vector is unique in that it is a cold-shock vector that expresses the insert at low temperatures (18 °C) following induction, which prevents the transcription of leaky genes at 37°C (*309*). Additionally, this vector can be used to purify the protein of interest by either the GST- or His-tags, with human rhinovirus 3 C protease site (Leu-Glu-Val-Leu-Phen-Gln|Gly-Pro) and Factor Xa site (Ille-Glu-Gly-Arg) following their respective tags. After cleavage, a purified protein without the tags can be achieved. The pET-22b(+) vector (Novagen,, EMD Millipore, Billerica, MA) has a C-terminal His-tag. This unique vector has an N-terminal *pelB* signal for periplasmic localization, which increases solubility of the protein (*310*), and the signal peptidase cleavage sequence allows for cleavage just upstream of the insert.   Additionally, there is a C-terminal His-tag sequence that allows for purification using a Ni^{2+}-NTA resin column.

The inserts listed in Table 2.2 were cloned into the pCOLD-GST vector using a strategy previously reported in our laboratory (*144*). In short, the human MP6/IGF2R mini-receptor inserts (1-3F, 7-9F, and 11-13F) were restricted digested out of the pCMV5RIX vector using *Eco*RI at 5' end and *Xba*I at the 3' end. The resulting fragments were ligated into the pCOLD-GST vector that contained the 5' half of sequence encoding repeat 1 of the human M6P/IGF2R that also contains the signal sequence. The DDMPR R1-3F was PCR-amplified out of the pUC57 vector and ligated into an opened pCOLD-GST vector containing the first half of repeat 1 of the M6P/IGF2R, using *Eco*RI and *Xba*I. Diagnostic cuts were made to validate that we achieved the correct inserts into our vectors.

The DDMPR R3F insert was engineered to express bacterial codon usage and synthesized as a 477-base pair (bp) gBOCK by Intergrated DNA Tecnhologies (IDT, Coralville, IA), and contained a FLAG-tag sequence at the 3'-end. We engineered an *Spe*I cutsite into the gene for single cut restriction analysis. The gBlock was digested

with *Nco*I at the 5'-end and *Xho*I at the 3' end. The vector containing our DDMPR R3F

insert was validated using *Spe*I and sequencing.

R. Expression of the DDMPR and mini-receptor constructs

R.1. Expression of DDMPR R1-3F construct

Transient expression of DDMPR R1-3F was done in HEK 293 or 293T cells.

Transfection was carried out by a modification of the calcium phosphate method as

described previously (*305*). At 24 h post-transfection, the medium was replaced with

serum-free DMEM followed by incubation for 3 days to permit the cells to condition the

medium. To recover the secreted, epitope-tagged DDMPR, the conditioned medium

was recovered and cellular debris was pelleted on a tabletop centrifuge at 7,000 RPM

The medium was then concentrated to ~250 µL using Amicon Ultracel 10K centrifugal

filters as per the manufacturer's specifications or lyophilized and stored at -20°C until

use. To compare secreted vs non-secreted DDMPR, cells were harvested three days

post-transfection and lysates were prepared as described in section G. Additionally,

conditioned medium and lysates were analyzed as described in section G.

R.2. Bacterial expression of GST- or His-tagged proteins

The expression plasmids constructed in pCOLD-GST and pET-22b(+) vector

constructs as described in section N.1 were transformed into Rosetta 2 *E. coli*

competent cells, using a standard transformation procedure based on the transformation

protocol by New England Biolabs Transformed cells were plated on LB agar plates

containing the appropriate antibiotic(s) as listed in Table 2.2. The plates were incubated

overnight at 37°C, and a single colony from each plate was used to inoculate 50 mL of

Luria broth (LB) medium containing appropriate antibiotic(s) and incubated overnight at

37°C, 250 rpm. Larger 250 mL to 1 L LB cultures containing the appropriate antibiotic(s)

were inoculated with the overnight starter culture and grown at 37°C, 250 rpm. Once the culture reached an optical density at O.D.$_{600}$ = 0.6, a sample of culture was taken for SDS-PAGE analysis and the culture was inducted with 0.25 to 1 mM Isopropyl β-D-1-thiogalactopyranoside (IPTG) (final concentration). IPTG is a mimic of allolactose that binds the lac repressor and allows for expression of T7 RNA polymerase and the protein of interest. Following induction, the cell culture was allowed to grow for another 3-4 h in the conditions listed in Table 2.2. A post-induction sample was removed for SDS-PAGE analysis, and the pre- and post-inducing aliquots were compared by loading equal amount of protein by normalizing to 500 μL with an O.D.$_{600}$ = 0.5. The sample was centrifuged at 13,000 rpm for 1 min and resuspended in 15 μL 2x loading buffer, boiled for 5 min and analyzed following the electrophoresis protocol followed by Coomassie blue R-250 staining. The induced culture was harvested by centrifugation at 10,000 rpm for 15 min. The supernatant was discarded and the cell pellet was stored at -20°C for future use.

S. Purification of His/FLAG-tagged mini-receptors

Following expression of our proteins of interest, the proteins were purified via their His-tags. The bacterial cell pellets were resuspended in a lysis buffer (10 mL per 100mL to 1 L of culture: 10 mL 1x PBS, 2 m M PMSF in isopropanol, 1% NP-40, 1 m M DTT, 1:1600 His-tag protease inhibitor cocktail (PIC). Cells were lysed on a French Press, and the cellular debris removed from the lysate via centrifugation (16,500 rpm, 1 h, 4°C). An aliquot of the supernatant and pellet representing the soluble and insoluble fractions, respectively, were electrophoresed on either a 10% or 15% SDS-PAGE gel and stained with Coomassie blue.

For purification of the soluble fraction, the supernatant was applied to a Ni^{2+} column pre-equilibrated with ÄKTA Buffer A (1x PBS, 20 mM imidazole, and 1 DTT at pH 7.4). ÄKTA Buffer A contains a low concentration of imidazole that reduces non-specific binding to the resin column. Imidazole rings in the His-tag have two lone pair electrons that chelate to the metal ions in the column; thus, the protein of interest may be purified using this strategy with increasing concentrations of imidazole for elution. The column was washed with 4 column volumes (20 mL) following the sample injection with ÄKTA Buffer A, and the His-tagged proteins were eluted with a gradient of ÄKTA Buffer B (1 M imidazole and 1 mM DDT, at pH 7.4. The fractions containing protein were indicated as peaks in the elution profile, and these fractions were analyzed using SDS-PAGE. The fractions containing the protein were pooled and dialyzed in dialysis buffer (1x PBS with 1 mM DTT) to remove the imidazole. Slide-A-Lyzer dialysis cassettes with a 10,000 MWCO were used, and the samples were dialyzed in 2x 2L of dialysis buffer at 4°C for 4 h and then 16 h with gentle stirring.

For purification of the insoluble fraction, the pellet was re-solubilized in ÄKTA urea Buffer A (1x PBS, 6 M urea, 20 mM imidazole, 28.5 mM 2-mercaptoethanol (β-ME), 1% Triton X-100, at pH 8.0-8.4). After re-solubilizing the pellet at 4°C, end-over-end, overnight, any remaining insoluble particles were pelleted at 16,500 rpm, 4°C, 1 h. The re-solubilized fraction was purified following the soluble fraction purification with the following change: ÄKTA Buffer B was substituted with ÄKTA urea Buffer B (1x PBS, 6 M urea, 1% Triton X-100, 1M imidazole, at pH 8.0-8.4).

The N-terminal GST-tag was not removed until after refolding. To remove the GST-tag, the proteins were cut with Turbo 3 C (Accelagen; San Diego, CA, USA) (2 units/1 µL; 1 unit/ 100 µg), end-over-end, 4°C, for 24-72 h. Aliquots of before and after cleavage were analyzed via SDS-PAGE and Coomassie blue staining.

T. Refolding of His/FLAG-tagged mini-receptors

The proteins purified from the insoluble fraction were completely unfolded due to DTT and the high concentration of urea. Refolding occurred in one of several refolding buffers as listed in Table 2.3. The protein refolding followed one of two protocols.

1. Direct dilutions:

Protein was allowed to unfold in ÄKTA urea Buffer A for 1 h at 4°C. Protein was diluted directly with volumes (1:0 control; 1:1; 1:5; 1:10; 1:20) of refolding buffer, briefly vortexed to mix, then allowed to rest at 4°C for 24-48 h for refolding. Conversely, only half of the refolding buffer was added at 12 h while the second half was added at 24 h.

2. Dialysis:

Protein was dialyzed in refolding buffer supplemented with decreasing concentrations of of urea (4 M, 2 M, 1 M, 0 M) over the course of 6 days.

After following either protocol for protein refolding, the refolded protein was dialyzed in dialysis buffer (1x PBS or 1x TBS) in a two-step process overnight. Following dialysis, the protein was subjected to biophysical or functional assays to determine proper and functional folding of the mini-receptors.

Protein Name	Vector	M_w (kDa)	M_w (kDa) +GST	Cell Line	Antibiotics	Induction
DDMPR R1-3F	pCOLD-GST	51.1	78	C41	Amp	18°C 250 rpm
DDMPR R1-3F	pCOLD-GST	51.1	78	JRC1	Amp/Cam	18°C 250 rpm
DDMPR R1-3F	pCOLD-GST	51.1	78	JRC3	Amp/Cam	18°C 250 rpm
1-3F	pCOLD-GST	49.4	77	C41	Amp	18°C 250 rpm
1-3F	pCOLD-GST	49.4	77	JRC1	Amp/Cam	18°C 250 rpm
1-3F	pCOLD-GST	49.4	77	JRC3	Amp/Cam	18°C 250 rpm
7-9F	pCOLD-GST	49.4	76	C41	Amp	18°C 250 rpm
7-9F	pCOLD-GST	49.4	76	JRC1	Amp/Cam	18°C 250 rpm
7-9F	pCOLD-GST	49.4	76	JRC3	Amp/Cam	18°C 250 rpm
11-13F	pCOLD-GST	54	81	C41	Amp	18°C 250 rpm
11-13F	pCOLD-GST	54	81	JRC1	Amp/Cam	18°C 250 rpm
11-13F	pCOLD-GST	54	81	JRC3	Amp/Cam	18°C 250 rpm
DDMPR R3	pET-22b(+)	18.3		BL21	Amp	37°C 250 rpm

Table 2.2: Bacterial expression constructs were transformed into E. coli Rosetta 2 competent cell strains.

Received from Dr. Paul Sorgen, UNMC: C41, JRC1, JRC3, BL21
Recieviend from Dr. Steve Caplan, UNMC: pCOLD-GST
Abbreviations are as follows: C41, C41(DE3)pLysS; JRC1, C41(DE3)pRARE2pLysS; JRC3, C43(DE3)pRARE2pLysS; BL21, BL21(DE3); Cam, chloramphenicol, Amp, ampicillin

Refolding recipe, pH 8.0	Buffer*
50 mM Buffer*	Tris
1 mM EDTA	MES
1 M L-arginine	MOPS
0.1 mM PMSF	HEPES
3.7 mM Cystamine	Glycine
6.5 mM Cysteamine 2-mercaptoethylamine	1x PBS

Table 2.3: MPR mini-receptor refolding buffer conditions. The refolding buffer recipe contained the components in the left column, where the buffer* was substituted for a buffer in the column on the right.

U. PMP-Sepharose pull-down assay

Aliquots of HEK 293 cell conditioned media and lysates or soluble and re-solubilized pellet fractions from *E. coli* cells, containing equimolar amounts of expressed FLAG-tagged soluble receptors as determined by the bicinchoninic acid assay, were incubated with 5 µL of packed PMP-Sepharose 4B resin in (IMM2 buffer: 50 mM HEPES, pH 7.4, 0.15 M NaCl, 0.05% Triton X-100, pH 7.4) plus 1% BSA with or without increasing concentrtions of 5 mM M6P (0 mM to 20 mM) with mixing for 16 h at 4°C. The resin was collected by centrifugation at 8,000 x g for 30 s. The resulting resin pellets were washed twice with 1 mL IMM2 buffer. The resin complex was immunosorbed to 10% SDS-PAGE gels and probed with α-FLAG M2 antibody (1:1000) or α-His-tag antibody (1:1000) and processed as previously mentioned.

V. ^{125}I-PMP-BSA ligand blot analysis

Samples were prepared as for SDS-PAGE immunoblots in section I, except under non-reducing conditions (absence of DTT in the sample buffer). After electrophoresis, proteins were transferred to transferred to BA85 nitrocellulose membrane under non-reducing conditions (15 mM Tris, pH 8.3, 120 mM glycine). Blots were stripped of SDS in Ligand A buffer (10 mM TRIS, pH 7.4, 150 mM NaCl, 0.05% NaN$_3$, 3% NP-40) for 30 min, end-over-end, 4°C, blocked in Ligand B (10 mM TRIS, pH 7.4, 150 mM NaCl, 0.05% NaN$_3$, 1% BSA) for 2 h, end-over-end, 4°C, and probed in radioligand (Ligand B, 0.01% Tween-20, 2 million cpm or 0.5 nM ^{125}I-PMP-BSA) overnight, end-over-end, 4°C. After 3 x 15 min washes in Ligand C (10 mM TRIS, pH 7.4, 150 mM NaCl, 0.05% NaN$_3$, 0.1% Tween-20), end-over-end, 4°C, blots were dried and detected by means of autoradiography and quantified using Typhoon 9410 PhosphorImager analysis (Amersham Biosciences Corp., Piscataway, NJ, USA).

W. Statistical Methods

Comparative analysis among multiple experimental groups were done using a one-way analysis of variance (ANOVA) with Dunnett's test as a post-hoc analysis that compared specific group means (e.g. PMP-ligands, IGF-II, etc.) to a control group mean (medium + vehicle). Differences were considered significant at $P < 0.05$.

Chapter III

Exploitation of the Ligand-Binding Properties of the Mannose 6-Phosphate/Insulin-like Growth Factor II (IGF-II) Receptor to Inhibit IGF-II-Dependent Growth of Cancer Cells

The material covered in this chapter is the topic of the following article in preparation authored by:

Zavorka, M.E., Connelly, C.M, Grosely, R., and MacDonald, R.G.

A.   Summary

The M6P/IGF2R binds M6P-capped ligands and IGF-II at different binding sites within the EC domain and mediates ligand internalization and trafficking to the lysosome. Multivalent M6P-based ligands can cross-bridge the M6P/IGF2R which increases their rate of internalization, permitting IGF-II binding as a passenger ligand and subsequent trafficking to the lysosome, where the IGF-II is degraded. This unique feature of the receptor can be exploited to design novel therapeutic agents against IGF-II-dependent cancers that will lead to decreased bioavailable IGF-II within the tumor microenvironment. Our studies demonstrate that our bivalent M6P-based ligands bind to the M6P/IGF2R with high affinity and decrease growth of cancer cells by causing an accelerated increase of IGF-II internalization and degradation.

B.   Rationale

The main function of the M6P/IGF2R is in lysosomal biogenesis by transporting newly synthesized lysosomal enzymes and other M6P-capped glycoproteins from the TGN to the lysosome. Additionally, the receptor captures other glycosylated and non-glycosylated ligands from the cell surface and internalizing these ligands for transport to the lysosome for degradation. The M6P/IGF2R at the cell surface is constitutively internalized regardless of bound ligand (*6, 153, 160, 161*). However, it was noted that the homotetrametic lysosomal enzyme β-glucuroidase (hGUS), which has multiple M6P-capped oligosaccharides, increased the rate of internalization of receptor-bound IGF-II; this accelerated internalization was attributed to the multiple M6P glycosylations on the lysosomal enzyme that were able to cross-bridge the M6P-binding sites on M6P/IGF2R monomers, stabilizing the dimeric receptor. This dimerization of the M6P/IGF2R accelerates the rate of internalization of bound ligands 3-4-fold (*131*), although the exact

mechanism by which this occurs is unknown. Monovalent ligands for the M6P/IGF2R, such as M6P and IGF-II, are unable to produce this effect, supporting the hypothesis that dimerization or oligomerization of the M6P/IGF2R is important for rapid internalization, which monovalent ligands are unable to achieve. Moreover, the cellular repressor of E1A-stimulated genes (CREG), which is a secreted M6P-capped glycoprotein, can facilitate the internalization and disposal of IGF-II in the lysosome by regulating M6P/IGF2R; this caused a cell-cycle arrest in NIH 3T3 fibroblasts, human vascular smooth muscle cells, and a teratocarcinoma cell line, NTERA-2 (*228, 229, 311*). Altogether, these studies suggest that binding of multivalent M6P-capped ligands to the M6P/IGF2R enhances the receptor's rate of internalization of IGF-II leading to decreased cell growth/proliferation. Our hypothesis is that this functional activity of the M6P/IGF2R may be exploited to design novel treatments for IGF-II-dependent cancers. To our knowledge, there have not been any studies to directly test whether bi- or multivalent M6P-based ligands could enhance the internalization rate of M6P/IGF2R-IGF-II complex through direct binding of the M6P-binding sites that inhibits IGF-II-dependent growth of cancer cells.

Our laboratory has designed a panel of bi- and multidentate M6P-based ligands of decreasing molecular size and number of M6P moieties to evaluate their ligand-binding properties for the M6P/IGF2R. The aim of the current study was to assess the effect of these high-affinity, bivalent ligands on IGF-II-dependent cell growth and their ability to deplete IGF-II from the conditioned medium. The long-term goal of this project is to utilize these compounds as a potential therapeutic agent for the treatment of IGF-II-dependent cancers. Previously, two panels of phosphatase-resistant, M6P-based, bidentate compounds were synthesized, but none were able to bind the receptor with high affinity indicative of bivalency (*312, 313*). The lack of effectiveness of these ligands

has been attributed to the design, with insufficient distance between or improper orientation of the M6P groups to permit interaction with two M6P-binding sites on the receptor dimer simultaneously. Thus, we synthesized a panel of multidentate pentamannosyl 6-phosphate (PMP)-based pseudoglycoproteins and –peptides as proof-of-principle studies. This panel of PMP-ligands was designed to have decreasing molecular sizes and number of M6P moieties to determine the smallest possible M6P-based ligand that could achieve high-affinity, bivalent binding for the M6P/IGF2R, allowing for stabilization of the receptor dimer and accelerated internalization of IGF-II as a passenger ligand. One of the most important features of these ligands is that the protein and peptide scaffolds constrain the conformational flexibility of the PMP functional groups to allow more favorable orientation for binding to the receptor. Radioligand displacement analysis indicate that these PMP-ligands bound to the M6P/IGF2R with high affinity compared to the monovalent binding of M6P, indicating achievement of bivalent binding. Our cell growth studies suggest that these compounds can decrease IGF-II-dependent cell viability in a number of cancer cell lines. Additionally, this reduction of cell viability from PMP-ligand treatment can be attributed to the internalization and degradation of extracellular IGF-II, as evidenced by our ^{125}I-IGF-II degradation assays. The subsequent mechanism of growth suppression has not been definitively elucidated, but apoptosis, cell cycle arrest, and migration are all possible mechanisms that need to be investigated further. To our knowledge, we have designed the first panel of high-affinity, bivalent M6P-ligands for the M6P/IGF2 that can decrease IGF-II-dependent cell viability.

C.   Results

C.1.   Synthesis and purification of pentamannosyl 6-phosphate (PMP) ligands

We synthesized a panel of ligands varying in molecular size to determine the minimal size needed to achieve high-affinity binding in order to cross-bridge the receptor. Pentamannosyl 6-phosphate (PMP), derived from the yeast natural byproduct phosphomannan, was coupled by reductive amidation to protein scaffolds of different sizes as previously reported (*144, 152*).   PMP is hydrolyzed from *P. holsii* phosphomannan, and the PMP chain structure contains five mannose rings that are coupled through α(1,3) linkages, where the distal mannose ring (furthest from the reducing end) has a phosphate on the sixth carbon and the proximal two mannose rings are linked through an α(1,2) linkage (*300, 301*). The most proximal mannose ring is then coupled through the reducing end to any free amine group on the protein or peptide scaffold.

Our lab has coupled PMP to a panel of proteins consisting of albumin (PMP-BSA), ovalbumin (PMP-OVA), and insulin (PMP-INS). We have also chemically linked PMP to two tripeptides: lysyl-tyrosyl-lysine (PMP-KYK) and seryl-tyrosyl-lysine (PMP-SYK). After the coupling phase, the PMP-pseudoglycoproteins were purified by dialysis and analyzed by SDS-PAGE; Coomassie staining of the gels revealed that the purified products' molecular masses showed upward shifts corresponding to their predicted masses based on the known molecular masses of the core proteins and assuming 100% derivatization of PMP to bovine serum albumin (BSA), OVA, and INS (Table 3.1). The PMP-glycopeptides were purified by anion-exchange and size-exclusion chromatography to apparent homogeneity by the criterion of SDS-PAGE with Coomassie staining, and analyzed by MALDI-TOF mass spectrometry, which suggested

that the PMP-peptides were heterogeneous in size with mass differences corresponding

to differences in extent of derivatization by the PMP chains (data not shown).

PMP-ligand	Precursor	Predicted MW	Approximate PMP Groups
PMP-BSA	Bovine Serum Albumin	90,000	24
PMP-OVA	Chicken Egg Ovalbumin	58,000	13
PMP-INS	Bovine Insulin	8,800	3
PMP-KYK	Lysyl-Tyrosyl-Lysine	3,600	3
PMP-SYK	Seryl-Tyrosyl-Lysine	2,400	2

Table 3.1: PMP-pseudoglycoproteins and –peptides. The panel of PMP-ligands was designed to encompass a molecular size range to determine the smallest M6P-based ligand capable of high-affinity binding to the M6P/IGF2R. For BSA, ovalbumin and insulin, molecular weights (MW) were measured by migration on reducing SDS-PAGE. For the tripeptide conjugates, MW was estimated by MALDI-TOF mass spectrometry.

C.2.   Validation of PMP-Ligand binding to the M6P/IGF2R

The PMP-pseudoglycoproteins and peptides were validated for their ability to bind to the bovine M6P/IGF2R and characterized for their binding properties.   In previous studies, using radioligand displacement assays where ^{125}I-PMP-BSA used as the tracer, all PMP-ligands were able to bind to the soluble bovine M6P/IGF2R that was immobilized to Sepharose 4B resin. In this assay, a high concentration of M6P was able to competitively displace the PMP-ligands from the receptor with IC_{50} values in the nM range. M6P alone is used as a control for monovalent binding (with a K_D near 8 µM (*93*), while G6P is used as a negative control because the 2-hydroxyl group is in the equatorial state and prevents formation of a key hydrogen bond enabled by the axial state. Nevertheless, binding of PMP-OVA (Figure 3.1) as well as the other PMP-ligands (data not shown) exhibited a non-linear regression curve that shifted to the left, indicative of high-affinity, bivalent binding.   The IC50 and RBA values indicate that PMP-OVA binds with nM affinity similar to hGUS (Table 3.2).   These ligands produced affinity consistent with a bivalent mode of binding for the M6P/IGF2R that was similar but not quite as high as hGUS.

In order to produce bivalent binding, these ligands must cross-bridge the dimeric M6P/IGF2R. In a previous gel-shift assay done by Dr. Chris Connelly during his doctoral work, PMP-BSA was able to stabilize the dimeric, soluble M6P/IGF2R, as the molecular mass of the receptor shifted to a mass that was unable to be clearly resolved on the gel (data not shown). As PMP-BSA concentration increased, the amount of monomeric, soluble M6P/IGF2R decreased.   However, PMP-BSA did not shift the monomeric receptor to a dimeric form as well as hGUS (data not shown), indicating that hGUS may be more efficient at inducing dimerization while PMP-BSA is able to stabilize a pre-formed dimeric structure while having reduced ability to initiate dimerization.   Also of

note, hGUS has the preferred α(1,2) linkages between the distal and penultimate mannose rings while PMP-BSA has α(1,3) linkages that gives up some affinity for the receptor.

The pseudoglycoprotein ligand PMP-BSA shows a preference for binding to the M6P-binding site in domain 3, as indicated by mutagenesis and pull-down studies previously done by Dr. Connelly (data not shown). FLAG-tagged constructs bearing mutations in the M6P-binding sites or truncated forms of the receptor deleting M6P-binding sites (*128*) were designed to regulate the number of available M6P-binding sites per receptor. Using a FLAG-tagged pull-down approach, the binding of PMP-ligands to the receptor constructs was determined. PMP-OVA and PMP-SYK have preferential binding to domain 3 over domain 9, but each binds with lower affinity than the positive control natural ligand, hGUS. It is important to note that hGUS had some binding for domain 9 even though it primarily binds through domain 3, suggesting that hGUS may have a different binding mechanism than our PMP-ligands.

In order to determine if PMP-ligands can inhibit cell viability, we first determined the stability of the PMP-ligands in serum-containing medium. Our ligands are heavily phosphorylated, making them susceptible to phosphatase cleavage, which would render them incapable of altering cell viability due to their inability to bind the M6P/IGF2R. To validate that our ligands are stable throughout the duration of a multi-day cell culture experiment, we incubated radiolabeled PMP-BSA with different concentrations of serum-containing medium at 37 °C and compared ligand integrity at different time points to that of ^{125}I-PMP-BSA in a serum-free control (Figure 3.2). Aliquots taken over the course of this study were resolved on SDS-PAGE, and the gel was dried and analyzed by autoradiography. Over the course of 24 hours, the intensity and migration of ^{125}I-PMP-BSA was comparable to the 0 h time point of the serum-free control, indicating that our
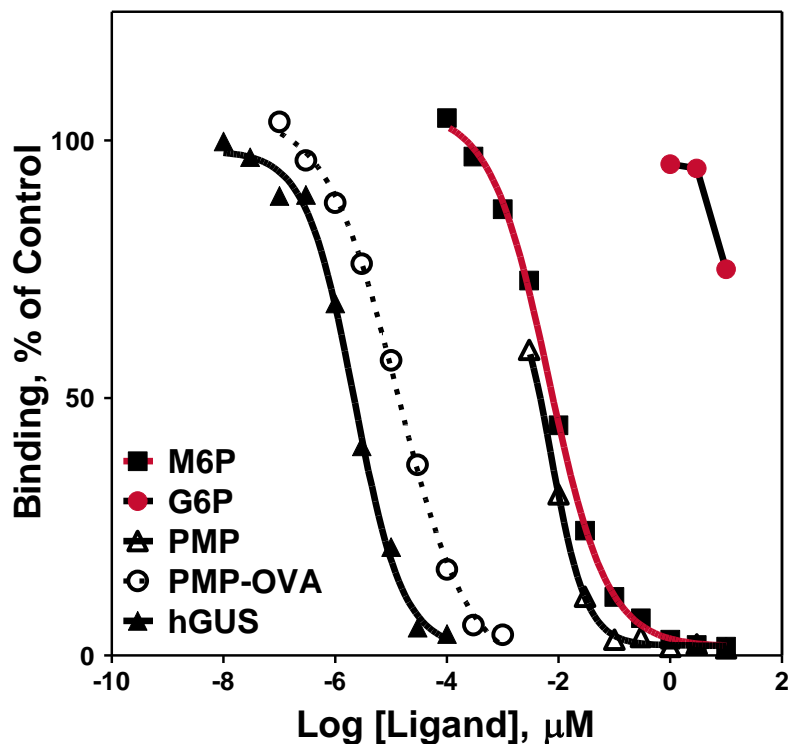
Figure 3.1. Competitive Binding Analysis of PMP and PMP-OVA in Displacement of PMP-BSA from M6P/IGF2R-Sepharose. M6P is the reference for monovalent, low-affinity binding. G6P is the negative control. hGUS is a reference for bivalent, high-affinity binding. PMP has the same low, monovalent binding affinity as M6P. PMP-OVA's shift to the left indicates higher affinity of this ligand and is a potential for bivalency. These data are representative of three replicate experiments; the binding parameters calculated from the data are shown in Table 3.2.

Ligand	IC_{50}^{a}, µM (n)	RBA^{b}
M6P	4.6 ± 0.99 (3)	1
G6P	> 10,000 (3)	N.A.
PMP	7.5 (1)	0.62
PMP-OVA	0.015 ± .011 (3)	620 ± 155
hGUS	.002 (1)	1643

Table 3.2: Binding Properties of PMP-Ligands for M6P/IGF2R.

a. IC_{50} values for competitive displacement of radiolabeled PMP-BSA from the receptor (n = # of trials). b. RBA = relative binding affinity, normalized to free M6P.

PMP-ligands are stable in conditions that mimic those that would be used in cell culture experiments. To determine whether the stability of the radioligand declines with time following incubation with cells, Capan-1 (human pancreatic adenocarcinoma cell line) cells were incubated with 400,000 cpm ^{125}I-PMP-BSA under reduced (1%) serum conditions for up to 48 h. Aliquots of the conditioned medium at different time points were then immobilized in a soluble M6P/IGF2R-Sepharose 4B assay with or without 5 mM M6P, which competitively displaces the ^{125}I-PMP-BSA, and then the radioactivity was counted on a gamma counter (Figure 3.2). At the 1-h time point, some of the radioactive counts were absent from the conditioned medium, indicating that some of the ligand was internalized. After 6 hours, the internalization appeared to stabilize with only a slow decrease in counts throughout the 48-h assay. The addition of M6P to the pull-down assay displaced the radioactive counts, indicating that the assay was indeed pulling down the ^{125}I-PMP-BSA ligand. Thus, we concluded that our ligand is stable for at least 48 h *in vitro*.

C.3.   PMP-ligands decrease viability of cells in culture

Our laboratory previously used a short-term growth assay to determine whether the high-affinity binding of the PMP-ligands to the M6P/IGF2R can induce cytotoxic effects similar to those observed with CREG. A mouse L-cell fibroblast cell line that stably over-expressed wild-type bovine M6P/IGF2R was used, since this cell line was also used by York *et al.* to demonstrate that multivalent M6P-ligands induce rapid uptake of IGF-II by the M6P/IGF2R (*131*). In Dr. Chris Connelly's doctoral work, mouse L-cells incubated with as little as 10 nM PMP-OVA or PMP-SYK had a significant inhibition of cell viability over a 4-day time course. M6P up to a concentration of 10 mM did not produce an effect on its own, but when it was added to the PMP-ligand

Figure 3.2: Resistance of PMP-ligands to degradation. A) ^{125}I-PMP-OVA was added to serum containing medium or serum-free (SF) medium for up to 24 h. Aliquots were resolved by SDS-PAGE. PMP-OVA was stable in serum-containing medium for up to 24 h, as degradation of the radioactive material was not seen in this cell-free assay. B) Mouse L-cells were incubated with ^{125}I-PMP-BSA for up to 48 h. Aliquots of the conditioned medium were taken at the indicated time points and subjected to a sM6P/IGF2R-Sepharose 4B pull-down to determine the amount of radioactive counts able to bind the resin. M6P (10 mM) was used to competitively displace the ^{125}I-PMP-BSA to determine the amount of radioactive counts contributing to specific M6P-based binding to the immobilized receptor, which indicates the integrity of the PMP-ligand following incubation with cells.
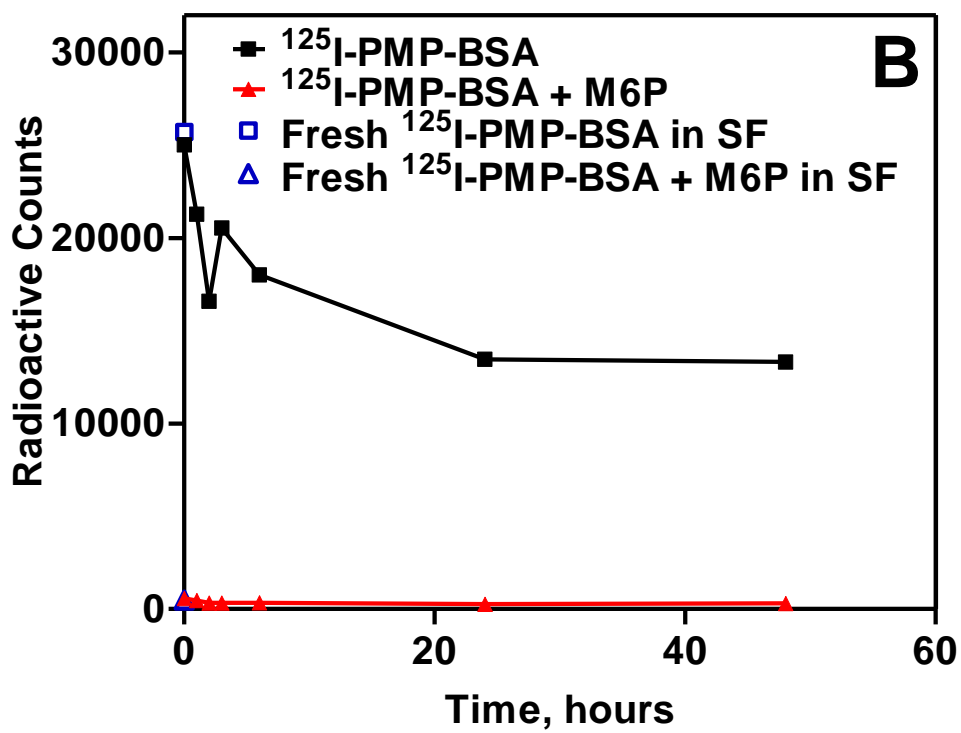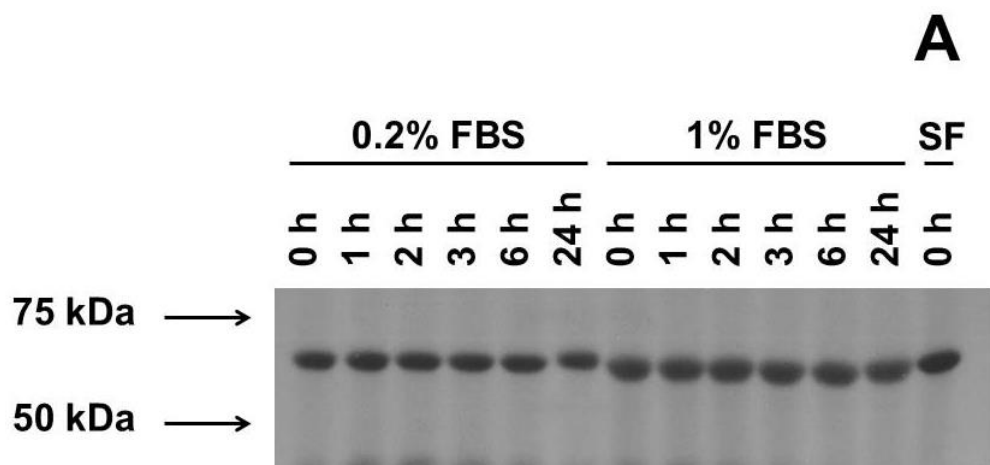
treatment, it was able to rescue the reduction on cell viability due to competitive displacement of the bivalent ligand. This indicated that the PMP-ligands were binding to the M6P/IGF2R in a M6P-dependent manner. It is hypothesized that these PMP-ligands function by depleting excess IGF-II from the cell milieu by way of the M6P/IGF2R. In the mouse L-cells, 10 nM IGF-II slightly increased the cell viability, but this growth factor was able to completely rescue the decrease in cell viability back to the level of the control. Therefore, decreased cell viability caused by the PMP-ligands is both a M6P- and IGF-II-dependent phenomenon.

Mouse L-cells were utilized for these proof-of-principle studies due to their high over-expression of the M6P/IGF2R. Given our long-term goals for the use of these ligands, various human cancer cell lines were used as more relevant models to study the PMP-ligand effects. Hepatocellular carcinoma (HuH-7) and choriocarcinoma (JEG-3) cells were initially used as several studies demonstrated that these cell lines express all the requisite components of the IGF-axis as well as exhibit an IGF-II-driven autocrine loop (*264, 274, 314*). Previous work by Dr. Connelly demonstrated that these two cancer cell lines responded to the PMP-ligand treatment in the same manner as the L-cells (data not shown). PMP-OVA at a concentration of 200 nM was able to significantly reduce the cell viability, and addition of 10 mM M6P reversed the effects. However, it was necessary to increase the concentration of PMP-ligands 20-fold higher than what was needed in the mouse L-cells in order to see a significant inhibition of cell viability in HuH-7 and JEG-3 cells. This may be due to the fact that the mouse L-cells have a higher concentration of M6P/IGF2R on the cell surface than the cancer cell lines or that the mouse L-cells do not produce as much IGF-II acting in an autocrine loop as the cancer cells.

We next wanted to validate the activity of our PMP-ligands in various types of cancer cell lines to determine if our ligand is effective in treating these cancers. Our lab determined through western blotting the expression of M6P/IGF2R in multiple cancer cell lines (Figure 3.3). Additionally, two well-differentiated adenocarcinoma cell lines, S2-013 and Capan-1 (*315*) expressed the receptor well. Dr. Connelly determined through RT-PCR that S2-013 cells express high levels of IGF-II, but Capan-1 cells express very little to no IGF-II (data not shown).This would provide both autocrine and paracrine loop model systems for our studies. Both pancreatic cancer cell lines responded well to IGF-II and -I, with increased cell viability in response to as little as 0.01 nM IGF-II. Using soluble M6P/IGF2R as an IGF-II ligand-trap, S2-013 did not show a decrease in cell viability, indicating that this cell line produces enough IGF-II to overcome the trap or that the growth factor may be working in an intracrine fashion, i.e. not fully released into the milieu before being recaptured by the cell, that a ligand-trap did not affect the cell growth. In contrast, Capan-1 had a moderate decrease in cell viability when treated with soluble M6P/IGF2R over a five-day assay (Figure 3.4). These data suggest that Capan-1, which relies on the IGF-II in the medium, has some dependency on IGF-II for growth, but this cell line is not solely dependent on the IGF-II pathway for mitogenesis and survival. Accordingly, treating Capan-1 with 50 nM PMP-OVA revealed a moderate decrease in cell viability, not quite to the extent as the ligand-trap (Figure 3.4). Furthermore, the PMP-OVA treatment did not affect the cell viability of S2-013 cells, similar to the soluble M6P/IGF2R treatment.
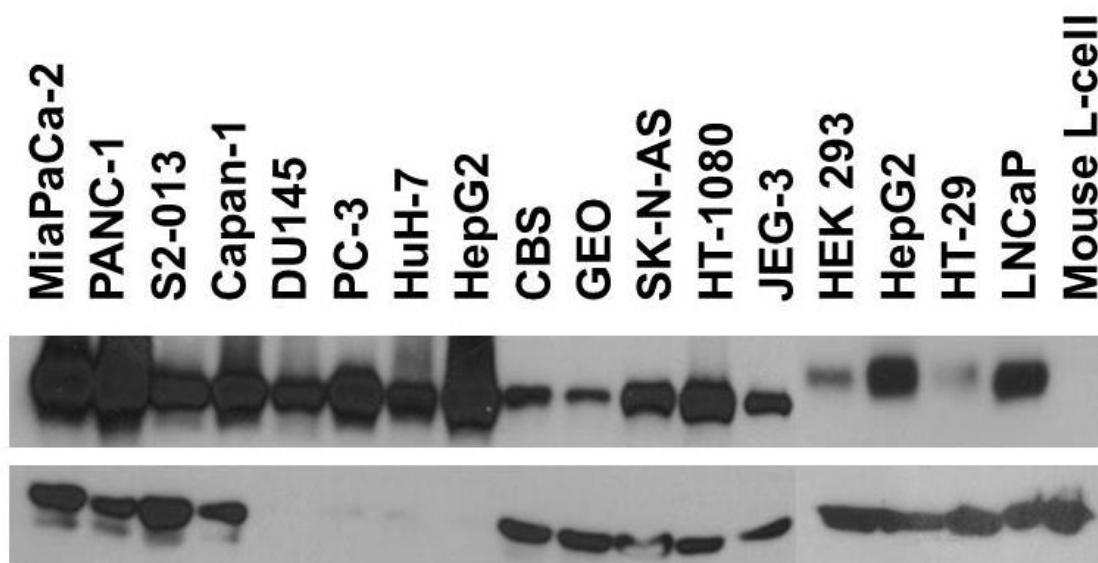
Figure 3.3: M6P/IGF2R expression by cancer cell lines. A) Lysates of various cancer cell lines were subjected to SDS-PAGE and immunoblot analysis, probing with α-CD222 antibody. Pancreatic cancer cell lines: MiaPaCa-2, PANC-1, S2-013, Capan-1; prostate cancer cell lines: DU145, PC-3, LNCaP; hepatocellular carcinoma cell lines: HuH-7, HepG2; colon cancer cell lines: CBS, GEO, HT-29; neuroblastoma cell line: SK-N-AS; fibrosarcoma cell line: HT-1080, choriocarcinoma cell line: JEG-3; human embryonic kidney cells: HEK 293; mouse L-cells are a kidney fibroblast cell line. Notice that our stable human M6P/IGF2R expression cell line (mouse L-cell) had lost the expression of the receptor, which explains why subsequent experiments using this cell line failed.
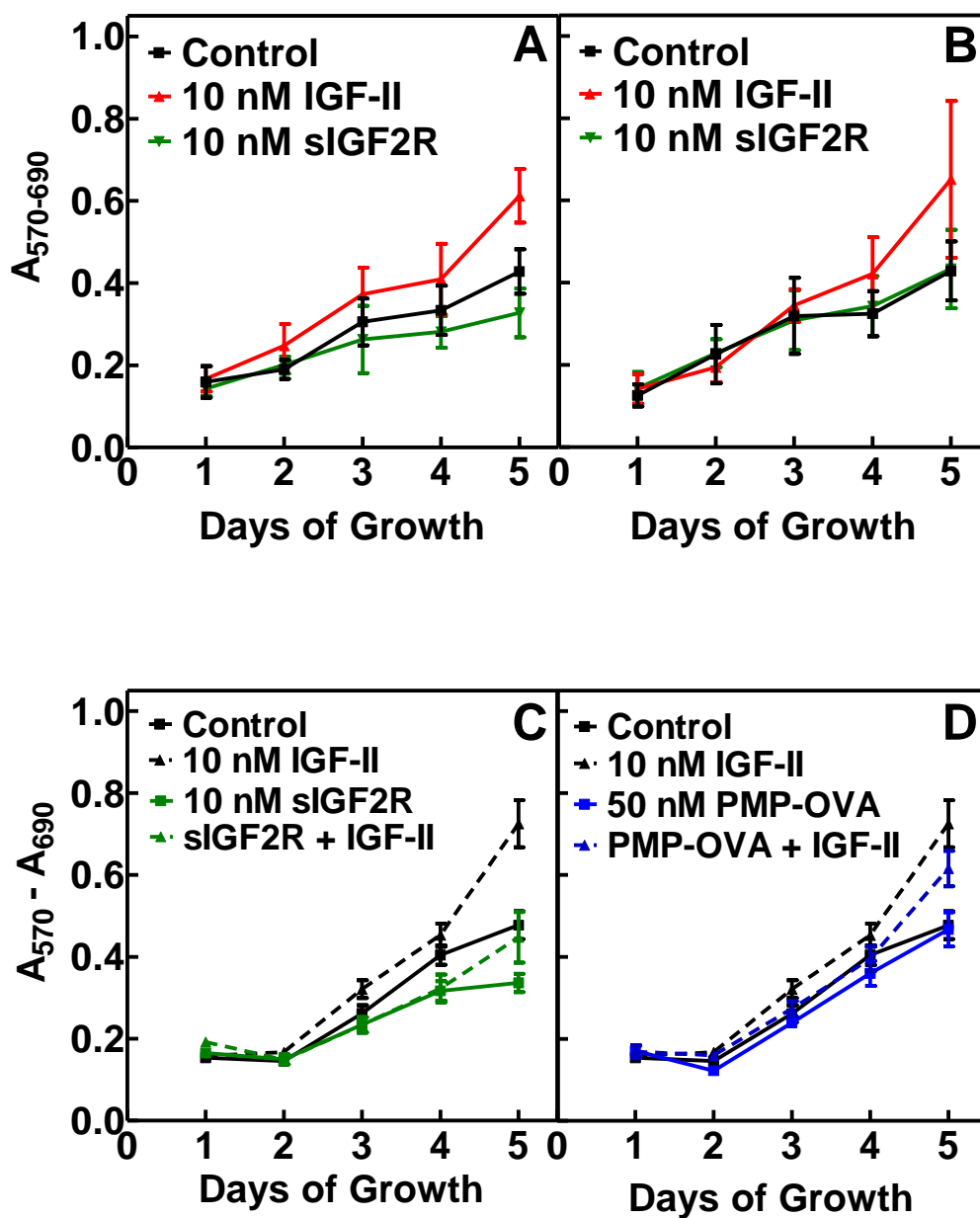
Figure 3.4: Inhibition of pancreatic cancer cell growth by multivalent M6P-based ligands. A) Capan-1 and B) S2-013 were differentially responsive to IGF-II and the IGF-II ligand trap, sIGF2R (sM6P/IGF2R). Capan-1 grew better in response to IGF-II than S2-013, and this growth was inhibited by sequestering IGF-II. C) IGF-II was able to partially rescue the growth inhibition effect caused by soluble M6P/IGF2R. D) PMP-OVA inhibits the IGF-II-dependent growth of Capan-1 cells, which is rescued by the addition of exogenous IGF-II.

We next wanted to determine whether other pancreatic cancer cells could be targeted by our PMP-ligands. The moderately poorly differentiated pancreatic carcinoma cell lines MiaPaCa-2 and PANC-1 were used to lend further support to the use of our ligands against pancreatic cancer. These two cell lines did not respond to IGF-II and soluble M6P/IGF2R functioning as a ligand trap, indicating that these cell lines are not IGF-dependent and would not be good models for our studies.

We next expanded our studies outside of the digestive tract (i.e., liver and pancreas) and focused on another major cancer type, prostate. DU145, a moderately differentiated prostate carcinoma cell line, was used as a representative prostate cancer cell line, as it has been shown to be IGF-II-responsive and express the necessary components of the IGF axis (*178*). Prostate cancer has a relatively high overall five-year survival rate, yet it is still the second-leading cause of cancer death in men, according to the American Cancer Society. In the early stages of prostate cancer progression, the prostate cancer cells are dependent on androgen and express the androgen receptor (*316*), which allows androgen-deprivation therapy to be an effective treatment option. However, many patients progress to a castration-resistant prostate cancer, which leads to over-activation of the androgen receptor (AR)-dependent pathway and further drives metastasis. The IGF-axis may play a role in the progression of prostate cancer following androgen-deprivation therapy (*317*). Therefore, we were interested in knowing if our PMP-ligands can inhibit prostate cancer cell growth and serve as a potential therapeutic agent for advanced forms of prostate cancer. DU145 cells do not express AR and thus may serve as castration-resistant prostate cancer cell line. DU145 responded moderately well to PMP-OVA treatment (data not shown). PMP-ligands may decrease cell viability in prostate cancer cells that are dependent on IGF-II.

The IGF-axis is highly expressed in the developing and mature central nervous system. The IGFs are important in neurodevelopment and neuroprotection (*318*). However, it is also known that IGF-II is a major autocrine contributor to neuroblastoma growth and promotes resistance to retinoic acid (RA), a metabolite of vitamin A that functions through RA receptors to modulate transcription of genes and is a known neuronal differentiation molecule (*319*). We thus utilized the embryonal neuroblastoma cell line, SK-N-AS, to determine if PMP-ligands can also function in this system. This poorly differentiated cancer cell line expresses all of the major components of the IGF-axis (IGF-II, IGF1R, and M6P/IGF2R), including IGF-II functioning in an autocrine loop (*203*). SK-N-AS cells were slightly, but not significantly, sensitive to the PMP-OVA treatment at 100 nM concentration. Additionally, the cell lines that we have tested are summarized in Table 3.3.

Taken together, these data may suggest that our ligands function best in well-differentiated IGF-II-dependent cancer cells, with the most prominent response being a cancer that is easily accessible through the bloodstream, in which the tumor has high expression of the M6P/IGF2R, such as hepatocellular carcinoma. However, our PMP-ligands are not limited to this type of cancer, as it proved effective on many types of cancer that are responsive to IGF-II.

Cell Line	Cancer Type	Differentiation	Ligand Trap Response
Capan-1	Pancreatic	WD	++
S2-013	Pancreatic	WD	-
MiaPaCa-2	Pancreatic	PD-MD	-
PANC-1	Pancreatic	PD	-
HuH-7	Hepatocellular	WD	++
JEG-3	Choriocarcinoma	WD	++
DU145	Prostate	MD	+
SK-N-AS	Neuroblastoma	PD	+

Table 3.3: Comparison of cancer cell lines and their response to ligand trap (sM6P/IGF2R) or PMP-ligand treatment. The cell lines from different sources had a different response to the ligand trap (sM6P/IGF2R) or PMP-ligand treatment as indicated by -, no response; +, mild response; ++, moderate response. Abbreviations: WD, well differentiated; MD, moderately differentiated; PD, poorly differentiated.

C.4.   PMP-ligands decreased IGF-II in the conditioned medium of cancer cells

Since the effect of PMP-ligands on cells is M6P-dependent, indicating that the PMP-ligands bind to the M6P/IGF2R through a M6P-binding site, and IGF-II-dependent as indicated by add-back of IGF-II, which rescues the effect, we hypothesized that the PMP-ligands work to deplete IGF-II from the medium. To detect the low concentrations of IGF-II in the conditioned medium, we employed many approaches until we were able to achieve the highest sensitivity to detect minute differences in the level of IGF-II among media conditioned by cells from different treatment groups.

Capan-1, S2-013, and HuH-7 cells were treated with 10 nM IGF-II or the vehicle control, HBS (HEPES buffered saline). Conditioned medium (CM) was collected 72 hours after treatment and proteins were separated under reducing conditions on 15% or 8-16% SDS-PAGE gels and then immunoblotted with rabbit αIGF-II antibody. The sensitivity of the αIGF-II antibody was estimated to be about 3.75 ng based on detection of recombinant IGF-II from a serial dilution that was electrophoresed without being exposed to cells (Figure 3.5A), but was not sensitive enough to directly detect IGF-II in the conditioned medium after exposure to Capan-1, S2-013, or HuH-7 cells (data not shown). The samples were then concentrated 16-fold using ultracentrifugation, which improved electrophoresis by eliminating salts. However, there was only about a 50% recovery of the IGF-II from the centrifugal concentrators as determined by immunoblotting of an internal control using the αIGF-II antibody (Figure 3.5B). Recovery was not improved following washes with a salt-free Tris-EDTA buffer (data not shown). Fresh CM from the cells was then concentrated via lyophilization, which worsened the electrophoretic separation causing smearing of the proteins. Again, the antibody was not sensitive enough to detect differences in the IGF-II from the concentrated CM. Continuing with this immunoblotting approach, we next attempted to detect IGF-II via the
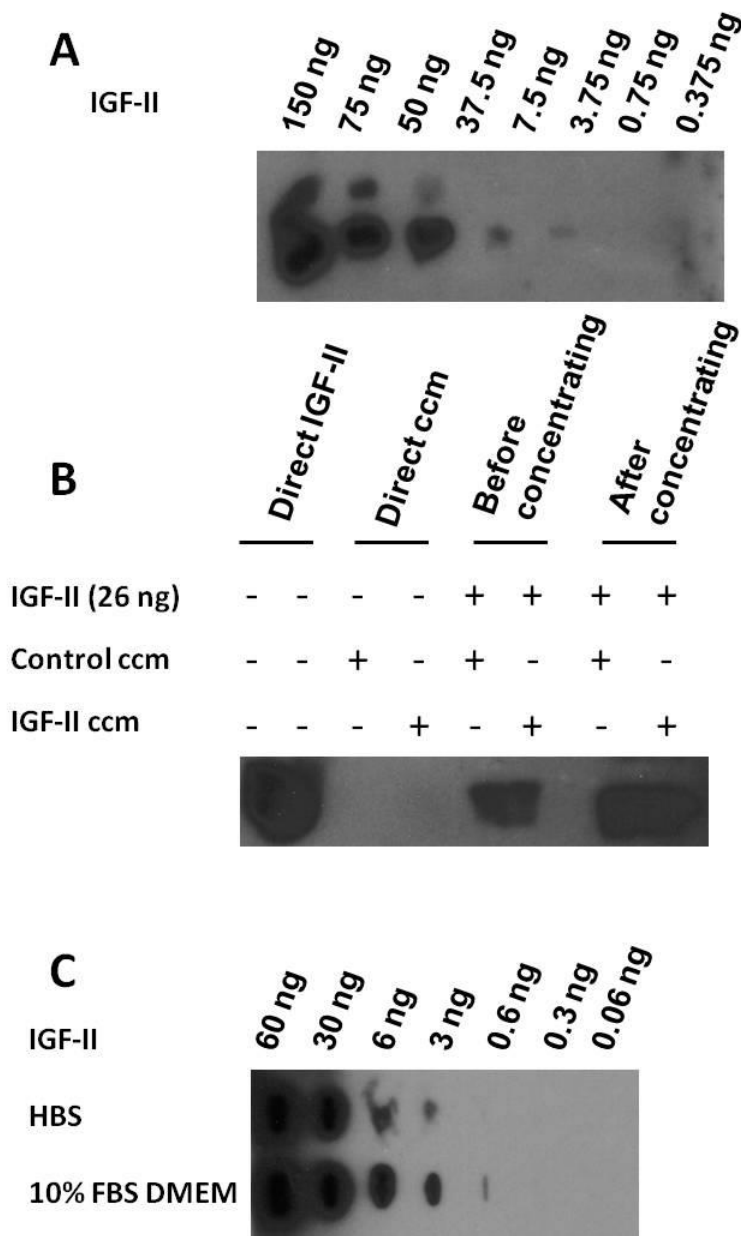
Figure 3.5: Detection of IGF-II through immunoblot and dot blot analysis. A) A standard curve for IGF-II was made by SDS-PAGE and immunoblotting with an αIGF-II antibody, where the lowest detection limited achieved was 3.75 ng. B) The amount of IGF-II recovered from conditioned medium by concentration using centrifugal filters was determined by spiking IGF-II before or after concentrating. There was less than 50% recovery from the concentrators. C) Dot blot analysis of decreasing cold carrier IGF-II and ^{125}I-IGF-II in serial dilutions in either HBS or 10% FBS DMEM as a carrier. The lowest detection limit was 0.6 ng in the 10% FBS DMEM and 3 ng in the HBS samples.

dot blot method. We estimated that IGF-II detection was in the range of 0.6-3 ng using radiolabeled IGF-II as an internal control, with only a 30% recovery of ^{125}I-IGF-II in 10% serum-containing medium that was not exposed to cells (Figure 3.5C). Using CM from cells, the amount of IGF-II was undetected, indicating that this approach was not sensitive enough (data not shown). This may be due to the prevalence of too many proteins adhering to the nitrocellulose membrane, reducing the possibility of IGF-II to bind. We then needed to find an alternative detection method with high sensitivity.

We next tried to concentrate and partially purify aliquots of 3% serum-containing medium spiked with 500,000 cpm ^{125}I-IGF-II using a trichloroacetic acid (TCA) protein precipitation followed by electrophoresis and immunoblotting. Unfortunately, this did not work either, as the TCA could not be removed from the protein pellet even with acetone washing, and subsequent electrophoresis of the re-dissolved proteins was impossible (data not shown).

To improve detection of IGF-II, we miniaturized a chromatographic purification procedure followed by radioimmunoprecipitation assay (RIA) as previously done by Park *et al.* with some modifications (*307*). Fresh 1% serum-containing medium was lyophilized and reconstituted in 1 M acetic acid and run through a BioGel P10 gel filtration column using a 0.1 M acetic acid mobile phase. Fractions were collected for 2 min per tube and protein concentration was analyzed using the absorbance at 280 nm. After conditioning the column for several runs, radiolabeled IGF-II with unlabeled IGF-II carrier was fractionated. IGF-II consistently eluted between fractions 17-24 from this column (Figure 3.6A). In subsequent experiments, these pooled fractions were lyophilized and reconstituted in 1 M HCl before IGF-II concentrations were determined via radioimmunoassay (RIA). These experiments indicated that our sensitivity in this assay was 1.5 ng with a 60% recovery (Figure 3.6B). For detection of IGF-II in the

Figure 3.6: IGF-II concentration determined by size exclusion chromatography and ^{125}I-IGF-II RIA. A) The bulk protein eluted from the size exclusion column fractionated into two predominant peaks: large, excluded proteins in fractions 7-10 and small, included proteins in fractions 30-40 as indicated in the blue line. ^{125}I-IGF-II was used to determine the fractions in which IGF-II elutes, which was in fractions 17-24. The peak before and the peak after the ^{125}I-IGF-II represent components of the IGF-II preparation, radiolabeled BSA and degraded fragments, respectively. B) ^{125}I-IGF-II RIA determined that amount of IGF-II recovered in the assay using medium spiked with 50-150 ng of cold IGF-II and 0.3 nM ^{125}I-IGF-II. C) The ^{125}I-IGF-II RIA was too insensitive and inconsistent to detect small changes in IGF-II levels in conditioned medium (CM).
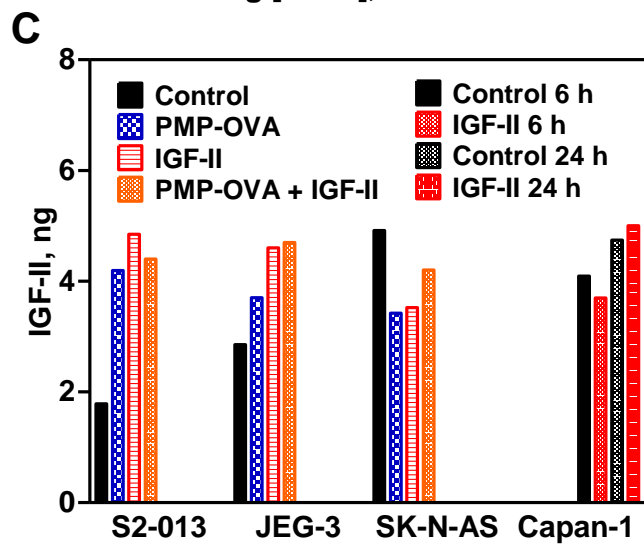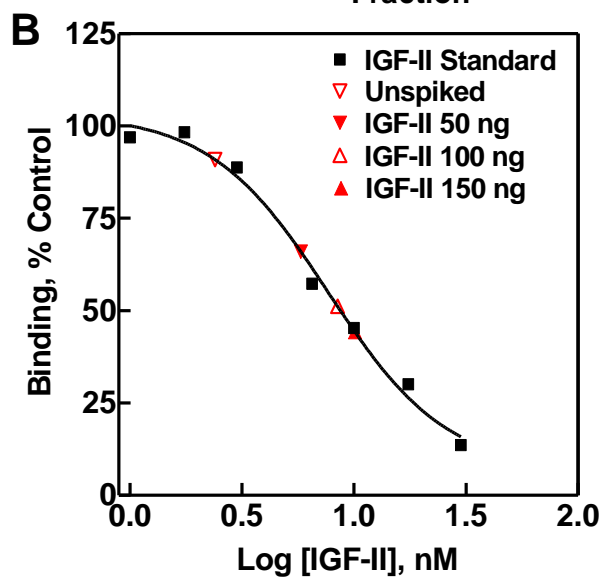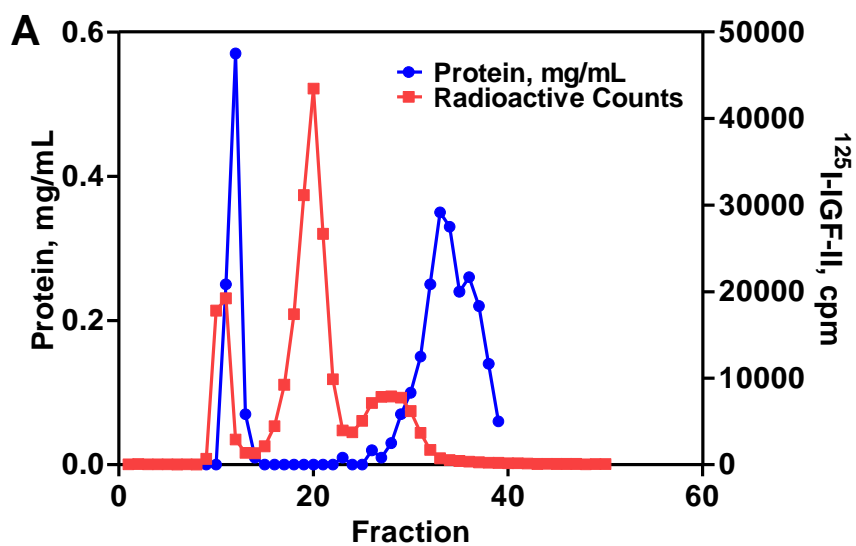
conditioned media of cells, Capan-1, SK-N-AS and JEG-3 cells were seeded in 6-cm dishes and treated with 200 nM PMP-OVA, 10 nM IGF-II, 200 nM PMP-OVA + 10 nM IGF-II, or vehicle control (HBS). After 24 h, the conditioned media were collected and lyophilized. IGF-II in the samples was determined following the aforementioned column fractionation protocol. All treatment conditions produced IGF-II values that were well within the IGF-II RIA standard range of detection, but were all comparable (Figure 3.6C). Temporal studies in Capan-1 and JEG-3 revealed that this assay was again not sensitive enough to detect the differences, if any, in the very low IGF-II concentrations in the CM.

Han *et al.* were able to see internalization of IGF-II with overexpression of CREG in human vascular smooth muscle cells, using a mouse IGF-II ELISA kit (*231*). Furthermore, knock-down of CREG or blocking the ability of IGF-II to bind to the M6P/IGF2R using neutralizing antibodies reversed the IGF-II internalization effect. However, Han *et al.* did not do the key experiment to demonstrate that CREG is decreasing IGF-II in the medium by binding to the M6P/IGF2R through a M6P-based mechanism that is displaceable with M6P. Knowing that we had not yet achieved an assay sensitive enough to detect minute differences in IGF-II in the conditioned medium of cultured cells, we decided to take an indirect internalization yet direct degradation of IGF-II assay approach. We added ^{125}I-IGF-II tracer to the low-serum (3%) growth medium at time zero of the treatment period, and then tracked recovery in the conditioned medium for up to 72 h by counting the TCA-soluble and insoluble radioactive material remaining in the conditioned medium over time. Intact IGF-II precipitates when the CM is treated with 46% TCA while any low-molecular weight (degraded) radiolabeled fragments of IGF-II are recovered in the supernatant. The rationale behind this approach is that M6P/IGF2R-mediated uptake of the labeled IGF-II by cells followed by

intracellular ligand degradation would tend to deplete the intact IGF-II from CM and increase the amount of radiolabeled breakdown products released.

To test this approach, SK-N-AS, HuH-7 and Capan-1 cells were grown in 24-well plates until near confluency. The treatments were initiated by adding low-serum medium supplemented with 0.3 nM ^{125}I-IGF-II and 1 nM cold carrier IGF-II. Cells were treated with 50-100 nM PMP-OVA, 100 or 200 nM IGF-II, 10 mM M6P, 50 nM sM6P/IGF2R, combinations of the treatments, or vehicle control HBS. Aliquots were taken at 0, 6, 24, 48, and 72 h time points. The purpose of adding the cold carrier IGF-II was two-fold: 1) it served to block binding of the radiolabeled IGF-II to binding proteins and non-specific extracellular binding surfaces and proteins, such as vitronectin (*308*) and 2) to simulate a reasonable concentration of pericellular IGF-II as might be encountered *in vivo*. Additionally, we increased the concentration of IGF-II to 100-200 nM in the treatment groups in order to function as a negative control to completely displace the radiolabeled IGF-II from the receptor, thereby increasing the amount of ^{125}I-IGF-II in the insoluble pellet (intact ^{125}I-IGF-II). From our results we were able to indirectly detect internalization of ^{125}I-IGF-II from the CM and directly detect degradation of the radiolabled growth factor in all cell lines tested, including HuH-7, Capan-1, SK-N-AS, JEG-3, and S2-013. The ^{125}I-IGF-II was internalized, degraded, and secreted back into the conditioned medium at a steady rate over the course of the assay as seen by a time-dependent increase in radioactive counts in the TCA supernatant and a corresponding decrease of counts in the TCA pellet in HuH-7 cells (Figure 3.7A). With the addition of PMP-OVA, there was an increase in IGF-II internalization as indicated by a sharp drop in the amount of TCA-precipitable IGF-II compared to the control after 2-3 days of incubation with the PMP-OVA. Additionally, there was a more pronounced increase of radioactive material in the TCA supernatant (degraded IGF-II) when PMP-OVA was

added to the cells. Interestingly, the overwhelming concentration of IGF-II (100-200 nM) behaved similarly to the control instead of protecting the ^{125}I-IGF-II from degradation. However, when PMP-OVA and IGF-II are co-incubated, the multivalent M6P-based ligand is able to further promote IGF-II internalization and degradation, although not as strongly as the PMP-OVA alone. Furthermore, M6P and sM6P/IGF2R partially inhibited PMP-OVA's effect on internalization of the ^{125}I-IGF-II. In all treatment groups throughout the course of the assay, the radioactive material in the TCA supernatant and pellet yielded approximately an 80-100% recovery in amount of total cpm added to the assay (Table 3.3). Therefore, from our ^{125}I-IGF-II internalization assay, we can conclude that PMP-ligands are able to bind to the M6P/IGF2R and promote internalization and degradation of extracellular IGF-II as a passenger ligand.

Figure 3.7: Precipitation of ^{125}I-IGF-II from CM by trichloroacetic acid (TCA). HuH-7 cells were seeded into 24-well plates in complete medium and allowed to attach for 24 h before switching to reduced-serum medium supplemented with the various treatments plus 0.3 nM ^{125}I-IGF-II and 1 nM cold carrier IGF-II. The treatments were: IGF-II (100 nM), PMP-OVA (100 nM) ± IGF-II (100 nM), or vehicle control. At the indicated times, aliquots of the conditioned medium were treated with TCA (46% final concentration). After incubation on ice for 1 h, the samples were centrifuged and the amounts of radioactivity recovered in the pellet and supernatant fractions were measured. A) These data were converted to percent recovery based on input radioactive IGF-II and plotted as indicated. PMP-OVA treatment caused a significant increase radioactive material in the soluble fraction and a significant decrease in that of the insoluble fraction at both 24 h and 48 h compared to the control at 24 h and 48 h. Data represent mean ± SEM (n=4); *, $P<0.001$. B) The ratio of the TCA-soluble to TCA-insoluble radioactive material recovered at each time point was calculated and plotted vs. time for each treatment group. Data represent mean ± SEM (n=3); *, $P<0.01$.
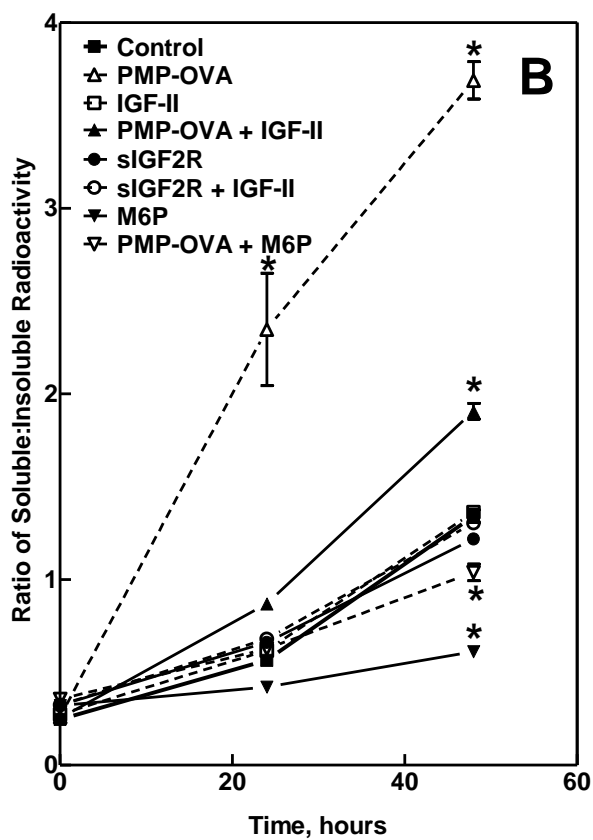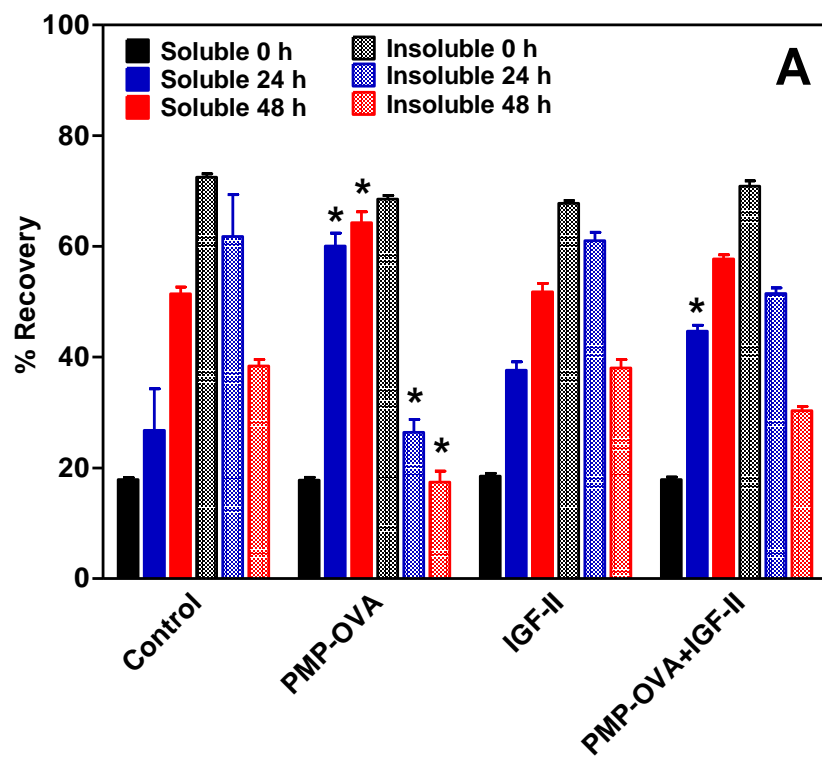
Time Point	% Recovery, Soluble	% Recovery, Insoluble
0 h	19.0	70.1
24 h	21.6	69.8
48 h	22.4	69.5
72 h	23.4	66.2

Table 3.3: Percentage of precipitable ^{125}I-IGF-II in medium over the course of the ^{125}I-IGF-II degradation assay. The soluble fraction is the TCA supernatant (degraded IGF-II). The insoluble fraction is the TCA precipitated protein (intact IGF-II). Medium was incubated in dishes and was not exposed to cells to determine the stability of the ^{125}I-IGF-II over the course of the study. Since cells are not present to degrade the ^{125}I-IGF-II, the percent recovery of the radioligand from each fraction remained constant. Thus, we are able to determine the amount of radioactive counts that are attributed to ^{125}I-IGF-II and not radioactive background.

C.5.   PMP-ligand effect on apoptosis in cancer cells

Upon activation of the IGF1R or hybrid of IGF1R/IR-A via IGF-II binding, several different downstream signaling pathways can become activated. One such final end-state effect mediated through the PI3K/Akt survival pathway is decreased apoptosis, or programmed cell death. To determine if PMP-ligands stimulate apoptosis due to IGF-II depletion, we performed a series of apoptotic studies. Capan-1 and S2-013 pancreatic cancer cell lines and SK-N-AS neuroblastoma cells were seeded into 24-well plates and treated with 100 nM PMP-OVA, 10 nM IGF-II, PMP-OVA + IGF-II, or vehicle control HBS. A set of wells was also treated with 400 µM palmitic acid as a positive control for apoptosis (*320*). After 24 or 48 hours, cells were treated with DAPI, a fluorescent stain that binds A-T-rich regions of DNA, and tends to accumulate to a higher concentration indicated by increased fluorescence intensity in cells undergoing apoptosis (*321, 322*). Apoptotic and total cells were counted manually under fluorescence microscopy. Capan-1 cells treated with 100 nM PMP-OVA exhibited about a 5-fold higher number of apoptotic nuclei compared to the control (Figure 3.8A and 3.8C). The addition of 10 nM IGF-II eliminated the increase in apoptosis back to the level of the vehicle control, while IGF-II on its own had fewer apoptotic nuclei than the control. S2-013 cells had an overall similar response as the Capan-1 cells, with a 2.5-fold increase in apoptotic nuclei over the control in the PMP-OVA treatment and a slight but non-significant decrease in IGF-II-treated cells (Figure 3.8B and 3.8C). The SK-N-AS cells had a higher resting number of apoptotic nuclei per 100 cells than the other cell lines, yet PMP-OVA increased the number of apoptotic nuclei approximately 3-fold compared to the control. The IGF-II-treated cells had a non-significant reduction in apoptotic nuclei while the add-back of IGF-II again rescued PMP-OVA's pro-apoptotic response (Figure 3.8B and 3.8C). The ability of M6P to rescue this effect of the PMP-ligands was not tested with this design.

A

	24h		48h	
	DAPI	Phase Contrast	DAPI	Phase Contrast

Control

PMP-OVA

IGF-II

PMP-OVA +
IGF-II

B

	SK-N-AS 24h		S2-013 24h	
	DAPI	Phase Contrast	DAPI	Phase Contrast

Control

PMP-OVA
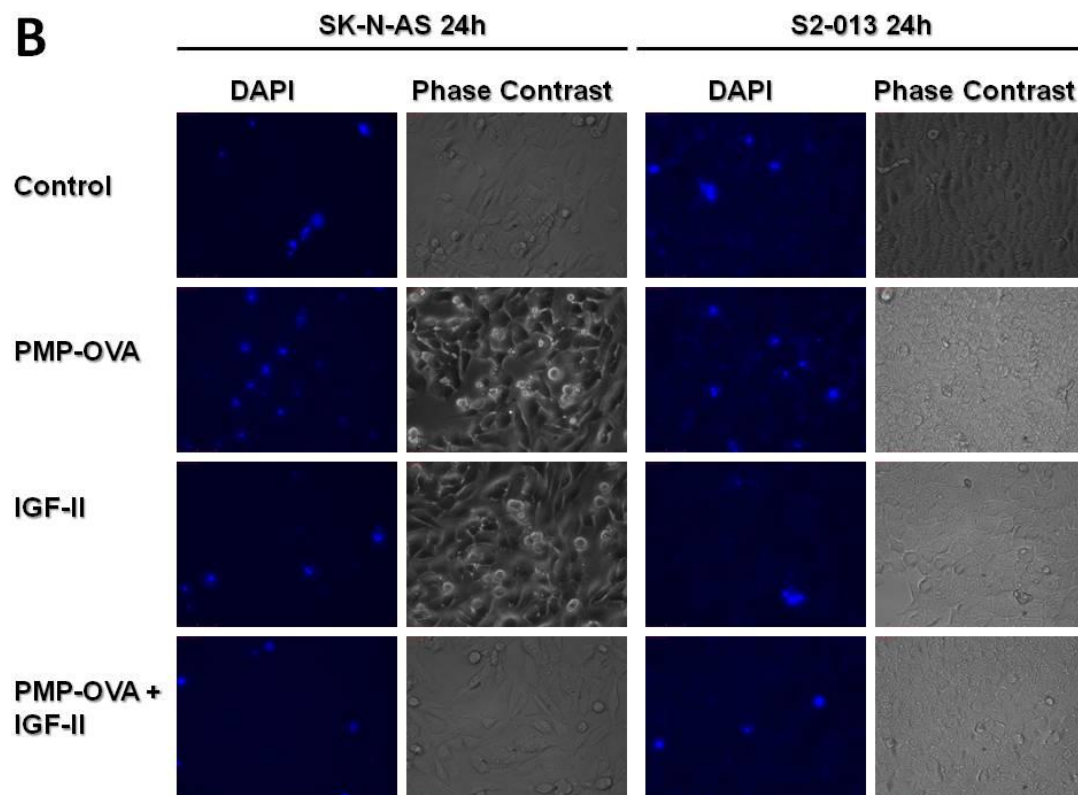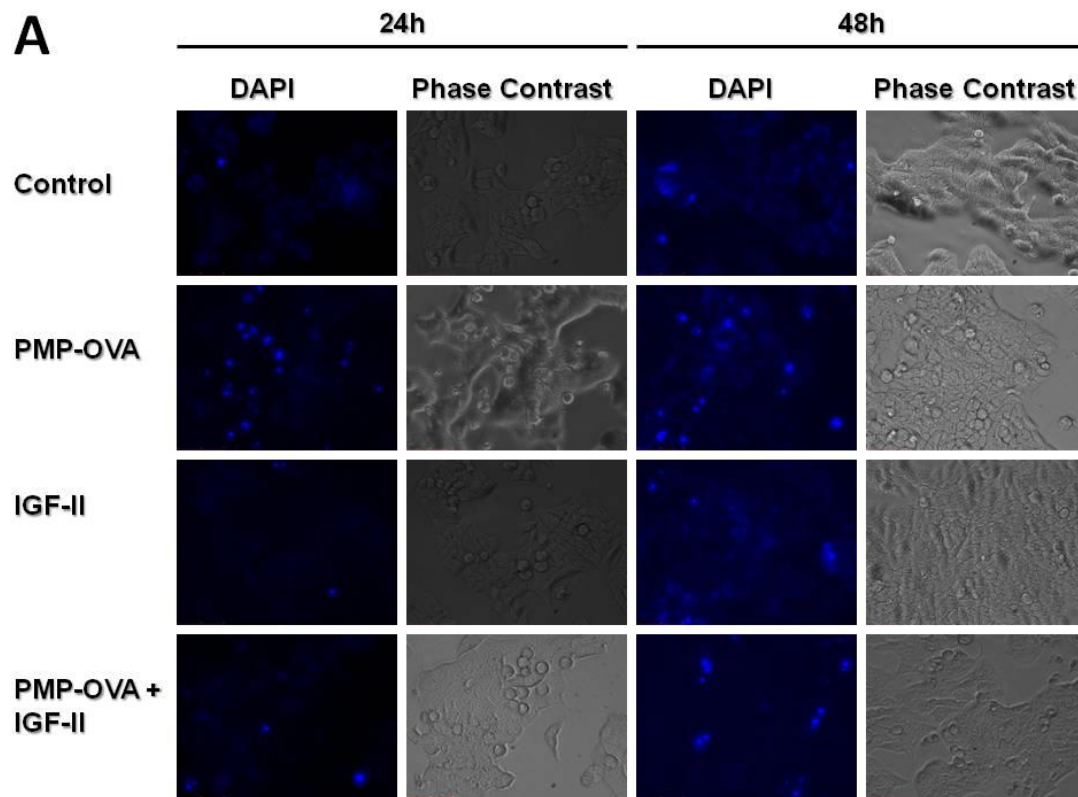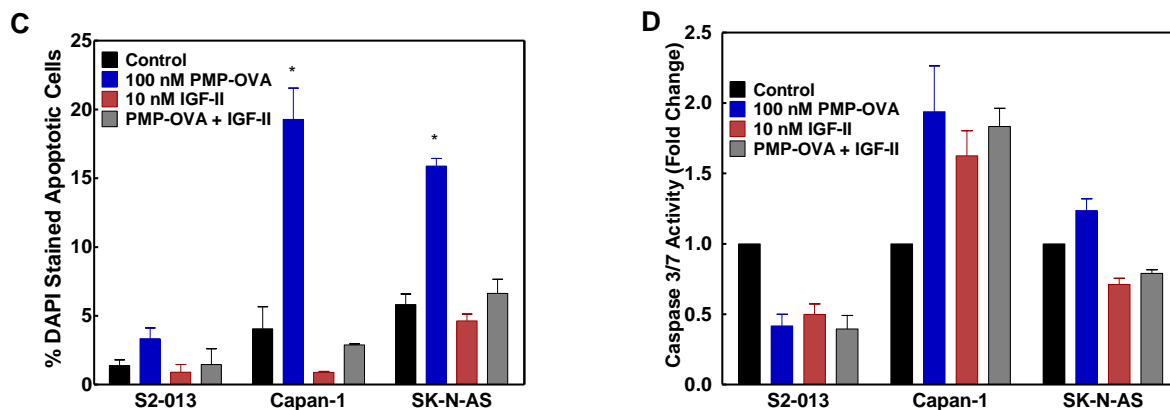
IGF-II

PMP-OVA +
IGF-II

Figure 3.8: Effects of PMP-OVA and IGF-II on apoptosis of cancer cell lines. Cancer cells were treated as indicated prior to DAPI staining of apoptotic nuclei. A) Capan-1 cells were treated for 24 h and 48 h and B) S2-013 and SK-N-AS were treated for 24 h. Cells were stained with DAPI and representative images were taken through fluorescence and phase contrast channels. Apoptotic nuclei that appeared enlarged with bright staining or fragmented were counted manually from a field of 70-150 total cells. C) The quantification of DAPI staining from the three cell lines tested with their respective SEM values plotted, (n=3). PMP-OVA treatment in Capan-1 and SK-N-AS cells had significant differences compared to control, $p < 0.001$. D) S2-013, Capan-1, and SK-N-AS cells were treated for 24 h before the caspase 3/7 activity assay was used to determine the amount of caspase activation.

To confirm via a biochemical indicator that apoptosis is induced by PMP-ligand treatment, S2-013 and Capan-1 cells and SK-N-AS cells were seeded into black, clear-bottom 96-well plates. Following a 24-hour incubation period of 100 nM PMP-OVA, 10 nM IGF-II, PMP-OVA + IGF-II, or vehicle control HBS, a caspase 3/7 activity assay was performed following manufacturer's instructions. Interestingly, there was no significant increase in caspase activation in the S2-013 cell line, in contradiction to the DAPI staining, as all treatment conditions were lower than that of the control (Figure 3.8D). However, all treatment groups (PMP-OVA, IGF-II, and PMP-OVA + IGF-II) were 1.7-2-fold higher in caspase 3/7 activity compared to the control in the Capan-1 cells. Moreover, SK-N-AS cells showed no significant change in the caspase 3/7 activity among the various treatment groups (Figure 3.8D). From these data, the slight increase in apoptotic nuclei detected in the DAPI staining assay does not appear to be correlated with caspase 3/7 activation.

To further investigate the role of apoptosis, we performed immunoblot analysis of different apoptotic markers in cell lysates following treatment with the aforementioned groups after a 24-hour incubation period. Poly ADP ribose polymerase (PARP) is a nuclear-resident family of proteins involved in DNA repair that detects single-strand DNA breaks (SSB) by binding to the break and inducing a conformational change to recruit the DNA repair machinery. In apoptosis, PARP is a downstream target of caspase 3 and becomes cleaved, rendering it inactive and unable to bind to damaged DNA (*323*). We therefore looked at PARP1 to determine if the 116-kDa active protein is cleaved to 89 kDa after PMP-OVA treatment. Immunoblots of cell lysates treated with the various treatment groups. The S2-013 pancreatic cancer cell line had a slight steady-state activation of PARP cleavage, and PMP-OVA slightly increased this activation (Figure 3.9A and 3.9C). Cells treated with the pan-caspase inhibitor Z-VAD-FMK (50 μM),

without the addition of PMP-OVA, showed no cleavage of PARP, but PMP-OVA slightly increased the PARP cleavage back to that of the control. Leupeptin (230 µM) is a protease inhibitor that inhibits cysteine, serine, and threonine peptidases, such as cathepsins. To determine if the slight apoptotic activation was a result of a caspase-independent mechanism, we inhibited cathepsins with leupeptin, which increased the PARP cleavage, and PMP-OVA slightly though non-significantly synergized with leupeptin to enhance this effect. Staurosporine (2 nM) is a kinase inhibitor (protein kinase C IC_{50}=3 nM; cAMP-dependent protein kinase IC_{50}=8 nM; p60v-src IC_{50}=6 nM; IR IC_{50}= 61 nM; IGF1R IC_{50}=6,150 nM (*324*)) that was used as a positive control for apoptosis. SK-N-AS neuroblastoma cells did not have a significant difference in PARP cleavage among the treatment groups and the control apart from the staurosporine treatment (Figure 3.9B and 3.9C).

Myeloid cell leukemia-1 (Mcl-1) is a protein homologous to B-cell CLL/lymphoma 2 (Bcl-2) and promotes cell viability, which mediates Bcl-2 antagonist killer (Bax) activity. Higher expression of Mcl-1 protects the cell from apoptosis (*325-328*). Higher expression of Mcl-1 in tumor cells leads to poorer prognosis in patients with certain cancers, such as of the breast (*327*). Alternatively, suppression of Mcl-1 expression in gastric cancers can increase the effectiveness of apoptosis-promoting chemotherapy (*325*) but knockout in normal murine hepatocytes leads to liver damage caused by increased apoptosis (*326*). We investigated the expression of Mcl-1 using αMcl-1 immunoblots that probed for both the long and short isoforms, where the long isoform enhances cell survival by inhibiting apoptosis and the short promotes apoptosis. Immunoblots probing for Mcl-1 were inconclusive for the S2-013 cell line, as we were unable to achieve a clear image with this antibody (Figure 3.9A). Interestingly, it appears as if the cells express both isoforms under almost all of the conditions, except

staurosporine treatment, in which case cells expressed the long (cell survival) while the short (pro-apoptosis) was not detected. We expected that the results for staurosporine would have been reversed. SK-N-AS cells also showed interesting results, in which PMP-OVA treatment expressed the Mcl-1 long isoform more than any other treatment (Figure 3.9B and 3.9D). IGF-II-treated cells, which we expected to have enhanced survival, expressed the short isoform, while staurosporine had very limited detection of either isoform yet normalized to higher expression of the short isoform. The data from the Mcl-1 blots confound our DAPI staining data.

The pro-apoptotic protein p53 upregulated modulator of apoptosis (PUMAα/β) inhibits cell growth by increasing apoptosis. S2-013 pancreatic cancer cells expressed PUMA under all treatments. Additionally, all treatments had elevated PUMA expression compared with the control, with even greater levels in the conditions treated with inhibitors against cathepsins (leupeptin), caspases (Z-VAD-FMK), or kinases (staurosporine) (Figure 3.9A and 3.E). Treatment with these inhibitors increased activation of apoptosis, and co-treatment with PMP-OVA may further enhance the effect. However, PMP-OVA alone showed only a mild increase over the control, and rescue with IGF-II brought the levels of PUMA back to that of the control. Staurosporine did not have as dramatic an impact on PUMA as it otherwise does on PARP cleavage, and unexplainably the DMSO vehicle control had increased PUMA.

A

PARP

MCL-1

PUMA

Cyclin D1

Actin

Labels: Control, IGF-II, PMP-OVA, PMP-OVA + IGF-II, Leupeptin, PMP-OVA + Leupeptin, Z-VAD-FMK, PMP-OVA + FMK, DMSO Vehicle, Staurosporine

B

PARP

MCL-1 short exposure

MCL-1 long exposure

Cyclin D1

Actin

Labels: Control, IGF-II, PMP-OVA, PMP-OVA + IGF-II, Leupeptin, PMP-OVA + Leupeptin, Fmk, PMP-OVA + Fmk, DMSO Vehicle, Staurosporine
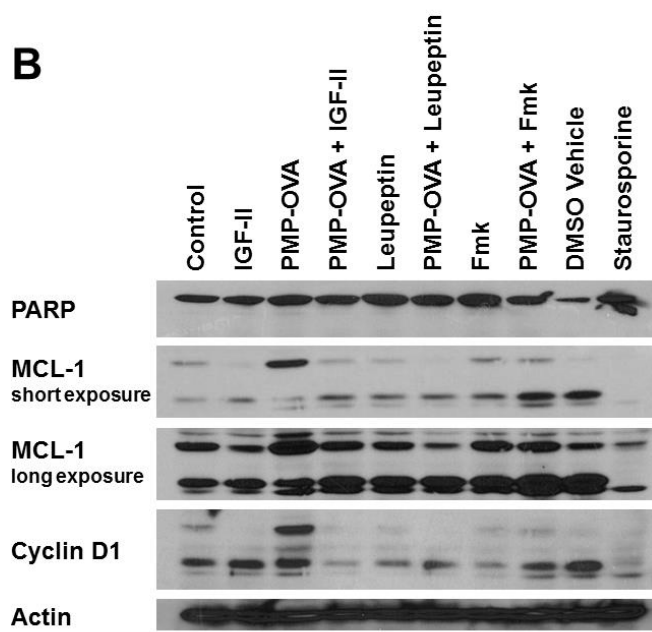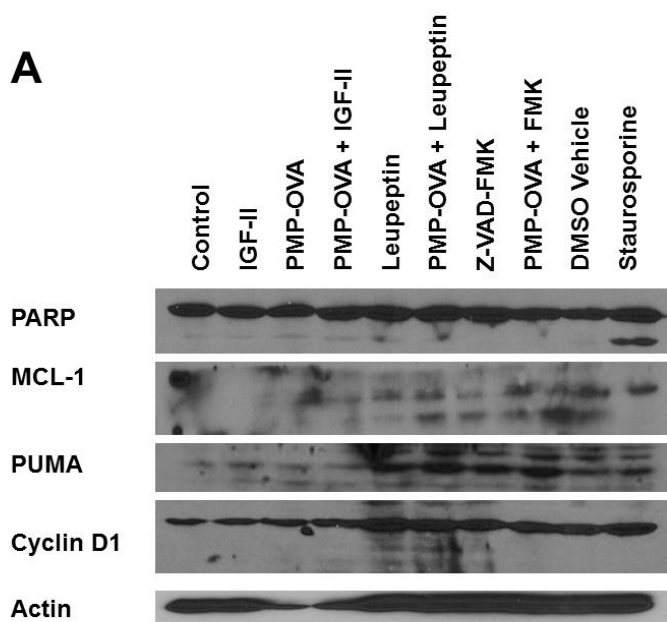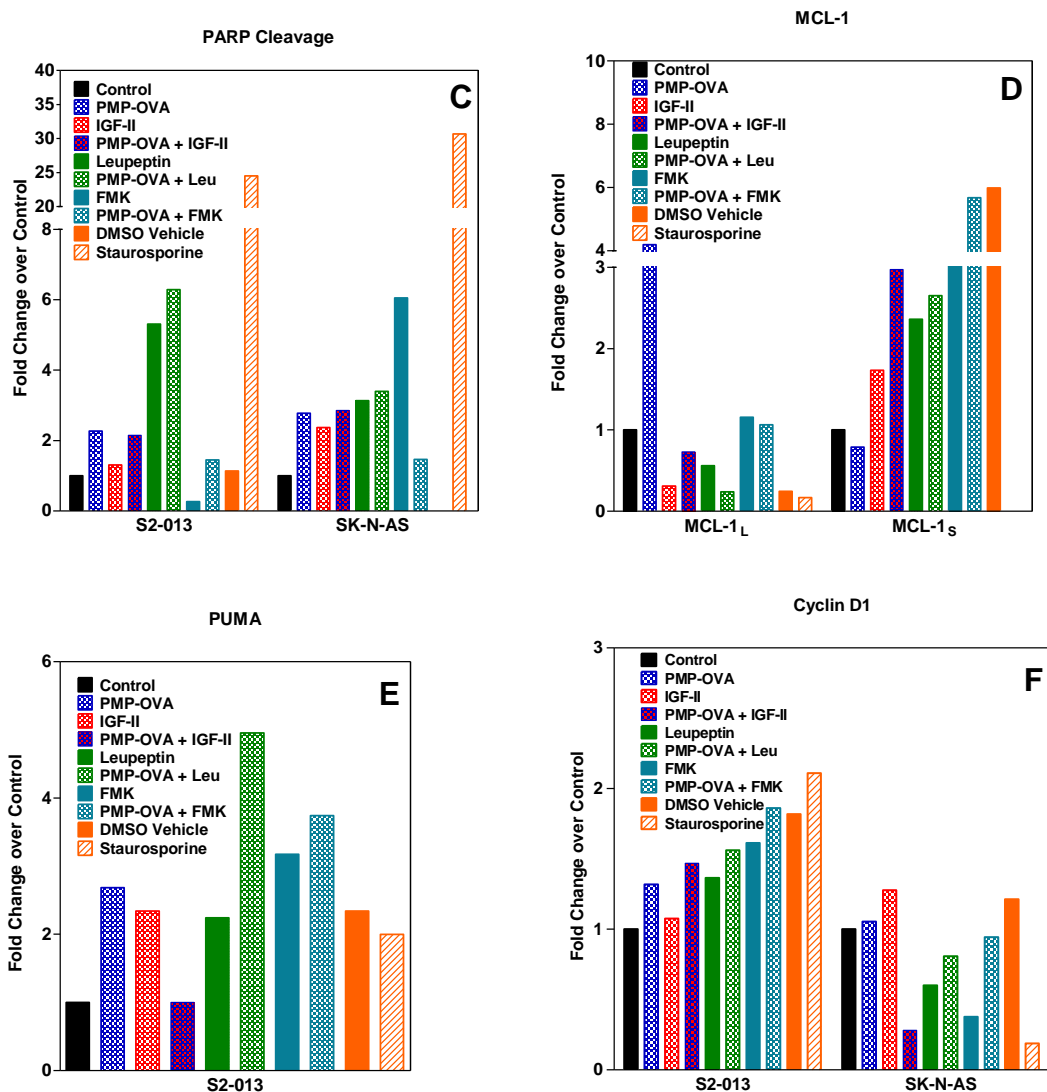
Figure 3.9: Effect of PMP-OVA and IGF-II on markers of apoptosis in cancer cells. A) S2-013 and B) SK-N-AS cells were incubated with various treatments: PMP-OVA at 100 nM, IGF-II at 10 nM, Leupeptin (Leu) at 230 µM, the proteasome inhibitor FMK at 50 µM, and staursporine at 2 nM. Whole-cell lysates were prepared after 24 hours and subjected to immunoblot analysis to determine status of apoptosis markers. C) PARP cleavage of S2-013 and SK-N-AS; D) MCL-1 long (pro-survival) and short (pro-apoptosis) isoforms of SK-N-AS; E) PUMA of S2-013 cells; and F) Cyclin D1. The MCL-1 blot of the S2-013 cells was difficult to quantify and was excluded from plots in panels C-F.

To further test if apoptosis is the cause of reduced cell viability, fluorescently labeled annexin V and propidium iodide (PI) staining using flow cytometry to visualize early and late stage apoptosis vs necrosis was used. Annexin V is a calcium-dependent phospholipid-binding protein that specifically binds to phosphatidylserine (PS) residues on the outer cell membrane of cells targeted to undergo apoptosis. The scramblase Xk-related protein 8 (Xkr8), which is a type of flipase, flips PS from the inner to the outer leaflet of the plasma membrane when apoptosis is initiated (*329*). Annexin V binds to the outer leaflet of the cell membrane and the allophycocyanin (APC) conjugated to annexin V fluoresces at a wavelength of 650/660 nm which indicates the stage of apoptosis. PI is a fluorescent molecule that intercalates DNA and is a representative of total DNA content, which fluoresces at 535/617 nm. With annexin V and PI staining, cells without staining for either molecule are the live population. Cells stained with low annexin V but high PI are early-stage apoptotic cells, while cells with high annexin V and high PI staining are late-stage apoptotic cells. The population that stains with high PI but low annexin V is considered to be the necrotic cells, i.e., the cells that are lysed quickly that do not have time for Xkr8 to flip the PS for annexin V to bind. JEG-3 cells were treated with 200 nM PMP-OVA and compared to vehicle control (HBS) and the positive apoptosis control treatment, staurosporine (2 nM), and were analyzed on a Calibur III flow cytometer after 6 and 24 h treatments. Unfortunately, the JEG-3 cells that were used for this experiment exhibited an unusually high background staining of annexin V that confounded interpretation of the results, as there was a high necrotic population following annexin V + PI staining in contradiction to the status of the cells prior to staining (Figure 3.10A). Annexin V with PI staining was then repeated using Capan-1 and HuH-7 cell lines. These cell lines had better results than the JEG-3, but still had an increase in the necrotic population, even in the control group, indicating an issue with the staining protocol. Nonetheless, there was an increase (8.2%) in early apoptosis with a

decrease of total cell viability (80%) following the 6-hour staurosporine treatment in the Capan-1 cells, which indicates that our positive control for apoptosis worked in this cell line. However, there was no change between the 200 nM PMP-OVA treatments at 6 and 24 hours and the control in the different subpopulations (Figure 3.10C). In the HuH-7 cells, there was not a change in the subpopulations within the staurosporine-treated cells and the 200 nM PMP-OVA or control groups, suggesting that this was a failed experiment, as any results could not be considered a true representation since the positive control for apoptosis did not work (Figure 3.10B). These studies were performed only once in each cell line and would need to be repeated to have a proper n value in order to do statistical analysis for determination of the apoptotic effect from PMP-ligand treatments.

In toto for the cell death studies, PMP-ligand treatment on its own may slightly increase apoptosis compared to the vehicle control in IGF-II-dependent cancer cells. However, the results do not fully agree from experiment to experiment using different biomarkers for cell death, which may be accounted for by differences in responsiveness to IGF-II, potency of different ligand preparations, or loss of the IGF-II-dependent growth in cells from many potential causes.

Figure 3.10: Effects of PMP-OVA on apoptosis of cancer cell lines using annexin V staining and flow cytometry analysis. A) JEG-3 choriocarcinoma, B) HuH-7 hepatocellular carcinoma, and C) Capan-1 pancreatic carcinoma cells were treated with PMP-OVA or the positive apoptosis inducer staurosporine for 6 to 24 h and then stained with annexin V and 7AAD prior to flow cytometry analysis. Viable (black), early apoptosis (blue), late apoptosis (purple), and necrotic (red) cells were gated and the number of cells determined.

Annexin V Staining
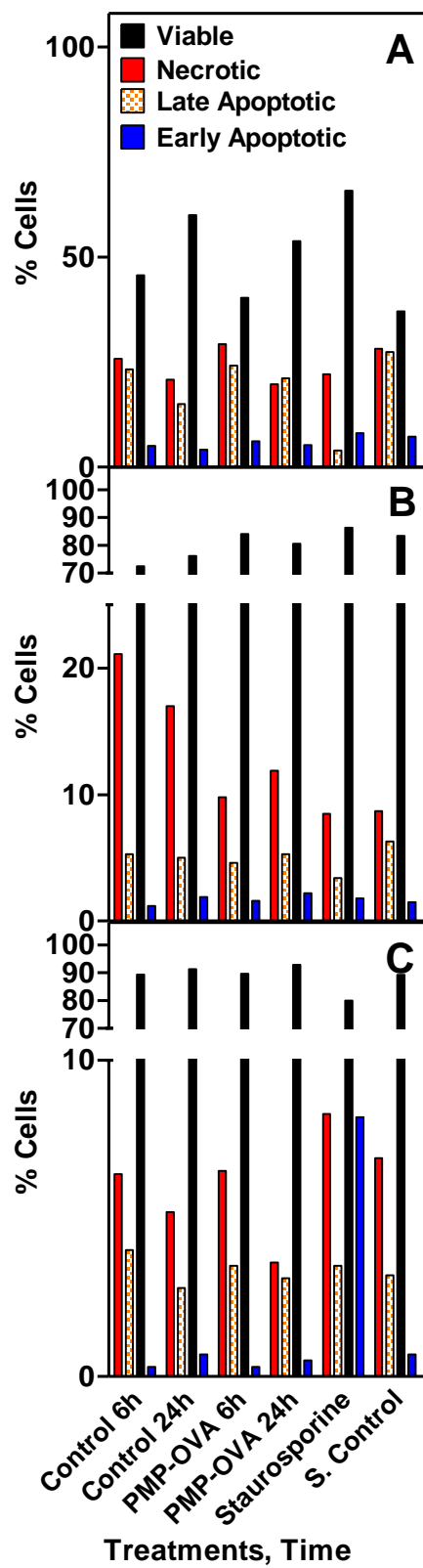
To determine if autophagy may play a role either by decreasing apoptosis and increasing cell survival in control cells or if our PMP-ligands interfere with autophagy that they initiate cell death, we investigated the formation of autophagosomes. To study this, we used a series of confocal and fluorescent microscopy approaches as well as immunoblot analysis of LC3-I conversion to LC3-II, mTOR activation, and subsequent p70S6 kinase activation, which is a main effector targeted by activated mTOR (*330*).

SK-N-AS cells were grown to 70-80% confluency and then treated with 200 nM PMP-OVA, 10 nM IGF-II, 200 nM PMP-OVA, + 10 nM IGF-II, or vehicle control (HBS) for 24 hours. Whole-cell extracts were prepared and subjected to immunoblot analysis. IGF-II increased mTOR phosphorylation compared to control, but PMP-OVA did not affect phosphorylation of mTOR (Figure 3.11A and 3.11B). The addition of the IGF-II ligand trap (soluble M6P/IGF2R) decreased phosphorylation of mTOR, as predicted. These results were extended to the phosphorylation of mTOR's substrate, p70S6K, where IGF-II enhanced phosphorylation of this protein but PMP-OVA did not have much of an effect. The decreased activation of mTOR in the sM6P/IGF2R cells was not seen in the phosphorylation of p70S6K (Figure 3.11A and 3.11C). In the LC3 immunoblot, SK-N-AS cells experience a steady-state of conversion of LC3-I to LC3-II. All treatments had slightly more LC3-II than the control but differences were not significant (Figure 3.11A and 3.11D). However, these data do not necessarily indicate changes in autophagy flux, as LC3-II becomes degraded by autophagy (*331*). Furthermore, there may not be an issue with the autophagosome formation but the fusion of autophagosomes with lysosomes, which would not be detected through immunoblot analysis.
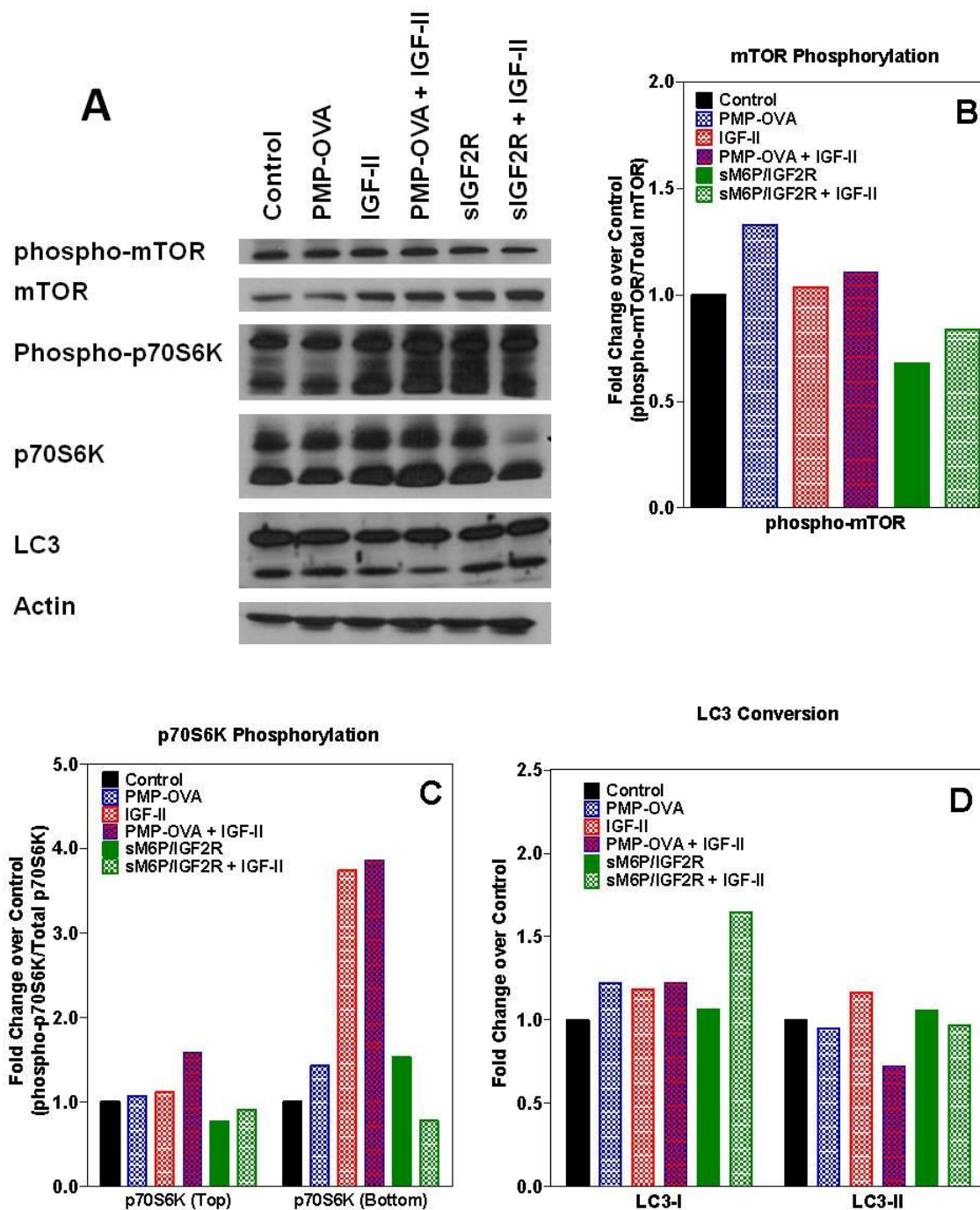
Figure 3.11: Effect of PMP-OVA on autophagy markers in SK-N-AS cancer cells.
A) Immunoblots of autophagy markers: LC3 conversion, and phosphorylation of mTOR and the mTOR target p70S6K. Quantification of change caused by the treatments compared to control for B) mTOR phosphorylation normalized to total mTOR; C) p70S6K phosphorylation normalized to total p70S6K for both the upper (80 kDa) and lower (75 kDa) bands; and LC3-I conversion to LC3-II.

We next grew SK-N-AS cells on collagen-coated coverslips for immunofluorescent microscopy. We treated the cells with 100 nM PMP-OVA and vehicle control HBS with or without 50 nM bafilomycin for 24 h. Bafilomycin is an inhibitor of vacuolar-type H^+-ATPase that blocks the maturation of autophagosomes by preventing the fusion of autophagosomes with lysosomes (*332*). The bafilomycin was then washed out and cells were incubated with their treatments for an additional 1 to 9 h. The cells were fixed, permeablized and incubated with an α-LC3 (marker of autophagosomes) antibody and LAMP1 (marker of lysosomes) antibody. Cells were then incubated with secondary antibodies conjugated to AlexaFluor 488 (LC3) and 568 (LAMP1) as well as DAPI to stain the nucleus. The subcellular compartments were then visualized on a confocal microscope. Initial studies did not reveal much difference among the various treatment groups when comparing the autophagosome size and number to the lysosomes (data not shown). There was also not a distinct difference in colocalization of the two markers, indicating that there was not a significant difference in autophagy among the different treatments. Interestingly, the morphology of the PMP-OVA-treated groups had changed slightly compared to the control or other treatment groups. The PMP-OVA-treated cells were more elongated with a disordered plasma membrane, and the nuclei appeared to be larger and more bi- and multinucleated compared to the control. The experiment was repeated using phalloidin (a dye that binds specifically to elongated actin filaments) and DAPI staining to visualize any actin cytoskeleton rearrangement that may occur due to PMP-OVA treatment, and the cells were viewed on both confocal and fluorescent microscopes (Figure 3.12). Upon treatment with PMP-OVA, the actin cytoskeletal structure appeared to reorganize in more parallel bundles that appeared to avoid the nuclei while the control actin cytoskeleton revealed a cell that was more at rest with actin bundles crossing different directions, including over the nuclei. The size of the cell appeared larger in the PMP-
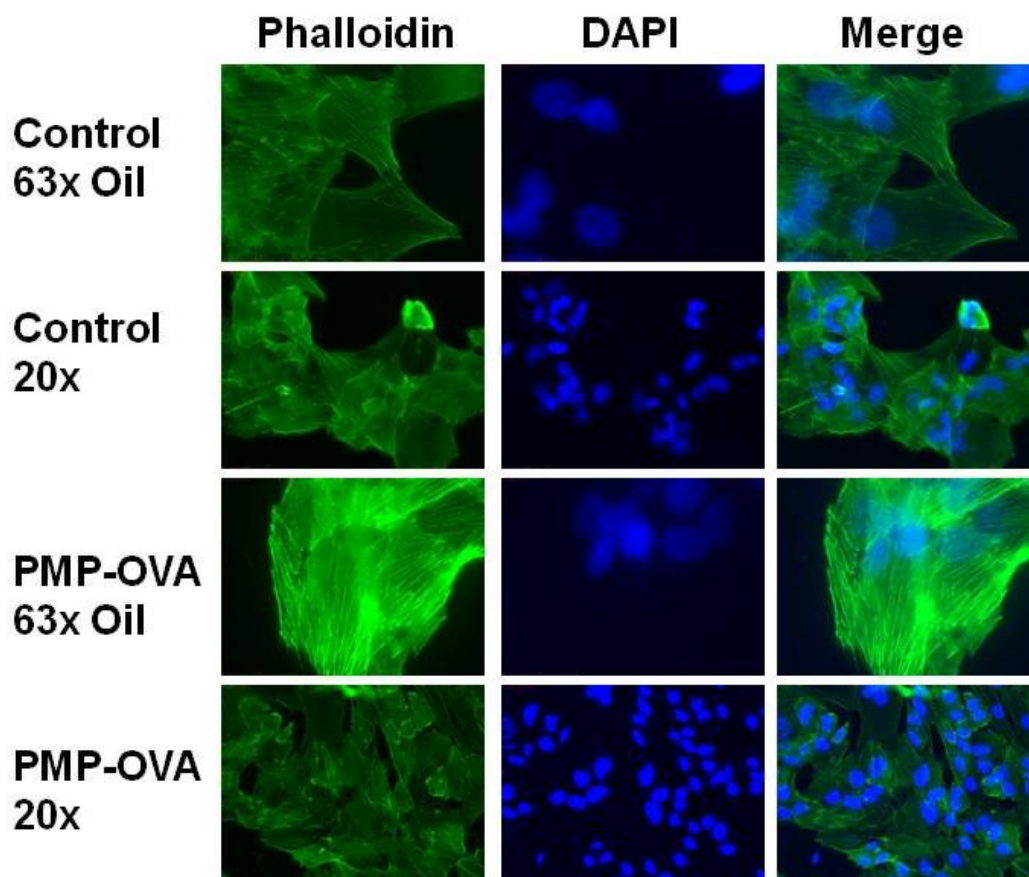
Figure 3.12 Anomalous effect of PMP-OVA on the actin cytoskeleton. Actin filaments were stained with phalloidin (green) and the nuclei were stained with DAPI (blue) to visualize morphological changes and actin bundling as a result of treatment of the cells with 200 nM PMP-OVA for 24 h. Cells treated with PMP-OVA displayed changes in actin bundling and appeared larger than control cells.

OVA treatment, similar to the previous studies. In conclusion from these studies, PMP-ligand treatment affects the cancer cells in some way, but whether it is downstream of IGF-II depletion or an off-target effect of the ligand directly is still not known and would need to be investigated further.

C.6. PMP-ligand effect on cell cycle progression in cancer cells

Our laboratory has seen that PMP-ligand treatment reduces cell viability, but it is unknown what the underlying mechanism that decreases cell number is. Mitogenic IGF-II activation of IGF1R and IGF1R/IR-A leads to accelerated cell cycle progression and proliferation via mitosis (*203*). The cell cycles of S2-013, SK-N-AS, JEG-3, Capan-1, and HuH-7 cancer cell lines were investigated using flow cytometry by three different methods.

Initial experiments examined cell cycle progression in S2-013 cells following 100 nM PMP-OVA treatment with or without 10 nM IGF-II, 10 nM IGF-II, or vehicle control HBS and compared to the apoptotic positive control staurosporine using propidium iodide (PI) staining, which binds DNA following permeabilization of the plasma membrane prior to analysis on a Calibur I flow cytometer. Results revealed small, but not significant differences within the G0/G1 and G2 phases between the PMP-OVA- and control-treated groups, with only a slight yet non-significant decrease in the S-phase of PMP-OVA-treated cells (Figure 3.13A). There was a distinct G2 cell cycle arrest in the positive control staurosporine. The lack of cell cycle arrest following PMP-OVA treatment may be due to the fact that S2-013 cells are not responsive to IGF-II or our PMP-ligands. The cell cycle arrest analysis was then performed using SK-N-AS cells. The control and PMP-OVA-treated cells were comparable, but the PMP-OVA cells had a

slight increase in the G2 but not the subsequent decrease in G1 that would further support cell cycle arrest (Figure 3.13B). The lack of a significant difference in the cell cycle phases between the treatment groups may be due to the fact that these cells were asynchronous with pools of cells in various points of their cell cycle, and they progress through their cell cycle relatively slowly (doubling t = 39 h). To test the effect in synchronized cells, we did a double thymidine block over the course of 40 h before the cells were treated with 200 nM PMP-OVA and compared to vehicle control (HBS). A plate of cells was collected and fixed every 2 hours until 12 h as well as a 24 h time point before staining with PI following flow cytometry analysis. Much to our disappointment, the cell cycle histograms of PMP-OVA appeared very similar to the histograms representing the control (Figure 3.13C). There was not a gradual progression through the cell cycle phases that may be attributed to the slow progression of these cells or that these cells were not released from the double thymidine block. JEG-3 cells were used for their faster cell cycle progression (doubling t ≈ 24 h); these cells were synchronized after serum deprivation for 72 hours, and then treated with 200 nM PMP-OVA or vehicle control (HBS). The histograms of the two groups over the course of the study revealed a progression through the cell cycle in which the PMP-OVA-treatment lagged slightly behind the control (Figure 3.13D). At the 10-h time point, the PMP-OVA-treated cells had a slight decrease in the G1 phase with a slight increase in the G2 phase compared to the control that progressed to a greater difference at 24 h. This indicates that the PMP-OVA is causing a slower cell cycle progression in JEG-3 cells, but is not necessarily causing cell cycle arrest.

A S2-013 Cell Cycle Analysis

B SK-N-AS Cell Cycle Analysis

C Synchronized SK-N-AS Cell Cycle

D Synchronized JEG-3 Cell Cycle
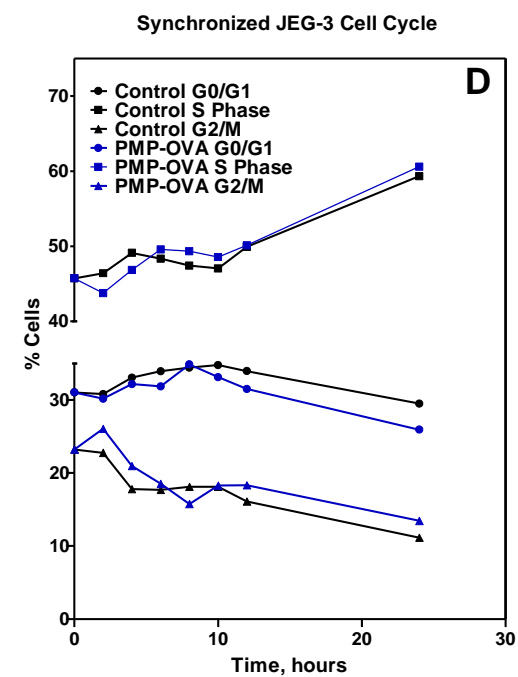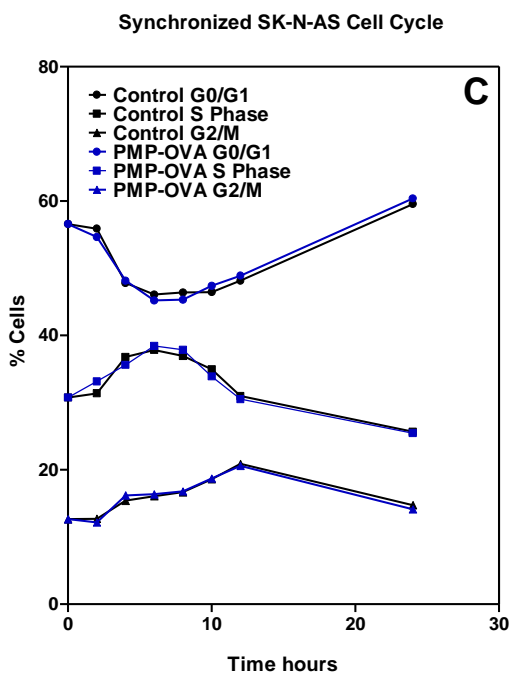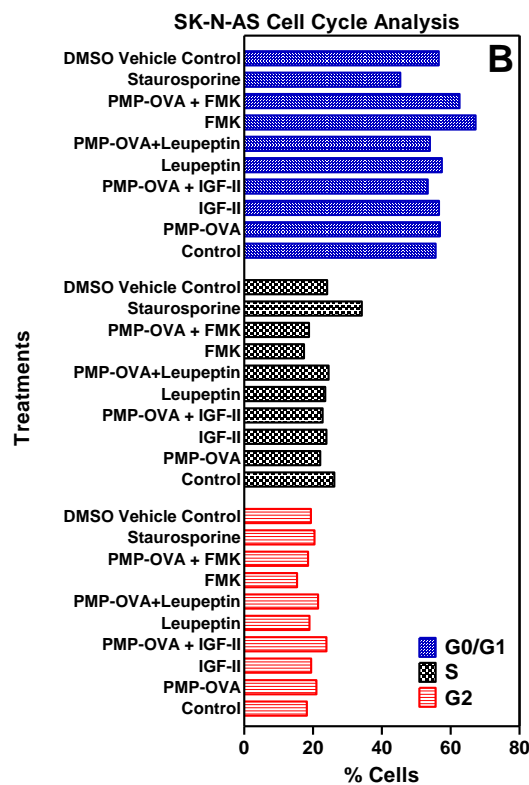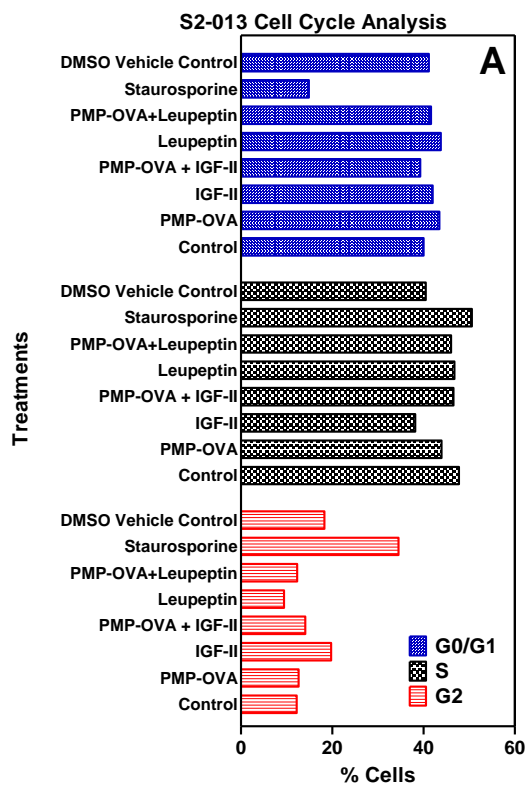
Figure 3.13: Analysis of the effects of PMP-OVA on the cell cycle in S2-013 and SK-N-AS. Unsynchronized A) S2-013 pancreatic cancer cells and B) SK-N-AS neuroblastoma cells were treated with 200 nM PMP-OVA, 10 nM IGF-II, 230 µM leupeptin (leu), 50 µM Z-VAD-FMK (FMK), 2 nM staurosporine, combinations of these or control (HBS) for 24 h prior to PI staining and flow cytometry analysis. Each bar depicts the number of cells gated in each cell-cycle phase in the various treatment groups. C) SK-N-AS neuroblastoma cells were synchronized using a double thymidine block prior to 24 h incubation with 200 nM PMP-OVA or the control. D) JEG-3 choriocarcinoma cells were synchronized using a 48 h serum deprivation protocol prior to 24 h incubation with 200 nM PMP-OVA or the control. Both SK-N-AS and JEG-3 cells were fixed and stained at the time indicated before flow cytometry analysis. These cell lines were not effectively released from their cell cycle blocks.

	S2-013			SK-N-AS		
Treatment	**G0/G1**	**S**	**G2/M**	**G0/G1**	**S**	**G2/M**
Control	40	48	12	56	26	18
PMP-OVA	43	44	13	57	22	21
IGF-II	42	38	20	57	24	19
PMP-OVA + IGF-II	39	47	14	53	23	24
Leupeptin	44	47	9	57	24	19
PMP-OVA + Leu	42	46	12	54	25	22
FMK				67	17	15
PMP-OVA + FMK				63	19	19
Staurosporine	15	51	35	45	24	19
DMSO	41	41	18	57	34	20

Table 3.4: Summary of flow cytometry analysis of PI-stained S2-013 and SK-N-AS. Unsynchronized cancer cells were treated as indicated in Figure 3.14. These data are tabulated as percentage of cells gated in G0/G1, P, or G2/M phases.

Although PI staining alone through flow cytometry analysis is one of the standard methods of cell cycle progression, this type of analysis visualizes total DNA content within the different phases at a certain point in time. However, it does not take into consideration the number of cells that have progressed through DNA synthesis to different phases. We were interested to see how many cells were currently undergoing DNA replication following treatment by using 5-bromo-2'-deoxyuridine (BrdU) incorporation coupled with PI staining and analysis using flow cytometry. BrdU is a homolog of thymidine that is incorporated into the DNA during DNA synthesis in replicating cells. Following a fixation/permeabilization and DNA nicking step, a fluorescently tagged antibody recognizes incorporated BrdU in the DNA. SK-N-AS cells were treated for 24 h with 100-200 nM PMP-OVA with or without 10 nM IGF-II, 10 nM IGF-II, or the cell cycle inhibitor paclitaxel (5 or 50 nM) and compared with the vehicle control. Following a 3-h incubation with BrdU, the cells were fixed and permeabilized, treated with DNase and an αBrdU-APC antibody, and analyzed on a Calibur III flow cytometer. Studies have shown that when cells are treated with paclitaxel at a concentration below the IC_{50} value, cells undergo G2/M cell cycle arrest (*333*); treatment with higher concentrations induce apoptosis. Therefore, we used two concentrations to find which provided cell cycle arrest without inducing apoptosis. When SK-N-AS cells were treated with 5 nM paclitaxel for 24 h, there were more cells in G2/M with fewer in G0/G1, indicative of a G2/M block. Paclitaxel at 50 nM for 6 h was also able to induce G2/M cell cycle arrest, but it was not as dramatic as the cells treated with the longer, lower concentration (Figure 3.14). PMP-OVA at 200 nM had fewer cells in the G0/G1 phase, although there was not a corresponding increase in the S- or G2/M phases. This study was performed only once in one cell line and needs to be validated to determine if PMP-ligands are affecting the proliferation in cancer cells.
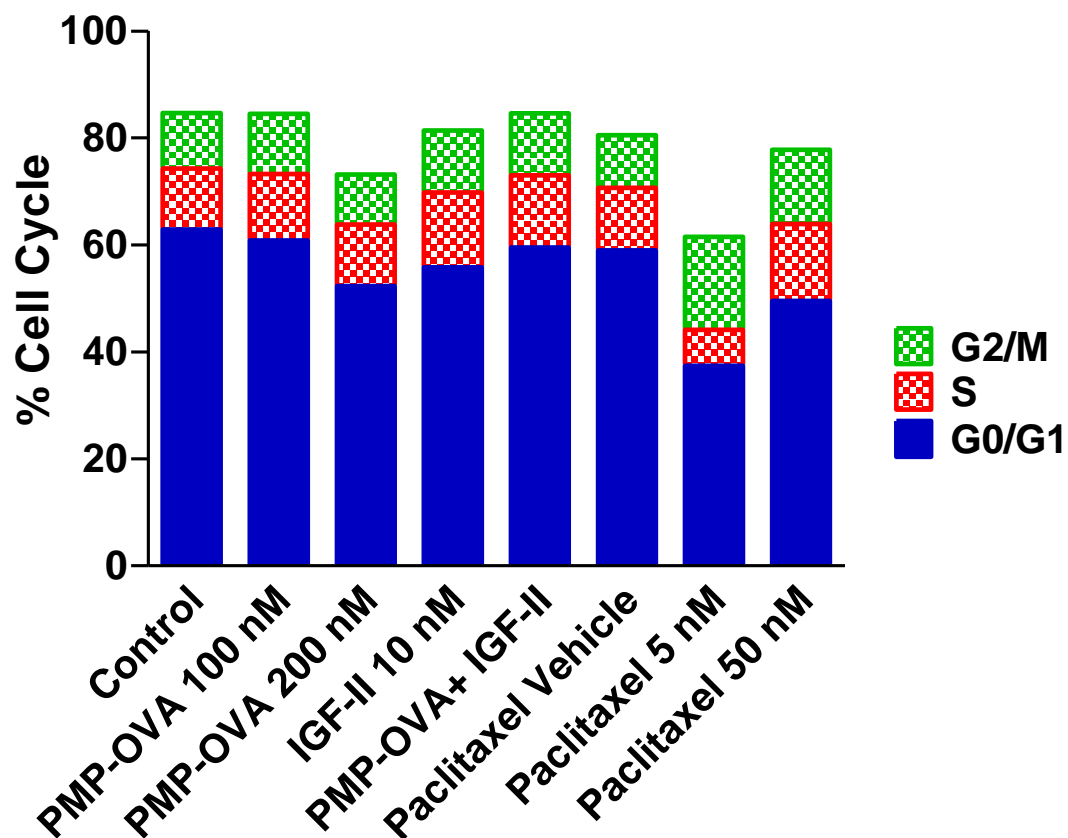
Figure 3.14: BrdU incorporation of SK-N-AS following treatments to determine cell cycle progression. Actively dividing cells incorporated BrdU into their DNA, and a APC-lablled BrdU and 7AAD stain indicated the cell cycle phase of cells. Notice that 200 nM PMP-OVA and 24 h of 5 nM paclitaxel had fewer cells that could be gated, indicating a cytotoxicity event.

To investigate the signaling that influences cell cycle progression, immunoblots of key effectors in the Akt and ERK pathways were performed to measure possible activation by phosphorylation. SK-N-AS cells were grown to 70-80% confluency and treated with 100 nM PMP-OVA, 10 nM IGF-II, PMP-OVA + IGF-II, 10 nM sM6P/IGF2R, sM6P/IGF2R + IGF-II, or vehicle control (HBS) for 24 hours. Whole-cell extracts were then subjected to SDS-PAGE followed by immunoblot analysis. The phosphorylation of Akt at Thr308 or Ser473 was not noticeably different among the treatment groups compared to control (Figure 3.15). However, there was an increase in ERK1/2 phosphorylation as a result of IGF-II treatment. Furthermore, PMP-OVA did not affect ERK1/2 phosphorylation, but it appears that IGF-II is signaling through the MAPK/ERK pathway upon activation of the receptor tyrosine kinases in these cells. Additionally, p53 in SK-N-AS cells was investigated, as this protein is an important master regulator of the cell that has many targets, including cell cycle arrest and initiation of apoptosis (*334*). However, there was no change in p53 levels among the different treatments and further investigation of the literature revealed that this cell line has a mutant but inactivated p53 protein; thus, p53 is not regulating the cell cycle or apoptosis in these cells at all. Cyclin D1 protein levels in both cell lines were also not significantly different from the control cells (Figure). This may be because the whole-cell lysates used in these immunoblots were from non-synchronized cells. Clearer results of more minute differences may be obtained by first synchronizing the cells prior to treatment.

In summary, our cell cycle analyses indicate that it appears as if IGF-II signals through the MAPK/ERK pathway in these cells, but the presence of PMP-OVA does not inhibit this signaling. Additionally, there may be a slight slow-down in cell cycle progression due to PMP-OVA, but our ligand does not completely initiate

Figure 3.15: Effect of PMP-OVA on mitogenic and survival response to PMP-OVA treatment in SK-N-AS cells. Cells were treated with 200 nM PMP-OVA, 10 nM IGF-II, 10 nM sM6P/IGF2R (sIGF2R), or combinations for 24 h and compared to the control (HBS). A) Immunoblot analysis of cell lysates probing for effectors of mitogenic and survival signaling. Quantification of phosphorylation of B) Akt at Thr308 and Ser 473 and C) ERK1/2. Note the scale difference between pAkt and pERK, as pAkt appears to have a higher basal activity in all treatments, but pERK seems to have a higher activation from IGF-II treatment.

A

phospho-Akt (Thr308)
phospho-Akt (Ser473)
Akt
phospho-ERK
ERK
Actin
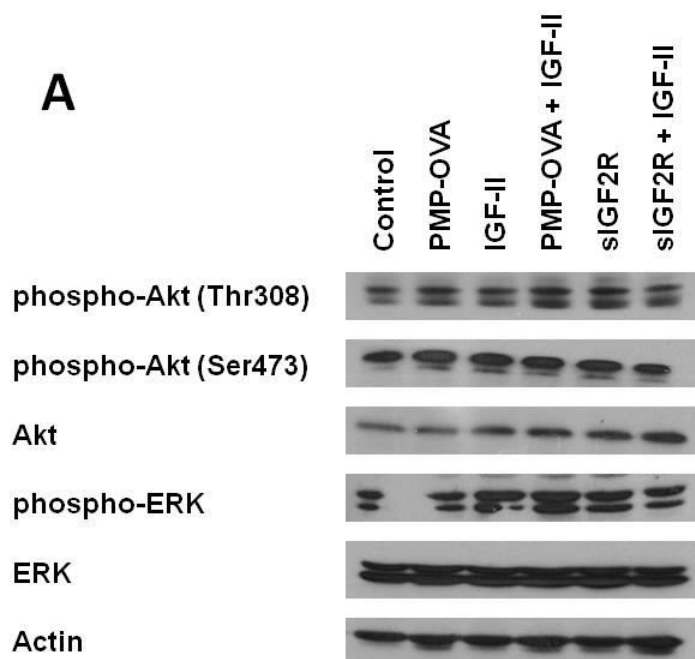
Phosphorylation of Akt
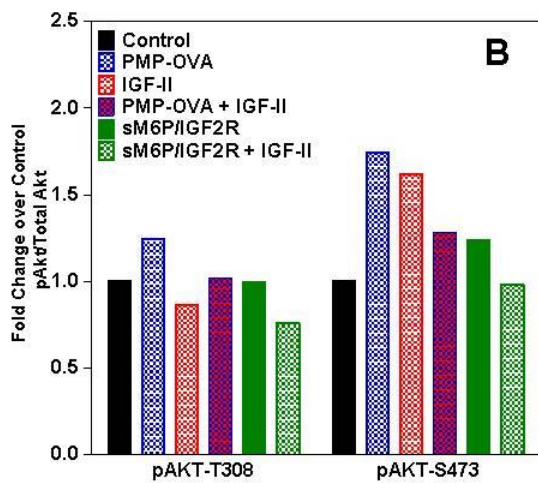
Phosphorylation of ERK1/2

B

C
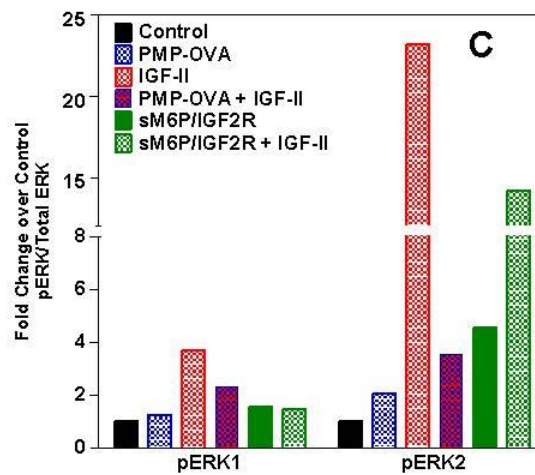
cell cycle arrest. These experiments need to be validated with synchronized cells to determine if the PMP-ligands are truly regulating the cell cycle.

C.7. PMP-ligand effect on migration of cancer cells

To determine if PMP-ligands affect the migration potential of cancer cells, we performed scratch wound healing assays and transwell migration assays using microscopy and fluorescent microscopy, respectively. HuH-7, Capan-1, and JEG-3 cells were seeded into 6-well plates and grown to 80% confluency. Three scratches per well were made using a sterile pipette tip and 6 images per well were taken, designated as the 0 hour time point. Cells were treated with 100 or 200 nM PMP-OVA, 10 nM IGF-II, or vehicle control HBS. Images were taken every 24 hours until 96 hours. Interestingly, PMP-OVA did not inhibit the migration potential of the cancer cells but rather increased the rate of wound closure. This may be due to the fact that such a high concentration of PMP-ligand was used that may have caused a more chemotactic response and closure of the wound. Additional studies using lower concentrations of PMP-ligand need to be performed to validate the wound closure data.

In the transwell migration assay, HuH-7 cells were seeded into 24-well inserts in serum-free medium and inserted into the well of the 24-well plate, which contained the treatments (100 nM PMP-OVA, 10 nM IGF-II, PMP-OVA + IGF-II, or vehicle control HBS) in 3% serum-containing medium. After 24 hours, the membranes were retrieved, cells were fixed and stained with DAPI, and the membranes were imaged under fluorescent microscopy. In this preliminary study that was performed only once, PMP-OVA appeared to limit the number of cells that migrated across the membrane.
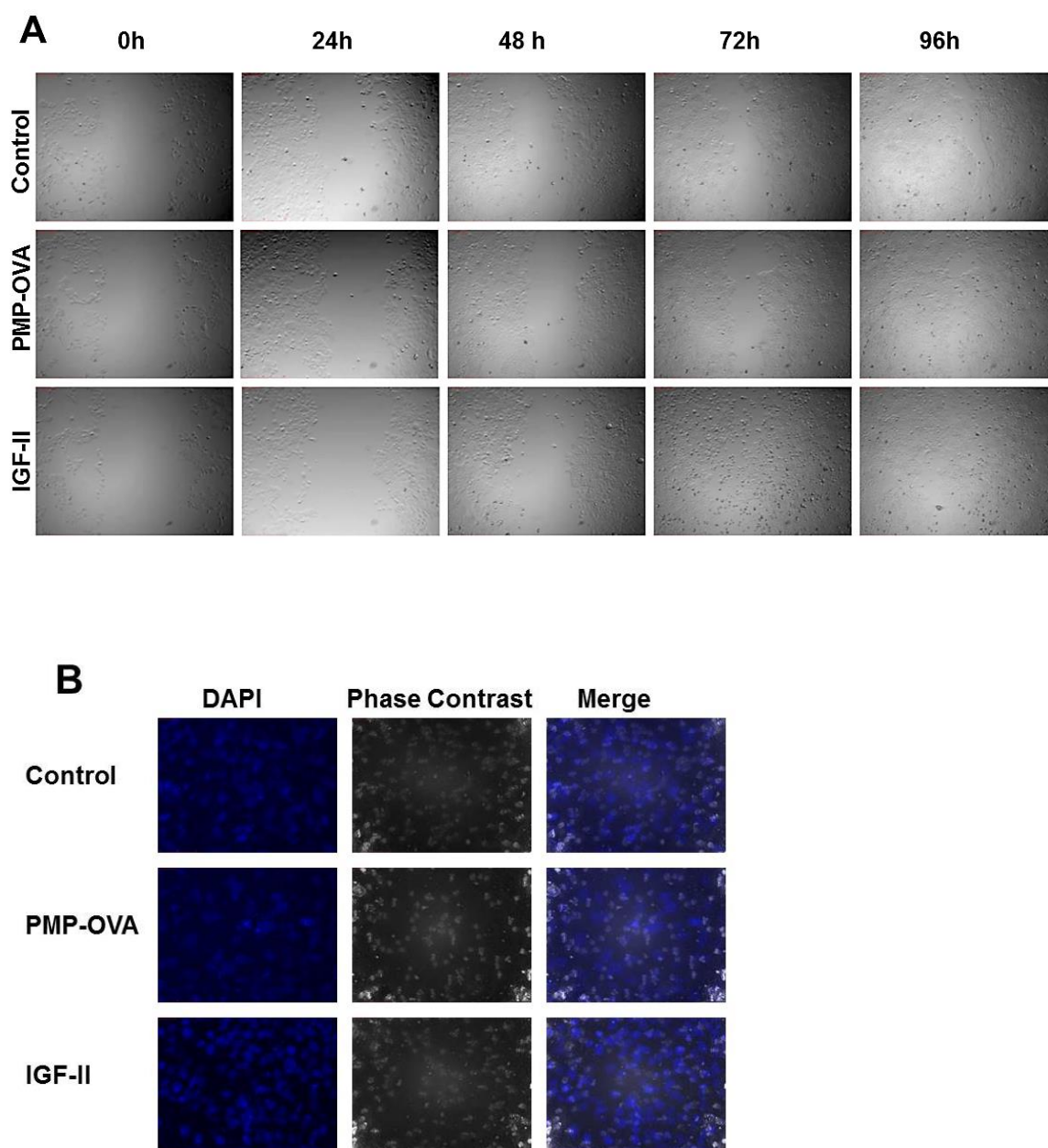
Figure 3.16: Effect of PMP-OVA on migration of cancer cell lines.

A) A representative set of images from a 96-h scratch assay of Capan-1 cells.

B) A representative set of images from a 48-h transwell assay of HuH-7 cells.

Interestingly, IGF-II did not enhance the migration as we expected. These preliminary results need to be validated with more replicates and additional cell lines.

D.   Discussion

The M6P/IGF2R functions to transport acid hydrolases to the lysosome as well as traffic extracellular M6P-tagged glycoproteins and non-glycosylated proteins to the lysosome for degradation. These proteins bind to the receptor at different binding sites, where M6P-tagged proteins bind with high affinity to repeats 3 and 9, lower affinity to repeat 5, with very low binding to repeat 15, while IGF-II binds to repeat 11 with the aid of the fibronectin-like type II domain (FnII) of repeat 13 (*46, 101, 279*). Having these distinct binding domains allows the M6P/IGF2R to be multifunctional. Multivalent M6P-based biding accelerates the M6P/IGF2R internalization rates 3-4-fold above its steady-state constitutive internalization, while simultaneously allowing IGF-II to bind to a separate location and act as a passenger ligand (*131*). This enhanced internalization was due to ligand-induced M6P/IGF2R dimerization, which may occur through increasing receptor's internalization signals within the cytoplasmic tail or a conformational change that allows the internalization signal to be presented in a more optimum manner (*131*). Furthermore, the M6P-modified glycoprotein, CREG, could bind to the M6P/IGF2R and induce cell cycle arrest via increased internalization of IGF-II from the cell milieu (*163, 228, 229, 335*). To date, no studies have clearly characterized this multivalent binding interaction and subsequent IGF-II degradation, but this led us to exploit the M6P/IGF2R as a potential therapeutic approach in targeting IGF-II-dependent cancers. Having a role in development and differentiation, IGF-II expression is often increased in cancers (*243-247, 336*). Therefore, our laboratory developed and tested a panel of pseudoglycoprotein ligands with varying molecular sizes and number of M6P

moieties to determine whether high affinity, bi- or multivalent M6P-based ligands could bind to the M6P/IGF2R and decrease cell viability. The goal of this study was to determine if these high-affinity M6P-based ligands could force internalization, degradation and consequent depletion of extracellular IGF-II and thereby decrease cell viability.

There have been only a few studies that have targeted the M6P/IGF2R as a therapeutic measure. Human serum albumin modified with M6P moieties has been used to target the M6P/IGF2R as a conduit to deliver both anti-fibrotic and anticancer drugs into cells (*337, 338*). Also, synthetic M6P-mimetics have been developed that bind to the M6P/IGF2R with similar or slightly better affinity than the monovalent ligand M6P (*312, 313, 339, 340*), but some of these mimetics did not have cytotoxic effects on cells (*340*). Therefore, to date there are no reports of synthetic M6P-based ligands that are capable of binding the M6P/IGF2R with bivalent binding similar to the natural ligand hGUS. Consequently, we are the first lab to our knowledge to design such ligands to help provide proof-of-principle evidence that they may be useful in treating IGF-II-dependent cancers.

Tong *et al.* determined that a ligand bearing two M6P moieties bound to the M6P/IGF2R with 100-1000-fold higher affinity than what the monovalent M6P is able to achieve (*93*). Previous studies determined that our PMP-ligand panel does bind to the M6P/IGF2R with high-affinity implying bivalency, fulfilling this increased affinity requirement (Figure 3.1); even the smallest bidentate PMP-tripeptide (PMP-SYK) could achieve bivalency. Moreover, these ligands can stabilize the dimeric M6P/IGF2R and bind to M6P-binding repeats on different monomers of the dimeric receptor, which is also required for rapid internalization of the M6P/IGF2R as seen with hGUS (*131*). These ligands were also able to decrease cell viability in a M6P- and IGF-II-dependent manner.

The aim of the current study was to determine if IGF-II in the conditioned medium was internalized and degraded in a similar fashion as CREG (*163, 335*) and to delineate the effect(s) these PMP-ligands have on cellular function.

Incubation with the PMP-ligand PMP-OVA reduced viability of mouse L-cells and two cancer cell lines (HuH-7 and JEG-3). This was dependent on binding through the M6P moieties of our PMP-ligand as M6P competitively displaced our ligand. Furthermore this effect appeared to decrease cell viability through the depletion of IGF-II, as exogenous IGF-II rescued the growth inhibition effect. We therefore applied the cell viability assay in several cancer cell types. We first screened cells for their ability to respond to exogenous, recombinant IGF-II and determined whether they have an intact autocrine or paracrine loop (Figures 3.4). In summary, cells that were poorly differentiated tend to be less IGF-II-dependent and had a decreased responsiveness to our PMP-ligands. These included the pancreatic carcinoma cell lines MiaPaCa-2 and PANC-1, and the prostate carcinoma cell line DU145. Several cell lines responded moderately well, which happen also to be moderately-to-well differentiated cancer cell lines. These include pancreatic adenocarcinoma cell line Capan-1, hepatocellular carcinoma cell line HuH-7, choriocarcinoma cell line JEG-3, and embryonal neuroblastoma SK-N-AS. However, the well-differentiated cell line S2-013 did not have much of a response, indicating that all well-differentiated cancer cells may not be equal. The poorly differentiated cell lines may have additional genetic alterations that allow for more aggressive cell growth, resistance to therapy, and lack of IGF-II-dependency making it difficult for the PMP-ligands to overwhelm the cells with IGF-II-deprivation and decreased cell viability. They may also have a higher basal activation of the receptor tyrosine kinases that make it more difficult to inhibit the activation of these receptors and subsequent pro-survival signals. The moderately well differentiated cells may have

more intact IGF signaling and a greater dependency on IGF-II, even in cell systems that produce their own IGF-II, that our PMP-ligand treatment deprives the cells of endogenous and exogenous IGF-II more readily, leading to the greater decrease in cell viability. If this is true, then our ligands will work most effectively in perhaps earlier-stage tumors that have not lost their differentiation status and that retain dependency on IGF-II. Additionally, the differences in response to PMP-ligand treatment in the various cancer cell lines could also be partly explained by the number of available M6P/IGF2R on their plasma membranes. The cancer cell lines all have varying concentrations of M6P/IGF2R on their plasma membranes, which allows for varying potentials of PMP-ligand binding to a dimer or oligomer. In the case of IGF-II-dependent tumors that do not express the M6P/IGF2R, our ligands may still work at inhibiting tumor growth by targeting cells within the tumor microenvironment that express M6P/IGF2R, such as normal fibroblasts or cancer-associated fibroblasts (CAFs), and thereby decrease IGF-II in the tumor EC matrix via a bystander effect. However, this would need to be investigated further.

In order to validate that our PMP-ligands work the same way as CREG, in which multivalent M6P-ligands inhibit cell viability by increasing the rate of internalization of IGF-II (*163, 228, 229, 335*), we needed to design an internalization assay sensitive enough to detect the minute changes in IGF-II within the conditioned medium following the different treatments. Our ^{125}I-IGF-II internalization assay followed by TCA-based precipitation revealed that 100 nM PMP-OVA was able to deplete intact IGF-II from the medium and increase the amount of radiolabeled species derived from IGF-II degradation (Figure 3.7). These observations strongly imply that the PMP-ligand treatment accelerated the internalization and subsequent degradation of ^{125}I-IGF-II from the conditioned medium compared to the vehicle control. IGF-II is precipitable in TCA as

demonstrated by our validating assay, so the increase in radioactive material in the TCA supernatant fraction reflects the amount of ^{125}I-IGF-II that was internalized and degraded, with the soluble remnants secreted back out into the conditioned medium. As expected, the addition of 100 nM IGF-II protected the ^{125}I-IGF-II tracer from this process, as indicated by increased radioactive counts in the TCA pellet. Much to our surprise, cells that are not as responsive to our PMP-ligands still have a slight enhancement of ^{125}I-IGF-II internalization following treatment with the multivalent M6P-based ligand. This may be due to the cells expressing the M6P/IGF2R on their plasma membranes despite the lack of IGF-II stimulation of the receptor tyrosine kinases.

It is evident that our synthetic, multivalent M6P-based ligands bind to the M6P/IGF2R and accelerate IGF-II internalization, but the mechanism by which cell viability was decreased appears to be a complex story following IGF-II depletion. Apoptosis is occurring at a basal level in the cancer cells we investigated. PMP-OVA treatment appears to increase the number of apoptotic nuclei in IGF-II-dependent cancer cells, but may not be completely dependent on caspase 3 activation. The depletion of IGF-II from the cell milieu would cause decreased activation of the IGF1R and IGF1R/IR-A hybrids. Since inhibiting apoptosis and promoting survival are downstream outcomes of receptor tyrosine kinase activation, it is expected that apoptosis would increase. However, we did not see a significant activation of pro-apoptotic proteins from PMP-OVA alone. This may not be attributed to an increase of apoptosis initiation but rather cells are unable to inhibit the progression of apoptosis following exposure to our multivalent M6P-based ligands. Apoptosis is reversible to a point, until it reaches a point of no return (*341*). Perhaps our ligands cause the cells to have a deficiency in reversing the apoptosis initiation. In the apoptotic immunoblot analysis, PMP-OVA alone did not have much of an effect but enhanced the MCL-1 and PUMA protein quantification in response

to leupeptin or Z-VAD-FMK. This raises the possibility that PMP-OVA may work synergistically with another drug in a combination approach. This is a possibility that would need further investigation.

Autophagy is a cellular process that can result in caspase-independent cell death. We investigated the conversion of LC3-I to LC3-II between PMP-OVA-treated cells and control. There was not a significant change in LC3 conversion that was noticed in immunoblots of whole cell lysates or immunofluorescent staining of the cells. However, this does not indicate that autophagy flux is unchanged, as there could be an issue with the fusion of autophagosomes to lysosomes, which was not investigated in our studies.

Migration and wound closure studies were only preliminary investigations and need to be addressed further. However, our data support the need to validate these studies. The scratch wound healing assay gives the impression that PMP-OVA treatment may accelerate the rate of closure. However, this may be a chemotactic phenomenon given the high concentrations of the ligand used, and that this preparation was different from the ligand used in earlier scratch assays. Much to our surprise, IGF-II did not enhance the closure of the wound in our assays. Conversely, PMP-OVA seemed to attenuate the migration of cells across the membrane of a transwell assay, but it did not inhibit migration completely. IGF-II also did not enhance migration in this study. It is hoped that additional studies will clarify these contradictory results.

In conclusion, our studies further contribute to the understanding of high-affinity, multivalent M6P-based binding to the M6P/IGF2R and the subsequent implications for cancer cell biology. Based on these data and what we currently know about the receptor biology, rapid internalization of the M6P/IGF2R occurs through dimerization, where

multiple contacts of the monomers across the EC domain are made (*140*). This dimerization is stabilized with multivalent M6P-based ligands that bind to the M6P-binding sites on each monomer of the receptor dimer. Our PMP-ligands are believed to bind to repeat 3 on the receptor dimers and mediate the accelerated internalization of IGF-II. Our hypothesis is supported by work done using CREG, a glycoprotein with multiple M6P moieties, and hGUS, a highly glycosylated lysosomal hydrolase. However, further studies need to be done to determine the exact mechanism by which the depletion of IGF-II from the cell milieu reduces cell viability following treatment with our PMP-ligands. We have designed the first synthetic high-affinity, bivalent M6P-based ligands that bind to the M6P/IGF2R, providing support for exploiting this receptor in IGF-II-dependent cancers.

Chapter IV

A Panel of Phosphatase-inert M6P-based Surrogates as "Molecular Rulers" for the M6P/IGF2R

The material covered in this chapter is the topic of the following article in preparation authored by:

Zavorka, M.E., Connelly, C.M,,Fei, X., Malik, G., Berkowitz D.B., and MacDonald, R.G.

A.   Summary

Bivalent M6P-based ligands bind to the M6P/IGF2R with high affinity and cause increased internalization and subsequent degradation of IGF-II in the lysosome, which has potential as a novel therapeutic approach against IGF-II-dependent cancers. Our laboratory has synthesized a panel of high-affinity, bivalent ligands to target the M6P/IGF2R; however, our ligands are susceptible to hydrolysis by phosphatases, rendering them ineffective in an *in vivo* system, such as mouse or human. Thus, in collaboration with Dr. David Berkowitz's lab in the Department of Chemistry at the University of Nebraska-Lincoln, we synthesized phosphatase- and protease-resistant analogs of M6P-based ligands. Two panels of bidentate mannose 6-phosphonate ligands (termed "molecular rulers") have been synthesized using different chemical strategies and their binding to the M6P/IGF2R was examined. The first set of ligands used different linker structures to determine if the linker influences binding of the M6P-based surrogates to the M6P-binding site. Our data indicate that the linkers in the cisoid conformation produce better binding than those in the transoid conformation. The second set of M6P-based surrogates had varying tether links to determine the distance required to span the M6P binding sites of the dimeric M6P/IGF2R. Increased binding affinity is correlated with increased tether length until a certain number of atoms is achieved, after which the affinity decreased most likely due to conformational flexibility and instability of the tether linker. Although our M6P-based surrogates bind the M6P/IGF2R, we were unable to produce true bivalent interaction, as determined through competitive displacement assays in comparison with the known monovalent binding of M6P. However, synthesis of a phosphatase-resistant ligand for the M6P/IGF2R could impact the treatment of IGF-II-dependent cancers by offering a more stable molecule that, if it binds with high-affinity and increases the internalization rate of IGF-II, can be an effective chemotherapeutic agent.

B.   Rationale

The M6P/IGF2R binds M6P-capped ligands with high affinity and traffics them to the lysosome, while IGF-II binds to a separate EC domain of the receptor and is internalized and degraded in the lysosome. Having separate binding sites for the different types of ligands allows this receptor to function as a novel tumor suppressor that can be exploited as a possible therapeutic target against IGF-II-dependent cancers. Our PMP-ligands discussed in chapter III of this dissertation bound to the M6P/IGF2R with high-affinity bivalency that was able to decrease cell viability by internalization of IGF-II and subsequent degradation of the growth factor. A shortcoming of our panel of M6P-based ligands is that they are susceptible to degradative activities—hydrolysis by glycosidases, proteases and phosphatases, and thus may not survive in the circulation long enough to target a tumor. Therefore, we set out to design a panel of M6P-mimetics that would bind with high affinity to the M6P/IGF2R yet resist hydrolysis and degradative inactivation.

It was determined that there are two M6P-binding sites per monomer of M6P/IGF2R (*93*). Simultaneous contacts with two separate M6P groups on distinct oligosaccharides or a single oligosaccharide with at least two M6P caps can bind to the M6P/IGF2R's binding sites with high affinity (*95*). This interaction can improve the binding affinity by 100- to 1000-fold by lowering the dissociation constant, when compared to a monovalent interaction, such as binding of M6P alone. The increased binding affinity of the M6P-containing ligands for the M6P/IGF2R promotes intermolecular cross-bridging interactions by the oligosaccharide occupying M6P-binding sites on both monomers of a dimeric receptor (*93*). A lysosomal enzyme containing multiple M6P moieties, human β-glucuronidase (hGUS), is able to increase the rate of ^{125}I-IGF-II internalization while a bivalent synthetic tripeptide can bind both M6P-binding sites on the same M6P/IGF2R monomer simultaneously is unable to accelerate the rate

of internalization through intramolecular contacts (*131*). This indicates that the accelerated internalization of the M6P/IGF2R results from intermolecular cross-bridging as opposed to intramolecular interactions.

Greater binding affinity of the M6P moiety to the M6P/IGF2R can be achieved with an α(1,2)-glycosidic linkage between the ultimate and penultimate mannose groups on the oligosaccharide. There is a slight reduction when this linkage is α(1,3) (*95*). Additionally, a synthetic panel of multivalent ligands for the M6P/IGF2R that was prepared using a glycopeptide approach demonstrated that compounds containing two M6P residues bonded to a core peptide of three to five amino acid residues were more suitable for high-affinity binding to the M6P/IGF2R (*342*). This suggested that bivalent binding was occurring. Incidentally, further investigation showed that the affinity of the high-affinity tripeptide was attributed to anthranilic acid on the lysine ε-amino group that increased binding by 1500-fold compared to M6P. Removal of this anthranoyl group decreased the binding affinity by 20-fold (*342*), indicating that this group was a contributor for the high-binding affinity, possibly through interactions with a hydrophobic patch near the M6P-binding site on the receptor. As expected, this compound was unable to stabilize a dimeric M6P/IGF2R (*131*). Thus, there is currently no small synthetic compound able to bivalently bind to the M6P/IGF2R through an entirely M6P-based approach.

Work presented herein is a continuation of previous studies (*312, 313*) using new approaches to produce M6P-based synthetic ligands. Our goal, in collaboration with the Berkowitz laboratory from the University of Nebraska-Lincoln, was to synthesize phosphatase- and hydrolase-resistant M6P-based surrogates that would bivalently bind to the cell-surface M6P/IGF2R with high affinity and increase IGF-II internalization by cells; thus, these compounds would function as a more stable therapeutic agent against IGF-II-dependent cancer than our PMP-ligands.

In the first set of phosphatase-resistant M6P-mimics, replacing the phosphate with a phosphonate (Figure 4.1) appeared to bind the M6P-binding sites of the M6P/IGF2R with similar IC_{50} and RBA values of M6P, while malonyl ether and malonate had decreased affinities for the receptor (*312*). The advantage of the phosphonate is that by eliminating the esters and amide bonds of the phosphate, greater resistance to hydrolysis and proteolysis is increased. In order to improve efficacy to work against IGF-II-dependent growth of cancer cells, these ligands must bind with high affinity, i.e., bivalently to the M6P/IGF2R. However, these ligands bound to the M6P/IGF2R with an affinity equivalent to M6P, indicating monovalent binding. These studies indicated that phosphonates are able to bind to the receptor but the tether length of 4 carbons was too short to allow the ligand to span the dimeric M6P/IGF2R to produce bivalent binding (*312*).

The second set of M6P-surrogate ligands was synthesized with increasing tether lengths of 6 to 36 atoms, most of which were carbon (*313*). Work done by the Dahms group estimated that the distance between the M6P-binding sites in domains 3 and 9 of the M6P/IGF2R is about 45 Å apart, while they estimated that the interphosphate distance between M6P groups on a bis-phosphorylated oligosaccharide is about 30 Å (*343*). In contrast, the estimated distance between the two phosphorus atoms on each of the synthetic M6P-mimetic ligands was 16-26 Å, indicating that they may be too short to span the dimeric M6P/IGF2R or even to span the two M6P-binding sites within one monomer of the receptor (*313*). As such, these ligands bound to the M6P/IGF2R with just slightly better affinity than M6P.

Thus, we wanted to synthesize a panel of ligands that would be able to cross-bridge the dimeric receptor in order to produce bivalent binding. Using ^{125}I-PMP-BSA displacement assays with immobilized sM6P/IGF2R, we determined the relative binding affinity (RBA) of each compound synthesized by our collaborators in the Berkowitz
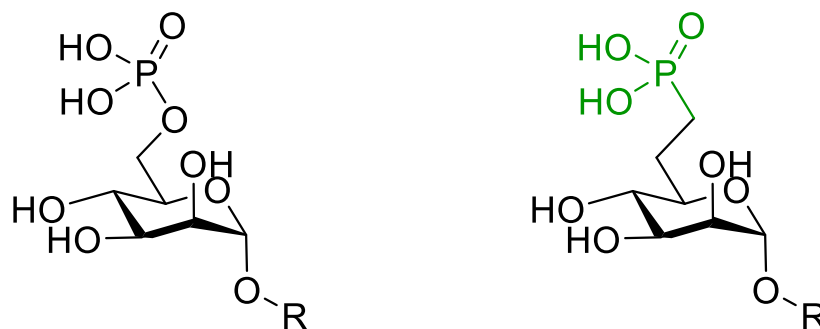
Figure 4.1: ChemDraw schematic drawing of M6P (left) and mannose 6-phosphonate (right). The methylene replaces the methylester bond, improving resistance to hydrolysis.

laboratory. Unfortunately, these ligands all bounds with affinities near that of M6P, indicating that we still have not yet achieved bivalent binding to the M6P/IGF2R. There may be other factors at play besides tether length, such as orientation of the phosphonates or flexibility in the tether that may result in the inability of bivalent binding to occur. Thus, we set out to further our understanding of the binding of the M6P-based ligands for the M6P/IGF2R.

C.   Results

C.1.   Synthesis of bidentate mannose 6-phosphonate surrogates

Xiang Fei and Guillaume Malik in the Berkowitz lab synthesized a panel of mannose 6-phosphonate surrogates using a combination of five different types of chemistries to create diversified ligands (Figure 4.2). The monomeric precursor 4'-azido butyl α-D-mannosyl 6-phosphonate underwent a series of reactions yielding the diversified linkers, while polybutylene glycol (PBG) served as the tether. Global debenzylation of two aza-ylide intermediates yielded compounds with either an amide linkage (amide linkage: BL1) or a triphenylphosphine trapped between the amide linker and tether (amide-triphenylphosphine linker: BL2).   The copper(I)-catalyzed azide-alkyne cycloaddition (CuAAC), or otherwise known as "click chemistry" focuses on 1,4-triazole. Using this chemistry, linkage diversity could be introduced to any azide-terminated molecule (1,4-triazole linker: BL3) (*344, 345*). Another form of CuAAC, Ru(II)-mediated AAC (RuAAC) was also used to target 1,5-triazole as a linker (1,5-triazole linker: BL4). Additionally, Sharpless-Demko cycloaddition/S_NAr sequence (*346*) could be used to provide tetrazole ligands and was conducive to assembly of ligands with spacers of variable length (1,5-tetrazole linker: BL5) (Figure 4.2A). Additionally, polyethylene glycol (PEG) was used as a tether to yield a set of ligands under the same

conditions as BL5 in order to vary the tether lengths (BL6-BL10). By altering the ligation

chemistry, five different linkages were assembled to form ten ligands with variable tether

lengths (Figure 4.2B).

C.2.   Receptor binding properties of the varying polybutylene glycol-linked

mannose 6-bisphosphonate surrogates

The RBAs of the synthetic M6P-based surrogates for the M6P/IGF2R were

determined by ^{125}I-PMP-BSA displacement assays in the presence of increasing

concentrations of unlabeled synthetic ligands (Figure 4.3, Table 4.1). Many features of

the synthetic ligands influence the binding of these ligands for the receptor, such as

number of hydrogen bond donors and acceptors that affect the extent of hydration,

molecular weight, and shape/trajectory of the linker. The IC_{50} values and RBAs for the

compounds with BL1, BL3, BL4, and BL5 (compounds XF-VIII-99, XF-VI-100, XF-VIII-1,

and XF-XV-25, respectively) linkers were all similar to slightly better than those values of

M6P. However, the slight increase in binding of these ligands for the receptor may be

attributed to the availability of two M6P-binding sites per mole of receptor available for

binding, rather than to enhanced interaction with the receptor. Thus, these synthetic

ligands do not appear to be producing bivalent binding that spans the dimeric

M6P/IGF2R. The synthetic ligand with BL2 linker (XF-XV-77) had IC_{50} and RBA values

worse than those of M6P itself, suggesting that the proximal structures in the ligand

interfered with binding. When comparing the features of these ligands, it appears as if

the ligand shapes influence the RBA values the most. The cisoid (bent) link (BL4 and

BL5) is favored over transoid (linear) link (BL2 and BL3). For example, the 1,5-triazole

linkage (BL4) had an RBA that was 3-fold higher than the 1,4-triazole linkage (BL3).

Furthermore, amide bonds have conformational flexibility and can freely rotate between

cisoid and transoid isomers. However, when the amide bond is anchored into a trans-

Figure 4.2. Schematic drawings of the M6P-based surrogates. A) Compounds BL1-BL5 differ in chemistry of the linker, as described in the text, which presents different orientations of the two mannose 6-phosphonate functional groups. B) Compounds BL6-BL10 vary in tether lengths of 4 to 12 repeating unit of PEG to determine the distance required to span the dimeric M6P/IGFR.

A

BL1
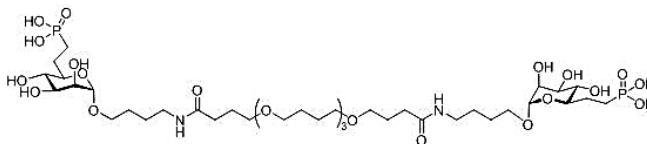
BL2
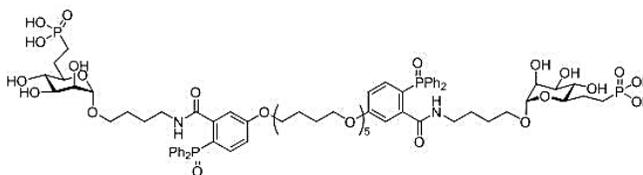
BL3
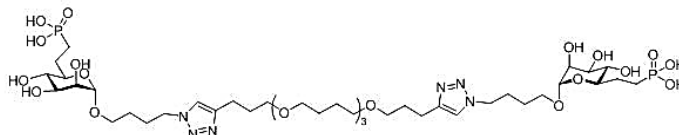
BL4
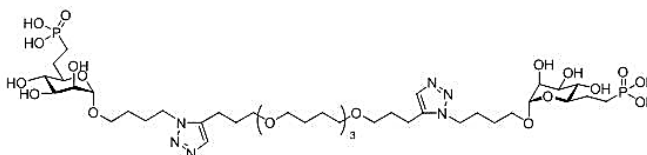
BL5
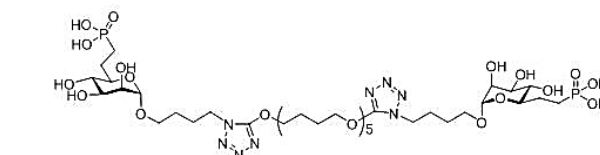
B

BL6
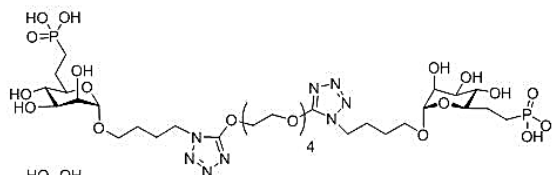
BL7
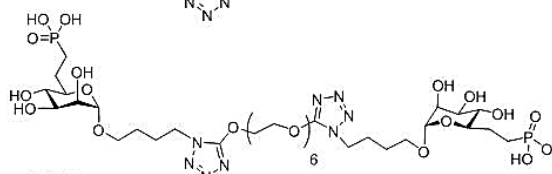
BL8
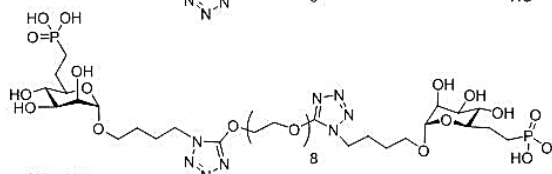
BL9
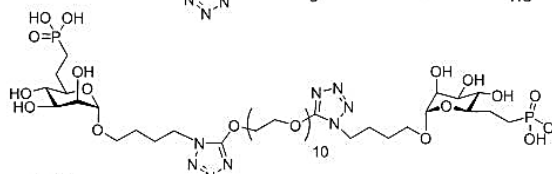
BL10
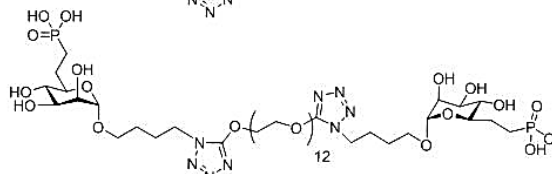
conformation through an intramolecular hydrogen bond, such as between the hydrogen from the amine and an oxygen as seen in BL2, there is a reduction in binding affinity most likely due to the inflexibility of this ligand as locked into an unfavorable trajectory. Nonetheless, all of these ligands achieved binding similar to M6P, indicating that we have not yet achieved bivalent binding.

Ligand	$IC_{50}{}^a$, µM (n)	RBA^b
M6P	11.6 ± 1.7 (6)	1
G6P	>10 mM (n)	N.A.
BL1	2.7 ± 1.4 (3)	2.1 ± 1.1
BL2	18.0 ± 3.3 (3)	0.67 ± 0.12
BL3	5.2 ± 3.3 (3)	1.3 ± 0.84
BL4	1.7 ± 1.3 (3)	3.9 ± 2.9
BL5	6.3 ± 4.2 (3)	2.4 ± 1.6
hGUS	0.02 (1)	640

Table 4.1: Binding Properties of phosphatase-resistant M6P-surrogates BL1-BL5 for M6P/IGF2R.

a. IC_{50} values for competitive displacement of radiolabeled PMP-BSA from the receptor (n = # of trials).

b. RBA = relative binding affinity, normalized to free M6P.
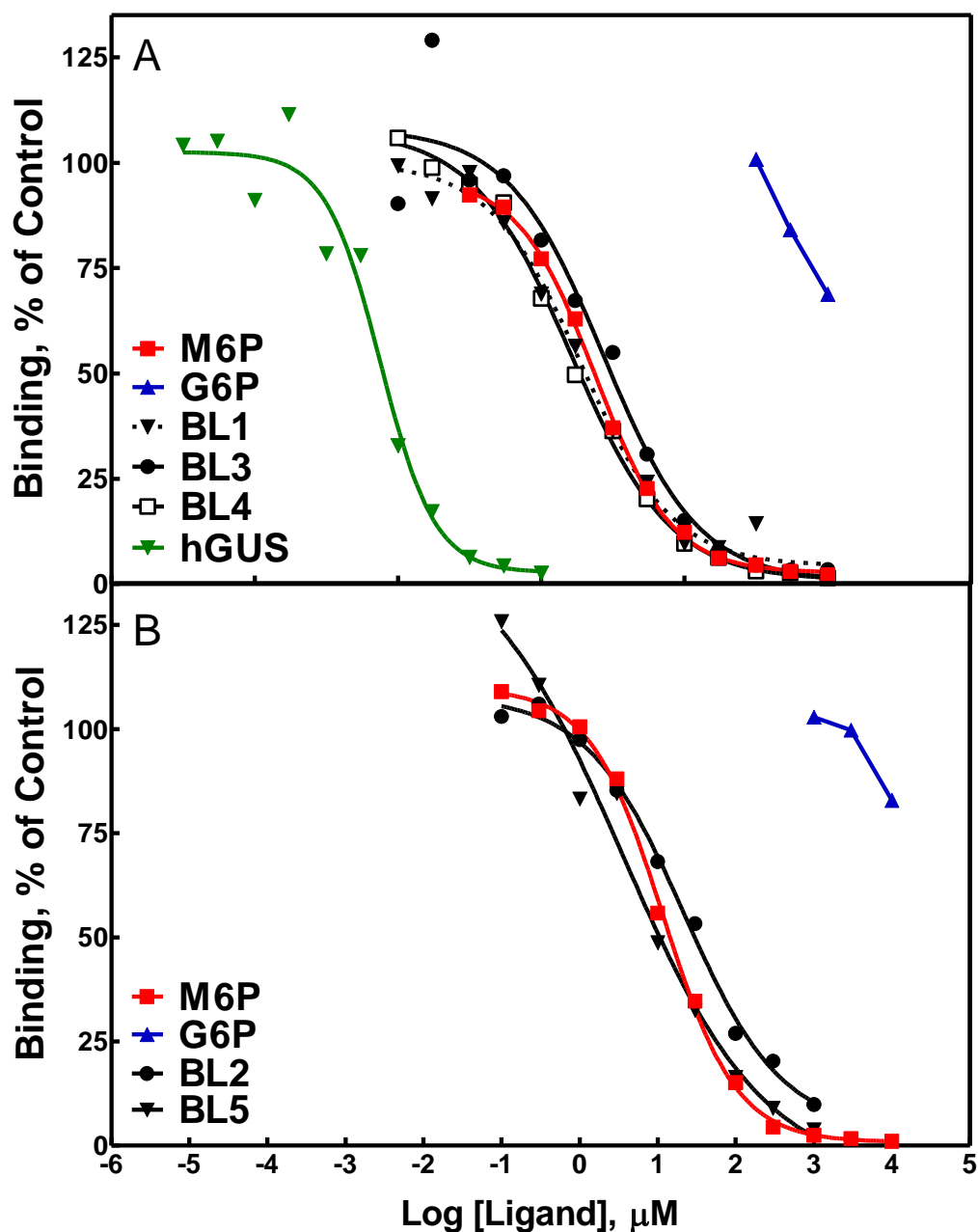
Figure 4.3: Competitive binding analysis of phosphatase-resistant M6P-surrogates BL1-5 in displacement of PMP-BSA from M6P/IGF2R-Sepharose. A) and B) All five compounds bound to the M6P/IGF2R with monovalent binding, similar to M6P. Human β-glucuronidase (hGUS) was employed as a high-affinity, bivalent control whose displacement curve is shifted to the left. Glucose 6-phosphate (G6P) served as a low-affinity or negative control. The binding properties of these ligands are summarized in Table 4.1.

C.3.   Receptor binding properties of the varying PEG-linked mannose 6-bisphosphonate surrogates

Five M6P-based surrogates were designed with increasing number of PEG units within the tether region as a molecular ruler. Interestingly, the RBA values improved as the tether length increased until a length of 8 PEG units (BL8; compound XF-XV-46) was achieved (Figure 4.4 and Table 4.2). From there, the RBA decreased with addition of further PEG units. Although these ligands are predicted to be long enough to cross-bridge the dimeric M6P/IGF2R, it is possible that the increased tether lengths may render them too flexible and unstable such that they fold back on themselves and are unable to produce a conformation favorable to bivalent binding. Additionally, the orientation of the phosphonates may not be positioned correctly to bind both M6P-binding sites simultaneously. Even though there is mild improvement in the RBAs of these ligands, they are still similar to M6P's binding affinity, indicating that these ligands are binding monovalently.

Ligand	$IC_{50}{}^{a}$, µM (n)	RBA^{b}
M6P	11.6 ± 1.7 (6)	1
G6P	>10 mM (n)	N.A.
BL6	5.7 ± 2.4 (5)	1.6 ± 0.69
BL7	3.2 ± 1.5 (4)	2.1 ± 0.94
BL8	1.4 ± 1.1 (4)	3.8 ± 3.0
BL9	4.1 ± 1.2 (6)	1.3 ± 0.37
BL10	5.7 ± 2.9 (4)	1.2 ± 0.59
hGUS	0.02 (1)	640

Table 4.2: Binding Properties of phosphatase-resistant M6P-surrogates BL1-BL5 for M6P/IGF2R.

a. IC_{50} values for competitive displacement of radiolabeled PMP-BSA from the receptor (n = # of trials).

b. RBA = relative binding affinity, normalized to free M6P.
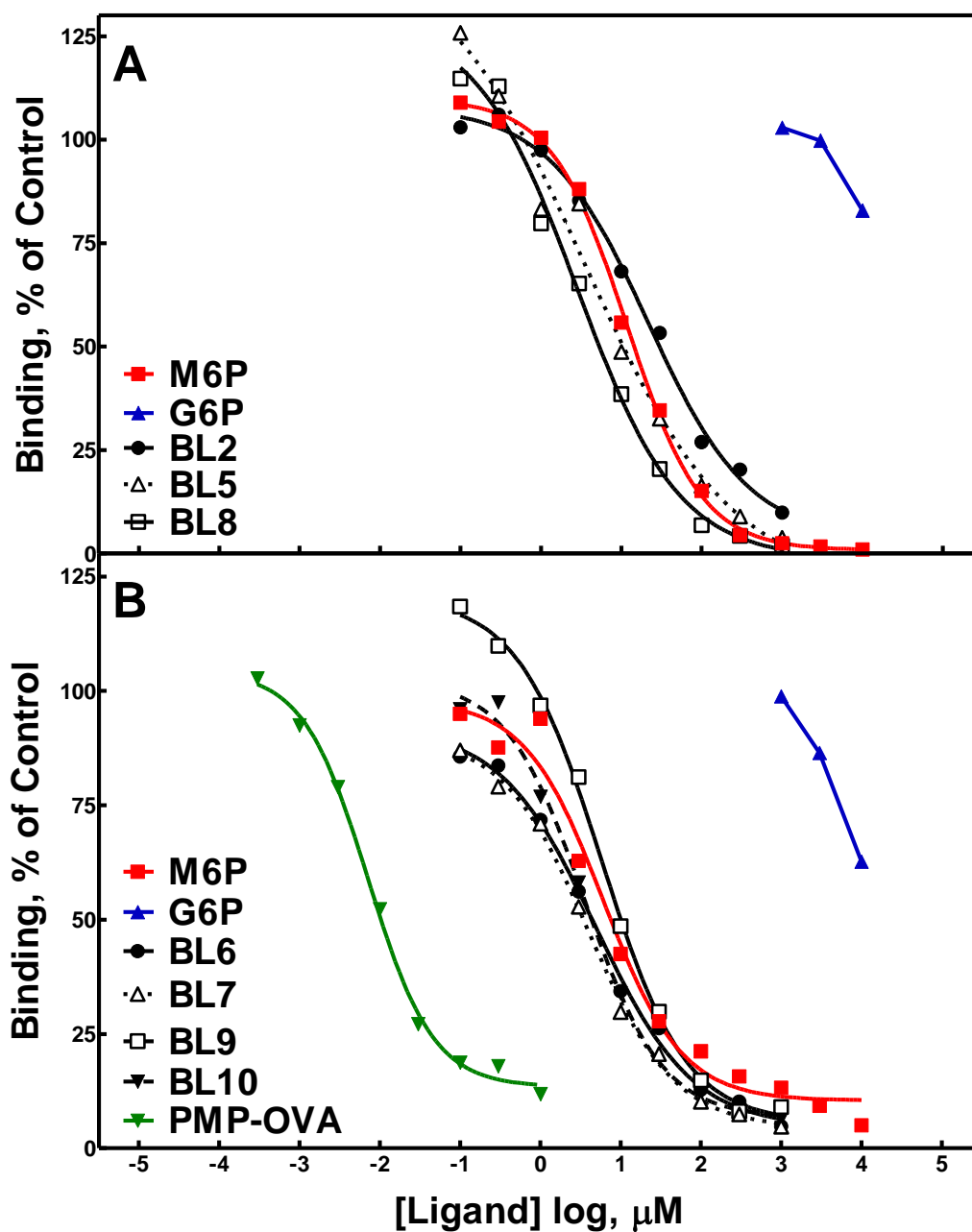
Figure 4.4: Competitive binding analysis of phosphatase-resistant M6P-surrogates BL6-10 in displacement of PMP-BSA from M6P/IGF2R-Sepharose. A) and B) All five compounds bound to the M6P/IGF2R with monovalent binding, similar to M6P. β-glucuronidase (hGUS) and glucose 6-phosphate were run as high-affinity and low-affinity controls, respectively. BL5 was used as a comparison between the two sets of phosphonate compounds, which indicated that both sets bound in the same manner to the receptor

D.   Discussion

Although the compounds with increased tether length were unable to achieve high-affinity binding consistent with bi- or multivalent binding, we have expanded our set of compounds that function as "molecular rulers" to measure the distance between two M6P-binding sites that would clarify intra- vs intermolecular bivalent binding to the M6P/IGF2R. These ligands were synthesized to display diverse linkers to determine if linker orientation influenced the binding affinity, which it did. Some conformations are clearly detrimental to binding to the M6P/IGF2R. Additionally, the tether length was increased to measure the distance between the M6P-binding sites. As the length increased, the RBA increased until 8 PEG units were incorporated. Anything larger than this may be too flexible and have too high of an entropic cost. The amount of enthalpy gained from the interaction with the second binding site is insufficient to compensate for the loss of degrees of freedom of the tether; thus these ligands are unable to produce bivalent binding. In order to complete these studies, we need to address the design concerns that may be affecting our ligand binding affinities. The increased tether length may be long enough, but we would need to stabilize the tether or linker so that these longer compounds do not flex so much or fold back on themselves, rendering them too short to bind in a bivalent manner. Additionally, the trajectory of the ligand matters. Once the first phosphonate binds to one M6P-biniding site, the second phosphonate needs to be either locked into the correct orientation and trajectory (cisoid) or flexible enough that it may rotate to find optimal binding. It is possible that these ligands are not able to rotate to allow both phosphnates to bind two M6P-binding sites at the same time. Once these issues have been addressed and we have achieved high-affinity, bivalent binding, will we need to validate that these synthetic M6P-based ligands are able to decrease the IGF-II-dependent growth of cancer cells. These ligands need to be able to cross-bridge the dimeric M6P/IGF2R and accelerate their internalization, and need to

bind in such a way that leaves domain 11 of the receptor available for binding any bioavailable EC IGF-II. These ligands must promote internalization and subsequent degradation of IGF-II in order to function as a potential therapeutic agent against cancer.

Our latest panel of M6P-based surrogates was designed to fit the known minimal requirements needed to produce high-affinity, bivalent binding to the M6P-binding domains of the M6P/IGF2R. Two M6P groups on separate oligosaccharides or a single oligosaccharide containing at least two M6P caps can bind to the M6P/IGF2R's M6P-binding sites with high affinity, representing a 100-1000-fold increase in binding affinity than the monovalent binding of M6P (*93*). Our bidentate synthetic M6P-based surrogates have two mannose 6-phosphonate groups per molecule of ligand that are capable of binding the M6P/IGF2R. Furthermore, the high-affinity binding of M6P-based ligands is attributed to the negatively charged phosphate groups, as a 25-100-fold decrease in affinity occurs when the phosphates are removed or replaced with sulfate, as seen in unpublished data in our laboratory (Dr. Christopher Connelly, unpublished data). The crystal structure for the bovine M6P/IGF2R domains 1-3 determined that Ser386 within domain 3 interacts with the phosphate oxygens and a water molecule (*63*), and substitution of Ser386 with Ala decreased the recognition of M6P by 100-fold (*103*). Therefore, conservation of these negative charges were necessary to produce appropriate recognition and binding within the M6P-binding pocket. Lastly, it is estimated that the M6P-binding sites within a single M6P/IGF2R monomer are about 45 Å apart yet the maximum distance between phosphates on oligosaccharides is approximately 30 Å (*343*). Since increased internalization results from cross-bridging the receptor, the distance between the M6P-binding sites on the different monomers must be about 30 Å apart. Therefore, our M6P-based surrogates should be long enough to span the dimeric receptor.

Despite our failure of achieve bivalent interactions with this panel of new ligands, this work has promise. The resistance to hydrolysis and phosphatase cleavage is advantageous as an anti-cancer agent. We need to address the issues with the flexibility of the tether lengths and the trajectory of the linkers in order to achieve high-affinity binding ligands. Even though our ligands are long enough to span the dimeric structure of the M6P/IGF2R, these studies indicate how important the precise orientation of the phosphonates is in order to achieve bivalent binding.

Chapter V

A Putative MP6 Receptor Identifed in *Dictyostelium discoideum:*

Chacterization of the M6P-based Binding of the MRH Domains

The material covered in this chapter is the topic of the following article in preparation authored by:

Zavorka, M.E., Connelly, C.M, Fei, X., Malik, G., Nelson, D.L., Berkowitz D.B., and MacDonald, R.G.

A. Summary

The M6P/IGF2R binds many types of M6P-capped glycosylated and non-glycosylated ligands and traffics them to the lysosome. This receptor is mostly involved in lysosomal biogenesis; its role is to bind newly synthesized acid hydrolases in the TGN and transport them to the early endosome. However, the M6P/IGF2R can also bind and internalize IGF-II and other non-glycosylated proteins from the extracellular (EC) milieu. The vast array of ligands that bind the M6P/IGF2R can be attributed to the receptor's 15 EC homologous repeating domains that have high sequence identity to each other and to the one EC domain of CD-MPR. Additionally, each repeating domain has a similar tertiary fold, the MRH domain. The MPRs share overlapping yet distinct roles of transporting ligands and are evolutionarily conserved. However, it is thought that the MPRs may have arisen from a common ancestor and that the M6P/IGF2R (containing 15 EC repeats) may have evolved from multiple gene duplications. However, the most primitive form of the MPRs capable of binding M6P to date has been discovered in the bivalve mollusk, of the genus *unio,* while MPR-like proteins have been identified in *Drosophila melanogaster*. Identification of the earliest forms of the MPRs can provide insights into the origin of the receptors and their functions. *Dictyostelium discoideum*, a social amoeba, has a lysosomal system in which its lysosomal enzymes have been shown to bind the mammalian M6P/IGF2R. However, a MPR has yet to be identified in this organism. We have identified a putative *D. discoideum* MPR (DDMPR), through sequence alignment and bioinformatics studies using multiple mammalian M6P/IGF2Rs as references. The putative DDMPR possesses 5 potential MRH domains with conserved key amino acid residues and cysteines involved in disulfide bonds to form a functional M6P-binding pocket. Additionally, we have analyzed the M6P-binding activity of this putative receptor through PMP-resin affinity chromatography using recombinant

MRH domain mini-receptors that we expressed and purified. In summary, our data demonstrate that *D. discoideum* has a putative MPR, which would be the most primitive MPR known to date, and this finding may have implications on our understanding of the MPRs and lysosomal biogenesis.

B.   Rationale

The M6P/IGF2R (300 kDa) and the CD-MPR (46 kDa) are the only two members of the P-type lectin family that function to transport newly synthesized lysosomal enzymes by recognizing M6P monoester or M6P diester moieties found on the glycoproteins (*46*). Upon recognition and binding of these glycoproteins to the MPRs in the TGN, the complex is transported to the early endosome. Additionally, any M6P-containing glycoprotein that is mis-sorted to the plasma membrane and secreted or any additional EC M6P-capped protein can bind the M6P/IGF2R, but not the CD-MPR, and it is internalized through clathrin-coated pits and shuttled in vesicles to the endosomal-lysosomal system. In the late endosome, the MPRs release their cargo once the acidic pH of below 6 is encountered. Late endosomes containing the cargo fuse with the lysosome while the MPRs are recycled back to the TGN or plasma membrane for another round of trafficking (*46, 160-162, 347*).

As type I integral membrane glycoproteins, the MPRs have an N-terminal signal sequence, an EC domain that contains ligand-binding sites, a transmembrane domain, and a C-terminal cytoplasmic tail. The M6P/IGF2R has 15 EC repeating domains that have high homology (~147) to one another and to the single EC domain of CD-MPR (154 residues) (*348*). It has been shown that the CD-MPR folds into a carbohydrate recognition domain that can bind ligands with high affinity (*62, 349, 350*). The

M6P/IGF2R, with each EC domain having 14-28% identity (*20*), has a conserved pattern of cysteine residues between each domain and also the EC of the CD-MPR. This allows for each domain to fold into its own MRH domain, allowing for 15 potential binding sites in M6P/IGF2R and 1 in CD-MPR. The CD-MPR, in fact, does bind a single mole of M6P per mole of monomeric receptor even though it exists as a dimer or tetramer in the membrane (*94*), but equilibrium dialysis studies have shown that the M6P/IGF2R binds only 2 moles of M6P with high affinity per mole of receptor (*93*). The high-affinity M6P-binding sites of the M6P/IGF2R have been localized to domains 3 and 9 (*106, 107*), with a low-affinity M6P-binding site in domain 5, which interestingly has a preference for M6P diester modifications (*105, 351*). Recently, another low-affinity M6P-binding site has been identified in domain 15 (*101*). The high-affinity M6P-binding sites are not functionally equivalent, as determined by studies using mutant full-length receptors with only one functional M6P-binding site (*352*). Additionally, a glycan microarray analysis of *N*-glycan isoforms that had zero to two M6P-GlcNAc phosphodiesters or M6P monoesters was used to determine specificity of the CD-MPR and M6P/IGF2R; the latter receptor is able to recognize a larger repertoire of glycosylated ligands than CD-MPR, due to the different ligand-binding domains within the EC domain (*353*). Furthermore, when either MPR is knocked out in mice or cells, the results indicate that the M6P/IGF2R is more efficient at targeting lysosomal enzymes than the CD-MPR (*354, 355*). The M6P/IGF2R has a higher binding affinity and recognizes a broader array of lysosomal enzymes than the CD-MPR (*356, 357*). However, one receptor cannot fully compensate for the loss of the other, indicating that, even though there are redundancies, they are both important for proper lysosome biogenesis (*88, 89*). Nonetheless, the M6P/IGF2R has enhanced lysosomal enzyme trafficking over the CD-MPR in addition to the CD-MPR's inability to bind ligands at the cell surface as this

environment is not at the pH optiumum for ligand binding. These functions of the M6P/IGF2R may have evolved from an earlier form of the receptor.

Dictyostelium discoideum, a social amoeba or slime mold, in the vernacular, has a lysosomal system, and its lysosomal enzymes have been well characterized in axenic cells (*358*). These lysosomal enzymes have *N*-linked oligosaccharides possessing M6P residues in methyldiester linkages or mannose 6-sulfate (M6S) moieties (*41, 43, 99, 359*). *D. discoideum* lysosomal enzymes, such as α-mannosidase and β-glucosidase, can bind the mammalian M6P/IGF2R in domains 3 and 5 with high affinity (*105, 108, 360*). The ability of the mammalian M6P/IGF2R to recognize M6P moieties in diesters and M6S may be due to broader binding pockets of domains 3 and 5 that would accommodate these larger modifications, which is expected to exist in the MPR of *D. discoideum* (*63, 104, 351*). Furthermore, the sulfate and phosphate monoester both have one negative charge rather than the two charges that phosphate possesses, which may attribute to differences in binding preference. The precursors for α-mannosidase and β-glucosidase are membrane-bound, and following proteolytic cleavage, become soluble and are transported to the lysosome, yet to date, there has not been an MPR identified in *D. discoideum* (*40, 361*).

Recently, our laboratory in collaboration with David Berkowitz's laboratory at the University of Nebraska-Lincoln has identified a putative MPR in *D. discoideum* (DDMPR). Thus, the goal of this study was to characterize the structure and ligand-binding properties of this putative receptor in comparison to the mammalian M6P/IGF2R. To do this, initial studies performed multiple sequence alignments and homology modeling that compared the M6P-binding domains of the CD-MPR and domains 3, 5, and 9 of the M6P/IGF2R, revealing 5 potential MRH domains within the putative DDMPR amino acid sequence (Figure 5.1). Furthermore, regions 3 of the MRH domains in the

Figure 5.1: Schematic of the DDMPR gene with 5 MRH domains. The five MRH domains (R1-R5) are shown in red with R3 having the highest identity to domain 3 of the mammalian M6P/IGF2R.   The G1 and G2 regions may encode possible glycotransferase domains just N-terminal to the transmembrane domain (TM).   The putative DDMPR sequence is 2441 amino acids in length.

DDMPR have the cysteine patterning and conserved amino acid residues that are involved in M6P-binding comparable to the MPRs. A recombinant mini-receptor of DDMPR R1-3 was expressed in the mammalian expression system and ligand binding studies were performed by pulling down the mini-receptors (DDMPR or human mini-receptors) with PMP-Sepharose resin and competitively displaced with M6P to determine relative binding affinities. Additionally, repeat 3 of the MRH domains in the DDMPR was expressed in the bacterial expression system and subsequently purified and characterized *in vitro*. From these preliminary studies, we have identified a putative MPR in *D. discoideum* that binds M6P, suggesting that the M6P binding function of the MPRs arose at an earlier stage in evolution than previously thought, and may serve as a more simplistic model for studying lysosomal enzyme targeting and lysosomal storage diseases.

C.   Results

C.1.   Identification of a putative MPR in *D. discoideum* via bioinformatics and previous binding studies

There are several proteins that have MRH domains, but these domains within the MPRs have been the only ones found to bind M6P (*25, 46*). Since *D. discoideum* lysosomal enzymes have been shown to bind to the mammalian M6P/IGF2R (*108*), it was hypothesized that this slime mold species may have a similar protein containing MRH domains. Therefore, several bioinformatics-based searches were conducted previously by David Nelson in our collaborator David Berkowitz's lab at the University of Nebraska-Lincoln, to identify any genes/open reading frames within the *D. discoideum* genome that might encode MRH domains and could serve as orthologs of the

mammalian M6P/IGF2R. First, the putative *D. discoideum* M6P-like receptor (DDMPR) needed to have at least one MRH domain, as well as retain key cysteine residues forming disulfide bonds and essential binding residues within the MRH domain that have been identified in the CD-MPR and M6P/IGF2R. Lastly, the MRH domain needed to retain the canonical anti-parallel flattened β-barrel found in the known receptors' M6P-binding domains. If the putative DDMPR fit the above criteria, it may serve as the most evolutionarily primitive form of the MPRs known to date.

Using a basic local alignment search tool (BLAST) and InterProScan analyses that allows searches within various genomes for similar sequences and motifs, respectively, two nucleotide sequences that encode hypothetical protein sequences that have significant homology with the bovine M6P/IGF2R domain 3 sequence were identified in chromosome 5 of *D. discoideum* AX-3 strain (Hit 1 nucleotide accession: XM_630458.1; Hit 1 protein accession: XP_63550.1; Hit 2 nucleotide accession: XM_630374.1; Hit 2 protein accession: XP_635466). These proteins met the aforementioned criteria and had five contiguous MRH domains. Further analysis of these two hypothetical proteins yield 1526 amino acid residues for Hit 1 and 2441 amino acid residues for Hit 2. The two sequences are very similar with minor differences, yet further study indicates that Hit 1 appears to be an incomplete version of Hit 2; therefore, we believe that Hit 1 may not encode an actual protein. Based on the sequence alignment and conservation of cysteines, it was hypothesized that the third MRH domain (repeat 3, or R3) of the putative DDMPR would have a similar overall tertiary structure with domain 3 of the bovine M6P/IGF2R. Indeed, through a series of bioinformatic analyses (Jmol and Spartan 04) to study the 3-dimensional structure of the DDMPR MRH domains compared to the crystal structure of the bovine M6P/IGF2R domain 3 (Protein Data Bank I.D.: 1ISZO) revealed that the DDMPR R3 retains the anti-parallel

flattened β-barrel sandwich (Figure 5.2) needed for a MRH domain. Additionally, DDMPR domains 2-4 were similar to the structure and fold of the bovine M6P/IGF2R domains 1-3 with slight differences in amino acid side-chain positioning. Further studies determined the likelihood of M6P interacting with DDMPR R3 in a dynamic simulation (AutoDock 4 software; The Scripps Research Institute), which revealed that M6P does indeed dock within the potential binding site of DDMPR R1-R3, but it eventually dissociates, unlike docking of the bovine M6P/IGF2R domains 1-3. This dissociation most likely occurs because the DDMPR R1-R3 domain forms a larger binding pocket that may accommodate a molecule that is larger than M6P; this possibility has not yet been explored, but is consistent with the M6P-methylester modifications found on *D. discoideum* lysosomal enzymes. The DDMPR is unique from the other known MPRs in that there are two motifs corresponding to glycosyltransferase domains, which are not present in the higher order MPRs. It has yet to be determined if these domains are part of a catalytic activity of the receptor. A hydrophobic region was detected using Kyte and Doolittle analysis (*362*), indicating that this protein has an N-terminal transmembrane domain. In Dr. Chris Connelly's doctoral work, Vector NTI® Align X program (Invitrogen, Carlsbad, CA) was used to do a multiple species sequence alignment of the DDMPR R3 against the M6P/IGF2R domain 3. It predicted that DDMPR R3 was the best candidate, sharing 17% identity with all mammalian receptor species used in this alignment and 21.4% identity with the human M6P/IGF2R. Furthermore, DDMPR R3 has high identity of conserved residues involved in disulfide bonds and M6P-binding in the mammalian proteins, with this domain containing 6 cysteines that resemble the pattern of cysteins in domain 3 of the bovine M6P/IGF2R. The MRH domains of the M6P/IGF2R and CD-MPR are about 150 amino acid residues in length having a pattern of cysteine residues. Ten MRH domains of the M6P/IGF2R have 8 cysteines, one domain (domain 13) has 12 cysteines with 4 of those cysteines residing in the fibronectin type II domain, one domain

has 9 cysteines, and three domains of the M6P/IGF2R as well as the single MRH domain of the CD-MPR all have 6 cysteines (*20*). One final similarity of the DDMPR MRH domain to that of CD-MPR is the conservation of His105 that allows formation of a hydrogen bond with the phosphate group of the incoming M6P moiety upon binding (*98*). Following the bioinformatics analysis of the conserved sequence alignment and amino acid residues and maintaining the tertiary fold similar to the MRH domains of the M6P/IGF2R, a DDMPR C-terminally FLAG-tagged construct encompassing R1-R3 was designed and synthesized by Dr. Chris Connelly in his doctoral work (unpublished).

Using a similar cloning strategy that was done previously in our laboratory by Chad Byrd during his doctoral work to make the human mini-receptors of the M6P/IGF2R followed by a C-terminal FLAG-tag (1-3F, 1-8F, 7-9F, 1-15F) (*144*), DDMPR R1-R3 was synthesized by GenScript Corporation (Piscataway, NJ) and engineered using human codon usage tables to be expressed in mammalian cells (HEK 293 and HEK 293T cells). The DDMPR FLAG-tagged cDNA was cloned into pCMV5RIX/1-3F vector (the pCMV5 vector with a mutated *Eco*RI restriction endonuclease site in the multiple cloning sequence) using *Eco*RI at the 5'-end and *Xba*I at the 5'-end, thereby dropping out the 3'-half of the sequences encoding the human M6P/IGF2R domain 1 and the full domains 2 and 3. Therefore, the new DDMPR-containing vector would have the human M6P/IGF2R leader sequence expressed at the N-terminal end for proper localization and expression (Figure 5.3). Dr. Connelly validated the DDMPR construct to be about 76 kDa according to SDS-PAGE analysis and αFLAG immunoblots and was expressed in both the lysate and conditioned medium (data not shown). Additionally, Dr. Connelly tested the ability of the DDMPR to bind PMP-Sepharose resin, in which the M6P-groups on the
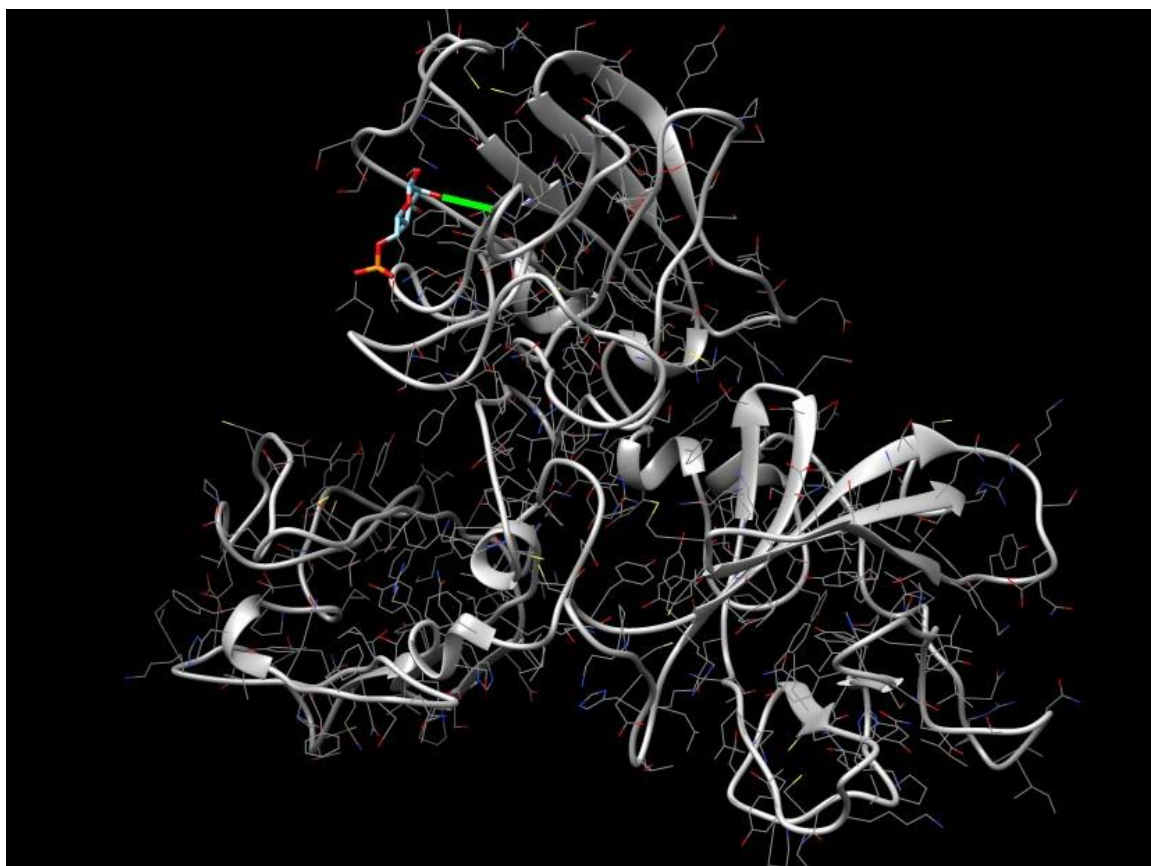
Figure 5.2: Ribbon structure of MRH regions 1-3 of the putative DDMPR. The sequence coding the first three MRH domains were aligned with the crystal structure of the bovine M6P/IGF2R (PDB: 1ISZO) to create a PDB file using SWISS-MODEL (Swiss Institute of Bioinformatics, Lausanne, Switzerland), and docked with M6P (blue mannose ring with red oxygens) using SwissDoc (Swiss Institute of Bioinformatics). The overall structure is predicted to fold into flattened β-barrels similar to the MRH domains of the M6P/IGF2R. This docking structure was visualized using the PDB docking file in USCF Chimera version 1.10.1 (University of California, San Fransico, CA).
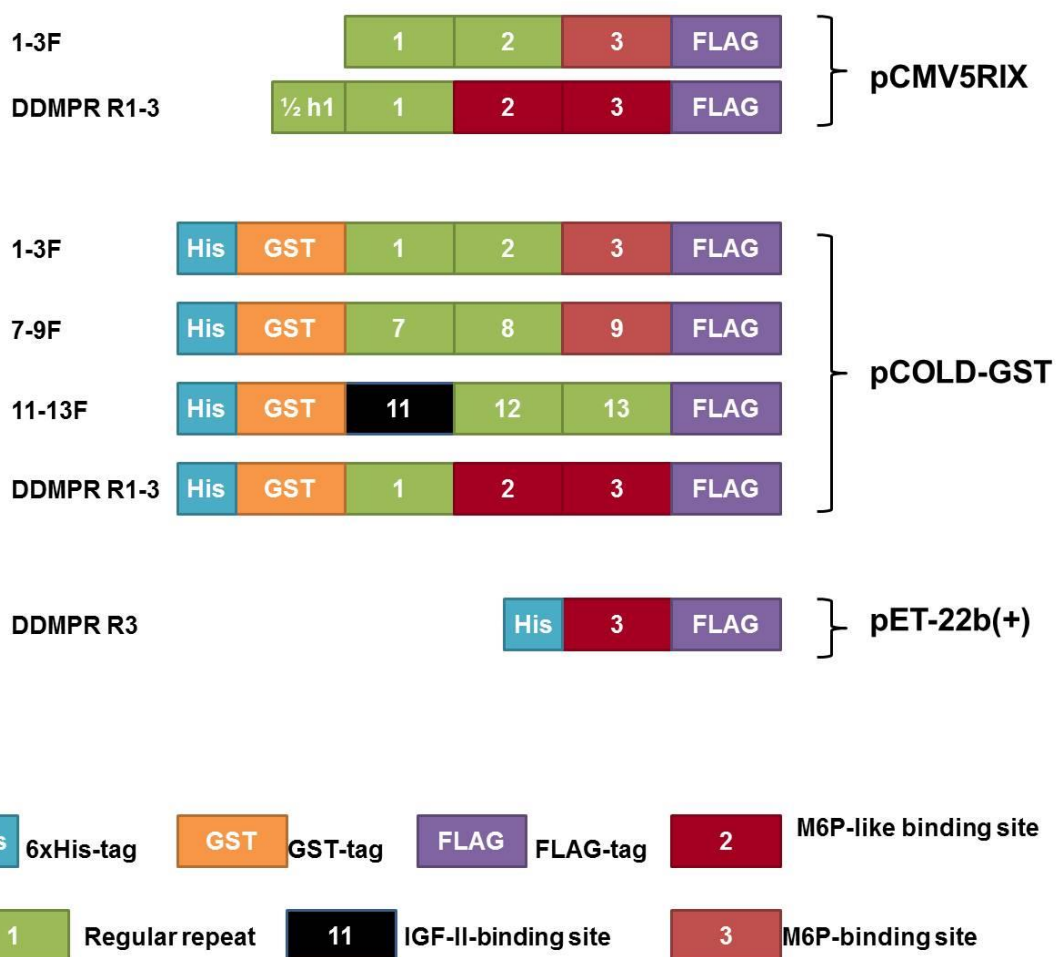
Figure 5.3: Schematic of the DDMPR and human M6P/IGF2R mini-receptor constructs. The pCMV5RIX vector constructs were expression in HEK 293 and 293T cells. DDMPR R1-3 has the first half of the human domain 1 as a leader sequence for proper protein expression. The pCOLD-GST vector constructs were expressed in *E. coli*. Constructs 13-F, 7-9F, and 11-13F represent the human M6P/IGF2R mini-receptors encompassing those domains, while DDMPR R1-3 encompasses the first 3 MRH domains of the putative DDMPR. All 4 constructs have an N-terminal His- and GST-tag. The pET-22b(+) vector construct was expressed in BL21 cells and has an N-terminal His-tag. The DDMPR R3 encompasses only MRH region 3.

immobilized PMP should bind the potential M6P-binding pocket of the DDMPR. Interestingly, he found that DDMPR R1-3 is pulled down by the PMP-Sepharose resin, but the addition of 10 mM M6P appeared to enhance paradoxically the binding rather than competitively displace the DDMPR R1-3, and the addition of NaCl slightly increased binding compared to his DDMPR R1-3 alone group. Another interesting observation from the pull-down experiment done by Dr. Chris Connelly is that he was unable to pull down the human 7-9F mini-receptor in lysates or conditioned medium. However, since the human 1-15F mini-receptor was readily pulled down (possibly through the binding of domain 3), this supported these assays as a valid way to determine DDMPR R1-3 binding. Nevertheless, these preliminary studies supported the hypothesis that DDMPR R1-3 does bind M6P but needed further investigation.

C.2. DDMPR secreted into conditioned medium by transfected 293 cells binds M6P but differs from mammalian M6P/IGF2R

In order to characterize the binding of DDMPR, we expressed DDMPR domains 1-3F and human mini-receptors in HEK 293 and HEK 293T cells using a standard calcium phosphate protocol as previously described (*305*). All constructs expressed well in the lysates and conditioned medium (Figure 5.4A). Previous experiments by Dr. Connelly showed that DDMPR R1-3 and human 1-15F mini-receptors bind PMP-Sepharose resin, indicating that the DDMPR R1-3 mini-receptor's MRH domain can bind M6P moieties. To determine the extent of M6P-based binding to DDMPR R1-3, we used a series of pull-downs and immuno- or ligand blotting studies with increasing concentrations of M6P or the negative control glucose 6-phosphate (G6P). In the first sets of experiments, DDMPR R1-3 was pulled down using PMP-Sepharose resin, electrophoresed on 10% SDS-PAGE gels, and probed with αFLAG antibody in an immunoblot and compared to the positive control human 1-3F to determine that we have

proper folding of the mini-receptors (Figure 5.4B). In a set of samples from each receptor, 20 mM M6P was co-incubated during the pull-down phase to competitively displace the mini-receptors. Interestingly, DDMPR R1-3 can be pulled down only from the conditioned medium pool and not from lysates. This may indicate that the receptor harbored within the cells does not have the proper conformation to acquire ligand-binding function, whereas the properly folded receptor that is capable of being secreted has attained its native conformation and thus, biological function. Additionally, there could also be such high translational rates of the receptor (especially in 293T cells) that it escapes proper folding and becomes trapped within the intracellular compartments instead of achieving proper folding in the TGN necessary for secretion into the conditioned medium. Nonetheless, DDMPR R1-3 bound well to the PMP-resin, but interestingly was not displaced by 20 mM M6P. The positive control 1-3F mini-receptor from cell lysate bound to the PMP-resin and was displaced by M6P as expected, while the negative control empty vector pCMV5 lysate did not bind at all as expected considering that it does not express a mini-receptor.

We next tried displacing the DDMPR from the resin using a broader range of M6P concentrations to determine which levels of M6P interfere with receptor binding to the PMP-Sepharose resin. In theory, as the concentration of M6P increases, it will compete for the M6P-binding sites on the receptors that, after washes of the resin, will result in full dissociation of the receptor from the resin. In this experiment, M6P did not interrupt binding of the DDMPR R1-3 to the PMP-resin even at concentrations as high as 50 mM, but rather appeared to enhance binding slightly (Figure 5.4C). Conversely, even the lowest concentration of M6P (1 mM) that we tested with the human 1-3F disrupted binding and released the protein from the resin. However, the negative control G6P also inhibited binding of the human 1-3F, which was not expected. We next used smaller

increments of ligand concentrations to determine if different amounts of M6P could modulate DDMPR R1-3 binding. It appeared as if low concentrations of M6P (0.1-1 mM) progressively increased the DDMPR R1-3 binding to the PMP-Sepharose (Figure 5.4D). However, 0.5 mM M6P significantly decreased the binding of human 1-3F to PMP-Sepharose and no binding was detected at 5 mM M6P and higher. Again, G6P was also affecting human 1-3F binding. To explain this, we may have had an unfortunate M6P contamination in our G6P stock, which would explain why DDMPR R1-3 has an increased binding with 5 mM G6P but human 1-3F was competitively displaced. Confusingly, an additional experiment revealed that 0.01 and 0.05 mM M6P decreased the DDMPR R1-3 binding to the PMP-resin, but 0.1-0.5 mM enhanced binding. The addition of 1, 5, and 10 mM significantly decreased the binding of DDMPR R1-3 while 0.01-10 mM G6P did not have much effect, and DDMPR R1-3 bound well under these conditions (Figure 5.4D).

To account for the possibility that the human 1-3F mini-receptor may be more sensitive to improper folding or more readily displaced, we conducted PMP-Sepharose pull-down experiments with soluble bovine M6P/IGF2R (^{125}I-sM6P/IGF2R) that contains the first 14 EC domains and part of domain 15. DDMPR R1-3 conditioned medium or ^{125}I-sM6P/IGF2R was incubated end-over-end at 4°C overnight with the resin in the presence or absence of increasing concentrations of M6P or G6P. Following the pull-down assay and subsequent washes of the resin, the samples were electrophoresed and the ^{125}I-sM6P/IGF2R gel dried down before exposure to radiographic film. The DDMPR R1-3 gel underwent transfer and immunoblotting, probing with αFLAG antibody. The ^{125}I-sM6P/IGF2R bound to the PMP-resin and appeared to tolerate the addition of M6P until 0.03 mM, which greatly disrupted binding of the receptor for the resin (Figure 5.5). At 1 mM M6P, no bound radiolabeled receptor was detectable following
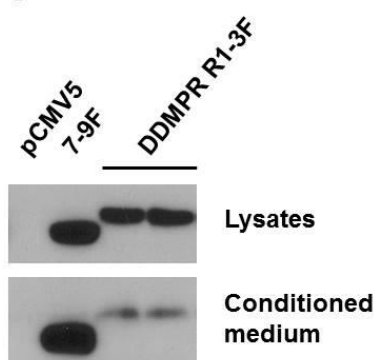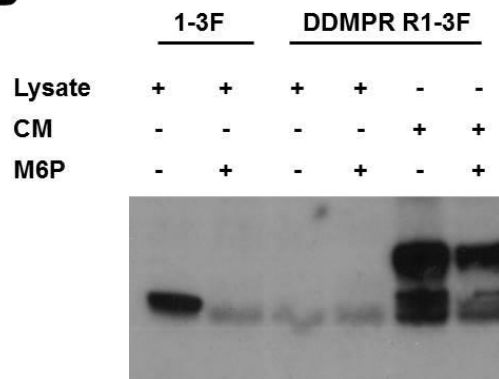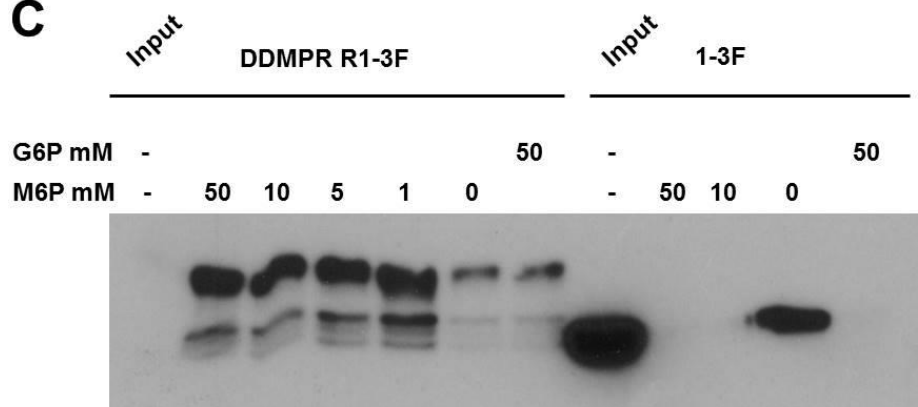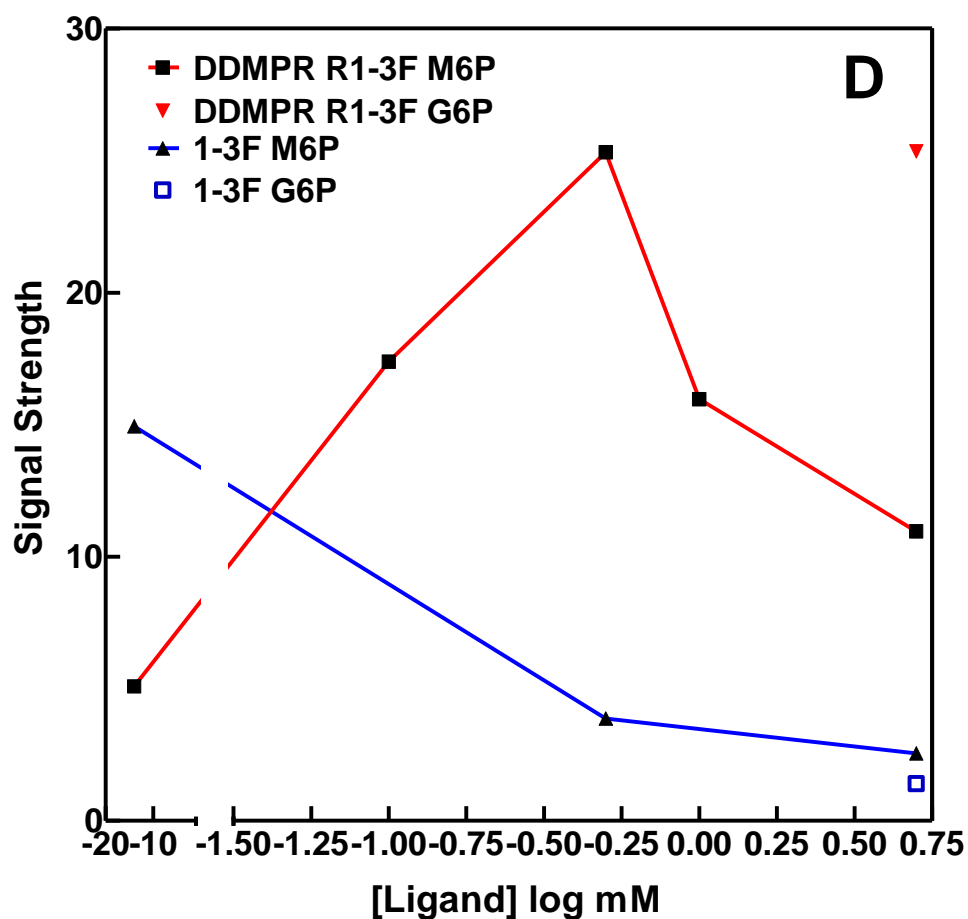
Figure 5.4: Mammalian expression and analysis of DDMPR R1-3F in lysates and conditioned medium of HEK 293 cells. A) Transfected cells expressed the DDMPR mini-receptor and all human mini-receptors in lysates and the conditioned medium, as detected by α-FLAG immunoblot analysis. B) DDMPR R1-3F from CM, but not lysates, pulled down with PMP-Sepharose resin, which binds to the mini-receptor's M6P-binding domain. M6P (10 mM) was able to partially disrupt the binding of DDMPR R1-3 with the resin. C) M6P partially displaced DDMPR R1-3F from the PMP-Sepharose by competitively disrupting M6P-based binding, although M6P was far more effective at displacing human 1-3F. Note that DDMPR R1-3F in the CM has a lower contaminating band for an unknown reason. D) Quantification of the M6P displacement in C) confirmed that increasing concentrations of M6P improves DDMPR binding to the receptor-resin until maximal binding is reached at which point binding drops, while M6P hinders human 1-3F binding to the receptor-resin.

electrophoresis. In this blot, G6P up to a concentration of 20 mM had no effect on receptor binding to the resin, indicating that the binding is specific for M6P. With the DDMPR R1-3 immunoblot following this pull-down, we saw an interesting pattern of receptor binding to the PMP-resin, where 1 mM and 10 mM M6P or G6P improved binding, while there was a steady decrease in binding with the lower ligand concentrations (Figure 5.5). It is possible that the precise concentration of M6P can either aid or hinder the M6P-binding of DDMPR R1-3. Another possibility is the amount of endogenous M6P/IGF2R in the cell lysates from the HEK 293 cells may interfere with binding of DDMPR R1-3 to PMP-Sepharose; as M6P increases, it can displace the endogenous receptor and free up available binding sites for DDMPR R1-3 to bind. Together, these data suggest that the DDMPR binds M6P but not as tightly as the mammalian M6P/IGF2R, indicating that the DDMPR may have other ligands it prefers, such as M6S or M6P methyl ester.

At that point in the project, we had lost expression of our DDMPR R1-3 in lysates and conditioned medium. We attempted transfections using different reagents, concentrations of reagent and cDNA, different cell lines, and different techniques, all of which did not express the DDMPR R1-3 in the conditioned medium. However, these binding assays suggest that DDMPR is able to bind M6P-modified glycoproteins, but this receptor may prefer additional or structurally analogous but slightly different ligands, as M6P is unable to completely disrupt the binding of the receptor with PMP-Sepharose. Additional ligands that may be more suitable for DDMPR's binding pocket need to be tested to determine the relative binding affinity of these ligands for the putative receptor.
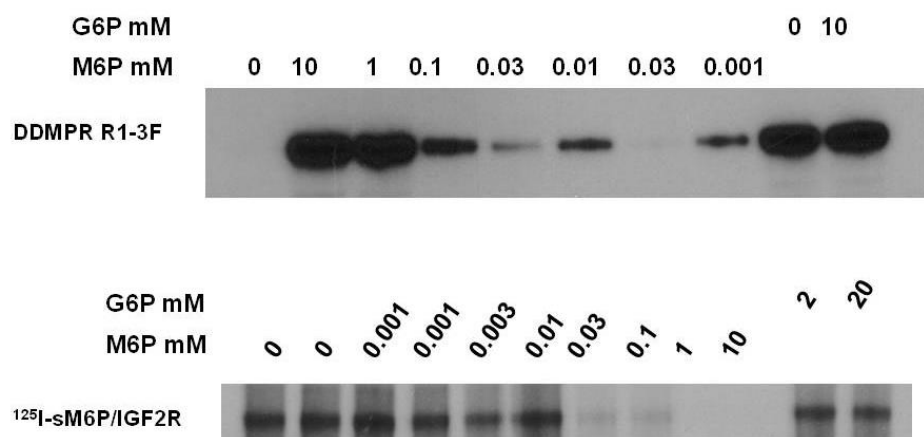
Figure 5.5: Differential Affinity of DDMPR R-3F versus sM6P/IGF2R to pull-down by PMP-Sepharose and to displacement with M6P. DDMPR R1-3F from the CM and ^{125}I-sM6P/IGF2R were pulled down with PMP-Sepharose resin with increasing concentrations of M6P and G6P. The DDMPR R1-3F had a different displacement profile than the ^{125}I-sM6P/IGF2R.

C.3.   Purification of endogenous DDMPR from Ax3 conditioned medium using *D. discoideum* lysosomal enzymes

Due to our inability to express large amounts of properly folded DDMPR R1-3 in the conditioned medium, we attempted to purify the endogenous receptor from *D. discoideum* Ax3 and Ax4 cultured cells. The endogenous DDMPR would be significantly larger (~270 kDa according to ExPASy ProtPram analysis using the protein sequence) than our mini-receptor. Since *D. discoideum* lysosomal enzymes are known to bind the mammalian M6P/IGF2R (*108*), we attempted to purify these enzymes using the soluble bovine M6P/IGF2R (sM6P/IGF2R) bound to Sepharose resin. Our goal was to use *D. discoideum* purified lysosomal enzymes to bind the endogenous DDMPR through affinity chromatography.   Following sIGF2R-Sepharose resin pull-down of the conditioned medium and ^{125}I-sM6P/IGF2R ligand blotting, M6P-capped proteins were pulled down in both Ax3 and Ax4 cell lines (Figure 5.6A). To improve separation of these M6P-capped proteins, we performed DEAE-Sepharose ion-exchange chromatography of the *D. discoideum* Ax3 conditioned medium in sodium phosphate buffer and eluted with a NaCl concentration gradient. After dialysis and lyophilization of the column fractions, the samples were electrophoresed and ligand-blotted with ^{125}I-sM6P/IGF2R as probe. The ligand blot showed improved separation of the M6P-capped proteins (Figure 5.6B). However, these ligands are not yet purified based on their M6P-content, as additional proteins at similar molecular weights and charges but that are not necessarily M6P-containing proteins could have migrated through the column. We then tried to purify these ligands using a sM6P/IGF2R-Sepharose affinity chromatography eluted with increasing concentrations of M6P. ^{125}I-sM6P/IGF2R ligand blot analysis revealed that some M6P-modified proteins eluted in the later M6P elution stages, but recovery of protein from the column was low (Figure 5.6C). This suggests that the endogenous *D.*
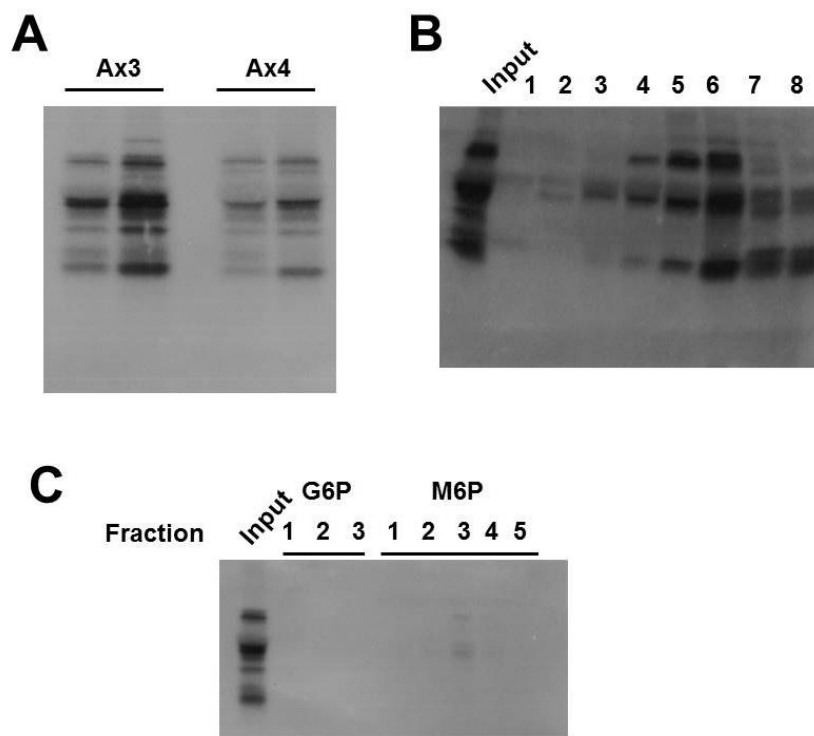
Figure 5.6: Purification of endogenous *D. discoideum* lysosomal enzymes. A) Whole cell lysates from *D. discoideum* Ax3 and Ax4 strains were electrophoresed under native conditions and probed with ^{125}I-sM6P/IGF2R to determine if these cells expressed M6P-capped glycoproteins. B)   Ax3 cell lysates were fractionated with ion-exhange chromatography eluted with a NaCl gradient and the fractions (1-8) were electrophoresed on 8-16% SDS-PAGE. The gel was transblotted to nitrocellulose probed with ^{125}I-sM6P/IGF2R under ligand blotting conditions, which revealed that there were multiple proteins eluting that bind to the bovine M6P/IGF2R C) sM6P/IGF2R-Sepharose purification of Ax3 cell lysates using M6P as the eluent demonstrated that this method may not be useful for purification of enough lysosomal enzymes for future studies.

discoideum ligands are not eluting off of the column, either because of increased affinity for the sM6P/IGF2R-resin or by non-specific binding to the resin that was lost due to incomplete column conditioning (i.e. incomplete blocking of the non-specific binding on the resin with BSA). Despite our efforts, we were unable to purify the endogenous *D. discoideum* M6P-containing ligands and immobilize them on a resin bed to capture the endogenous DDMPR. Perhaps a more specific receptor-specific antibody immobilized to resin would better serve our purposes of purifying the endogenous receptor, but this will have to await further experiments.

C.4. Cloning, expression, purification and folding of pCOLD-GST/DDMPR in a bacterial expression system

Several labs have purified, refolded, and performed structural studies, such as x-ray crystallography, on bovine M6P/IGF2R mini-receptors in ligand-bound and ligand-free states (domains 1-3, 5, 11, and 11-13) to characterize the receptor (*61, 63, 64, 101, 343, 363*). Since our laboratory, in collaboration with the Berkowitz laboratory, has discovered the putative M6PR in *D. discoideum*, we decided to express truncated forms of the putative receptor in a bacterial expression system. We engineered FLAG-tagged domain 3 of the DDMPR and tri-repeat mini-receptors of the human M6P/IGF2R (domains 1-3, 7-9, and 11-13) into a pCOLD-GST vector. This vector has N-terminal His- and GST-tags upstream of the constructs followed by a FLAG-tag to the carboxyl terminal end (Figure 5.3). A human rhinovirus 3 C protease site (Leu-Glu-Val-Leu-Phe-Gln|Gly-Pro) lies between the GST-tag sequence and upstream of the protein sequence, that can be cleaved with proteases such as HRV 3 C or Turbo 3 C. Additionally, there is

a Factor Xa site (Ile-Glu-Gly-Arg) following the His-tag sequence, adding to the versatility of this plasmid.

Using a similar cloning strategy to our previous DDMPR 1-3F construct, we PCR-amplified our DDMPR 1-3F fragment insert from the pUC57 vector and ligated it into the pCOLD-GST vector using an *Eco*RI site at the 5' end and an *Xba*I site at the 3' end. Additionally, human M6P/IGF2R fragments were sub-cloned from our previous expression vector pCMV5RIX (pCMV5 vector with an *Eco*RI site mutated out of the multiple cloning sequence) into the pCOLD-GST vector. We realized that our inserts were all engineered to be read in a mammalian expression system instead of a bacterial expression system. To account for this, we used three Rosetta 2 cell line derivatives that express several tRNA species capable of aiding in expression of proteins from human mRNAs: C41, JRC1, and JRC3. All of these *E. coli* BL21(DE3) lines are used for expression of toxic proteins or proteins with rare codons, i.e. mammalian codon usage. The C41(DE3) cells have at least one mutation that prevents cell death that is associated with expression of recombinant, toxic proteins (i.e., membrane proteins and some cytoplasmic proteins). JRC1 cells are C41(DE3) competent cells expressing the pRARE2 plasmid and are used for toxic proteins with rare codons (i.e., mammalian codons). JRC3 cells are C43(DE3) competent cells, which have a different set of mutations than C41(DE3) that prevents cell death upon expression of toxic proteins, expressing the pRARE2 plasmid and are used for toxic proteins with rare codons. In short, Jennifer L. Kopanic from Dr. Paul Sorgen's laboratory engineered the JRC1 and JRC3 cell lines during her doctoral dissertation work by combining the pLysS plasmid (pLysSRARE2) from Rosetta 2(DE3)pLysS cells with the C41(DE3)/C43(DE3) strains.

Using diagnostic restriction endonuclease digestion, we confirmed that the banding pattern of the DNA fragments on a 1% agarose gel correlated with the expected sizes. Once we made all clones, we followed the protocol illustrated in Figure 5.7 and transformed our constructs into the above three cell lines to determine which cell line would express our receptor fragments. This vector has a unique way of expressing inserts and therefore has a specific growth protocol that needed to be optimized. A growth culture was inoculated with starter culture following transformation and growth at 37°C, 250 rpm, until an $O.D._{600}$ of 0.4 was reached. Cells were then induced with 1 mM isopropyl β-D-1-thiogalactopyranoside (IPTG), which is an allolactose mimetic that binds the *lac* repressor to initiate transcription, and expression was allowed to continue for 16 h at 18°C, 180 rpm. Aliquots of whole cells taken pre-induction and after the overnight induction period were lysed with heat and SDS-PAGE loading buffer and electrophoresed on a 10% gel to measure expression. Coomassie staining revealed more intense bands at the correct molecular weights post-induction in all three cell lines, indicative of successful expression following IPTG induction, but an αFLAG immunoblot revealed that JRC1 and JRC3 had a greater expression of 1-3F than C41 (Figure 5.8).

Once bacterial expression was achieved, the cells were lysed using a French Press and then the lysates were centrifuged at 16,500 rpm for 1 h to separate the two fractions: soluble supernatant and the insoluble pellet. Aliquots of the soluble and insoluble fractions were electrophoresed on a 10% SDS-PAGE gel and stained using Coomassie blue. The stained gels revealed that the most constructs (1-3F, 7-9F, 11-13F, and DDMPR 1-3F) were expressed in the insoluble fraction (Figure 5.9). The insoluble fractions were then extracted with 6 M urea (ÄKTA Buffer A) to resolubilize the precipitated protein. Following an additional spin to discard insoluble cellular debris, the resolubilized fraction was affinity-purified on an ÄKTA FPLC using a HisTrap™ HP (Ni^{2+}
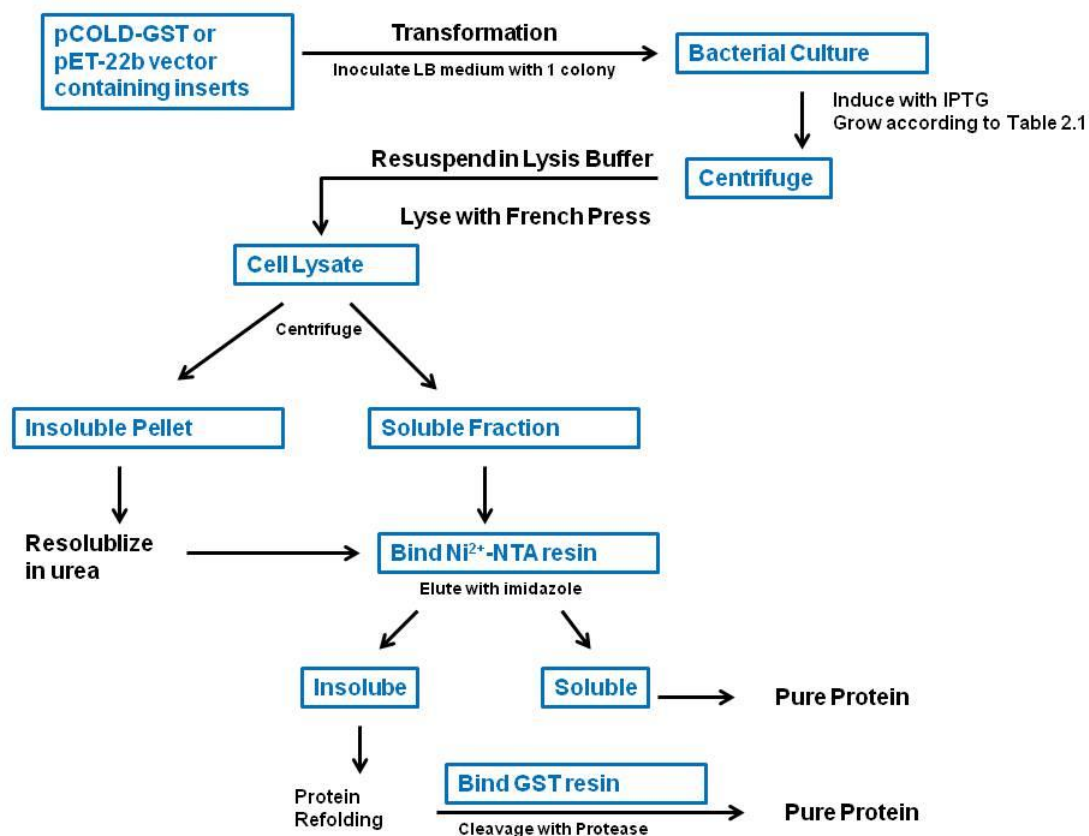
Figure 5.7: Purification of DDMPR and human mini-receptor constructs using the bacterial expression system. The mini-receptors were cloned into expression vectors and transformed into E. coli. Cultures were grown according to Table 2.2. Cells were collected through centrifugation, resuspended in lysis buffer, and lysed with French Press. The lysates were centrifuged to separate the insoluble pellet from the soluble fraction. The insoluble pellet was resolublized in urea. Both fractions, during different column runs, were purified on an Ni^{2+}-NTA resin column. The soluble fraction was considered pure protein. The insoluble fraction was refolded and the GST-tagged removed.
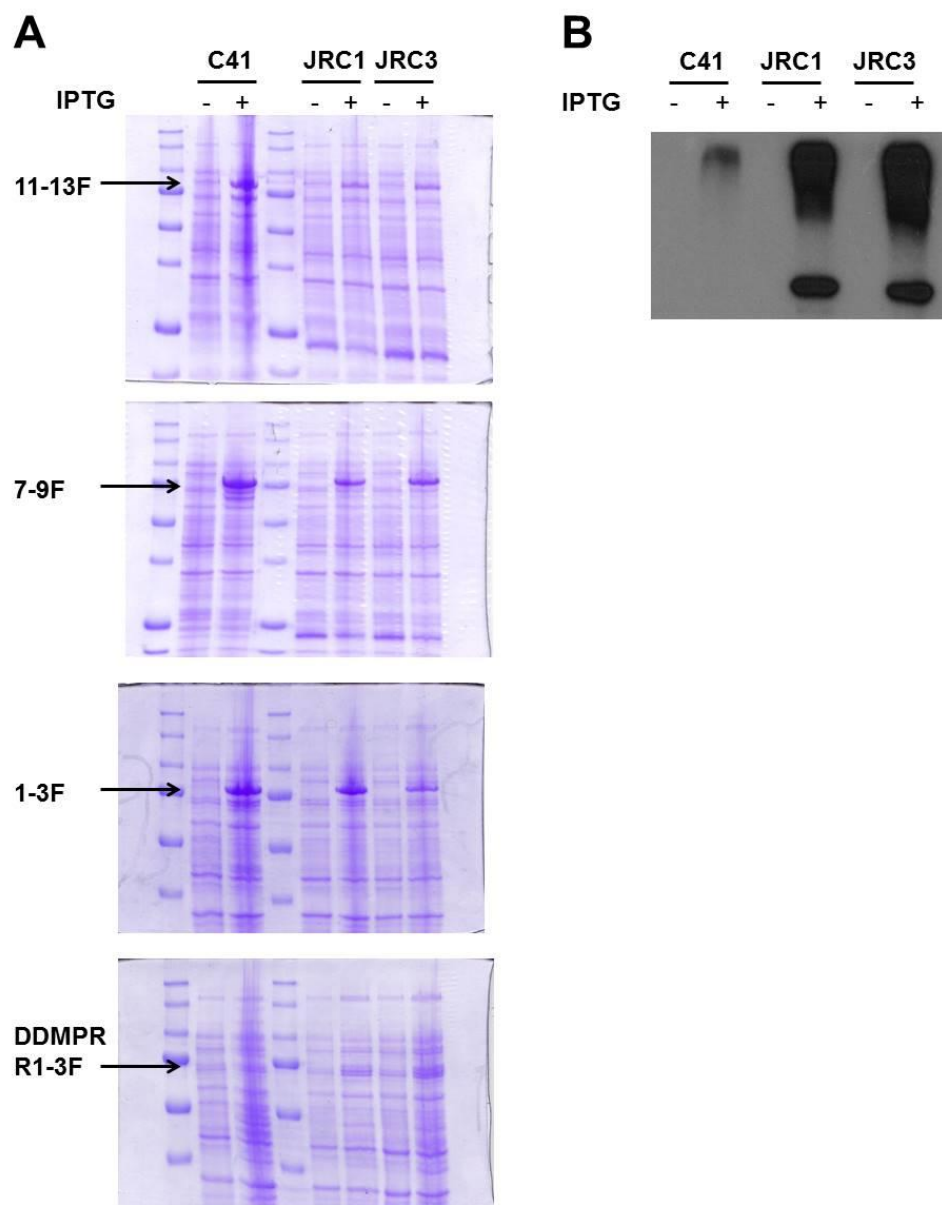
Figure 5.8: Expression of mini-receptors from *E. coli* using pCOLD-GST vector. A) DDMPR and human M6P/IGF2R mini-receptors cDNA were transformed into *E. coli* strains C41, JRC1, and JRC3. Whole-cell samples were electrophoresed and Coomassie stained. All constructs expressed in all cell lines following 1 mM IPTG induction. B) Immunoblot analysis probing with α-FLAG of 1-3F whole-cell samples revealed that JRC1 and JRC3 had higher expression of the FLAG-tagged mini-receptor than the C41 strain.
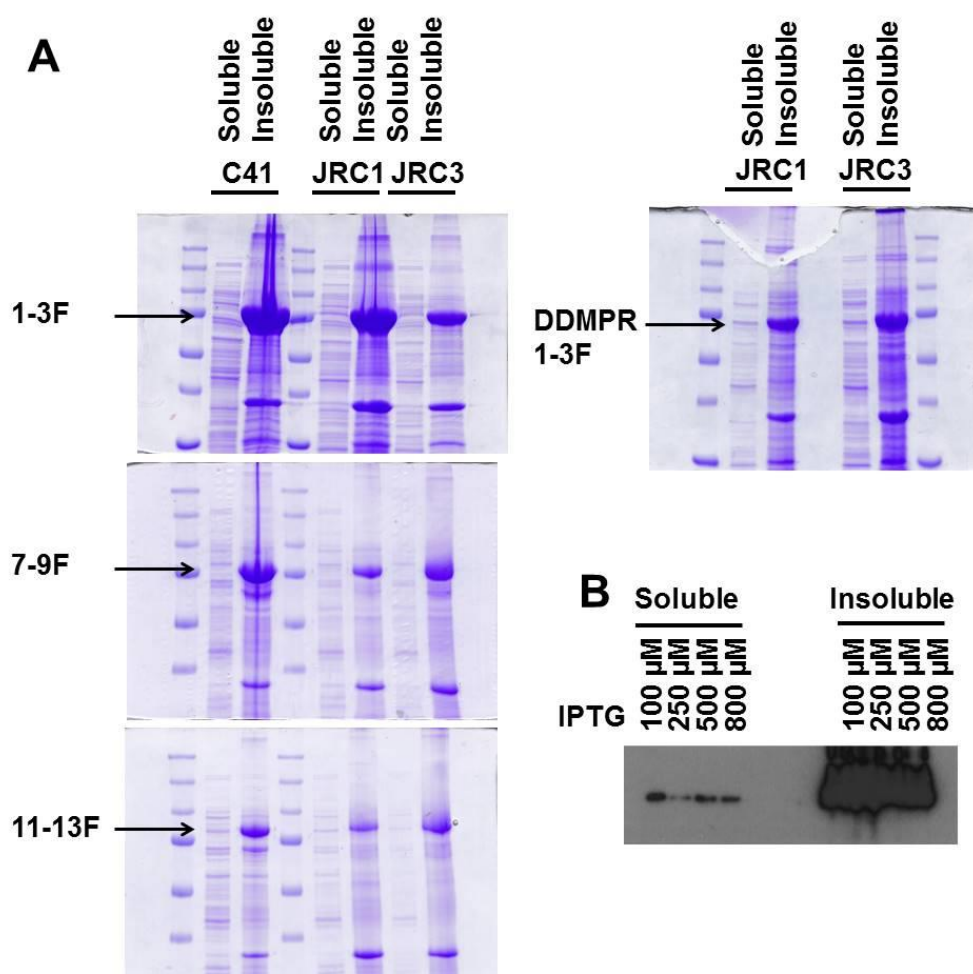
Figure 5.9: Solubility of the FLAG-tag mini-receptor proteins expressed in bacterial cells. A) Soluble and insoluble fractions were electrophoresed and Coomassie-stained to reveal that all strains expressed the majority of the FLAG-tagged proteins in the insoluble fraction. B) Immunoblot analysis probing for the FLAG-tag of human 1-3F mini-receptor expressed in C41 cells following increasing concentrations of IPTG.

resin) column, which binds the His-tag on the target protein with high affinity. An elution gradient of increasing imidazole concentration (ÄKTA Buffer B) determined that all proteins eluted in earlier fractions (near fraction 4-10) (Figure 5.10A). Aliquots of these fractions confirmed the presence or absence of protein on Coomassie blue-stained 10% acrylamide electrophoresed gels (Figure 5.10B). Fractions containing protein were pooled.

We selected the 1-3F mini-receptor for development of the folding methods. Refolding proved to be difficult as each mini-receptor contains 3-4 disulfide bonds that, if paired in a non-native manner, would result in a misfolded receptor that was defunct in binding ability. Refolding buffer was composed of a mixture of buffer and components to allow optimal oxidation/reduction (cystamine/cysteamine 2-mercaptoethylamine) reactions to allow the right cysteine pairs to bind and amino acid (L-arginine) to prevent protein aggregation. (See Materials and Methods for details.) With the first few attempts to refold the 1-3F mini-receptor, ratios using direct dilutions (1:0 unfolded control, 1:1, 1:5, and 1:10 in the first attempt and 1:0, 1:10, and 1:20 in the second attempt) of protein:refolding buffer were used, where the protein was subjected to ÄKTA Buffer A urea to completely unfold any protein that may have incidentally folded before refolding buffer was added. Either half of the refolding buffer was added at time 0 and time 24 h and the protein was allowed to fold for 48 h, or the entire amount of refolding buffer was added immediately at time 0 and the protein allowed to fold for 48 h. The GST-tag and His-tags were then cleaved from the target protein by using Turbo 3C (T3C) protease and the GST bound to glutathione resin and was pulled down, thereby leaving the folded protein in the supernatant (Figure 5.10C). The refolded protein was then analyzed using a ^{125}I-PMP-BSA ligand blot, in which the PMP on the radioligand should bind to the binding pocket of the properly folded 1-3F mini-receptor with high affinity. Unfortunately,

there was not any detectable properly folded protein in our samples when compared to the properly folded 1-3F expressed from HEK 293 lysates (data not shown). Additionally, the spectra from the circular dichroism data indicated that we did not achieve any folding (absence of detectable secondary structure) (data not shown). The protein was then concentrated using Amicon Ultra centrifuge filters and subsequently electrophoresed and stained with Coomassie blue to determine if the GST-tag was properly cleaved from the protein. Interestingly, increased exposure to T3C cleaved additional amounts of the GST-tag from the proteins, but the concentration of uncleaved protein remained high even after 72 h with the protease (Figure 5.10C). According to the manufacturer's product datasheet, small traces of urea can inhibit the activity of T3C, so we next dialyzed away the urea after refolding prior to the cleavage of the GST-tag. Unfortunately, the majority of the GST-tag remained intact with our protein. This may be due to misfolding of the protein that results in the HRV 3 C site being trapped inside the protein and is unavailable for cleavage by the protease. T3C is able to cleave some of the protein, which suggests that our protein was a heterogeneous population of different folding endpoints, i.e., folded differently but none correctly. A ^{125}I-PMP-BSA ligand blot confirmed that we did not have functional protein regardless of the GST-tag present (data not shown).

We attempted to refold the 1-3F mini-receptor using the refolding buffer as previously mentioned except substituting various the buffers (Tris, MES, MOPS, HEPES, glycine, or PBS) to determine if the base buffer made a difference in the outcome. Again, ^{125}I-PMP-BSA ligand blot revealed that there was no functional mini-receptor present (data not shown). All of the previous folding steps were performed in direct dilutions, where a volume of the refolding buffer was added at one time and the protein solution sits undisturbed for a given amount of time while it refolds. It is possible that our

mini-receptors need to refold in a timed concentration gradient as opposed to immediate folding. Therefore, we did a urea step-down dialysis in which the refolding buffer was replaced with fresh refolding buffer containing a lower concentration of urea (4 M, 2 M, 1 M, 0 M urea) every 24 h. Unfortunantely, we were unable to achieve a functional protein using these approaches.

We expressed 1-3F in JRC3 cells using reduced concentrations of IPTG for induction in order to improve solubility of the protein. IPTG at 100, 250, 500, or 800 μM was used to induce the JRC3 cells transformed with pCOLD-GST/1-3F. SDS-PAGE separation and Coomassie blue staining of the electrophoresed whole cell samples lysed under heat in SDS-PAGE loading buffer indicated that these lower concentrations of IPTG induced expression of our mini-receptor (Figure 5.9B). Additionally, lysing the cells on the French Press followed by SDS-PAGE analysis of the electrophoresed fractions showed that the majority of the 1-3F receptor resided in the insoluble fraction in all four samples. However, αFLAG immunobloting of these fractions determined that there is some expression of 1-3F in the soluble fractions (Figure 5.9B). These soluble fractions were purified on the ÄKTA using the aforementioned protocol, and fractions containing the protein were pooled and incubated with T3C protease to remove the GST-tag. We were again unable to cleave the GST-tag, indicating that the pCOLD-GST vector may not work to purify our mini-receptor constructs (data not shown).

Figure 5.10: Purification of His/GST/FLAG-tagged mini-receptors using Ni^{2+}-NTA affinity chromotography. A) Elution profile of mini-receptor from the ÄKTA purification system, which showed an absorbance reflecting protein eluting in fractions 2-9. B) Coomassie staining of electrophoresed fractions from chromotagraphy validated the fractions containing protein. C) Cleavage of GST-tag from mini-receptor using T3C protease following protein refolding

A

B

| Fraction | Flowthrow | Wash | 1 | 2 | 3 | 4 | 5 | 6 | 7 | 8 | 9 | 20 |

C

Refolding	1:0	1:1	1:5	1:10
72 h	- - +	- - +	- - +	- - +
60 h	- + -	- + -	- + -	- + -
Uncleaved	+ - -	+ - -	+ - -	+ - -

Uncleaved

Cleaved
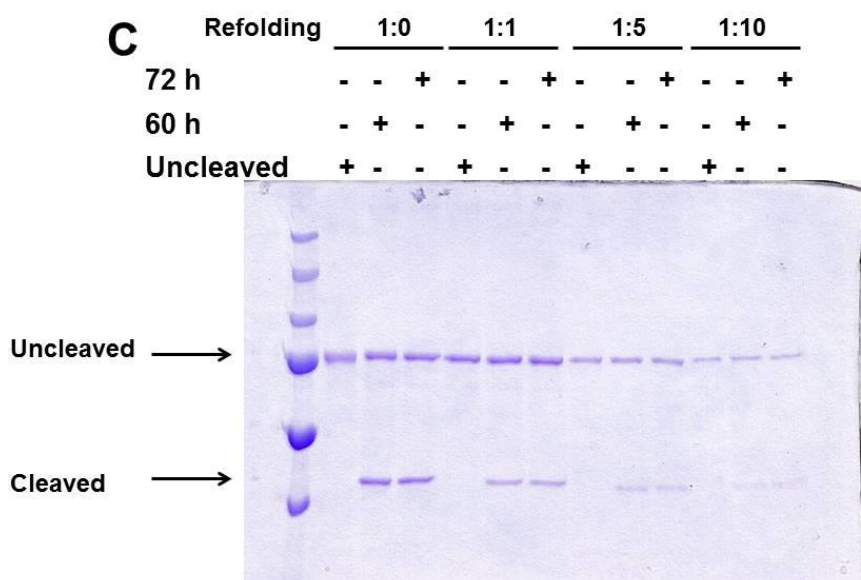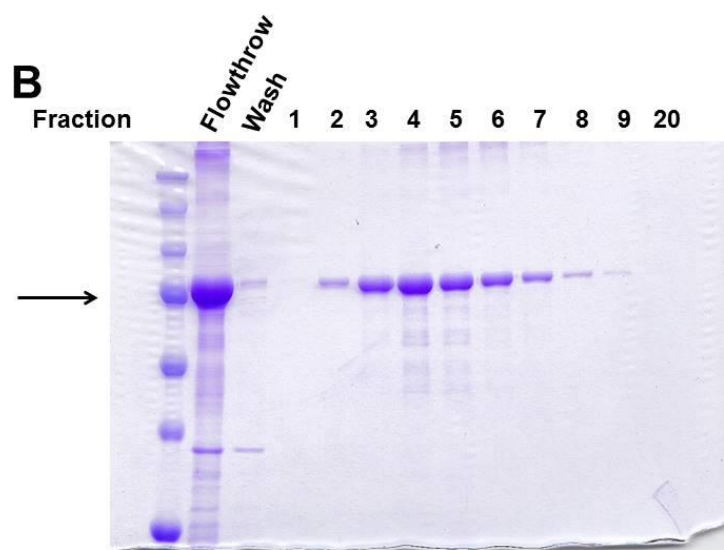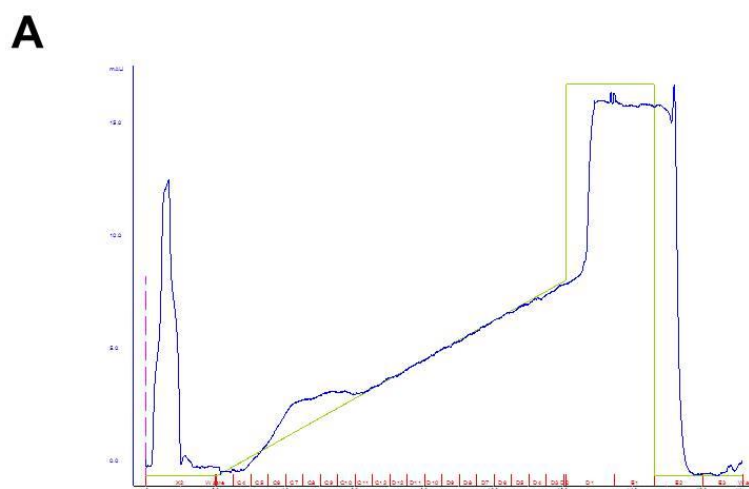
C.5. Cloning, expression, purification and folding of pET-22b(+)/DDMPR3F in a bacterial expression system

Since we were unable to purify and refold our mini-receptor constructs using the pCOLD-GST vector, we chose to clone DDMPR3F into a different bacterial expression vector, pET-22b(+), that was the same vector that Brown *et al.* used to clone M6P/IGF2R domain 11 (*61*). This unique vector has an N-terminal *pelB* signal for periplasmic localization, which increases solubility of the protein (*310*), and the signal peptidase cleavage sequence allows for cleavage just upstream of the insert. Additionally, there is a C-terminal His-tag sequence that allows for purification using a Ni^{2+}-NTA resin column. However, we decided to follow the protocol as done by Brown *et al.* (*61*), and therefore transformed our pET-22b/DDMPR3F vector into *E. coli* BL21(DE3) cells, which are unable to read mammalian codons. Therefore, we had to convert our codons to preferred bacterial codon usage, so we had a gBlock synthesized from Integrated DNA Technologies. We subcloned the DDMPR3F gBlock into the pET-22b(+) vector using *Nco*I and *Xho*I. We engineered our insert to have a *Spe*I restriction site, allowing for validation using a single restriction endonuclease digestion (data not shown). Additionally, sequencing revealed that our DDMPR3F receptor was correctly cloned into our vector. ExPasy Protein Parameters tool calculated the estimated molecular weight of our protein to be 18,332 with a theoretical pI of 7.64 and a molar extinction coefficient of 25,705 $M^{-1}cm^{-1}$.

We transformed our pET-22b/DDMPR3F vector into BL21(DE3) cells, and following inoculation of our growth culture with our starter culture, we monitored O.D.$_{600}$ until 0.6-0.8 at 37°C, 250 rpm. The cells were then induced with increasing concentrations of IPTG and maintained under the growth conditions for 3-4 more hours. SDS-PAGE analysis of the samples pre-induction and post-incubation indicated that the

DDMPR3F was expressed in these cells (Figure 5.11A). Cells were lysed on the French Press and aliquots of the two fractions were electrophoresed on a 15% SDS-PAGE gel and stained with Coomassie blue, which showed that the the vast majority of the protein was in the insoluble fraction as it had been in the pCOLD-GST mini-receptor experiments (Figure 5.11B). The insoluble fraction was resolubilized in 6 M urea and purified on the ÄKTA using a Ni^{2+}-NTA resin column as previously mentioned (Figure 5.11C). The eluted fractions indicated that the protein eluted in the first half of the gradient elution.

The expressed, resolubilized DDMPR3F was then refolded in the refolding buffers mentioned previously. Ratios (1:0 control, 1:1, 1:5, 1:10, and 1:20) of protein:refolding buffer were used in Tris, MES, MOPS, and HEPES refolding buffers for 48 h after a 1 h incubation with urea to unfold any potential contacts within the receptor. ^{125}I-PMP-BSA ligand blots revealed that the radioligand was unable to bind functional protein. However, our positive control 1-3F from HEK 293 lystate also did not bind the radioligand (data not shown). We next performed a circular dichroism (CD) analysis to determine if there was any folding that occurred within the DDMPR3F. The CD spectra observed that the refolding buffers absorbed near 200 nm, and subtracting the buffer spectra from the protein spectra revealed no protein folding (data not shown). This may be due to a component in the refolding buffer (L-arginine, cystamine, or cysteamine 2-mercapoethylamine) causing absorption that interferes with the spectra. Thus, CD analysis cannot be performed when these buffers are present. Therefore, a two-step Tris-buffer dialysis was performed to determine if the refolding buffer components could be eliminated. After two rounds of dialysis, residual refolding buffer components remain in the sample (data not shown), indicating that additional rounds of dialysis would be needed to remove the interference.
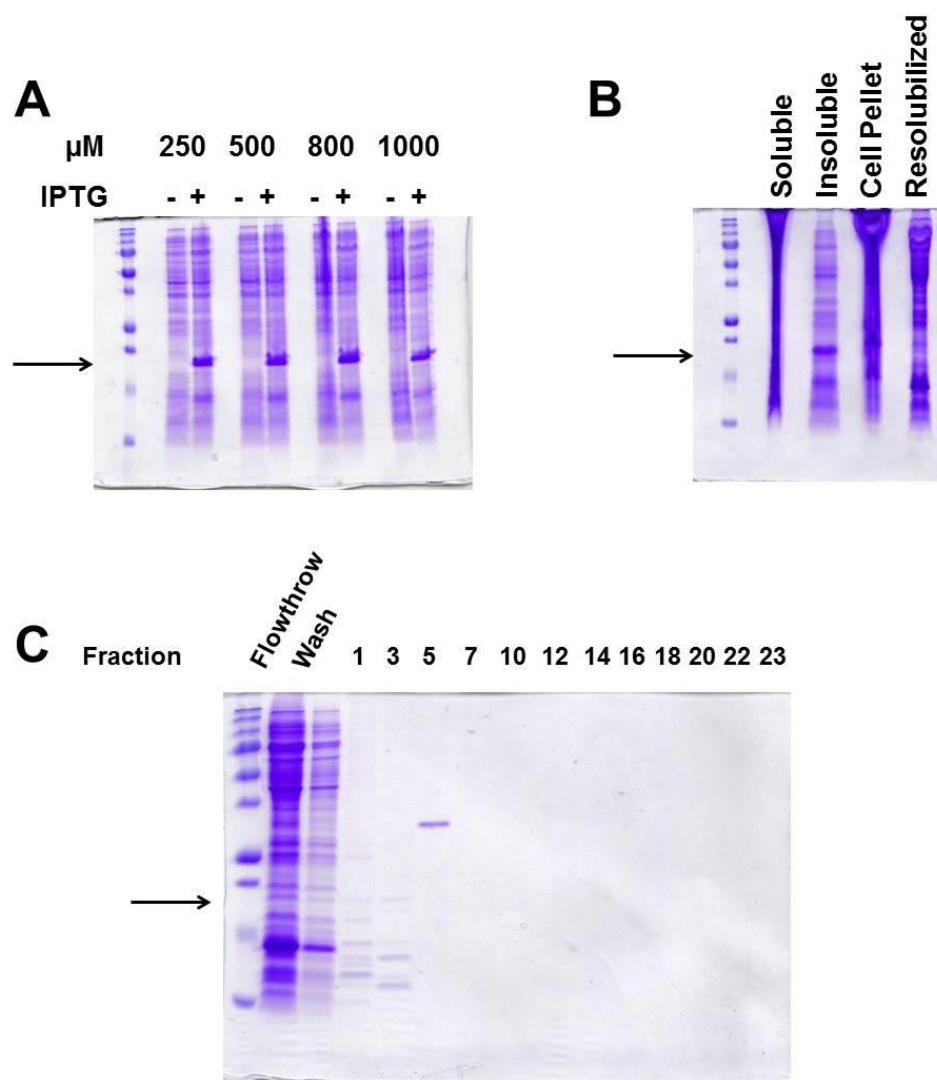
Figure 5.11: Purification of His/FLAG-tagged DDMPR R3 using Ni^{2+}-NTA affinity chromatography. A) DDMPR R3 was expressed in *E. coli* BL21 cells. Coomassie staining revealed that increasing concentrations of IPTG all effectively stimulated expression of the protein. B) Coomassie staining of the soluble and insoluble fractions revealed that most of the protein expressed was in the insoluble fraction and could be re-solubilized in urea. C) Coomassie staining of the Ni^{2+}-NTA affinity chromatography fractions showed that the DDMPR R3 protein eluted in fractions 1-10, with fraction 5 having most of the protein.

We attempted to refold the DDMPR3F before purification following protocols used by Gao *et al.* and Brown *et al.* (*61, 364*). The insoluble fraction, following expression and lysing the cells, was subjected to 6 or 8 M urea denaturing buffer, and the resolubilized fraction was diluted 10-fold in denaturing buffer before incubation with folding buffer in 12-h increments. Following refolding, the sample was Tris dialyzed to remove the urea, in which some proteins precipitated out of solution. The supernatant fractions of the collected samples were then concentrated by lyophilization. Interestingly, a ^{125}I-PMP-BSA ligand blot of the different fractions (soluble, folded, insoluble pellet following folding, and unfolded) showed that the only fraction that bound the radioligand was the soluble fraction (Figure 5.12). The soluble fraction was then subjected to ^{125}I-PMP-BSA ligand blots with or without 5 mM M6P, which competitively binds with M6P-containing ligands for M6P-binding sites. The half of the ligand blot with the presence of M6P during the introduction of ^{125}I-PMP-BSA resulted in a weaker signal than the other half of the ligand blot without M6P, indicating that M6P was able to displace some but not all of the radioligand (Figure 5.12). This is consistent with previous data in that M6P is able to only partially displace M6P-based ligands (PMP-ligands), which may be explained by the lack of preference for M6P, as DDMPR's binding domain may prefer ligands having diester structures or containing sulfur residues (i.e. M6S). Immunoblots of the His-tag on the DDMPR3F following a pull-down using PMP-Sepharose 4B resin resulted in either not enough protein concentration for detection or the lack of affinity of the receptor for the resin (data not shown). Dialysis and purification of the soluble fraction was unable to yield improved results of properly folded DDMPR3F. Thus, the most effective method to determine ligand binding preferences for the DDMPR in the bacterial expression system is to use the soluble fraction from BCL21(DE3) cells that were transformed with the pET-22b/DDMPR3F vector construct.
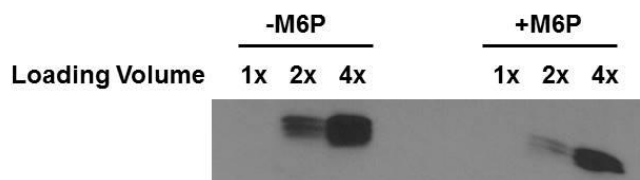
Figure 5.12: PMP-Sepharose pull-down of DDMPR R3 and displacement with M6P.
The soluble fraction of the DDMPR R3 expressed in BL21 cells following Ni^{2+}-NTA affinity chromatography was electrophoresed under non-reducing conditions and probed with ^{125}I-PMP-BSA with or without 10 mM M6P. M6P partially displaced the radioligand from the mini-receptor.

D.   Discussion

Dictyostellium discoideum is a social amoeba with a lysosomal system that is similar to the mammalian lysosomal system (*365*).   The lysosomal enzymes in *D. discoideum* often bear M6S and M6P methyldiester modifications, and it has been suggested that these acid hydrolases are transported by an unidentified receptor (*41, 43, 108, 359, 361, 366, 367*).   It has also been observed that *D. discoideum* lysosomal enzymes, when trafficked within the cells of this organism, are membrane-associated despite the lack of a TM domain until they reach the lysosome, suggesting that a receptor is involved in this process.   Additionally, lysosomal enzymes in this organism, namely α-mannosidase and β-glucosidase, can bind the mammalian M6P/IGF2R and are internalized by cultured human fibroblasts (*360*).   Despite the evidence that suggests a receptor related to the MPRs may be involved in lysosomal biogenesis of this social amoeba, one has not yet been found.   Identifying and characterizing a putative MPR in *D. discoideum* can help reveal the ancestral origins of the receptor as well as aid in our understanding of trafficking and lysosomal biogenesis.   The simplicity of this organism may provide an uncomplicated model system to study diseases associated with insufficient sorting or missorting of these enzymes.   Furthermore, the larger MPR in higher eukaryotes has 15 EC domains, which may have arisen from gene duplications (*25*), yet we still do not completely understand the function of all of these domains and defined their roles in normal and disease-associated biology.

The multiple-species sequence alignment in earlier work suggested that the putative DDMPR R3 retained all of the important amino acid residues that are necessary for M6P binding by the mammalian receptor. Additionally, the cysteine pattern predicts disulfide bonding that contributes to the tertiary architecture to fold into an MRH domain. Expression of recombinant DDMPR R1-3, which is similar in sequence and folds to

human M6P/IGF2R 1-3, can be pulled down using PMP-Sepharose resin in which the M6P residues on the PMP interact with the M6P-binding site of the receptor. This same resin is used to purify the M6P/IGF2R from bovine liver extracts and FBS, which allows for specific purification of the receptor as there are no other proteins known to bind M6P residues at neutral pH (*303*). Thus, given such strong similarities between the DDMPR and the mammalian M6P/IGF2R, our laboratory may have found the putative MPR in *D. discoideum*. Nevertheless, much work needs to be done to fully characterize the structure and function of this receptor. Interesting to note in our binding assays of the DDMPR R1-3 construct, M6P does not competitively displace the receptor from the PMP-Sepharose resin as mammalian M6P/IGF2R full-length and mini-receptors are displaced. Conversely, the DDMPR3R construct expressed from BCL21 cells was partially displaced as opposed to having enhanced binding. These contradictory pieces of data may be explained by the different expression systems and methods used. The DDMPR3R was expressed in a bacterial system that does not express an endogenous MPR, and our construct was purified through affinity chromatography before doing the binding analysis. Thus, our receptor was pure and the only protein present to bind the ^{125}I-PMP-BSA. However, our DDMPR R1-3 construct was expressed in HEK 293 that express endogenous M6P/IGF2R and CD-MPR, and crude conditioned medium was used in the pull-down procedure, which may have had soluble M6P/IGF2R present. In these experiments, some endogenous receptor may have initially bound to the PMP-resin, but as M6P concentration increased, its ability to displace the sM6P/IGF2R from the resin was also increased; thus, more functional groups may have become available on the resin for DDMPR R1-3 to bind. Furthermore, the inconsistencies in the ability of M6P to enhance or displace the DDMPR R1-3 from the PMP-Sepharose resin can also be attributed to the amount of endogenous sM6P/IGF2R present in the conditioned

medium that is released by protease activity that cleave the M6P/IGF2R in domain 15 (*287, 368*)

We have seen that M6P has a weaker affinity for the DDMPR than for the mammalian M6P/IGF2R, which may be attributed to the slightly larger binding pocket of DDMPR. NMR studies showed that the six cysteines in the structure of domain 5 of the bovine M6P/IGF2R allow for a broader binding pocket that may accommodate M6P-GlcNAc-phosphodiesters (*104*). DDMPR R3 also has six cysteines but lacks the critical tryptophan and tyrosine residues found in the ligand-binding pocket of M6P/IGF2R domain 5. On the other hand, DDMPR R3 has a histidine residue positioned at nearly the same position as His105 found in the CD-MPR's EC domain that coordinates hydrogen bonding with an incoming phosphate group on a M6P molecule. Alternatively, the imidazole ring in this histidine in DDMPR R3 could cause steric constraints that result in broadening the binding pocket as seen with other bulky amino acid residues within domain 5 of the M6P/IGF2R (*104*). The molecular modeling study of M6P docking with the DDMPR R1-3 that Dr. Connelly had simulated gave credence to the idea that DDMPR folds into a broader pocket. In his simulation, the rate of dissociation of M6P was increased as well as increased solvation compared to the binding pocket of the bovine M6P/IGF2R domains 1-3, indicating a larger binding pocket in DDMPR. The presence of additional water molecules within the binding pocket suggests that there is enough space to accommodate larger functional groups, such as M6P-methyldiester. Our binding studies support this, as 10 mM M6P, an amount that competitively displaces binding of PMP-Sepharose to the sM6P/IGF2R, does not completely disrupt binding of the DDMPR to PMP-resin. However, if we were to use a different type of ligand that may be better suited for the M6P-binding pocket (i.e. M6S or M6P-methyldiester) in DDMPR, we expect to see tighter binding of that ligand for DDMPR and thereby disrupt

the interaction with PMP-resin at much lower concentrations. This needs to be addressed to determine what ligands DDMPR prefers, which may help in understanding the evolutionary origin of the MPRs.

Another unique feature of the DDMPR that was discovered during the bioinformatics analysis was that this putative receptor has two glycosyltransferase motifs just upstream of the potential TM domain. These domains need further investigation to determine if they have, in fact, functional activity. If so, it is interesting to think that the ancestral MPR may have had dual roles in lysosomal biogenesis: transport of acid hydrolases and post-translational processing of M6P-based oligosaccharides. Additionally, it is interesting that the MPR in higher-order organisms evolved into the receptors we know today (i.e., acquired duplications of the MRH domains and IGF-II binding in the M6P/IGF2R) while the putative MPR of *D. discoideum* acquired glycosyltransferase motifs.

Nonetheless, we have found, for the first time, a putative MPR in *D. discoideum*, which would make this the most primitive MPR known to date. Studies need to be done to fully understand the binding preferences of this putative receptor compared to the M6P/IGF2R, and to identify the roles of the glycosyltransferase motifs. These studies may have an impact on the biomedical field, as understanding the evolution of the M6P/IGF2R may help in better targeting diseases that are affected by a compromised MPR.

Chapter VI

Conclusion and Future Directions

A.   Overview

The M6P/IGF2R is involved in lysosomal biogenesis and internalization of EC M6P-glycosylated and non-glycosylated ligands for transport to the lysosome. The *M6P/IGF2R* is thought of as a tumor suppressor by regulating the excess of ligands in the cell milieu, such as IGF-II. Additionally, the inability of M6P/IGF2R to transport newly synthesized acid hydrolases to the lysosome, such as defects in the glycosylation pathway limiting their ability to bind to the MPRs, can result in one of over 35 lysosomal storage diseases. Thus, this receptor is vital in multiple different functions of the cell. However, one of the most well studied features of this receptor is its role of M6P-based binding. High-affinity, bivalent M6P-based ligands, such as lysosomal enzymes, bind and stabilize the dimeric M6P/IGF2R at the cell surface, leading to its internalization at a faster rate than when there is no M6P-based ligand bound (*131*). Moreover, this accelerated internalization of the receptor allows for IGF-II to bind in a different binding domain and it is taken up by the receptor and trafficked to the lysosome at faster rate as a passenger along with a multivalent M6P-based ligand. Furthermore, a decrease in IGF-II concentration in the cell milieu as a result of rapid internalization by CREG led to cell cycle arrest and inhibited growth of several different cell types (*228, 229, 311*). Therefore, we were interested in producing a panel of M6P-based ligands capable of bi- or multivalent binding to the M6P/IGF2R that could suppress IGF-II-dependent growth of cancer cells. Additionally, the MPRs are well conserved through evolution, with the earliest form of "true" MPR known to date in the invertebrates such as mollusk. However, the social amoeba, *D. discoideum*, was found to produce lysosomal enzymes that bind to the M6P/IGF2R, a discovery that predated identification of a receptor capable of transporting these acid hydrolases within this organism. We provide evidence of a putative MPR protein that retains all the necessary components of an

MRH domain that also binds M6P. The studies presented in this dissertation further our understanding of the origin of the M6P/IGFR as well as increase our potential for exploiting this receptor as a potential target against IGF-II-dependent cancer.

B.   PMP-ligands

B.1.   Conclusions

Our bi- and multidentate panel of PMP-pseudoglycan ligands bind to the M6P/IGF2R with bivalent, high affinity about 100-1000-fold higher than M6P alone. Upon binding to the receptor *in vitro*, cell viability is decreased presumably through depletion of bioavailable IGF-II in the conditioned medium. Add-back of either 10 mM M6P or 10 nM IGF-II to the PMP-ligand-treated cells rescues the inhibition on cell viability effect, suggesting that our ligands operate in both a M6P- and IGF-II-dependent manner. Different cell lines had different levels of responsiveness to our ligands. As such, these cell lines exhibited varying levels of IGF-II dependency. This variation may be explained by differences in receptor density on the cell surface, resistance or sensitivity within the intracellular signaling pathways, cell-to-cell contact density, genetic mutations in oncogenes or tumor suppressors that are not related to the IGF axis yet contribute to cell growth, or slight batch-to-batch differences in our PMP-ligand preparations. Additionally, it was difficult to find an established cell line that has complete IGF-II-dependency, as all cell lines we tested had only a certain level of dependency. IGF-II over-expression has been shown in many tumors, yet if our cell lines are just partially IGF-II-dependent, our PMP-ligands would be able to operate only to the level of dependency. Patient samples resected from IGF-II-dependent tumors through the Rapid Autopsy Program at UNMC may provide a more responsive model for

our PMP-ligands. Nonetheless, some of our cell lines were responsive, which appeared to be established cell lines that were obtained from tumors classified as moderate-to-well differentiated. The poorly differentiated cell lines that we tested were not responsive to our PMP-ligands and had minimal or no response to IGF-II, indicating that these cancer cells are not IGF-II-dependent and would not be good candidates for therapy using our novel therapeutic agents. At best, it would seem that the PMP-ligands may be most efficacious in combination chemotherapy approaches.

We hypothesized that our PMP-ligands were functioning by stimulating internalization of IGF-II from the medium and causing degradation of the growth factor in the lysosome, thereby leaving the receptor tyrosine kinases such as the IGF1R less activated. Our ^{125}I-IGF-II internalization assay provided support for our hypothesis by showing an increase in TCA-soluble radioactive material (^{125}I-IGF-II degradation products) when our PMP-ligand is present. Conversely, the addition of unlabeled IGF-II or M6P abrogated the effect by protecting the ^{125}I-IGF-II in the conditioned medium, which resulted in more radioactive counts present in the TCA-insoluble pellet (intact ^{125}I-IGF-II).

As IGF-II is internalized at an accelerated rate when PMP-ligands are present, we expect to see the reduction of cell viability that is caused by reversal/blockade of the IGF-II signaling pathway. That is, we would expect to see cell cycle arrest as seen with CREG (*228, 229, 311*) or an increase in apoptosis/decrease in survival. We were unable to determine the exact mechanism of action that is a result from our PMP-ligands. We saw a slight increase in cell death in some experiments, but this finding was not entirely supported by the caspase 3/7 activity assay or caspase 3 cleavage immunoblot, nor did our annexin V staining support the increase in cell death. The annexin V staining may have had technical issues when doing these assays and would

need to be repeated. Also, the JEG-3 cells appeared to have a unique biology in that they may have a hyperactive flippase that flips the PS to the outer membrane of the plasma membrane even when apoptosis is not occurring. We also may not necessarily detect an increase in activation of the executioner caspases if caspase-independent cell death was occurring in our studies. We need to delve deeper into these apoptotic studies to determine if our PMP-ligands are inducing cell death, either through decreasing IGF-II activation or by off-target effects.

Our migration assays proved interesting and yielded unexpected results. In scratch assays, it appeared as if different ligand preparations caused different outcomes. The first sets of scratch assays were performed using PMP-OVA from one batch and the second sets of scratch assays with another. As such, the first set did not show a significant decrease in wound closure rates, but the ligand caused a slight reduction in closure compared to control. Interestingly, the IGF-II-treated groups did not close faster than the control. The second sets had the opposite outcome, wherein the PMP-OVA accelerated the wound closure rate. Upon closer examination, there may have been a chemotactic response occurring at the high concentration (200 nM) of PMP-ligand. In the earlier batch, the stock concentration was lower and it was slightly lower molecular weight than the second batch, indicating the possibility that there were fewer PMP groups per unit protein. This slight difference in molecular weight may have caused a ligand that is more potent at lower concentrations but causes an odd chemotactic response at higher concentrations. We would need to repeat these experiments with increasing concentrations of PMP-ligand in order to determine if there is a particular concentration that decreases migration. The preliminary data on the transwell assays suggest that our PMP-ligand may decrease migration, but more thorough analyses need to be done.

There is also the potential that our PMP-ligands alone are not potent enough to initiate cell death or cell cycle arrest. For example, the initiation of apoptosis is reversible until a certain point when the executioner caspases are activated (*341, 369*). It is possible that once apoptosis is initiated, our PMP-ligands may be enough to overcome the protection against apoptosis and drive the cell toward cell death. If so, this would greatly reduce the toxicity effects of chemotherapeutic drugs by allowing a smaller dose of the pro-apoptosis drug in combination with our PMP-ligands to cause cell death of the tumor. Further studies into the mechanism of PMP-ligand action as well as combination studies will contribute to novel treatments against IGF-II-dependent growth of cancer cells.

B.2. Future Directions

Our PMP-ligands reduce cell viability in an M6P- and IGF-II-dependent manner. However, we need to understand the mechanism of the inhibition of cell growth. Additional studies focusing on the apoptosis cascade can determine the cause of cell death. As of now, we do not know if this is a caspase-dependent or –independent apoptosis. There is a growing body of evidence that suggests many factors can interplay to initiate caspase-independent cell death, such as cathepsins (namely cathepsin B and D), calpains, and AIF-mediated cell death (*370*). We would need to investigate the activities of these caspase-independent apoptotic proteins to tease out which may play a role in mediating the cell death that we see with our PMP-ligand treatment.

We have seen *in vitro* that our PMP-ligands can reduce cell viability of IGF-II-dependent cancer cells, but in order for our ligands to function as potential

chemotherapeutic agents, we need to test the efficacy *in vivo*. One valid concern is that our PMP-ligands are capped with a number of M6P moieties (approximately 2 to 24), which have the potential to be cleavage by phosphates and proteases in the animal model. Our PMP-ligands are effective in conditioned medium up to 72 hours, as seen in ^{125}I-IGF-II internalization assays and PMP-ligands degradation assays. We would need to determine if our PMP-ligands are efficient at targeting the tumor and at what dosage and frequency we need to administer our agents. These are important questions that need to be answered in order to use our PMP-ligands against IGF-II-dependent cancer.

When we treated the cells with PMP-ligands, we were disappointed that the response from the cells was not always consistent. We would see a slight increase in cell death and possibly a slight delay in cell cycle progression. However, we did not see a robust enough response that would account for the reduction on cell viability. There is a possibility that our PMP-ligands are not potent enough to induce cell cycle arrest or apoptosis alone, but they may work synergistically with a chemotherapeutic agent. For example, we may see an increase in apoptosis following PMP-ligand treatment because the cells underwent a pro-apoptotic signal that they otherwise would recover from, but our agent was able to drive them to cell death. Decreasing IGF-II from the conditioned medium may be just enough to commit the cell to apoptosis. If so, the standard of therapy may call for less toxicity by allowing decreased concentrations of global cytotoxic drug in conjunction with our very specific agent. We need to test this first *in vitro* and then *in vivo* by providing a pro-apoptotic signal (such as staurosporine, TRAIL, or paclitaxel) in the presence of our specific PMP-ligand to measure the synergistic effects. If the two agents are synergistic, then we should see enhanced sensitivity to the cytotoxic agent in the presence of the PMP-ligand. This approach would have the potential to improve the therapeutic window for the cytotoxic drug.

M6P/IGF2R trafficking is continuous with constitutive internalization regardless of bound ligand (*46*). Furthermore, the presence of EC ligands can influence receptor localization to the plasma membrane to take up the additional ligands and transport them to the lysosome (*67, 219, 221*). It is not known if receptor localization and trafficking are affected upon PMP-ligand binding. We would hypothesize that as PMP-ligand binds to the M6P-binding sites within the EC domain of the M6P/IGF2R, the dimeric structure is stabilized and allows for rapid internalization of the receptor and all bound passenger ligands, such as IGF-II. From there, the complex would be trafficked to the early endosome for sorting to the lysosome for destined cargo, while the receptor is recycled. However, we need to verify that our PMP-ligands drive the receptor through the classical internalization pathway and do not promote internalization into a vesicle and mis-sorting or prevention of lysosome/endosome fusion. Additionally, it is presumed that our PMP-ligands bind with high affinity yet the low pH of the late endosome would cause the complex to dissociate so that the receptor may be recycled. We need to monitor the intracellular trafficking to demonstrate that the M6P/IGF2R is not becoming degraded along with the complex, which would limit the efficacy of our agents if the receptor cannot return to the cell surface to undergo another round of rapid internalization. Lastly, we need to validate that our PMP-ligands are, in fact, functioning through the M6P/IGF2R. We have concluded that our ligands are binding very specifically to the M6P-binding sites located within the receptor because the addition of M6P or IGF-II rescues the effect caused by our ligands. But we need to perform M6P/IGF2R knockout studies to validate the specificity of our ligands; that way, we would be able to identify any potential off-target effects employed by out agents. Targeting the M6P/IGF2R to enhance its tumor suppressor functions shows promise in treating IGF-II-dependent cancer and understanding the mechanism caused by the

ligand-receptor interaction can aid in the development of novel therapeutic agents against these types of cancer.

C.   A Panel of Phosphatase-inert M6P-based Surrogates as "Molecular Rulers" for the M6P/IGF2R

C.1.   Conclusions

The synthetic M6P-based, phosphatase-resistant surrogates bound to the M6P/IGF2R.   These bidentate molecules were designed to determine the binding preferences of the linker and to measure the distance that spans the dimeric receptor. It is important to determine the exact chemical preferences of the M6P-binding sites of the M6P/IGF2R in order to better design therapeutic agents that can target this receptor in IGF-II-dependent cancers. Several studies from different labs have contributed to our understanding of the M6P-based binding to this receptor, including the amino acids involved in recognition of the incoming M6P (*46*), preferred glycosidic linkages between mannose residues (*95*), and distance spanning the M6P-binding domains (*343*). Studies on the M6P recognition by the M6P/IGF2R has led to the design of M6P-based binding ligands in different labs.

In earlier studies in our lab, the phosphonate has been shown to be a suitable replacement for phosphate at the sixth carbon of the mannose ring (*312*). Another set of M6P-surrogates used various tether lengths to determine the distance needed to span the dimeric M6P/IGF2R. However, these ligands were unable to produce bivalent binding. Work presented in this dissertation investigated the binding of two new panels of synthetic M6P-based surrogates to determine if the linker chemistry affected the binding affinity and increased tether length would allow for cross-bridging the receptor.

Much to our disappointment, we were unable to achieve bi- or multivalent binding with these bidentate molecules. However, we were able to determine that the orientation of the linker impacts the binding affinity of these ligands for the M6P/IGF2R. A molecule in the cisoid orientation may offer a better presentation of the phosphonate ends to the M6P-binding sites, producing higher affinity binding. Additionally, increasing the tether length correlates with binding until the tether reaches a certain number of atoms. When the tether length exceeds 8 repeating units of PEG, we suspect that the tether is too flexible and folds back on itself instead of remaining outstretched and long enough to span the distance. Additionally, there may be too much flexibility and lack of stability of the orientation of the phosphonates so that after one phosphonate end binds to a M6P/IGF2R monomer, the other end is unable to achieve the correct orientation for productive binding. When the two ends are so conformationally independent, the first binding event would not reduce the entropic cost of the second event very much.

C.2.   Future Directions

Synthetic M6P-based ligands for the M6P/IGF2R that resist hydrolysis as well as phosphatase and protease cleavage would be valuable for treating IGF-II-dependent cancer. High-affinity, bivalent binding to the receptor leads to accelerated internalization of the receptor and any bound passenger ligand, such as IGF-II. By targeting this receptor to internalize at a faster rate, we can deplete the bioavailable IGF-II from the cell milieu that would subsequently lead to decreased IGF1R and IGF1R/IR-A activation. Work in our lab using our PMP-ligands supports this idea as our ligands decrease cell viability. Our collaborators in Lincoln were able to synthesize M6P-based ligands that are not cleavable by phosphatases and would have a longer half-life in *in vitro* and *in*

vivo studies. Since these ligands were unable to produce bivalent binding, we will need to design new panels of ligands that would be able to achieve bivalent binding. The linker affects binding, so we will need to keep the linker in mind when designing these new sets. The linker should support a cisoid configuration as opposed to transoid and should not be too bulky, as demonstrated with the loss of binding attributed to the triphenylphosphine linker in the BL2 compound. The tether length is important, as it needs to be able to span the dimeric receptor. However, we will need to introduce some stability into the flexible linker in order to prevent potential folding of the compound.

Once we are able to achieve high-affinity, bivalent binding to the M6P/IGF2R, we will need to validate these ligands *in vitro* to determine if they are able to decrease cell viability similar to the PMP-ligands. If successful, these ligands may be administered *in vivo* to decrease tumor burden in IGF-II-dependent cancers. Our mannose 6-phosphonate ligands would be advantageous as chemotherapeutic agents in these types of cancers, so further studies are necessary to develop them into a novel anti-cancer therapy.

D.   A Putative MP6 Receptor Identifed in *Dictyostelium discoideum:* Chacterization of the M6P-based Binding of the MRH Domains

D.1.   Conclusions

Previous work done by David Nelson and Dr. Chris Connelly identified a hypothetical protein in the *D. discoideum* genome that possesses MRH domains and appears to be a homolog to the MPRs. Further bioinformatics analysis revealed that the third MRH domain (DDMPR R3) retains the cysteine pattern observed in the mammalian M6P/IGF2R domain 3. A recombinant DDMPR R3 protein was shown to bind PMP-

Sepharose resin. M6P resulted in a different displacement pattern from this resin than for either human M6P/IGF2R 1-3F or ^{125}I-sM6P/IGF2R. The difference in the displacement pattern may be due to the preferences of ligands that each receptor prefers, where M6P and M6S have differet overall charges that affect binding We predict that M6P is a preferred ligand for the M6P/IGF2R but not for the DDMPR, which may explain why the addition of M6P can increase the binding of DDMPR to the PMP-resin. As M6P increases, it competitively displaces the endogenous M6P/IGF2R allowing more binding sites on the resin available for DDMPR. The DDMPR R3 that was purified from BL21 cells further supports that M6P is not the preferred ligand of this putative receptor, as 10 mM M6P only partially displaced the 125I-PMP-BSA from the ligand blot at the bands corresponding to the molecular weight of DDMPR R3. This was purified, recombinant protein, so other proteins would not be interfering with the results.

D.2.   Future Directions

We have seen that the putative DDMPR binds M6P-based ligands and can be partially displaced with M6P. We suspect that DDMPR may prefer sulfated ligands or those larger than M6P such as M6P-methyldisester modifications. The overlay of the DDMPR R3 modeled structure with the crystal structure of the bovine M6P/IGF2R domain 3 shows that these receptors have similar folding. However, minute changes within the DDMPR binding pocket allow for a slightly larger pocket similar to domain 5 of the mammalian receptor. Domain 5 of the M6P/IGF2R has been shown to bind phosphodiesters with high affinity and has lower affinity for M6P (*105*). We hypothesize that the DDMPR is similar in that it binds M6P but it prefers M6S and M6P-methylester. Additionally, lysosomal enzymes purified from *D. discoideum* have been shown to have

sulfated caps and M6P-methylesters (*99, 100*). Furthermore, the charges on the ligands differ, so the receptor transporting these types of ligands must have a binding pocket that can accommodate the size and charge of the ligand.

We are interested in knowing the binding preferences of this putative receptor for ligands. To determine this, we must express purified DDMPR R3 or expansions of the binding pocket (R1-5) and perform displacement assays using ^{125}I-PMP-BSA as a tracer. Increasing concentrations of different ligands that the receptor may prefer (M6S, M6P-methylester, mannose 6-sulfonate, mannose 6-sulfenate, mannose 6-phosphamine) should displace the DDMPR R3 from PMP-Sepharose resin or displace the radioligand from the ligand blot. Thus, IC_{50} and RBA values can be calculated and compared to those of M6P. We expect that M6S an M6P-methylester will bind with highest affinity for the DDMPR. Additionally, there are two potential glycosyltransferase domains within the C-terminal domain of this putative receptor. Investigation of this region will determine if these domains are enzymatically active; if so, it is interesting that this organism may have one multifunctional protein involved in lysosome biogenesis. Characterization of the ligand binding properties and structural features of the DDMPR may further our understanding in the origins of the MPRs and aid in lysosomal storage disease research.

E.   Summary

Our data support further investigation into exploiting the M6P/IGF2R as a potential therapeutic strategy for IGF-II-dependent cancers. High-affinity M6P-based ligands can bind the receptor and decrease cell viability in a M6P- and IGF-II-dependent manner. If we can design high-affinity ligands that are resistant to degradation *in vitro*, we can create a more stable anti-cancer agent that would function in IGF-II-dependent

cancer in combination chemotherapy that can lower the toxic effects seen in patients. Our M6P-based ligands would operate most efficiently in tumors or tumor microenvironments that express the IGF axis: IGF1R and/or IR-A, M6P/IGF2R and IGF-II. By limiting the concentration of IGF-II in the tumor microenvironment, we can inhibit IGF-II-dependent growth of the cancer cells and allow for a more specific approach to treating the tumor in a subset of patients. Further investigations will allow us to understand the biochemical mechanism in which our M6P-based ligands operate to decrease cell viability, and this knowledge will enable us to improve efficacy of these agents.

Chapter VII

References

1. Braulke, T., and Bonifacino, J. S. (2009) Sorting of lysosomal proteins, *Biochim Biophys Acta 1793*, 605-614.
2. Neufeld, E. F. (1991) Lysosomal storage diseases, *Annual review of biochemistry 60*, 257-280.
3. Parenti, G., Andria, G., and Ballabio, A. (2015) Lysosomal storage diseases: from pathophysiology to therapy, *Annu Rev Med 66*, 471-486.
4. Futerman, A. H., and van Meer, G. (2004) The cell biology of lysosomal storage disorders, *Nat Rev Mol Cell Biol 5*, 554-565.
5. Vellodi, A. (2005) Lysosomal storage disorders, *British journal of haematology 128*, 413-431.
6. Kornfeld, S., and Mellman, I. (1989) The biogenesis of lysosomes, *Annu. Rev. Cell Biol. 5*, 483-525.
7. Hickman, S., and Neufeld, E. F. (1972) A hypothesis for I-cell disease: defective hydrolases that do not enter lysosomes, *Biochem Biophys Res Commun 49*, 992-999.
8. Glaser, J. H., McAlister, W. H., and Sly, W. S. (1974) Genetic heterogeneity in multiple lysosomal hydrolase deficiency, *The Journal of pediatrics 85*, 192-198.
9. Hickman, S., Shapiro, L. J., and Neufeld, E. F. (1974) A recognition marker required for uptake of a lysosomal enzyme by cultured fibroblasts, *Biochem. Biophys. Res. Commun. 57*, 55-61.
10. Kaplan, A., Achord, D. T., and Sly, W. S. (1977) Phosphohexosyl components of a lysosomal enzyme are recognized by pinocytosis receptors on human fibroblasts, *Proc. Natl. Acad. Sci. U.S.A. 74*, 2026-2030.
11. Neufeld, E. F., Sando, G. N., Garvin, A. J., and Rome, L. H. (1977) The transport of lysosomal enzymes, *J. Supramol. Struct. 6*, 95-101.
12. Natowicz, M. R., Chi, M. M., Lowry, O. H., and Sly, W. S. (1979) Enzymatic identification of mannose 6-phosphate on the recognition marker for receptor-mediated pinocytosis of beta-glucuronidase by human fibroblasts, *Proc Natl Acad Sci U S A 76*, 4322-4326.
13. Steiner, A. W., and Rome, L. H. (1982) Assay and purification of a solubilized membrane receptor that binds the lysosomal enzyme α-L-iduronidase, *Arch. Biochem. Biophys. 214*, 681-687.
14. Hoflack, B., and Kornfeld, S. (1985) Lysosomal enzyme binding to mouse P388D1 macrophage membranes lacking the 215-kDa mannose 6-phosphate receptor: evidence for the existence of a second mannose 6-phosphate receptor, *Proc. Natl. Acad. Sci. U.S.A. 82*, 4428-4432.
15. Fischer, H. D., Gonzalez-Noriega, A., and Sly, W. S. (1980) β-Glucuronidase binding to human fibroblast membrane receptors, *J. Biol. Chem. 255*, 5069-5074.
16. Sahagian, G. G., Distler, J., and Jourdian, G. W. (1981) Characterization of a membrane-associated receptor from bovine liver that binds phosphomannosyl residues of bovine testicular β-galactosidase, *Proc. Natl. Acad. Sci. U.S.A. 78*, 4289-4293.
17. Rome, L. H., Weissmann, B., and Neufeld, E. F. (1979) Direct demonstration of binding of a lysosomal enzyme, alpha-L-iduronidase, to receptors on cultured fibroblasts, *Proc. Natl. Acad. Sci. U.S.A. 76*, 2331-2334.
18. Bhaumick, B., Bala, R. M., and Hollenberg, M. D. (1981) Somatomedin receptor of human placenta: solubilization, photolabeling, partial purification, and comparison with insulin receptor, *Proc. Natl. Acad. Sci. U.S.A. 78*, 4279-4283.
19. MacDonald, R. G., Pfeffer, S. R., Coussens, L., Tepper, M. A., Brocklebank, C. M., Mole, J. E., Anderson, J. K., Chen, E., Czech, M. P., and Ullrich, A. (1988) A

single receptor binds both insulin-like growth factor II and mannose-6-phosphate, *Science 239*, 1134-1137.

20. Lobel, P., Dahms, N. M., and Kornfeld, S. (1988) Cloning and sequence analysis of the cation-independent mannose 6-phosphate receptor, *J. Biol. Chem. 263*, 2563-2570.

21. Morgan, D. O., Edman, J. C., Standring, D. N., Fried, V. A., Smith, M. C., Roth, R. A., and Rutter, W. J. (1987) Insulin-like growth factor II receptor as a multifunctional binding protein, *Nature 329*, 301-307.

22. Hoflack, B., and Kornfeld, S. (1985) Purification and characterization of a cation-dependent mannose 6-phosphate receptor from murine P388D1 and macrophages and bovine liver, *J. Biol. Chem. 260*, 12008-12014.

23. Pohlmann, R., Nagel, G., Schmidt, B., Stein, M., and Lorkowski, G. (1987) Cloning of a cDNA encoding the human cation-dependent mannose 6-phosphate-specific receptor, *Proc. Natl. Acad. Sci., U.S.A. 84*, 5575-5579.

24. Laureys, G., Barton, D. E., Ullrich, A., and Francke, U. (1988) Chromosomal mapping of the gene for the type II insulin-like growth factor receptor/cation-independent mannose 6-phosphate receptor in man and mouse, *Genomics 3*, 224-229.

25. Nadimpalli, S. K., and Amancha, P. K. (2010) Evolution of mannose 6-phosphate receptors (MPR300 and 46): lysosomal enzyme sorting proteins, *Current protein & peptide science 11*, 68-90.

26. Oshima, A., Nolan, C. M., Kyle, J. W., Grubb, J. H., and Sly, W. S. (1988) The human cation-independent mannose 6-phosphate receptor. Cloning and sequence of the full-length cDNA and expression of functional receptor in COS cells, *J. Biol. Chem. 263*, 2553-2562.

27. Szebenyi, G., and Rotwein, P. (1994) The mouse insulin-like growth factor II/cation-independent mannose 6-phosphate (IGF-II/MPR) receptor gene: Molecular cloning and genomic organization, *Genomics 19*, 120-129.

28. Killian, J. K., Buckley, T. R., Stewart, N., Munday, B. L., and Jirtle, R. L. (2001) Marsupials and Eutherians reunited: genetic evidence for the Theria hypothesis of mammalian evolution, *Mamm. Genome 12*, 513-517.

29. Yandell, C. A., Dunbar, A. J., Wheldrake, J. F., and Upton, Z. (1999) The kangaroo cation-independent mannose 6-phosphate receptor binds insulin-like growth factor II with low affinity, *J Biol Chem 274*, 27076-27082.

30. Suresh, K., Vegiraju, S. R., and Nadimpalli, S. K. (2004) Molecular cloning of goat Mannose 6-phosphate receptors, MPR 300 and 46, *Glycoconjugate journal 20*, 257-265.

31. Clairmont, K. B., and Czech, M. P. (1989) Chicken and *Xenopus* mannose 6-phosphate receptors fail to bind insulin-like growth factor II, *J. Biol. Chem. 264*, 16390-16392.

32. Matzner, U., Hille-Rehfeld, A., von Figura, K., and Pohlmann, R. (1996) Expression of mannose 6-phosphate receptors in chicken, *Developmental dynamics : an official publication of the American Association of Anatomists 207*, 11-24.

33. Yerramalla, U. L., Nadimpalli, S. K., Schu, P., von Figura, K., and Hille-Rehfeld, A. (2000) Conserved cassette structure of vertebrate Mr 300 kDa mannose 6-phosphate receptors: partial cDNA sequence of fish MPR 300, *Comparative biochemistry and physiology. Part B, Biochemistry & molecular biology 127*, 433-441.

34. Gasanov, U., Koina, C., Beagley, K. W., Aitken, R. J., and Hansbro, P. M. (2006) Identification of the insulin-like growth factor II receptor as a novel receptor for binding and invasion by Listeria monocytogenes, *Infect Immun 74*, 566-577.

35. Yadavalli, S., and Nadimpalli, S. K. (2008) Mannose-6-phosphate receptors (MPR 300 and 46) from the highly evolved invertebrate Asterias rubens (Echinodermate): biochemical and functional characterization of MPR 46 protein, *Glycoconjugate journal 25*, 889-901.

36. Nadimpalli, S. K., Yerramalla, U. L., Hille-Rehfeld, A., and von Figura, K. (1999) Mannose 6-phosphate receptors (MPR 300 and MPR 46) from a teleostean fish (trout), *Comparative biochemistry and physiology. Part B, Biochemistry & molecular biology 123*, 261-265.

37. Nadimpalli, S. K., and von Figura, K. (2002) Identification of the putative mannose 6-phosphate receptor (MPR 46) protein in the invertebrate mollusc, *Bioscience reports 22*, 513-521.

38. Dennes, A., Cromme, C., Suresh, K., Kumar, N. S., Eble, J. A., Hahnenkamp, A., and Pohlmann, R. (2005) The novel Drosophila lysosomal enzyme receptor protein mediates lysosomal sorting in mammalian cells and binds mammalian and Drosophila GGA adaptors, *J Biol Chem 280*, 12849-12857.

39. Whyte, J., R C, and Munro, S. (2001) A yeast homolog of the mammalian mannose 6-phosphate receptors contributes to the sorting of vacuolar hydrolases, *Curr. Biol. 11*, 1074-1078.

40. Mierendorf, R. C., Jr., Cardelli, J. A., and Dimond, R. L. (1985) Pathways involved in targeting and secretion of a lysosomal enzyme in Dictyostelium discoideum, *J Cell Biol 100*, 1777-1787.

41. Freeze, H. H., and Wolgast, D. (1986) Structural analysis of N-linked oligosaccharides from glycoproteins secreted by Dictyostelium discoideum. Identification of mannose 6-sulfate, *J Biol Chem 261*, 127-134.

42. Freeze, H. H. (1985) Interaction of Dictyostelium discoideum lysosomal enzymes with the mammalian phosphomannosyl receptor. The importance of oligosaccharides which contain phosphodiesters, *J Biol Chem 260*, 8857-8864.

43. Freeze, H. H., and Wolgast, D. (1986) Biosynthesis of methylphosphomannosyl residues in the oligosaccharides of Dictyostelium discoideum glycoproteins. Evidence that the methyl group is derived from methionine, *J Biol Chem 261*, 135-141.

44. Freeze, H. H., Yeh, R., Miller, A. L., and Kornfeld, S. (1983) Structural analysis of the asparagine-linked oligosaccharides from three lysosomal enzymes of Dictyostelium discoideum. Evidence for an unusual acid-stable phosphodiester, *J Biol Chem 258*, 14874-14879.

45. Brissenden, J. E., Ullrich, A., and Francke, U. (1984) Human chromosomal mapping of genes for insulin-like growth factors I and II and epidermal growth factor, *Nature 310*, 781-784.

46. Dahms, N. M., and Hancock, M. K. (2002) P-type lectins, *Biochim. Biophys. Acta 1572*, 317-340.

47. Pohlmann, R., Nagel, G., Schmidt, B., Stein, M., Lorkowski, G., Krentler, C., Cully, J., Meyer, H. E., Grzeschik, K. H., Mersmann, G., and et al. (1987) Cloning of a cDNA encoding the human cation-dependent mannose 6-phosphate-specific receptor, *Proc Natl Acad Sci U S A 84*, 5575-5579.

48. Szebenyi, G., and Rotwein, P. (1994) The mouse insulin-like growth factor II/cation-independent mannose 6-phosphate (IGF-II/MPR) receptor gene: molecular cloning and genomic organization, *Genomics 19*, 120-129.

49.   Killian, J. K., and Jirtle, R. L. (1999) Genomic structure of the human M6P/IGF2 receptor, *Mamm Genome 10*, 74-77.

50.   Kalscheuer, V. M., Mariman, E. C., Schepens, M. T., Rehder, H., and Ropers, H. H. (1993) The insulin-like growth factor type-2 receptor gene is imprinted in the mouse but not in humans, *Nat. Genet. 5*, 74-78.

51.   Riesewijk, A. M., Schepens, M. T., Welch, T. R., van den Berg-Loonen, E. M., Mariman, E. M., Ropers, H.-H., and Kalscheuer, V. M. (1996) Maternal-specific methylation of the human *IGF2R* gene is not accompanied by allele-specific transcription., *Genomics 31*, 158-166.

52.   Nolan, C. M., Killian, J. K., Petitte, J. N., and Jirtle, R. L. (2001) Imprint status of M6P/IGF2R and IGF2 in chickens, *Development genes and evolution 211*, 179-183.

53.   Livingstone, C. (2013) IGF2 and cancer, *Endocr Relat Cancer 20*, R321-339.

54.   Matzner, U., von Figura, K., and Pohlmann, R. (1992) Expression of the two mannose 6-phosphate receptors is spatially and temporally different during mouse embryogenesis, *Development 114*, 965-972.

55.   Nissley, Kiess, W., and Sklar, M. (1993) Developmental expression of the IGF-II/mannose 6-phosphate receptor, *Mol. Reprod. Dev. 35*, 408-413.

56.   Alexandrides, T., Moses, A. C., and Smith, R. J. (1989) Developmental expression of receptors for insulin, insulin-like growth factor I (IGF-I), and IGF-II in rat skeletal muscle, *Endocrinology 124*, 1064-1076.

57.   Funk, B., Kessler, U., Eisenmenger, W., Hansmann, A., Kolb, H., and Kiess, W. (1992) Expression of the human insulin-like growth factor II/mannose-6-phosphate receptor in multiple human tissues during fetal life and early infancy, *J. Clin. Endocrinol. Metab. 75*, 424-431.

58.   Wenk, J., Hille, A., and von Figura, K. (1991) Quantitation of Mr 46000 and Mr 300000 mannose 6-phosphate receptors in human cells and tissues, *Biochemistry international 23*, 723-731.

59.   Kornfeld, S. (1992) Structure and function of the mannose 6-phosphate/insulinlike growth factor II receptor, *Annu. Rev. Biochem. 61*, 307-330.

60.   Wylie, A. A., Pulford, D. J., McVie-Wylie, A. J., Waterland, R. A., Evans, H. K., Chen, Y. T., Nolan, C. M., Orton, T. C., and Jirtle, R. L. (2003) Tissue-specific inactivation of murine *M6P/IGF2R, Am. J. Pathol. 162*, 321-328.

61.   Brown, J., Esnouf, R. M., Jones, M. A., Linnell, J., Harlos, K., Hassan, A. B., and Jones, E. Y. (2002) Structure of a functional IGF2R fragment determined from the anomalous scattering of sulfur, *EMBO J. 21*, 1054-1062.

62.   Roberts, D. L., Weix, D. J., Dahms, N. M., and Kim, J.-J. P. (1998) Molecular basis of lysosomal enzyme recognition: three-dimensional structure of the cation-dependent mannose 6-phosphate receptor, *Cell 93*, 639-648.

63.   Olson, L. J., Dahms, N. M., and Kim, J.-J. P. (2004) The N-terminal carbohydrate recognition site of the cation-independent mannose 6-phosphate receptor, *J. Biol. Chem. 279*, 34000-34009.

64.   Brown, J., Delaine, C., Zaccheo, O. J., Siebold, C., Gilbert, R. J., van Boxel, G., Denley, A., Wallace, J. C., Hassan, A. B., Forbes, B. E., and Jones, E. Y. (2008) Structure and functional analysis of the IGF-II/IGF2R interaction, *EMBO J 27*, 265-276.

65.   Puertollano, R., Aguilar, R. C., Gorshkova, I., Crouch, R. J., and Bonifacino, J. S. (2001) Sorting of mannose 6-phosphate receptors mediated by the GGAs, *Science 292*, 1712-1716.

66. Corvera, S., Whitehead, R. E., Mottola, C., and Czech, M. P. (1986) The insulin-like growth factor II receptor is phosphorylated by a tyrosine kinase in adipocyte plasma membranes, *J. Biol. Chem. 261*, 7675-7679.

67. Corvera, S., Folander, K., Clairmont, K. B., and Czech, M. P. (1988) A highly phosphorylated subpopulation of insulin-like growth factor II/mannose 6-phosphate receptors is concentrated in a clathrin-enriched plasma membrane fraction, *Proc. Natl. Acad. Sci., U.S.A. 85*, 7567-7571.

68. Sahagian, G. G., and Neufeld, E. F. (1983) Biosynthesis and turnover of the mannose 6-phosphate receptor in cultured chinese hamster ovary cells, *J. Biol. Chem. 258*, 7121-7128.

69. Zhang, Q., Berggren, P.-O., and Tally, M. (1997) Glucose increases both the plasma membrane number and phosphorylation of insulin-like growth factor II/mannose 6-phosphate receptors, *J. Biol. Chem. 272*, 23703-23706.

70. MacDonald, R. G., and Czech, M. P. (1985) Biosynthesis and processing of the type II insulin-like growth factor receptor in H-35 hepatoma cells, *J. Biol. Chem. 260*, 11357-11365.

71. Goldberg, D. E., Gabel, C. A., and Kornfeld, S. (1983) Studies of the biosynthesis of the mannose 6-phosphate receptor in receptor-positive and -deficient cell lines, *J. Cell Biol. 97*, 1700-1706.

72. Kiess, W., Greenstein, L. A., Lee, L., Thomas, C., and Nissley, S. P. (1991) Biosynthesis of the insulin-like growth factor-II (IGF-II)/mannose-6-phosphate receptor in rat C6 glial cells: the role of N-linked glycosylation in binding of IGF-II to the receptor, *Mol. Endocrinol. 5*, 281-291.

73. Kiess, W., Haskell, J. F., Lee, L., Greenstein, L. A., Miller, B. E., Aarons, A. L., Rechler, M. M., and Nissley, S. P. (1987) An antibody that blocks insulin-like growth factor (IGF) binding to the type II IGF receptor is neither an agonist nor an inhibitor of IGF-stimulated biologic responses in L6 myoblasts, *J. Biol. Chem. 262*, 12745-12751.

74. Schmidt, B., Kiecke-Siemsen, C., Waheed, A., Braulke, T., and von Figura, K. (1995) Localization of the insulin-like growth factor II binding site to amino acids 1508-1566 in repeat 11 of the mannose 6-phosphate/insulin-like growth factor II receptor, *J. Biol. Chem. 270*, 14975-14982.

75. Thibault, C., Chan, J. K., Perdue, J. F., and Daughaday, W. H. (1984) Insulin-like growth factor II receptors. Molecular radius and molecular weight determination using quantitative polyacrylamide gel electrophoresis, *J. Biol. Chem. 259*, 3361-3367.

76. Corvera, S., Davis, R. J., Roach, P. J., DePaoli Roach, A., and Czech, M. P. (1986) Mechanism of receptor kinase action on membrane protein recycling, *Ann. N. Y. Acad. Sci. 488*, 419-429.

77. Corvera, S., Roach, P. J., DePaoli-Roach, A. A., and Czech, M. P. (1988) Insulin action inhibits insulin-like growth factor-II (IGF) receptor phosphorylation in H-35 hepatoma cells. IGF-II receptors isolated from insulin-treated cells exhibit enhanced in vitro phosphorylation by casein kinase II, *J. Biol. Chem. 263*, 3116-3122.

78. Méresse, S., and Hoflack, B. (1993) Phosphorylation of the cation-independent mannose 6-phosphate receptor is closely associated with its exit from the *trans*-Golgi network, *J. Cell Biol. 120*, 67-75.

79. Braulke, T., and Mieskes, G. (1992) Role of protein phosphatases in insulin-like growth factor II (IGF II)-stimulated mannose 6-phosphate/IGF II receptor redistribution, *J. Biol. Chem. 267*, 17347-17353.

80. Hu, K. Q., Backer, J. M., Sahagian, G., Feener, E. P., and King, G. L. (1990) Modulation of the insulin-like growth factor II/mannose 6-phosphate receptor in microvascular endothelial cells by phorbol ester via protein kinase C, *J. Biol. Chem. 265*, 13864-13870.

81. Liu, Q., Grubb, J. H., Huang, S. S., Sly, W. S., and Huang, J. S. (1999) The mannose 6-phosphate/insulin-like growth factor-II receptor is a substrate of type V transforming growth factor-β receptor, *J. Biol. Chem. 274*, 20002-20010.

82. Johnson, K. F., and Kornfeld, S. (1992) The cytoplasmic tail of the mannose 6-phosphate/insulin-like growth factor-II receptor has two signals for lysosomal enzyme sorting in the Golgi, *J. Cell Biol. 119*, 249-257.

83. Chen, H.-J., Yuan, J., and Lobel, P. (1997) Systematic mutational analysis of the cation-independent mannose 6-phosphate/insulin-like growth factor II receptor cytoplasmic domain. An acidic cluster containing a key aspartate is important for function in lysosomal enzyme sorting, *J. Biol. Chem. 272*, 7003-7012.

84. Zhu, Y., Doray, B., Poussu, A., Lehto, V. P., and Kornfeld, S. (2001) Binding of GGA2 to the lysosomal enzyme sorting motif of the mannose 6-phosphate receptor, *Science 292*, 1716-1718.

85. Takatsu, H., Katoh, Y., Shiba, Y., and Nakayama, K. (2001) Golgi-localizing, gamma-adaptin ear homology domain, ADP-ribosylation factor-binding (GGA) proteins interact with acidic dileucine sequences within the cytoplasmic domains of sorting receptors through their Vps27p/Hrs/STAM (VHS) domains, *J. Biol. Chem. 276*, 28541-28545.

86. Westcott, K. R., and Rome, L. H. (1988) Cation-independent mannose 6-phosphate receptor contains covalently bound fatty acid, *J. Cell. Biochem. 38*, 23-33.

87. Schweizer, A., Kornfeld, S., and Rohrer, J. (1996) Cysteine34 of the cytoplasmic tail of the cation-dependent mannose 6-phosphate receptor is reversibly palmitoylated and required for normal trafficking and lysosomal enzyme sorting, *J Cell Biol 132*, 577-584.

88. Pohlmann, R., Boeker, M. W., and von Figura, K. (1995) The two mannose 6-phosphate receptors transport distinct complements of lysosomal proteins, *J. Biol. Chem. 270*, 27311-21318.

89. Munier-Lehmann, H., Mauxion, F., Bauer, U., Lobel, P., and Hoflack, B. (1996) Re-expression of the mannose 6-phosphate receptors in receptor-deficient fibroblasts. Complementary function of the two mannose 6-phosphate receptors in lysosomal enzyme targeting, *J. Biol. Chem. 271*, 15166-15174.

90. Kasper, D., Dittmer, F., von Figura, K., and Pohlmann, R. (1996) Neither type of mannose 6-phosphate receptor is sufficient for targeting of lysosomal enzymes along intracellular routes, *J. Cell Biol. 134*, 615-623.

91. Sleat, D. E., Sohar, I., Lackland, H., Majercak, J., and Lobel, P. (1996) Rat brain contains high levels of mannose-6-phosphorylated glycoproteins including lysosomal enzymes and palmitoyl-protein thioesterase, an enzyme implicated in infantile neuronal lipofuscinosis, *J. Biol. Chem. 271*, 19191-19198.

92. Qian, M., Sleat, D. E., Zheng, H., Moore, D., and Lobel, P. (2008) Proteomics analysis of serum from mutant mice reveals lysosomal proteins selectively transported by each of the two mannose 6-phosphate receptors, *Molecular & cellular proteomics : MCP 7*, 58-70.

93. Tong, P. Y., Gregory, W., and Kornfeld, S. (1989) Ligand interactions of the cation-independent mannose 6-phosphate receptor. The stoichiometry of mannose 6-phosphate binding, *J. Biol. Chem. 264*, 7962-7969.

94.   Tong, P. Y., and Kornfeld, S. (1989) Ligand interactions of the cation-dependent mannose 6-phosphate receptor. Comparison with the cation-independent mannose 6-phosphate receptor, *J. Biol. Chem. 264*, 7970-7975.

95.   Distler, J. J., Guo, J., Jourdian, G. W., Srivastava, O. P., and Hindsgaul, O. (1991) The binding specificity of high and low molecular weight phosphomannosyl receptors from bovine testes. Inhibition studies with chemically synthesized 6-O-phosphorylated oligomannosides, *J. Biol. Chem. 266*, 21687-21692.

96.   Tomoda, H., Ohsumi, Y., Ichikawa, Y., Srivastava, O. P., Kishimoto, Y., and Lee, Y. C. (1991) Binding specificity of D-mannose 6-phosphate receptor of rabbit alveolar macrophages, *Carbohydr Res 213*, 37-46.

97.   Olson, L. J., Hindsgaul, O., Dahms, N. M., and Kim, J. J. (2008) Structural insights into the mechanism of pH-dependent ligand binding and release by the cation-dependent mannose 6-phosphate receptor, *J Biol Chem 283*, 10124-10134.

98.   Olson, L. J., Zhang, J., Dahms, N. M., and Kim, J. J. (2002) Twists and turns of the cation-dependent mannose 6-phosphate receptor. Ligand-bound versus ligand-free receptor, *J Biol Chem 277*, 10156-10161.

99.   Gabel, C. A., Costello, C. E., Reinhold, V. N., Kurz, L., and Kornfeld, S. (1984) Identification of methylphosphomannosyl residues as components of the high mannose oligosaccharides of Dictyostelium discoideum glycoproteins, *J. Biol. Chem. 259*, 13762-13769.

100.   Freeze, H. H. (1986) Modifications of lysosomal enzymes in Dictyostelium discoideum, *Molecular and cellular biochemistry 72*, 47-65.

101.   Olson, L. J., Castonguay, A. C., Lasanajak, Y., Peterson, F. C., Cummings, R. D., Smith, D. F., and Dahms, N. M. (2015) Identification of a fourth mannose 6-phosphate binding site in the cation-independent mannose 6-phosphate receptor, *Glycobiology 25*, 591-606.

102.   Reddy, S. T., Chai, W., Childs, R. A., Page, J. D., Feizi, T., and Dahms, N. M. (2004) Identification of a low affinity mannose 6-phosphate-binding site in domain 5 of the cation-independent mannose 6-phosphate receptor, *J Biol Chem 279*, 38658-38667.

103.   Hancock, M. K., Haskins, D. J., Sun, G., and Dahms, N. M. (2002) Identification of residues essential for carbohydrate recognition by the insulin-like growth factor II/mannose 6-phosphate receptor, *J Biol Chem 277*, 11255-11264.

104.   Olson, L. J., Peterson, F. C., Castonguay, A., Bohnsack, R. N., Kudo, M., Gotschall, R. R., Canfield, W. M., Volkman, B. F., and Dahms, N. M. (2010) Structural basis for recognition of phosphodiester-containing lysosomal enzymes by the cation-independent mannose 6-phosphate receptor, *Proc Natl Acad Sci U S A 107*, 12493-12498.

105.   Chavez, C. A., Bohnsack, R. N., Kudo, M., Gotschall, R. R., Canfield, W. M., and Dahms, N. M. (2007) Domain 5 of the cation-independent mannose 6-phosphate receptor preferentially binds phosphodiesters (mannose 6-phosphate N-acetylglucosamine ester), *Biochemistry 46*, 12604-12617.

106.   Dahms, N. M., Rose, P. A., Molkentin, J. D., Zhang, Y., and Brzycki, M. A. (1993) The bovine mannose 6-phosphate/insulin-like growth factor II receptor. The role of arginine residues in mannose 6-phosphate binding, *J. Biol. Chem. 268*, 5457-5463.

107.   Westlund, B., Dahms, N. M., and Kornfeld, S. (1991) The bovine mannose 6-phosphate/insulin-like growth factor II receptor. Localization of mannose 6-

phosphate binding sites to domains 1-3 and 7-11 of the extracytoplasmic region, *J. Biol. Chem. 266*, 23233-23239.

108.	Marron-Terada, P. G., Hancock, M. K., Haskins, D. J., and Dahms, N. M. (2000) Recognition of Dictyostelium discoideum lysosomal enzymes is conferred by the amino-terminal carbohydrate binding site of the insulin-like growth factor II/mannose 6-phosphate receptor, *Biochemistry 39*, 2243-2253.

109.	Lelbach, A., Muzes, G., and Feher, J. (2005) The insulin-like growth factor system: IGFs, IGF-binding proteins and IGFBP-proteases, *Acta physiologica Hungarica 92*, 97-107.

110.	Hawkes, C., and Kar, S. (2004) The insulin-like growth factor-II/mannose-6-phosphate receptor: structure, distribution and function in the central nervous system, *Brain Res. Rev. 44*, 117-140.

111.	Adams, T. E., Epa, V. C., Garrett, T. P., and Ward, C. W. (2000) Structure and function of the type 1 insulin-like growth factor receptor, *Cellular and molecular life sciences : CMLS 57*, 1050-1093.

112.	Dupont, J., and Holzenberger, M. (2003) Biology of insulin-like growth factors in development, *Birth defects research. Part C, Embryo today : reviews 69*, 257-271.

113.	LeRoith, D., and Roberts, C. T., Jr. (2003) The insulin-like growth factor system and cancer, *Cancer Lett. 195*, 127-137.

114.	Devi, G. R., Byrd, J. C., Slentz, D. H., and MacDonald, R. G. (1998) An insulin-like growth factor II (IGF-II) affinity-enhancing domain localized within extracytoplasmic repeat 13 of the IGF-II/mannose 6-phosphate receptor, *Mol. Endocrinol. 12*, 1661-1672.

115.	Linnell, J., Groeger, G., and Hassan, A. B. (2001) Real time kinetics of insulin-like growth factor II (IGF-II) interaction with the IGF-II/mannose 6-phosphate receptor, *J. Biol. Chem. 276*, 23986-23991.

116.	Garmroudi, F., Devi, G., Slentz, D. H., Schaffer, B. S., and MacDonald, R. G. (1996) Truncated forms of the insulin-like growth factor II (IGF-II)/mannose 6-phosphate receptor encompassing the IGF-II binding site: characterization of a point mutation that abolishes IGF-II binding., *Mol. Endocrinol. 10*, 642-651.

117.	Byrd, J. C., Devi, G. R., De Souza, A. T., Jirtle, R. L., and MacDonald, R. G. (1999) Disruption of ligand binding to the insulin-like growth factor II/mannose 6-phosphate receptor by cancer-associated missense mutations, *J. Biol. Chem. 274*, 24408-24416.

118.	Devi, G. R., De Souza, A. T., Byrd, J. C., Jirtle, R. L., and MacDonald, R. G. (1999) Altered ligand binding by insulin-like growth factor II/mannose 6-phosphate receptors bearing missense mutations in human cancers, *Cancer Res. 59*, 4314-4319.

119.	Zaccheo, O. J., Prince, S. N., Miller, D. M., Williams, C., Kemp, C. F., Brown, J., Jones, E. Y., Catto, L. E., Crump, M. P., and Hassan, A. B. (2006) Kinetics of insulin-like growth factor II (IGF-II) interaction with domain 11 of the human IGF-II/mannose 6-phosphate receptor: function of CD and AB loop solvent-exposed residues, *J. Mol. Biol. 359*, 403-421.

120.	Grimme, S., Honing, S., von Figura, K., and Schmidt, B. (2000) Endocytosis of insulin-like growth factor II by a mini-receptor based on repeat 11 of the mannose 6-phosphate/insulin-like growth factor II receptor, *J Biol Chem 275*, 33697-33703.

121.	Dahms, N. M., Bryzcki-Wessell, M. A., Ramanujam, K. S., and Seetharam, B. (1993) Characterization of mannose 6-phosphate receptors (MPRs) from opossum liver: opossum cation-independent MPR binds insulin-like growth factor-II, *Endocrinology 133*, 440-445.

122. Canfield, W. M., and Kornfeld, S. (1989) The chicken liver cation-independent mannose 6-phosphate receptor lacks the high affinity binding site for insulin-like growth factor II, *J. Biol. Chem. 264*, 7100-7103.

123. Killian, J. K., Byrd, J. C., Jirtle, J. V., Munday, B. L., Stoskopf, M. K., MacDonald, R. G., and Jirtle, R. L. (2000) *M6P/IGF2R* imprinting evolution in mammals, *Mol. Cell 5*, 707-716.

124. Yang, Y. W.-H., Robbins, A. R., Nissley, S. P., and Rechler, M. M. (1991) The chick embryo fibroblast cation-independent mannose 6-phosphate receptor is functional and immunologically related to the mammalian insulin-like growth factor-II (IGF-II)/mannose 6-phosphate receptor but does not bind IGF-II, *Endocrinology 128*, 1177-1189.

125. Zhou, M., Zhongmin, M., and Sly, W. S. (1995) Cloning and expression of the cDNA of chicken cation-independent mannose-6-phosphate receptor, *Proc. Natl. Acad. Sci. U.S.A. 92*, 9762-9766.

126. Mendez, E., Planas, J. V., Castillo, J., Navarro, I., and Gutierrez, J. (2001) Identification of a type II insulin-like growth factor receptor in fish embryos, *Endocrinology 142*, 1090-1097.

127. Nolan, C. M., McCarthy, K., Eivers, E., Jirtle, R. L., and Byrnes, L. (2006) Mannose 6-phosphate receptors in an ancient vertebrate, zebrafish, *Development genes and evolution 216*, 144-151.

128. Hartman, M. A., Kreiling, J. L., Byrd, J. C., and MacDonald, R. G. (2009) High-affinity ligand binding by wild-type/mutant heteromeric complexes of the mannose 6-phosphate/insulin-like growth factor II receptor, *FEBS J. 27*, 1915-1919.

129. MacDonald, R. G. (1991) Mannose-6-phosphate enhances cross-linking efficiency between insulin-like growth factor-II (IGF-II) and IGF-II/mannose-6-phosphate receptors in membranes, *Endocrinology 128*, 413-421.

130. Kiess, W., Thomas, C. L., Sklar, M. M., and Nissley, S. P. (1990) β-Galactosidase decreases the binding affinity of the insulin-like-growth-factor-II/mannose-6-phosphate receptor for insulin-like-growth-factor II, *Eur. J. Biochem. 190*, 71-77.

131. York, S. J., Arneson, L. S., Gregory, W. T., Dahms, N. M., and Kornfeld, S. (1999) The rate of internalization of the mannose 6-phosphate/insulin-like growth factor II receptor is enhanced by multivalent ligand binding, *J. Biol. Chem. 274*, 1164-1171.

132. Nykjaer, A., Christensen, E. I., Vorum, H., Hager, H., Petersen, C. M., Røigaard, H., Min, H. Y., Vihardt, F., Møller, L. B., Kornfeld, S., and Gliemann, J. (1998) Mannose 6-phosphate/insulin-like growth factor-II receptor targets the urokinase receptor to lysosomes via a novel binding interaction, *J. Cell Biol. 141*, 815-828.

133. Godár, S., Horejsi, V., Weidle, U. H., Binder, B. R., Hansmann, C., and Stockinger, H. (1999) M6P/IGFII-receptor complexes urokinase receptor and plasminogen for activation of transforming growth factor-β1, *Eur. J. Immunol. 29*, 1004-1013.

134. Kang, J. X., Li, Y., and Leaf, A. (1997) Mannose-6-phosphate/insulin-like growth factor-II receptor is a receptor for retinoic acid, *Proc. Natl. Acad. Sci. USA 95*, 13671-13676.

135. Lemansky, P., Fester, I., Smolenova, E., Uhlander, C., and Hasilik, A. (2007) The cation-independent mannose 6-phosphate receptor is involved in lysosomal delivery of serglycin, *Journal of leukocyte biology 81*, 1149-1158.

136. Wood, R. J., and Hulett, M. D. (2008) Cell surface-expressed cation-independent mannose 6-phosphate receptor (CD222) binds enzymatically active heparanase

independently of mannose 6-phosphate to promote extracellular matrix degradation, *J Biol Chem 283*, 4165-4176.

137. Leksa, V., Godár, S., Cebecauer, M., Hilgert, I., Breuss, J., Weidle, U. H., Horejsí, V., Binder, B. R., and Stockinger, H. (2002) The N terminus of mannose 6-phosphate/insulin-like growth factor 2 receptor in regulation of fibrinolysis and cell migration, *J. Biol. Chem. 277*, 40575-40582.

138. Kreiling, J. L., Byrd, J. C., Deisz, R. J., Mizukami, I. F., Todd, R. F., 3rd, and MacDonald, R. G. (2003) Binding of urokinase-type plasminogen activator receptor (uPAR) to the mannose 6-phosphate/insulin-like growth factor II receptor: Contrasting interactions of full-length and soluble forms of uPAR, *J. Biol. Chem. 278*, 20628-20637.

139. Ben-Zaken, O., Gingis-Velitski, S., Vlodavsky, I., and Ilan, N. (2007) Heparanase induces Akt phosphorylation via a lipid raft receptor, *Biochem Biophys Res Commun 361*, 829-834.

140. Kreiling, J. L., Byrd, J. C., and MacDonald, R. G. (2005) Domain interactions of the insulin-like growth factor II/mannose 6-phosphate receptor., *J. Biol. Chem. 280*, 21067-21077.

141. Byrd, J. C., Park, J. H. Y., Schaffer, B. S., Garmroudi, F., and MacDonald, R. G. (2000) Dimerization of the insulin-like growth factor II/mannose 6-phosphate receptor, *J. Biol. Chem. 275*, 18647-18656.

142. Perdue, J. F., Chan, J. K., Thibault, C., Radaj, P., Mills, B., and Daughaday, W. H. (1983) The biochemical characterization of detergent-solubilized insulin-like growth factor II receptors from rat placenta, *J Biol Chem 258*, 7800-7811.

143. Stein, M., Braulke, T., Krentler, C., Hasilik, A., and von Figura, K. (1987) 46-kDa mannose 6-phosphate-specific receptor; biosynthesis, processing, subcellular location and topology, *Biol. Chem. Hoppe-Seyler 368*, 937-947.

144. Byrd, J. C., and MacDonald, R. G. (2000) Mechanisms for high affinity mannose 6-phosphate ligand binding to the insulin-like growth factor II/mannose 6-phosphate receptor. Negative cooperativity and receptor oligomerization, *J. Biol. Chem. 275*, 18638-18646.

145. Goldstein, J. L., Brown, M. S., Anderson, R. G., Russell, D. W., and Schneider, W. J. (1985) Receptor-mediated endocytosis: concepts emerging from the LDL receptor system, *Annu Rev Cell Biol 1*, 1-39.

146. Griffiths, G., Hoflack, B., Simons, K., Mellman, I., and Kornfeld, S. (1988) The mannose 6-phosphate receptor and the biogenesis of lysosomes, *Cell 52*, 329-341.

147. Bleekemolen, J. E., Stein, M., von Figura, K., Slot, J. W., and Geuze, H. J. (1988) The two mannose 6-phosphate receptors have almost identical subcellular distributions in U937 monocytes, *Eur. J. Cell Biol. 47*, 366-372.

148. Klumperman, J., Hille, A., Veenendaal, T., Oorschot, V., Stoorvogel, W., von Figura, K., and Geuze, H. J. (1993) Differences in the endosomal distributions of the two mannose 6-phosphate receptors, *J. Cell Biol. 121*, 997-1010.

149. Waguri, S., Kohmura, M., Kanamori, S., Watanabe, T., Ohsawa, Y., Koike, M., Tomiyama, Y., Wakasugi, M., Kominami, E., and Uchiyama, Y. (2001) Different distribution patterns of the two mannose 6-phosphate receptors in rat liver, *J. Histochem. Cytochem. 49*, 1397-1405.

150. Scheel, G., and Herzog, V. (1989) Mannose 6-phosphate receptor in porcine thyroid follicle cells. Localization and possible implications for the intracellular transport of thyroglobulin, *European journal of cell biology 49*, 140-148.

151. Oka, Y., and Czech, M. P. (1986) The type II insulin-like growth factor receptor is internalized and recycles in the absence of ligand, *J. Biol. Chem. 261*, 9090-9093.

152. Braulke, T., Gartung, C., Hasilik, A., and von Figura, K. (1987) Is movement of mannose 6-phosphate-specific receptor triggered by binding of lysosomal enzymes?, *J. Cell. Biol. 104*, 1735-1742.

153. Oka, Y., Rozek, L. M., and Czech, M. P. (1985) Direct demonstration of rapid insulin-like growth factor II receptor initialization and recycling in rat adipocytes. Insulin stimulates ^{125}I-insulin-like growth factor II degradation by modulating the IGF-II receptor recycling process, *J. Biol. Chem. 260*, 9435-9442.

154. van Meel, E., and Klumperman, J. (2008) Imaging and imagination: understanding the endo-lysosomal system, *Histochemistry and cell biology 129*, 253-266.

155. Reitman, M. L., and Kornfeld, S. (1981) Lysosomal enzyme targeting. N-Acetylglucosaminylphosphotransferase selectively phosphorylates native lysosomal enzymes, *J. Biol. Chem. 256*, 11977-11980.

156. Waheed, A., Hasilik, A., and von Figura, K. (1982) UDP-N-acetylglucosamine:lysosomal enzyme precursor N-acetylglucosamine-1-phosphotransferase. Partial purification and characterization of the rat liver Golgi enzyme, *J Biol Chem 257*, 12322-12331.

157. Varki, A., and Kornfeld, S. (1980) Identification of a rat liver alpha-N-acetylglucosaminyl phosphodiesterase capable of removing "blocking" alpha-N-acetylglucosamine residues from phosphorylated high mannose oligosaccharides of lysosomal enzymes, *J Biol Chem 255*, 8398-8401.

158. Rohrer, J., and Kornfeld, R. (2001) Lysosomal hydrolase mannose 6-phosphate uncovering enzyme resides in the trans-Golgi network, *Mol Biol Cell 12*, 1623-1631.

159. Le Borgne, R., Alconada, A., Bauer, U., and Hoflack, B. (1998) The mammalian AP-3 adaptor-like complex mediates the intracellular transport of lysosomal membrane glycoproteins, *J Biol Chem 273*, 29451-29461.

160. Mullins, C., and Bonifacino, J. S. (2001) The molecular machinery for lysosome biogenesis, *Bioessays 23*, 333-343.

161. Dell'Angelica, E. C., and Payne, G. S. (2001) Intracellular cycling of lysosomal enzyme receptors: cytoplasmic tails' tales, *Cell 106*, 395-398.

162. Schweizer, A., Kornfeld, S., and Rohrer, J. (1997) Proper sorting of the cation-dependent mannose 6-phosphate receptor in endosomes depends on a pair of aromatic amino acids in its cytoplasmic tail, *Proc Natl Acad Sci U S A 94*, 14471-14476.

163. Sleat, D. E., Wang, Y., Sohar, I., Lackland, H., Li, Y., Li, H., Zheng, H., and Lobel, P. (2006) Identification and validation of mannose 6-phosphate glycoproteins in human plasma reveal a wide range of lysosomal and non-lysosomal proteins, *Molecular & cellular proteomics : MCP 5*, 1942-1956.

164. Liu, J., Sukhova, G. K., Sun, J. S., Xu, W. H., Libby, P., and Shi, G. P. (2004) Lysosomal cysteine proteases in atherosclerosis, *Arteriosclerosis, thrombosis, and vascular biology 24*, 1359-1366.

165. Muirden, K. D. (1972) Lysosomal enzymes in synovial membrane in rheumatoid arthritis. Relationship to joint damage, *Annals of the rheumatic diseases 31*, 265-271.

166. Nixon, R. A., Cataldo, A. M., Paskevich, P. A., Hamilton, D. J., Wheelock, T. R., and Kanaley-Andrews, L. (1992) The lysosomal system in neurons. Involvement

at multiple stages of Alzheimer's disease pathogenesis, *Ann N Y Acad Sci 674*, 65-88.

167. Zumkeller, W. (2001) IGFs and IGFBPs: surrogate markers for diagnosis and surveillance of tumour growth?, *Mol Pathol 54*, 285-288.

168. Jones, J. I., and Clemmons, D. R. (1995) Insulin-like growth factors and their binding proteins: biological actions, *Endocrine Rev. 16*, 3-34.

169. Pollak, M. (2008) Insulin and insulin-like growth factor signalling in neoplasia, *Nat Rev Cancer 8*, 915-928.

170. Kaplan, P. J., Mohan, S., Cohen, P., Foster, B. A., and Greenberg, N. M. (1999) The insulin-like growth factor axis and prostate cancer: lessons from the transgenic adenocarcinoma of mouse prostate (TRAMP) model, *Cancer Res. 59*, 2203-2209.

171. Pollak, M. N., Schernhammer, E. S., and Hankinson, S. E. (2004) Insulin-like growth factors and neoplasia, *Nat. Rev. Cancer 4*, 505-518.

172. Loechel, F., Fox, J. W., Murphy, G., Albrechtsen, R., and Wewer, U. M. (2000) ADAM 12-S cleaves IGFBP-3 and IGFBP-5 and is inhibited by TIMP-3, *Biochem Biophys Res Commun 278*, 511-515.

173. Gallagher, E. J., and LeRoith, D. (2011) Minireview: IGF, Insulin, and Cancer, *Endocrinology 152*, 2546-2551.

174. Wang, Y., Thinakaran, G., and Kar, S. (2014) Overexpression of the IGF-II/M6P receptor in mouse fibroblast cell lines differentially alters expression profiles of genes involved in Alzheimer's disease-related pathology, *PloS one 9*, e98057.

175. Wang, Y., Buggia-Prevot, V., Zavorka, M. E., Bleackley, R. C., MacDonald, R. G., Thinakaran, G., and Kar, S. (2015) Overexpression of the Insulin-Like Growth Factor II Receptor Increases beta-Amyloid Production and Affects Cell Viability, *Mol Cell Biol 35*, 2368-2384.

176. Martin-Kleiner, I., and Gall Troselj, K. (2010) Mannose-6-phosphate/insulin-like growth factor 2 receptor (M6P/IGF2R) in carcinogenesis, *Cancer Lett. 289*, 11-22.

177. Chanprasertyothin, S., Jongjaroenprasert, W., and Ongphiphadhanakul, B. (2015) The association of soluble IGF2R and IGF2R gene polymorphism with type 2 diabetes, *Journal of diabetes research 2015*, 216383.

178. Kimura, G., Kasuya, J., Giannini, S., Honda, Y., Mohan, S., Kawachi, M., Akimoto, M., and Fujita-Yamaguchi, Y. (1996) Insulin-like growth factor (IGF) system components in human prostatic cancer cell-lines: LNCaP, DU145, and PC-3 cells, *Int. J. Urol. 3*, 39-46.

179. Rinderknecht, E., and Humbel, R. E. (1978) The amino acid sequence of human insulin-like growth factor I and its structural homology with proinsulin, *J. Biol. Chem. 253*, 2769-2775.

180. Rinderknecht, E., and Humbel, R. E. (1978) Primary structure of human insulin-like growth factor II, *FEBS Lett. 89*, 283-289.

181. Daughaday, W. H., and Rotwein, P. (1989) Insulin-like growth factors I and II. Peptide, messenger ribonucleic acid and gene structures, serum and tissue concentrations, *Endocrine Rev. 10*, 68-91.

182. Delafontaine, P. (1995) Insulin-like growth factor I and its binding proteins in the cardiovascular system, *Cardiovascular research 30*, 825-834.

183. Puche, J. E., and Castilla-Cortazar, I. (2012) Human conditions of insulin-like growth factor-I (IGF-I) deficiency, *Journal of translational medicine 10*, 224.

184. Guntur, A. R., and Rosen, C. J. (2013) IGF-1 regulation of key signaling pathways in bone, *BoneKEy reports 2*, 437.

185. Constancia, M., Hemberger, M., Hughes, J., Dean, W., Ferguson-Smith, A., Fundele, R., Stewart, F., Kelsey, G., Fowden, A., Sibley, C., and Reik, W. (2002) Placental-specific IGF-II is a major modulator of placental and fetal growth, *Nature 417*, 945-948.

186. DeChiara, T. M., Robertson, E. J., and Efstratiadis, A. (1991) Parental imprinting of the mouse insulin-like growth factor II gene, *Cell 64*, 849-859.

187. Kaffer, C. R., Srivastava, M., Park, K. Y., Ives, E., Hsieh, S., Batlle, J., Grinberg, A., Huang, S. P., and Pfeifer, K. (2000) A transcriptional insulator at the imprinted H19/Igf2 locus, *Genes Dev 14*, 1908-1919.

188. Vu, T. H., and Hoffman, A. R. (1994) Promoter-specific imprinting of the human insulin-like growth factor-II gene, *Nature 371*, 714-717.

189. Li, X., Adam, G., Cui, H., Sandstedt, B., Ohlsson, R., and Ekstrom, T. J. (1995) Expression, promoter usage and parental imprinting status of insulin-like growth factor II (IGF2) in human hepatoblastoma: uncoupling of IGF2 and H19 imprinting, *Oncogene 11*, 221-229.

190. Baxter, R. C. (2014) IGF binding proteins in cancer: mechanistic and clinical insights, *Nat Rev Cancer 14*, 329-341.

191. Clemmons, D. R. (1997) Insulin-like growth factor binding proteins and their role in controlling IGF actions, *Cytokine & growth factor reviews 8*, 45-62.

192. Bergman, D., Halje, M., Nordin, M., and Engstrom, W. (2013) Insulin-like growth factor 2 in development and disease: a mini-review, *Gerontology 59*, 240-249.

193. Ullrich, A., Gray, A., Tam, A. W., Yang Feng, T., Tsubokawa, M., Collins, C., Henzel, W., Le Bon, T., Kathuria, S., Chen, E., Jacobs, S., Francke, U., Ramachandran, J., and Fujita-Yamaguchi, Y. (1986) Insulin-like growth factor I receptor primary structure: comparison with insulin receptor suggests structural determinants that define functional specificity, *EMBO J. 5*, 2503-2512.

194. Sachdev, D., and Yee, D. (2007) Disrupting insulin-like growth factor signaling as a potential cancer therapy, *Molecular cancer therapeutics 6*, 1-12.

195. Fulda, S., and Debatin, K. M. (2006) Extrinsic versus intrinsic apoptosis pathways in anticancer chemotherapy, *Oncogene 25*, 4798-4811.

196. Elmore, S. (2007) Apoptosis: a review of programmed cell death, *Toxicologic pathology 35*, 495-516.

197. Versteyhe, S., Klaproth, B., Borup, R., Palsgaard, J., Jensen, M., Gray, S. G., and De Meyts, P. (2013) IGF-I, IGF-II, and Insulin Stimulate Different Gene Expression Responses through Binding to the IGF-I Receptor, *Frontiers in endocrinology 4*, 98.

198. De Meyts, P., Wallach, B., Christoffersen, C. T., Urso, B., Gronskov, K., Latus, L. J., Yakushiji, F., Ilondo, M. M., and Shymko, R. M. (1994) The insulin-like growth factor-I receptor. Structure, ligand-binding mechanism and signal transduction, *Horm Res 42*, 152-169.

199. Pandini, G., Conte, E., Medico, E., Sciacca, L., Vigneri, R., and Belfiore, A. (2004) IGF-II binding to insulin receptor isoform A induces a partially different gene expression profile from insulin binding, *Ann N Y Acad Sci 1028*, 450-456.

200. Belfiore, A., Frasca, F., Pandini, G., Sciacca, L., and Vigneri, R. (2009) Insulin receptor isoforms and insulin receptor/insulin-like growth factor receptor hybrids in physiology and disease, *Endocrine reviews 30*, 586-623.

201. Ludwig, T., Eggenschwiler, J., Fisher, P., D'Ercole, A. J., Davenport, M. L., and Efstratiadis, A. (1996) Mouse mutants lacking the type 2 IGF receptor (IGF2R) are rescued from perinatal lethality in *Igf2* and *Igf1r* null backgrounds, *Dev. Biol. 177*, 517-535.

202. Di Cola, G., Cool, M. H., and Accili, D. (1997) Hypoglycemic effect of insulin-like growth factor-1 in mice lacking insulin receptors, *The Journal of clinical investigation 99*, 2538-2544.

203. Gallagher, E. J., and LeRoith, D. (2010) The proliferating role of insulin and insulin-like growth factors in cancer, *Trends in endocrinology and metabolism: TEM 21*, 610-618.

204. Entingh, A. J., Taniguchi, C. M., and Kahn, C. R. (2003) Bi-directional regulation of brown fat adipogenesis by the insulin receptor, *J Biol Chem 278*, 33377-33383.

205. Kim, J. J., and Accili, D. (2002) Signalling through IGF-I and insulin receptors: where is the specificity?, *Growth hormone & IGF research : official journal of the Growth Hormone Research Society and the International IGF Research Society 12*, 84-90.

206. Koster, A., von Figura, K., and Pohlmann, R. (1994) Mistargeting of lysosomal enzymes in M(r) 46,000 mannose 6-phosphate receptor-deficient mice is compensated by carbohydrate-specific endocytotic receptors, *Eur J Biochem 224*, 685-689.

207. Hille-Rehfeld, A. (1995) Mannose 6-phosphate receptors in sorting and transport of lysosomal enzymes., *Biochim. Biophys. Acta 1241*, 177-194.

208. Lee, S.-J., and Nathans, D. (1988) Proliferin secreted by cultured cells binds to mannose 6-phosphate receptors, *J. Biol. Chem. 263*, 3521-3527.

209. Faust, P. L., Chirgwin, J. M., and Kornfeld, S. (1987) Renin, a secretory glycoprotein, acquires phosphomannosyl residues, *J. Cell Biol. 105*, 1947-1955.

210. Herzog, V., Neumüller, W., and Holzmann, B. (1987) Thyroglobulin, the major and obligatory exportable protein of thyroid follicle cells, carries the lysosomal recognition marker mannose-6-phosphate, *EMBO J. 6*, 555-560.

211. Jirtle, R. L., Carr, B. I., and Scott, C. D. (1991) Modulation of insulin-like growth factor-II/mannose 6-phosphate receptors and transforming growth factor-β1 during liver regeneration, *J. Biol. Chem. 266*, 22444-22450.

212. Purchio, A. F., Cooper, J. A., Brunner, A. M., Lioubin, M. N., Gentry, L. E., Kovacina, K. S., Roth, R. A., and Marquardt, H. (1988) Identification of mannose 6-phosphate in two asparagine-linked sugar chains of recombinant transforming growth factor-beta 1 precursor., *J. Biol. Chem. 263*, 14211-14215.

213. Dennis, P. A., and Rifkin, D. B. (1991) Cellular activation of latent transforming growth factor β requires binding to the cation-independent mannose 6-phosphate/insulin-like growth factor type II receptor, *Proc. Natl. Acad. Sci. U.S.A. 88*, 580-584.

214. Munger, J., Harpel, J. G., Gleizes, P., Mazzieri, R., Nunes, I., and Rifkin, D. (1997) Latent transforming growth factor-beta: structural features and mechanisms of activation, *Kidney Int. 51*, 1376-1382.

215. Ghahary, A., Tredget, E. E., and Shen, Q. (1999) Insulin-like growth factor-II/mannose 6-phosphate receptors facilitate the matrix effects of latent transforming growth factor-β1 released from genetically modified keratinocytes in a fibroblast/keratinocyte co-culture system, *J. Cell. Physiol. 180*, 61-70.

216. Ghahary, A., Tredget, E. E., Shen, Q., Kilani, R. T., Scott, P. G., and Houle, Y. (2000) Mannose-6-phosphate/IGF-II receptors mediate the effects of IGF-1-induced latent transforming growth factor beta 1 on expression of type I collagen and collagenase in dermal fibroblasts, *Growth Factors 17*, 167-176.

217. Nguyen, G., and Contrepas, A. (2008) Physiology and pharmacology of the (pro)renin receptor, *Current opinion in pharmacology 8*, 127-132.

218. Jackson, D., and Linzer, D. I. (1997) Proliferin transport and binding in the mouse fetus, *Endocrinology 138*, 149-155.
219. Lonnroth, P., Assmundsson, K., Eden, S., Enberg, G., Gause, I., Hall, K., and Smith, U. (1987) Regulation of insulin-like growth factor II receptors by growth hormone and insulin in rat adipocytes, *Proc Natl Acad Sci U S A 84*, 3619-3622.
220. Corvera, S., Yagaloff, K. A., Whitehead, R. E., and Czech, M. P. (1988) Tyrosine phosphorylation of the receptor for insulin-like growth factor II is inhibited in plasma membranes from insulin-treated rat adipocytes, *Biochem. J. 250*, 47-52.
221. Corvera, S., and Czech, M. P. (1985) Mechanism of insulin action on membrane protein recycling: a selective decrease in the phosphorylation state of insulin-like growth factor II receptors in the cell surface membrane, *Proc. Natl. Acad. Sci. U.S.A. 82*, 7314-7318.
222. Chen, W. J., Goldstein, J. L., and Brown, M. S. (1990) NPXY, a sequence often found in cytoplasmic tails, is required for coated pit-mediated internalization of the low density lipoprotein receptor, *J. Biol. Chem. 265*, 3116-3123.
223. Ktistakis, N. T., Thomas, D., and Roth, M. G. (1990) Characteristics of the tyrosine recognition signal for internalization of transmembrane surface glycoproteins, *J. Cell Biol. 111*, 1393-1407.
224. Collawn, J. F., Stangel, M., Kuhn, L. A., Esekogwu, V., Jing, S. Q., Trowbridge, I. S., and Tainer, J. A. (1990) Transferrin receptor internalization sequence YXRF implicates a tight turn as the structural recognition motif for endocytosis, *Cell 63*, 1061-1072.
225. McGraw, T. E., Pytowski, B., Arzt, J., and Ferrone, C. (1991) Mutagenesis of the human transferrin receptor: two cytoplasmic phenylalanines are required for efficient internalization and a second-site mutation is capable of reverting an internalization-defective phenotype, *J Cell Biol 112*, 853-861.
226. Girones, N., Alverez, E., Seth, A., Lin, I. M., Latour, D. A., and Davis, R. J. (1991) Mutational analysis of the cytoplasmic tail of the human transferrin receptor. Identification of a sub-domain that is required for rapid endocytosis, *J Biol Chem 266*, 19006-19012.
227. Jadot, M., Canfield, W. M., Gregory, W., and Kornfeld, S. (1992) Characterization of the signal for rapid internalization of the bovine mannose 6-phosphate/insulin-like growth factor-II receptor, *J Biol Chem 267*, 11069-11077.
228. Di Bacco, A., and Gill, G. (2003) The secreted glycoprotein CREG inhibits cell growth dependent on the mannose-6-phosphate/insulin-like growth factor II receptor, *Oncogene 22*, 5436-5445.
229. Han, Y.-L., Guo, P., Sun, M.-Y., Guo, L., Luan, B., Kang, J., Yan, C.-H., and Li, S.-H. (2008) Secreted CREG inhibits cell proliferation mediated by mannose 6-phosphate/insulin-like growth factor II receptor in NIH3T3 fibroblasts, *Genes Cells 13*, 977-986.
230. Han, Y., Luan, B., Sun, M., Guo, L., Guo, P., Tao, J., Deng, J., Wu, G., Liu, S., Yan, C., and Li, S. (2011) Glycosylation-independent binding to extracellular domains 11-13 of mannose-6-phosphate/insulin-like growth factor-2 receptor mediates the effects of soluble CREG on the phenotypic modulation of vascular smooth muscle cells, *J Mol Cell Cardiol 50*, 723-730.
231. Han, Y., Cui, J., Tao, J., Guo, L., Guo, P., Sun, M., Kang, J., Zhang, X., Yan, C., and Li, S. (2009) CREG inhibits migration of human vascular smooth muscle cells by mediating IGF-II endocytosis, *Exp. Cell Res. 315*, 3301-3311.
232. Lamonerie, T., Lavialle, C., Haddada, H., and Brison, O. (1995) IGF-2 autocrine stimulation in tumorigenic clones of a human colon-carcinoma cell line, *Int. J. Cancer 61*, 587-592.

233. Foulstone, E., Prince, S., Zaccheo, O., Burns, J. L., Harper, J., Jacobs, C., Church, D., and Hassan, A. B. (2005) Insulin-like growth factor ligands, receptors, and binding proteins in cancer, *J Pathol 205*, 145-153.

234. Brouwer-Visser, J., and Huang, G. S. (2015) IGF2 signaling and regulation in cancer, *Cytokine & growth factor reviews 26*, 371-377.

235. Bruchim, I., Sarfstein, R., and Werner, H. (2014) The IGF Hormonal Network in Endometrial Cancer: Functions, Regulation, and Targeting Approaches, *Frontiers in endocrinology 5*, 76.

236. Grimberg, A., and Cohen, P. (2000) Role of insulin-like growth factors and their binding proteins in growth control and carcinogenesis, *J. Cell. Physiol. 183*, 1-9.

237. Ekstrom, T. J., Cui, H., Li, X., and Ohlsson, R. (1995) Promoter-specific IGF2 imprinting status and its plasticity during human liver development, *Development 121*, 309-316.

238. Cui, H., Cruz-Correa, M., Giardiello, F. M., Hutcheon, D. F., Kafonek, D. R., Brandenburg, S., Wu, Y., He, X., Powe, N. R., and Feinberg, A. P. (2003) Loss of IGF2 imprinting: a potential marker of colorectal cancer risk, *Science 299*, 1753-1755.

239. Dai, Y., Wang, Z., Li, J., Gu, X., Zheng, M., Zhou, J., Ye, X., Yao, J., Cui, I., Hu, Y., Cui, H. (2007) Imprinting status of IGF2 in cord blood cells of Han Chinese newborns, *Int. J. Mol. Sci. 8*, 273-283.

240. Rancourt, R. C., Harris, H. R., Barault, L., and Michels, K. B. (2013) The prevalence of loss of imprinting of H19 and IGF2 at birth, *FASEB journal : official publication of the Federation of American Societies for Experimental Biology 27*, 3335-3343.

241. Murphy, S. K., Huang, Z., Wen, Y., Spillman, M. A., Whitaker, R. S., Simel, L. R., Nichols, T. D., Marks, J. R., and Berchuck, A. (2006) Frequent IGF2/H19 domain epigenetic alterations and elevated IGF2 expression in epithelial ovarian cancer, *Molecular cancer research : MCR 4*, 283-292.

242. Qian, B., Katsaros, D., Lu, L., Canuto, E. M., Benedetto, C., Beeghly-Fadiel, A., and Yu, H. (2011) IGF-II promoter specific methylation and expression in epithelial ovarian cancer and their associations with disease characteristics, *Oncology reports 25*, 203-213.

243. Morison, I. M., and Reeve, A. E. (1998) Insulin-like growth factor 2 and overgrowth: molecular biology and clinical implications, *Molecular medicine today 4*, 110-115.

244. Ward, A. (1997) Beck-Wiedemann syndrome and Wilms' tumour, *Molecular human reproduction 3*, 157-168.

245. Ogawa, O., Eccles, M. R., Szeto, J., McNoe, L. A., Yun, K., Maw, M. A., Smith, P. J., and Reeve, A. E. (1993) Relaxation of insulin-like growth factor II gene imprinting implicated in Wilms' tumour., *Nature 362*, 749-751.

246. Feinberg, A. P. (1999) Imprinting of a genomic domain of 11p15 and loss of imprinting in cancer: an introduction, *Cancer Res. 59*, 1743s-1746s.

247. Zhan, S., Shapiro, D., Zhan, S., Zhang, L., Hirschfeld, S., Elassel, J., and Helman, L. J. (1995) Concordant loss of imprinting of the human insulin-like growth factor II gene promoters in cancer, *J. Biol. Chem. 270*, 27983-27986.

248. Balch, C., and Nephew, K. P. (2013) Epigenetic targeting therapies to overcome chemotherapy resistance, *Advances in experimental medicine and biology 754*, 285-311.

249. Breuhahn, K., Vreden, S., Haddad, R., Beckebaum, S., Stippel, D., Flemming, P., Nussbaum, T., Caselmann, W. H., Haab, B. B., and Schirmacher, P. (2004) Molecular profiling of human hepatocellular carcinoma defines mutually exclusive

interferon regulation and insulin-like growth factor II overexpression, *Cancer Res. 64*, 6058-6064.

250. Liu, M., Roth, A., Yu, M., Morris, R., Bersani, F., Rivera, M. N., Lu, J., Shioda, T., Vasudevan, S., Ramaswamy, S., Maheswaran, S., Diederichs, S., and Haber, D. A. (2013) The IGF2 intronic miR-483 selectively enhances transcription from IGF2 fetal promoters and enhances tumorigenesis, *Genes Dev 27*, 2543-2548.

251. Lederer, M., Bley, N., Schleifer, C., and Huttelmaier, S. (2014) The role of the oncofetal IGF2 mRNA-binding protein 3 (IGF2BP3) in cancer, *Seminars in cancer biology 29*, 3-12.

252. Liao, B., Hu, Y., Herrick, D. J., and Brewer, G. (2005) The RNA-binding protein IMP-3 is a translational activator of insulin-like growth factor II leader-3 mRNA during proliferation of human K562 leukemia cells, *J Biol Chem 280*, 18517-18524.

253. Suvasini, R., Shruti, B., Thota, B., Shinde, S. V., Friedmann-Morvinski, D., Nawaz, Z., Prasanna, K. V., Thennarasu, K., Hegde, A. S., Arivazhagan, A., Chandramouli, B. A., Santosh, V., and Somasundaram, K. (2011) Insulin growth factor-2 binding protein 3 (IGF2BP3) is a glioblastoma-specific marker that activates phosphatidylinositol 3-kinase/mitogen-activated protein kinase (PI3K/MAPK) pathways by modulating IGF-2, *J Biol Chem 286*, 25882-25890.

254. Ruiz i Altaba, A., Sanchez, P., and Dahmane, N. (2002) Gli and hedgehog in cancer: tumours, embryos and stem cells, *Nat Rev Cancer 2*, 361-372.

255. Ingram, W. J., Wicking, C. A., Grimmond, S. M., Forrest, A. R., and Wainwright, B. J. (2002) Novel genes regulated by Sonic Hedgehog in pluripotent mesenchymal cells, *Oncogene 21*, 8196-8205.

256. Hahn, H., Wojnowski, L., Specht, K., Kappler, R., Calzada-Wack, J., Potter, D., Zimmer, A., Muller, U., Samson, E., and Quintanilla-Martinez, L. (2000) Patched target Igf2 is indispensable for the formation of medulloblastoma and rhabdomyosarcoma, *J Biol Chem 275*, 28341-28344.

257. Tada, Y., Yamaguchi, Y., Kinjo, T., Song, X., Akagi, T., Takamura, H., Ohta, T., Yokota, T., and Koide, H. (2015) The stem cell transcription factor ZFP57 induces IGF2 expression to promote anchorage-independent growth in cancer cells, *Oncogene 34*, 752-760.

258. Lui, J. C., and Baron, J. (2013) Evidence that Igf2 down-regulation in postnatal tissues and up-regulation in malignancies is driven by transcription factor E2f3, *Proc Natl Acad Sci U S A 110*, 6181-6186.

259. Daughaday, W. H. (1990) The possible autocrine/paracrine and endocrine roles of insulin-like growth factors of human tumors., *Endocrinology 127*, 1-4.

260. Breuhahn, K., Longerich, T., and Schirmacher, P. (2006) Dysregulation of growth factor signaling in human hepatocellular carcinoma, *Oncogene 25*, 3787-3800.

261. Wilkin, F., Gagne, N., Paquette, J., Oligny, L. L., and Deal, C. (2000) Pediatric adrenocortical tumors: molecular events leading to insulin-like growth factor II gene overexpression, *J Clin Endocrinol Metab 85*, 2048-2056.

262. Lund, P., Schubert, D., Niketeghad, F., and Schirmacher, P. (2004) Autocrine inhibition of chemotherapy response in human liver tumor cells by insulin-like growth factor-II, *Cancer Lett 206*, 85-96.

263. Pollak, M., Beamer, W., and Zhang, J. C. (1998) Insulin-like growth factors and prostate cancer, *Cancer Metastasis Rev 17*, 383-390.

264. Nussbaum, T., Samarin, J., Ehemann, V., Bissinger, M., Ryschich, E., Khamidjanov, A., Yu, X., Gretz, N., Schirmacher, P., and Breuhahn, K. (2008) Autocrine insulin-like growth factor-II stimulation of tumor cell migration is a progression step in human hepatocarcinogenesis, *Hepatology 48*, 146-156.

265. Kaneda, A., Wang, C. J., Cheong, R., Timp, W., Onyango, P., Wen, B., Iacobuzio-Donahue, C. A., Ohlsson, R., Andraos, R., Pearson, M. A., Sharov, A. A., Longo, D. L., Ko, M. S., Levchenko, A., and Feinberg, A. P. (2007) Enhanced sensitivity to IGF-II signaling links loss of imprinting of IGF2 to increased cell proliferation and tumor risk, *Proc Natl Acad Sci U S A 104*, 20926-20931.

266. Rasmussen, A. A., and Cullen, K. J. (1998) Paracrine/autocrine regulation of breast cancer by the insulin-like growth factors, *Breast Cancer Res. Treat. 47*, 219-233.

267. Cohen, P., Peehl, D. M., Stamey, T. A., Wilson, K. F., Clemmons, D. R., and Rosenfeld, R. G. (1993) Elevated levels of insulin-like growth factor-binding protein-2 in the serum of prostate cancer patients, *J. Clin. Endocrinol. Metab. 76*, 1031-1035.

268. Ho, P. J., and Baxter, R. C. (1997) Insulin-like growth factor-binding protein-2 in patients with prostate carcinoma and benign prostatic hyperplasia, *Clin. Endocrinol. 46*, 333-342.

269. Timp, W., Levchenko, A., and Feinberg, A. P. (2009) A new link between epigenetic progenitor lesions in cancer and the dynamics of signal transduction, *Cell Cycle 8*, 383-390.

270. Sharon, E., Streicher, H., Goncalves, P., and Chen, H. X. (2014) Immune checkpoint inhibitors in clinical trials, *Chinese journal of cancer 33*, 434-444.

271. Hebert, E. (2006) Mannose-6-phosphate/insulin-like growth factor II receptor expression and tumor development, *Bioscience reports 26*, 7-17.

272. Jirtle, R. L. (1999) Genomic imprinting and cancer, *Exp Cell Res 248*, 18-24.

273. Zaina, S., and Squire, S. (1998) The soluble insulin-like growth factor (IGF-II) receptor reduces organ size by IGF-II-mediated and IGF-II-independent mechanisms, *J. Biol. Chem. 273*, 28610-28616.

274. O'Gorman, D. B., Weiss, J., Hettiaratchi, A., Firth, S. M., and Scott, C. D. (2002) Insulin-like growth factor-II/mannose 6-phosphate receptor overexpression reduces growth of choriocarcinoma cells *in vitro* and *in vivo*, *Endocrinology 143*, 4287-4294.

275. Oates, A. J., Schumaker, L. M., Jenkins, S. B., Pearce, A. A., DaCosta, S. A., Arun, B., and Ellis, M. J. C. (1998) The mannose 6-phosphate/insulin-like growth factor 2 receptor (*M6P/IGF2R*), a putative breast tumor suppressor gene, *Breast Cancer Res. Treat. 47*, 269-281.

276. DaCosta, S. A., Schumaker, L. M., and Ellis, M. J. (2000) Mannose 6-phosphate/insulin-like growth factor 2 receptor, a bona fide tumor suppressor gene or just a promising candidate?, *Journal of mammary gland biology and neoplasia 5*, 85-94.

277. De Souza, A. T., Hankins, G. R., Washington, M. K., Fine, R. L., Orton, T. C., and Jirtle, R. L. (1995) Frequent loss of heterozygosity on 6q at the mannose 6-phosphate/insulin-like growth factor II receptor locus in human hepatocellular tumors, *Oncogene 10*, 1725-1729.

278. Yamada, T., De Souza, A. T., Finkelstein, S., and Jirtle, R. L. (1997) Loss of the gene encoding mannose 6-phosphate/insulin-like growth factor II receptor is an early event in liver carcinogenesis, *Proc. Natl. Acad. Sci. U.S.A. 94*, 10351-10355.

279. Ghosh, P., Dahms, N. M., and Kornfeld, S. (2003) Mannose 6-phosphate receptors: new twists in the tale, *Nat. Rev. Mol. Cell Biol. 4*, 202-213.

280. De Souza, A. T., Hankins, G. R., Washington, M. K., Orton, T. C., and Jirtle, R. L. (1995) *M6P/IGF2R* gene is mutated in human hepatocellular carcinomas with loss of heterozygosity., *Nat. Genet. 11*, 447-449.

281. Hankins, G. R., De Souza, A. T., Bentley, R. C., Patel, M. R., Marks, J. R., Iglehart, J. D., and Jirtle, R. L. (1996) M6P/IGF2 receptor: a candidate breast tumor suppressor gene., *Oncogene 12*, 2003-2009.

282. Chappell, S. A., Walsh, T., Walker, R. A., and Shaw, J. A. (1997) Loss of heterozygosity at the mannose 6-phosphate insulin-like growth factor 2 receptor gene correlates with poor differentiation in early breast carcinomas, *Br. J. Cancer 76*, 1558-1561.

283. Rey, J.-M., Theillet, C., Brouillet, J.-P., and Rochefort, H. (2000) Stable amino-acid sequence of the mannose-6-phosphate/insulin-like growth-factor-II receptor in ovarian carcinomas with loss of heterozygosity and in breast-cancer cell lines, *Int. J. Cancer 85*, 466-473.

284. Kong, F.-M., Anscher, M. S., Washington, M. K., Killian, K. J., and Jirtle, R. L. (2000) *M6P/IGF2R* is mutated in squamous cell carcinoma of the lung, *Oncogene 19*, 1572-1578.

285. Gemma, A., Hosoya, Y., Uematsu, K., Seike, M., Kurimoto, F., Yoshimura, A., Shibuya, M., and Kudoh, S. (2000) Mutation analysis of the gene encoding the human mannose 6-phosphate/insulin-like growth factor 2 receptor (M6P/IGF2R) in human cell lines resistant to growth inhibition by transforming growth factor beta(1) (TGF-beta(1)), *Lung Cancer 30*, 91-98.

286. Li, J., and Sahagian, G. G. (2004) Demonstration of tumor suppression by mannose 6-phosphate/insulin-like growth factor 2 receptor, *Oncogene 23*, 9359-9368.

287. Kreiling, J. L., Montgomery, M. A., Wheeler, J. R., Kopanic, J. L., Connelly, C. M., Zavorka, M. E., Allison, J. L., and MacDonald, R. G. (2012) Dominant-negative effect of truncated mannose 6-phosphate/insulin-like growth factor II receptor species in cancer, *FEBS J. 279*, 2695-2713.

288. Janssen, J. A., and Varewijck, A. J. (2014) IGF-IR Targeted Therapy: Past, Present and Future, *Frontiers in endocrinology 5*, 224.

289. Pillai, R. N., and Ramalingam, S. S. (2013) Inhibition of insulin-like growth factor receptor: end of a targeted therapy?, *Translational lung cancer research 2*, 14-22.

290. Brahmkhatri, V. P., Prasanna, C., and Atreya, H. S. (2015) Insulin-like growth factor system in cancer: novel targeted therapies, *BioMed research international 2015*, 538019.

291. Prakash, J., Beljaars, L., Harapanahalli, A. K., Zeinstra-Smith, M., de Jager-Krikken, A., Hessing, M., Steen, H., and Poelstra, K. (2010) Tumor-targeted intracellular delivery of anticancer drugs through the mannose-6-phosphate/insulin-like growth factor II receptor, *Int J Cancer 126*, 1966-1981.

292. Poelstra, K., Beljaars, L., and Melgert, B. N. (2013) Cell-specific delivery of biologicals: problems, pitfalls and possibilities of antifibrotic compounds in the liver, *Drug discovery today 18*, 1237-1242.

293. Probst, O. C., Puxbaum, V., Svoboda, B., Leksa, V., Stockinger, H., Mikula, M., Mikulits, W., and Mach, L. (2009) The mannose 6-phosphate/insulin-like growth factor II receptor restricts the tumourigenicity and invasiveness of squamous cell carcinoma cells, *Int J Cancer 124*, 2559-2567.

294. Probst, O. C., Karayel, E., Schida, N., Nimmerfall, E., Hehenberger, E., Puxbaum, V., and Mach, L. (2013) The mannose 6-phosphate-binding sites of M6P/IGF2R determine its capacity to suppress matrix invasion by squamous cell carcinoma cells, *The Biochemical journal 451*, 91-99.

295. Puxbaum, V., Nimmerfall, E., Bauerl, C., Taub, N., Blaas, P. M., Wieser, J., Mikula, M., Mikulits, W., Ng, K. M., Yeoh, G. C., and Mach, L. (2012) M6P/IGF2R

modulates the invasiveness of liver cells via its capacity to bind mannose 6-phosphate residues, *J Hepatol 57*, 337-343.

296. Harper, J., Burns, J. L., Foulstone, E. J., Pignatelli, M., Zaina, S., and Hassan, A. B. (2006) Soluble IGF2 receptor rescues Apc(Min/+) intestinal adenoma progression induced by Igf2 loss of imprinting, *Cancer Res. 66*, 1940-1948.

297. Prince, S. N., Foulstone, E. J., Zaccheo, O. J., Williams, C., and Hassan, A. B. (2007) Functional evaluation of novel soluble insulin-like growth factor (IGF)-II-specific ligand traps based on modified domain 11 of the human IGF2 receptor, *Molecular cancer therapeutics 6*, 607-617.

298. Soh, C. L., McNeil, K., Owczarek, C. M., Hardy, M. P., Fabri, L. J., Pearse, M., Delaine, C. A., and Forbes, B. E. (2014) Exogenous administration of protease-resistant, non-matrix-binding IGFBP-2 inhibits tumour growth in a murine model of breast cancer, *Br J Cancer 110*, 2855-2864.

299. Chen, W. J., Ho, C. C., Chang, Y. L., Chen, H. Y., Lin, C. A., Ling, T. Y., Yu, S. L., Yuan, S. S., Chen, Y. J., Lin, C. Y., Pan, S. H., Chou, H. Y., Chang, G. C., Chu, W. C., Lee, Y. M., Lee, J. Y., Lee, P. J., Li, K. C., Chen, H. W., and Yang, P. C. (2014) Cancer-associated fibroblasts regulate the plasticity of lung cancer stemness via paracrine signalling, *Nature communications 5*, 3472.

300. Murray, G. J., and Neville, D. M., Jr. (1980) Mannose 6-phosphate receptor-mediated uptake of modified low density lipoprotein results in down regulation of hydroxymethylglutaryl-CoA reductase in normal and familial hypercholesterolemic fibroblasts, *J. Biol. Chem. 255*, 11942-11948.

301. Ferro, V., Fewings, K., Palermo, M. C., and Li, C. (2001) Large-scale preparation of the oligosaccharide phosphate fraction of Pichia holstii NRRL Y-2448 phosphomannan for use in the manufacture of PI-88, *Carbohydr Res 332*, 183-189.

302. Braulke, T., Causin, C., Waheed, A., Junghans, U., Hasilik, A., Maly, P., Humbel, R. E., and von Figura, K. (1988) Mannose 6-phosphate/insulin-like growth factor II receptor: distinct binding sites for mannose 6-phosphate and insulin-like growth factor II, *Biochem. Biophys. Res. Commun. 150*, 1287-1293.

303. Garmroudi, F., and MacDonald, R. G. (1994) Localization of the insulin-like growth factor II (IGF-II) binding/cross-linking site of the IGF-II/mannose 6-phosphate receptor to extracellular repeats 10-11, *J. Biol. Chem. 269*, 26944-26952.

304. Valenzano, K. J., Kallay, L. M., and Lobel, P. (1993) An assay to detect glycoproteins that contain mannose 6-phosphate, *Anal. Biochem. 209*, 156-162.

305. Pear, W. S., Nolan, G. P., Scott, M. L., and Baltimore, D. (1993) Production of high-titer helper-free retroviruses by transient transfection, *Proc. Natl. Acad. Sci. U.S.A. 90*, 8392-8396.

306. Denizot, F., and Lang, R. (1986) Rapid colorimetric assay for cell growth and survival: modifications of the tetrazolium dye procedure giving improved sensitivity and reliability., *J. Immunol. Meth. 89*, 271-277.

307. Park, J. H. Y., McCusker, R. H., Vanderhoof, J. A., Mohammadpour, H., Harty, R. F., and MacDonald, R. G. (1992) Secretion of insulin-like growth factor II (IGF-II) and IGF-binding protein-2 by intestinal epithelial (IEC-6) cells: implications for autocrine growth regulation, *Endocrinology 131*, 1359-1368.

308. Upton, Z., Webb, H., Hale, K., Yandell, C. A., McMurtry, J. P., Francis, G. L., and Ballard, F. J. (1999) Identification of vitronectin as a novel insulin-like growth factor-II binding protein, *Endocrinology 140*, 2928-2931.

309. Hayashi, K., and Kojima, C. (2008) pCold-GST vector: a novel cold-shock vector containing GST tag for soluble protein production, *Protein Expr Purif 62*, 120-127.

310. Sockolosky, J. T., and Szoka, F. C. (2013) Periplasmic production via the pET expression system of soluble, bioactive human growth hormone, *Protein Expr Purif 87*, 129-135.

311. Han, Y. L., Xu, H. M., Deng, J., Hu, Y., Kang, J., Liu, H. W., and Yan, C. H. (2006) [Over-expression of the cellular repressor of E1A-stimulated genes inhibits the apoptosis of human vascular smooth muscle cells in vitro.], *Sheng li xue bao : [Acta physiologica Sinica] 58*, 324-330.

312. Berkowitz, D. B., Maiti, G., Charette, B., Dreis, C. D., and MacDonald, R. G. (2004) Mono- and Bivalent Ligands Bearing Mannose 6-Phosphate (M6P) Surrogates: Targeting the M6P/insulin-like growth factor II receptor, *Org. Lett. 6*, 4921-4924.

313. Fei, X., Connelly, C. M., MacDonald, R. G., and Berkowitz, D. B. (2008) A set of phosphatase-inert "molecular rulers" to probe for bivalent mannose 6-phosphate ligand-receptor interactions, *Bioorg. Med. Chem. Lett. 18*, 3085-3089.

314. O'Gorman, D. B., Costello, M., Weiss, J., Firth, S. M., and Scott, C. D. (1999) Decreased insulin-like growth factor-II/mannose 6-phosphate receptor expression enhances tumorigenicity in JEG-3 cells, *Cancer Res. 59*, 5692-5694.

315. Burdick, M. D., Harris, A., Reid, C. J., Iwamura, T., and Hollingsworth, M. A. (1997) Oligosaccharides expressed on MUC1 produced by pancreatic and colon tumor cell lines, *J Biol Chem 272*, 24198-24202.

316. Jin, J. K., Dayyani, F., and Gallick, G. E. (2011) Steps in prostate cancer progression that lead to bone metastasis, *Int J Cancer 128*, 2545-2561.

317. Bellmunt, J., and Oh, W. K. (2010) Castration-resistant prostate cancer: new science and therapeutic prospects, *Therapeutic advances in medical oncology 2*, 189-207.

318. O'Kusky, J., and Ye, P. (2012) Neurodevelopmental effects of insulin-like growth factor signaling, *Frontiers in neuroendocrinology 33*, 230-251.

319. Melino, G., Stephanou, A., Annicchiarico-Petruzzelli, M., Knight, R. A., Finazzi-Agro, A., and Lightman, S. L. (1993) Modulation of IGF-2 expression during growth and differentiation of human neuroblastoma cells: retinoic acid may induce IGF-2, *Neurosci Lett 151*, 187-191.

320. Mu, Y. M., Yanase, T., Nishi, Y., Tanaka, A., Saito, M., Jin, C. H., Mukasa, C., Okabe, T., Nomura, M., Goto, K., and Nawata, H. (2001) Saturated FFAs, palmitic acid and stearic acid, induce apoptosis in human granulosa cells, *Endocrinology 142*, 3590-3597.

321. Cazanave, S. C., Mott, J. L., Elmi, N. A., Bronk, S. F., Werneburg, N. W., Akazawa, Y., Kahraman, A., Garrison, S. P., Zambetti, G. P., Charlton, M. R., and Gores, G. J. (2009) JNK1-dependent PUMA expression contributes to hepatocyte lipoapoptosis, *J Biol Chem 284*, 26591-26602.

322. Natarajan, S. K., Ingham, S. A., Mohr, A. M., Wehrkamp, C. J., Ray, A., Roy, S., Cazanave, S. C., Phillippi, M. A., and Mott, J. L. (2014) Saturated free fatty acids induce cholangiocyte lipoapoptosis, *Hepatology 60*, 1942-1956.

323. Boulares, A. H., Yakovlev, A. G., Ivanova, V., Stoica, B. A., Wang, G., Iyer, S., and Smulson, M. (1999) Role of poly(ADP-ribose) polymerase (PARP) cleavage in apoptosis. Caspase 3-resistant PARP mutant increases rates of apoptosis in transfected cells, *J Biol Chem 274*, 22932-22940.

324. Meggio, F., Boldyreff, B., Marin, O., Issinger, O. G., and Pinna, L. A. (1995) Phosphorylation and activation of protein kinase CK2 by p34cdc2 are independent events, *Eur J Biochem 230*, 1025-1031.

325. Akagi, H., Higuchi, H., Sumimoto, H., Igarashi, T., Kabashima, A., Mizuguchi, H., Izumiya, M., Sakai, G., Adachi, M., Funakoshi, S., Nakamura, S., Hamamoto, Y., Kanai, T., Takaishi, H., Kawakami, Y., and Hibi, T. (2013) Suppression of myeloid cell leukemia-1 (Mcl-1) enhances chemotherapy-associated apoptosis in gastric cancer cells, *Gastric cancer : official journal of the International Gastric Cancer Association and the Japanese Gastric Cancer Association 16*, 100-110.

326. Vick, B., Weber, A., Urbanik, T., Maass, T., Teufel, A., Krammer, P. H., Opferman, J. T., Schuchmann, M., Galle, P. R., and Schulze-Bergkamen, H. (2009) Knockout of myeloid cell leukemia-1 induces liver damage and increases apoptosis susceptibility of murine hepatocytes, *Hepatology 49*, 627-636.

327. Ding, Q., He, X., Xia, W., Hsu, J. M., Chen, C. T., Li, L. Y., Lee, D. F., Yang, J. Y., Xie, X., Liu, J. C., and Hung, M. C. (2007) Myeloid cell leukemia-1 inversely correlates with glycogen synthase kinase-3beta activity and associates with poor prognosis in human breast cancer, *Cancer Res 67*, 4564-4571.

328. Smolewska, E., Stanczyk, J., Robak, T., and Smolewski, P. (2006) Inhibited apoptosis of synovial fluid lymphocytes in children with juvenile idiopathic arthritis is associated with increased expression of myeloid cell leukemia 1 and XIAP proteins, *The Journal of rheumatology 33*, 1684-1690.

329. Marino, G., and Kroemer, G. (2013) Mechanisms of apoptotic phosphatidylserine exposure, *Cell research 23*, 1247-1248.

330. Astrinidis, A., and Henske, E. P. (2005) Tuberous sclerosis complex: linking growth and energy signaling pathways with human disease, *Oncogene 24*, 7475-7481.

331. Mizushima, N., and Yoshimori, T. (2007) How to interpret LC3 immunoblotting, *Autophagy 3*, 542-545.

332. Yamamoto, A., Tagawa, Y., Yoshimori, T., Moriyama, Y., Masaki, R., and Tashiro, Y. (1998) Bafilomycin A1 prevents maturation of autophagic vacuoles by inhibiting fusion between autophagosomes and lysosomes in rat hepatoma cell line, H-4-II-E cells, *Cell structure and function 23*, 33-42.

333. Das, G. C., Holiday, D., Gallardo, R., and Haas, C. (2001) Taxol-induced cell cycle arrest and apoptosis: dose-response relationship in lung cancer cells of different wild-type p53 status and under isogenic condition, *Cancer Lett 165*, 147-153.

334. Bieging, K. T., Mello, S. S., and Attardi, L. D. (2014) Unravelling mechanisms of p53-mediated tumour suppression, *Nat Rev Cancer 14*, 359-370.

335. Schähs, P., Weidinger, P., Probst, O. C., Svoboda, B., Stadlmann, J., Beug, H., Waerner, T., and Mach, L. (2008) Cellular repressor of E1A-stimulated genes is a bona fide lysosomal protein which undergoes proteolytic maturation during its biosynthesis, *Exp. Cell Res. 314*, 3036-3047.

336. Feinberg, A. P., Ohlsson, R., and Henikoff, S. (2006) The epigenetic progenitor origin of human cancer, *Nature reviews. Genetics 7*, 21-33.

337. Beljaars, L., Olinga, P., Molema, G., de Bleser, P., Geerts, A., Groothuis, G. M., Meijer, D. K., and Poelstra, K. (2001) Characteristics of the hepatic stellate cell-selective carrier mannose 6-phosphate modified albumin (M6P$_{28}$-HSA), *Liver 21*, 320-328.

338. Beljaars, L., Meijer, D. K., and Poelstra, K. (2002) Targeting hepatic stellate cells for cell-specific treatment of liver fibrosis, *Frontiers in bioscience : a journal and virtual library 7*, e214-222.

339. Gary-Bobo, M., Nirde, P., Jeanjean, A., Morere, A., and Garcia, M. (2007) Mannose 6-phosphate receptor targeting and its applications in human diseases, *Curr. Med. Chem. 14*, 2945-2953.

340. Jeanjean, A., Gary-Bobo, M., Nirde, P., Leiris, S., Garcia, M., and Morére, A. (2008) Synthesis of new sulfonate and phosphonate derivatives for cation-independent mannose 6-phosphate receptor targeting, *Bioorg. Med. Chem. Lett. 18*, 6240-6243.

341. Tang, H. L., Yuen, K. L., Tang, H. M., and Fung, M. C. (2009) Reversibility of apoptosis in cancer cells, *Br J Cancer 100*, 118-122.

342. Franzyk, H., Christensen, M. K., Jørgensen, R. M., Meldal, M., Cordes, H., Mouritsen, S., and Bock, K. (1997) Constrained glycopeptide ligands for MPRs. Limitations of unprotected phosphorylated building blocks, *Bioorg. Med. Chem. 5*, 21-40.

343. Olson, L. J., Yammani, R. D., Dahms, N. M., and Kim, J.-J. P. (2004) Structure of uPAR, plasminogen, and sugar-binding sites of the 300 kDa mannose 6-phosphate receptor, *EMBO J. 223*, 2019-2028.

344. Kolb, H. C., and Sharpless, K. B. (2003) The growing impact of click chemistry on drug discovery, *Drug discovery today 8*, 1128-1137.

345. Kalia, J., and Raines, R. T. (2010) Advances in Bioconjugation, *Current organic chemistry 14*, 138-147.

346. Demko, Z. P., and Sharpless, K. B. (2002) A click chemistry approach to tetrazoles by Huisgen 1,3-dipolar cycloaddition: synthesis of 5-sulfonyl tetrazoles from azides and sulfonyl cyanides, *Angew Chem Int Ed Engl 41*, 2110-2113.

347. Le Borgne, R., and Hoflack, B. (1998) Protein transport from the secretory to the endocytic pathway in mammalian cells, *Biochim Biophys Acta 1404*, 195-209.

348. Olson, L. J., Zhang, J., Dahms, N. M., and Kim, J.-J. P. (2002) Twists and turns of the CD-MPR: ligand-bound versus ligand-free receptor, *J. Biol. Chem. 277*, 10156-10161.

349. Marron-Terada, P. G., Bollinger, K. E., and Dahms, N. M. (1998) Characterization of truncated and glycosylation-deficient forms of the cation-dependent mannose 6-phosphate receptor expressed in baculovirus-infected insect cells, *Biochemistry 37*, 17223-17229.

350. Dahms, N. M., Lobel, P., and Kornfeld, S. (1989) Mannose 6-phosphate receptors and lysosomal enzyme targeting, *J. Biol. Chem. 264*, 12115-12118.

351. Bohnsack, R. N., Song, X., Olson, L. J., Kudo, M., Gotschall, R. R., Canfield, W. M., Cummings, R. D., Smith, D. F., and Dahms, N. M. (2009) Cation-independent mannose 6-phosphate receptor: a composite of distinct phosphomannosyl binding sites, *J Biol Chem 284*, 35215-35226.

352. Marron-Terada, P. G., Brzycki-Wessell, M. A., and Dahms, N. M. (1998) The two mannose 6-phosphate binding sites of the insulin-like growth factor-II/mannose 6-phosphate receptor display different ligand binding properties, *J. Biol. Chem. 273*, 22358-22366.

353. Castonguay, A. C., Lasanajak, Y., Song, X., Olson, L. J., Cummings, R. D., Smith, D. F., and Dahms, N. M. (2012) The glycan-binding properties of the cation-independent mannose 6-phosphate receptor are evolutionary conserved in vertebrates, *Glycobiology 22*, 983-996.

354. Sohar, I., Sleat, D., Liu, C.-G., Ludwig, T., and Lobel, P. (1998) Mouse mutants lacking the cation-independent mannose 6-phosphate/insulin-like growth factor II receptor are impaired in lysosomal enzyme transport: comparison of cation-independent and cation-dependent mannose 6-phosphate receptor-deficient mice, *Biochem. J. 330*, 903-908.

355. Stein, M., Zijderhand-Bleekemolen, J. E., Geuze, H., Hasilik, A., and von Figura, K. (1987) Mr 46,000 mannose 6-phosphate specific receptor: its role in targeting of lysosomal enzymes, *EMBO J. 6*, 2677-2681.

356. Hoflack, B., Fujimoto, K., and Kornfeld, S. (1987) The interaction of phosphorylated oligosaccharides and lysosomal enzymes with bovine liver cation-dependent mannose 6-phosphate receptor, *J. Biol. Chem. 262*, 123-129.

357. Sleat, D. E., and Lobel, P. (1997) Ligand binding specificities of the two mannose 6-phosphate receptors, *J. Biol. Chem. 272*, 731-738.

358. Cardelli, J. A. (1993) Regulation of lysosomal trafficking and function during growth and development of *Dictyostellium discoideum. Advances in Cell and Molecular Biology of Membranes 1,* 341-390.

359. Freeze, H. H., Lammertz, M., Iranfar, N., Fuller, D., Panneerselvam, K., and Loomis, W. F. (1997) Consequences of disrupting the gene that encodes alpha-glucosidase II in the N-linked oligosaccharide biosynthesis pathway of Dictyostelium discoideum, *Developmental genetics 21*, 177-186.

360. Freeze, H. H., Miller, A. L., and Kaplan, A. (1980) Acid hydrolases from Dictyostelium discoideum contain phosphomannosyl recognition markers, *J Biol Chem 255*, 11081-11084.

361. Cardelli, J. A., Golumbeski, G. S., and Dimond, R. L. (1986) Lysosomal enzymes in Dictyostelium discoideum are transported to lysosomes at distinctly different rates, *J Cell Biol 102*, 1264-1270.

362. Kyte, J., and Doolittle, R. F. (1982) A simple method for displaying the hydropathic character of a protein, *J. Mol. Biol. 157*, 105-132.

363. Uson, I., Schmidt, B., von Bulow, R., Grimme, S., von Figura, K., Dauter, M., Rajashankar, K. R., Dauter, Z., and Sheldrick, G. M. (2003) Locating the anomalous scatterer substructures in halide and sulfur phasing, *Acta crystallographica. Section D, Biological crystallography 59*, 57-66.

364. Gao, G. F., Gerth, U. C., Wyer, J. R., Willcox, B. E., O'Callaghan, C. A., Zhang, Z., Jones, E. Y., Bell, J. I., and Jakobsen, B. K. (1998) Assembly and crystallization of the complex between the human T cell coreceptor CD8alpha homodimer and HLA-A2, *Protein Sci 7*, 1245-1249.

365. Dimond, R. L., Burns, R. A., and Jordan, K. B. (1981) Secretion of Lysosomal enzymes in the cellular slime mold, Dictyostelium discoideum, *J Biol Chem 256*, 6565-6572.

366. Cardelli, J. A., Golumbeski, G. S., Woychik, N. A., Ebert, D. L., Mierendorf, R. C., and Dimond, R. L. (1987) Defining the intracellular localization pathways followed by lysosomal enzymes in Dictyostelium discoideum, *Methods in cell biology 28*, 139-155.

367. Richardson, J. M., Woychik, N. A., Ebert, D. L., Dimond, R. L., and Cardelli, J. A. (1988) Inhibition of early but not late proteolytic processing events leads to the missorting and oversecretion of precursor forms of lysosomal enzymes in Dictyostelium discoideum, *J Cell Biol 107*, 2097-2107.

368. MacDonald, R. G., Tepper, M. A., Clairmont, K. B., Perregaux, S. B., and Czech, M. P. (1989) Serum form of the rat insulin-like growth factor II/mannose 6-phosphate receptor is truncated in the carboxyl-terminal domain, *J. Biol. Chem. 264*, 3256-3261.

369. Geske, F. J., Lieberman, R., Strange, R., and Gerschenson, L. E. (2001) Early stages of p53-induced apoptosis are reversible, *Cell death and differentiation 8*, 182-191.

370. Broker, L. E., Kruyt, F. A., and Giaccone, G. (2005) Cell death independent of caspases: a review, *Clin Cancer Res 11*, 3155-3162.